ANALYSIS OF DATA FROM THE VOYAGER PLASMA SCIENCE EXPERIMENT USING THE FULL CUP RESPONSE

by

ALAN SETH BARNETT
S.B. Massachusetts Institute of Technology
1977

Submitted to the Department of
Physics
in Partial Fulfillment of the
Requirements for the Degree of

DOCTOR OF PHILOSOPHY

at the

MASSACHUSETTS INSTITUTE OF TECHNOLOGY
May 1983

Signature of Author_____
Department of Physics, 29 April 1983

Certified by_____
Thesis Supervisor

Accepted by_____
Chairman, Department Committee on Graduate Students

This work was funded in part by JPL contract 95733 and NASA contract NAGW-165

ANALYSIS OF DATA FROM THE VOYAGER PLASMA SCIENCE EXPERIMENT USING THE FULL CUP RESPONSE

by

ALAN SETH BARNETT

Submitted to the Department of Physics
on 29 May 1983 in partial fulfillment of the
requirements for the degree of
Doctor of Philosophy in Physics

ABSTRACT

The Voyager Plasma Science experiment consists of four modulated grid Faraday cups which measure positive ions and electrons in the energy-per-charge range of 10-5950 volts. A formula for the full response function of each of the cups is derived from the solution to the equations of motion for a charged particle inside the cup. The current in each of the energy-per-charge channels of the detector can be expressed as the difference between two integrals over velocity space of the product of the response function and the distribution function which describes the plasma. The integrals are performed for two special cases when the distribution function is a convected Maxwellian.

For the case when the sonic Mach number of the flow is large ("cold plasma" approximation), we approximated the dependence of the distribution function on the components of the flow perpendicular to the cup normal by a Dirac delta function, permitting the integrals over those components to be performed trivially. The remaining integral must be performed numerically.

For the more general case when the sonic Mach number is not large, we approximated the analytic expressions for the response function by a functional form which permits the integration over the components of velocity transverse to the cup normal to be performed analytically. Once again, the integral over the normal component of the velocity must be performed numerically. We developed a special integration scheme which greatly reduces the computer time required for the numerical computation of the remaining integral.

The formula for the response function was tested by using the solar wind as a test beam when the spacecraft was rotating during a cruise maneuver. Analysis of the data taken during the maneuver using the "cold plasma" approximation confirmed the accuracy of our response function for angles of incidence of up to 70° for the main sensor cups and up to at least 55° for the side sensor cup. By using data from all four cups simulatneously, we are able to determine the solar wind direction with a precision of better than 0.5°.

We then present analysis of data taken in the vicinity of the Jovian satellite Io. The interaction between Io and the Jovian magnetosphere is a topic of considerable interest due to the fact that the decametric radio emmision from Jupiter appears to be modulated by the satellite. Unfortunately, the problem of determining the plasma parameters near Io is extremely difficult due to the low Mach number of the flow, the

large angle of the flow with respect to the cup look directions, and the presence of several different ioic species. Under the assumption that the only ions present are O^+, O^{++}, S^+, and SO_2^+ and that all of the ionic species have the same thermal speed, we obtain estimates of the plasma parameters by fitting seven spectra taken in the vicinity of Io. We interpret our results in terms of a model of the interaction between Io and the Jovian ionosphere due to Neubauer (1980). The results indicate qualitative agreement with the model that the flow is analogous to the potential flow of an incompressible fluid around an infinitely long cylinder.

Thesis Supervisor: Dr. Stanislaw Olbert

Title: Professor of Physics

Acknowledgements

Acknowledgements

For helpful discussions and encouragement, I wish to thank Professors John Belcher and Ralph McNutt, and Drs. Alan Lazarus and Fran Bagenal.

For his assistance in the seemingly futile endeavor to tame the recalcitrant computer, I wish to thank Dr. George Gordon.

For their patience with my plottapes, I wish to thank Pamela Milligan and Mary Terkoski.

For her general helpfulness and cheerfulness, I wish to thank Anne Bowes.

For his amazing ability to find money to support me term after term, I wish to thank Professor Herb Bridge.

There is more to life than physics, and I would not have been able to finish this thesis and retain my sanity without the help of many other people. In particular;

For his companionship as partner in frequent attempts to boldly sail where no windsurfer has sailed before, I wish to thank Dr. Paul Gazis.

For providing (too?) many hours of extremely enjoyable distractions, I wish to thank the staff of the Sailing Pavilion and the members of the MIT Nautical Association.

For greatly enriching my life through the joy of music, I wish to thank all of the people with whom I have played chamber music over the past six years, in addition to the conductor, accompanist, and members of the MIT Choral Society.

For their frequent company and deep friendship, I wish to thank Peter Shaw, Leslie Silverfine, Penelope Metzidakis, Roland Vanderspek, Donna Hewitt, and Norman (Gil) Bristol, Jr..

For their love and moral support throughout my entire life, I wish to thank my parents.

And most important, for his many stimulating discussions of physics and other topics, his infinite patience, his encouragement to help me through the all too frequent discouraging moments, his great generosity with his time, and numerous other things great and small, I wish to thank Professor Stanislaw Olbert.

Table of Contents

Title Page	p	1
Abstract	p	2
Acknowledgements	p	4
Table of Contents	p	6
Chapter 1 Introduction	p	8
Chapter 2 Derivation of the Response Function of the Voyager Plasma Science Experiment	p	13
Section 2.1 Location and Orientation of the Instrument	p	14
Section 2.2 Structure and Operation of the Main Sensor Cups	p	15
Section 2.3 Response Function of the Main Sensor	p	17
Section 2.3a The Grid Transparency	p	18
Section 2.3b The Sensitive Area	p	20
Section 2.4 Structure and Operation of the Side Sensor	p	24
Section 2.4a The Grid Transparency	p	25
Section 2.4b The Sensitive Area	p	26
Section 2.5 The "Cold Plasma" Approximation	p	29
Section 2.6 The "Hot Plasma" Approximation for the Main Sensor	p	32
Section 2.7 The "Hot Plasma" Approximation for the D-Cup	p	37
Chapter 3 Experimental Test of the Response Function	p	38
Section 3.1 The Cruise Maneuver	p	39
Section 3.2 Analysis of Data Taken During the Cruise Maneuver	p	41
Section 3.3 Discussion and Conclusions	p	45

Chapter 4 The Theory of the Interaction Between Io and the Jovian Magnetosphere p 49

Section 4.1 Introduction p 50

Section 4.2 The Equations Which Describe the Plasma at Io p 52

Section 4.3 The Io-Magnetosphere Interaction p 59

Chapter 5 Analysis of Plasma Data Taken in the Vicinity of Io by Voyager I p 73

Section 5.1 The Io Flyby p 74

Section 5.2 Analysis of the Data p 75

Section 5.3 The Flow Around the Alfven Wing p 82

Section 5.4 Summary p 89

References p 92

Tables p 94

Figure Captions p 100

Figures p 113

Appendix A p 166

Appendix B p 178

Appendix C p 182

Appendix D p 186

Chapter I

Introduction

On 20 August 1977, a spacecraft named Voyager II was launched from the Kennedy Space Center in Florida, bound for the outer solar system. Voyager I, its sister ship, was launched two weeks later on September 5. Both spacecraft were targeted for close encounters with Jupiter and Saturn. Voyager II will also fly close to Uranus and Neptune.

One of the experiments carried by both of these spacecraft was a set of four modulated grid Faraday cups called the Plasma Science Experiment (PLS). The PLS experiment measures positive ions and electrons in the energy range of 10-5950 eV. It was designed and constructed at MIT, and includes several novel features (Bridge et al). Three of its four cups are very shallow, resulting in an extremely wide field of view. These same three cups are arrayed about an axis of symmetry such that their fields of view overlap. This region of overlap includes the direction of the solar wind flow throughout most of the mission. By analyzing positive ion data taken by all three of these cups simultaneously, it is possible to determine the direction of the solar wind flow to better than one-half degree and its magnitude to within a few km/sec.

The fourth cup is more conventional in design, and it looks in a direction perpendicular to the symmetry axis of the main cluster. During the interplanetary, or cruise, phase of the mission, this cup is used to measure electrons. In addition, during the inbound pass of planetary encounters, this cup looks in the direction of the corotating plasma, measuring both electrons and positive ions.

The main sensor cups were designed in such a way that for a wide range of sonic Mach numbers and flow directions, including all of the situations which one expects to encounter during the cruise phases of the mission, almost all

of the particles which enter the aperture and are not stopped by the modulator voltage do reach the collector. During planetary encounters, however, the facts that the Mach number is frequently low and that the flow is highly oblique to the cups makes the "unity response" approximation not valid. In order to analyze data taken at these times, a knowledge of the full response function of the cups is required.

This thesis presents a derivation of the full response function based on a calculation of the trajectories of charged particles inside the cups. The current measured by the sensors is given by the integral over velocity space of the product of the plasma distribution function and the cup response function. A computer program which performs this integration numerically has already been written by V. Vasyliunas, one of the designers of the instrument. Unfortunately, his algorithm is very slow. Not only is it impossible to use it to perform any iterative fitting procedure to determine the macroscopic plasma parameters, but it is even too slow to use at all for simulating the high resolution (M-mode) energy-per-charge spectra. We have overcome this difficulty by approximating the analytic expression for the response function by a functional form which permits the integrations over the components of velocity perpendicular to the cup normal to be performed analytically for the case where the distribution function is a convected Maxwellian. This derivation is the topic of Chapter 2.

In order to test the response function derived in Chapter 2, it is neccessary to have an extremely narrow test beam. Since such a beam is very difficult to make in the laboratory and the quiet solar wind has just these properties, we have tested the response function by analyzing data taken by Voyager I during a cruise maneuver. During the cruise maneuver, the

spacecraft performed a series of rotations which changed the orientation of the spacecraft, causing the solar wind to enter the cups from a wide variety of angles. The use of the data taken during the cruise maneuver to test our cup response functions is the topic of Chapter 3.

On the outbound pass of its Jupiter encounter, Voyager I flew about 20,000 km above the south pole of the satellite Io. As the decametric radio burst from Jupiter are known to be correlated with the phase angle of Io, the interaction between Io and the magnetospheric plasma is a topic of considerable interest. During the Io flyby, the sonic Mach number of the plasma was low (about 2) and the flow direction was perpendicular to the main sensor symmetry axis. This situation makes knowledge of the full response function neccessary for the analysis of the data taken during this period. This stretch of data was chosen for the first use of the full response function in analyzing data.

The satellite Io appears to have a high electrical conductivity. Drell, Foley and Ruderman (1965) have shown that any conductor which moves through a magnetized plasma will be a source of Alfven waves. If the velocity of the conductor with respect to the ambient medium does not change with time, there will be a standing wave pattern in the rest frame of the conductor consisting of a pair of Alfven "wings" which extend away from the conductor in the direction of the Alfven characteristics. Neubauer (1980) has shown that the plasma flow around each of these wing is analogous to the potential flow of an incompressible fluid around an infinite cylinder.

The final two chapters of the thesis are concerned with Io's interaction with the Jovian magnetospheric plasma. Chapter 4 contains a discussion and critique of Neubauer's theory, while Chapter 5 consists of analysis of the

data taken by Voyager I during the Io flyby. We conclude that the data is consistent with the overall picture that the plasma flows around the Alfven wing as if the wing were a long, cylindrical obstacle.

Chapter 2

Derivation of the Response Function

of the

Voyager PLS Experiment

2.1 Location and Orientation of the Instrument

The Voyager Plasma Science Experiment consists of four modulated grid Faraday cups. A sketch of the instrument is shown in Figure 2.1. Three of the cups, called the A-cup, B-cup, and C-cup, comprise the main sensor. These three cups have the same pentagonal shape and are arrayed with their cup normals 20° from an axis of symmetry. The fourth cup, called the side sensor or D-cup, has a circular aperture. The normal to the D-cup aperture points in a direction 88° from the main sensor symmetry axis.

Figure 2.2 shows the location and orientation of the plasma instrument on the spacecraft. The instrument is mounted on the science boom, a metal support structure which extends away from the main body of the spacecraft. Also on the science boom are the cosmic ray, imaging, UV spectrometry, IR spectrometry, photopolarimetry, and low energy charged particle experiments.

The system of coordinates called spacecraft coordinates is defined as follows: The spacecraft center of mass is taken as the origin. The unit vector $\hat{z}_{sc}$ points along the axis of the main antenna, with $+\hat{z}_{sc}$ pointing into the antenna. The unit vector $\hat{y}_{sc}$ lies in the plane containing the $\hat{z}_{sc}$ and the axis of symmetry of the science boom. It is perpendicular to the $\hat{z}_{sc}$ and makes an acute angle with the science boom. The unit vector $\hat{x}_{sc}$ is defined so as to make a right-handed system (see Fig. 2.2).

The outward pointing symmetry axis of the PLS main sensor is parallel to $-\hat{z}_{sc}$. As this axis is also parallel to the axis of the main antenna, it is pointed at the earth during most of the mission. Since the angular separation between the earth and the sun as seen from the outer solar

system is small, the solar wind flow direction is substantially into the main sensor. The D-cup is oriented such that it looks into corotating flow during the inbound pass of a planetary flyby. The relative orientations of the cup apertures as viewed from along the main sensor symmetry axis is shown in Fig. 2.3.

During the interplanetary, or cruise, phase of the mission, the main sensor measures positive ions and the side sensor measures electrons. During planetary encounters, the D-cup is also used to measure positive ions.

2.2 Structure and Operation of the Main Sensor Cups

A vertical cross section of a main sensor cup is shown in Figure 2.4, and a top view is shown in Figure 2.5. The collector of the cup has the shape of home plate on a baseball field with the corners smoothed out. The aperture is similar in shape, differing in that it is smaller and its parallel sides are shorter with respect to its other sides. The aperture area (A_{ap}) is 102 cm^2. Around the edge of the collector is a rim of metal. The collector plane is considered to be the plane defined by the top of this rim. The distance (h) from the aperture to this plane is 4.1 cm.

The cup has nine parallel grids. Each grid consists of a woven mesh of two perpendicular sets of parallel wires. When measuring ions, the suppressor grid is held at -95V relative to the collector, and the same positive voltage square wave is impressed on all three modulator grids. The rest of the grids and the collector are grounded to the spacecraft.

When a square wave voltage is impressed on the modulator grids, the

collector current is a square wave differing in phase by 180°, as shown in Figure 2.6. The amplitude of this square wave is the information which is telemetered back to Earth. During operation, a sequence of such square waves is used. The frequency of the wave is 400hz, and the limiting voltages are changed every 0.240 secs. The voltages are changed such that the higher voltage of any one square wave is the lower voltage of the next. In this way the voltage range of 10-5950 volts is divided into contiguous channels. In the low resolution (L-)mode there are 16 channels; in the high resolution (M-)mode there are 128 channels. Hereafter, we will label the channels with a subscript k. Appendix A includes a table which lists the threshold voltage ϕ_k, the voltage width $\Delta\phi_k$ $(\phi_{k+1} - \phi_k)$, and the average voltage $\bar{\phi}_k$ $((\phi_{k+1} + \phi_k)/2)$ for each channel in each of the positive ion modes (L and M). A more thorough description of the instrument and its operation is given in Bridge et al (1977).

In order to define the threshold speeds v_k we will use a coordinate system called cup coordinates. We take as the origin the center of the long side of the aperture (point 0 in Figure 2.5). The unit vector $\hat{z}_{cup}$ is perpendicular to the aperture plane and points into the cup, the unit vector $\hat{x}_{cup}$ is defined by the vector cross product of $\hat{z}_{sc}$ with $\hat{z}_{cup}$, and the unit vector $\hat{y}$cup is defined to make a right-handed coordinate system.

Consider a parallel beam of positive monoenergetic ions incident on the cup. The only particles to reach the collector will be those with a z-component of velocity greater than v_k given by

$$v_k=(2Z^* e\phi_k/Am_p)^{1/2} \qquad 2.1a$$

where Z^* is the charge state of the ion, e is the elementary charge, ϕ_m is the modulator voltage, A is the atomic weight and m_p is the proton mass. It is

convient to define the average proton speed $\bar{v}_k$ and the channel width Δv_k as

$$\bar{v}_k = (v_{k+1}+v_k)/2 \qquad 2.1b$$

$$\Delta v_k = v_{k+1}-v_k \qquad 2.1c$$

The values of $\bar{v}_k$ and Δv_k for each channel are included in Appendix A.

In terms of the distribution function $f(\vec{v})$ which describes the plasma environment of the spacecraft, the current in the k-th channel is given by Equations 2.2a and 2.2b.

$$I_k = I_k^* - I_{k+1}^* \qquad 2.2a$$

$$I_k^* = A_0 Z^* e \int_{-\infty}^{\infty}\int_{-\infty}^{\infty} dv_x dv_y \int_{v_k}^{\infty} dv_z v_z f(\vec{v}) R(\vec{v},v_k) \qquad 2.2b$$

where A_0 is the aperture area times the transparency at normal incidence and $R(\vec{v},v_k)$ is the cup response function, to be derived hereinafter. The quantity $f(\vec{v})$ in the above equation is the distribution function of a single species; if the plasma contains more than one species the current will be given by a sum of terms like Equation 2.2b, one for each type of ion.

The quantity I_k can be thought of as a function of $\bar{v}_k$. For the remainder of this thesis, the quantity $I_k(\bar{v}_k)/\Delta\phi_k$ will be referred to as the reduced distribution function. This is because when the unity response approximation is valid, $I_k/\Delta\phi_k$ is in fact proportional to the object which generally goes by that name (see McNutt et al (1981)).

2.3 Response Function of the Main Sensor

Our problem is to determine the function R. A particle incident on the aperture will reach the collector unless it is stopped by the modulator

voltage, it collides with a grid, or its trajectory is such that it misses the collector and collides with the side of the cup. The first effect is taken care of by the lower limit of the integration over v_z; the latter two effects are included in R. R can therefore by written as a product of two terms and a normalization constant,

$$R=TA/A_0 \qquad 2.3$$

where T is the transparency of the grids and A is the "sensitive" area of the collector. Note that R is normalized to unity at normal incidence. T and A are functions of velocity and channel number, while A_0 is a constant. We will first consider the effect of collisions with the grids (transparency).

2.3a The Grid Transparency

The transparency of a single grid is defined as the probability of an incident particle traversing the plane of the grid without colliding with the wires. We model a grid as a planar structure consisting of two perpendicular sets of parallel cylindrical wires. In the main sensor, the sets of wires of all of the grids are parallel to the x- and y- axes in cup coordinates. The transparency of the grid will be the product of the transparencies of each set of wires considered separately.

Consider the wires which run in the $\hat{x}$-direction. Since the transparency of these wires does not depend upon v_x, we only need to consider the projection of the motion into the y-z plane. The probability of a particle colliding with one of the wires is simply the ratio of the area of the wires to the area of the gaps between the wires projected into a plane perpendicular to the particle velocity vector (see Figure 2.7). Per unit length along the

wire, this ratio is

$$\text{Probability of collision} = \frac{d}{L \cos \alpha} = c \sec \alpha \qquad 2.4$$

where d is the wire diameter, L is the grid spacing, c(=1/42) is their ratio, and α is the angle between the particle velocity and the grid normal. The probability of a particle <u>not</u> colliding with the grid, is

$$\text{Probability of no collision} = 1 - (c \sec \alpha) \qquad 2.5$$

If $\vec{v}^*$ is the velocity of the particle as it crosses the grid plane, we see that the transparency of one grid is

$$T=[1-c(1+(\frac{v_x^*}{v_z^*})^2)^{1/2}][1-c(1+(\frac{v_y^*}{v_z^*})^2)^{1/2}] \qquad 2.6$$

Under the assumption that the potential inside the cup depends only on z,, $\vec{v}^*$ depends solely upon the velocity of the particle before it enters the cup and the voltage on the grid. The validity of this approximation will be discussed in the next section. An expression relating $\vec{v}^*$ with $\vec{v}$ is now found from energy conservation to be

$$v_x^* = v_x \qquad 2.7a$$

$$v_y^* = v_y \qquad 2.7b$$

$$v_z^* = (v_z^2 - 2e\phi/Am_p)^{1/2} \qquad 2.7c$$

The transparency of all of the grids is the product of the transparencies of the individual grids. It is given by

$$T=\prod_i [1-c(1+\frac{v_x^2}{v_z^2-\frac{2e\phi_i}{Am_p}})^{1/2}][1-c(1+\frac{v_y^2}{v_z^2-\frac{2e\phi_i}{Am_p}})^{1/2}] \qquad 2.8$$

where ϕ_i is the voltage on the i-th grid

Each cup has three modulator grids, one suppressor grid, and five grounded grids (see Fig. 2.4). The transparency is therefore given explicitly

by

$$T=[1-c(1+\frac{v_x^2}{v_z^2})^{1/2}]^5[1-c(1+\frac{v_x^2}{v_z^2(1-\frac{v_k^2}{v_z^2})})^{1/2}]^3[1-c(1+\frac{v_x^2}{v_z^2(1+\frac{v_s^2}{v_z^2})})^{1/2}]\times$$

$$[1-c(1+\frac{v_y^2}{v_z^2})^{1/2}]^5[1-c(1+\frac{v_y^2}{v_z^2(1-\frac{v_k^2}{v_z^2})})^{1/2}]^3[1-c(1+\frac{v_y^2}{v_z^2(1+\frac{v_s^2}{v_z^2})})^{1/2}] \qquad 2.9$$

The subscript s refers to the suppressor grid; v_s is defined in a manner analogous to the definition of v_k in Equation 2.1

$$v_s=(2Z^*e\phi_s/Am_p)^{1/2} \qquad 2.10$$

where ϕ_s is the voltage on the suppressor grid.

Note that for normal incidence $T=T_o=(1-c)^{18}=0.65$ and $A_0=66$ cm^2.

2.3b The Sensitive Area

The second factor in Equation 2.3 is the "sensitive area". This is defined to be the overlap of the area of the collector with the area of the image of the aperture in the plane of the collector.

Consider a beam of particles incident at an angle α to the cup normal. In the collector plane, the beam will have the shape of the aperture, but its position will be displaced because of the components of the particle velocity transverse to the cup normal direction, as shown in Figure 2.8. First we will compute the amount of the shift, and then we will discuss the functional dependence of the sensitive area on the shift vector.

We define a two dimensional vector $\vec{S}$, also shown in Figure 2.8, to be the displacement of the aperture image from a perpendicular projection of the

aperture into the plane of the collector. Figure 2.9 shows the projection into the x-z plane of a possible trajectory of a positive ion as it moves from the aperture to the collector of one of the main sensor cups. If the particles were not deflected by the electrostatic fields inside the cup, the shift would be given by

$$S_x = \frac{v_x}{v_z} h \qquad 2.11a$$

$$S_y = \frac{v_y}{v_z} h \qquad 2.11b$$

The effect of the fields is to bend the beam, thereby changing the amount of the shift. To compute the amount of the shift, we will solve the equations of motion for a charged particle moving in the electric field of one of the cups.

We will assume that the potential between the grids depends only upon z. This neglects the fine structure of the fields close to grids as well as the fringing fields near the edges of the grids.

The fine structure of the fields in the vicinity of the wires decays in a distance comparable to the mesh size of the grid. Since this distance is much less than the spacing between grids, the ripple in the fields near the wires can safely be ignored.

The fringing fields are important only in a region around the edge of the grids which has a width comparable to the grid spacing. Because of the cup goemetry, any particle whose trajectory includes the region where the fringing fields are important will miss the collector. As this will occur whether or not the fringing fields are used in computing the trajectory, these fields can be ignored.

The potential is therefore well approximated by a linear function of distance between any two neighboring grids. Figure 2.10a shows the potential

as a function of z for a typical channel. Using energy conservation and the fact that the fields are entirely in the z-direction the equation of motion is easily solved. The equations of motion of the particle are

$$v_x^* = \frac{dx}{dt} = v_x \qquad 2.12a$$

$$v_y^* = \frac{dy}{dt} = v_y \qquad 2.12b$$

$$v_z^* = \frac{dz}{dt} = (v_z^2 - \frac{2z^*e\phi(z)}{Am_p})^{1/2} \qquad 2.12c$$

with $\phi(z)$ given by

$$\phi(z) = \frac{z}{.762}\,\phi_k \qquad 0<z<.762 \qquad 2.13a$$

$$\phi(z) = \phi_k \qquad .762<z<1.143 \qquad 2.13b$$

$$\phi(z) = \frac{1.905-z}{.762}\,\phi_k \qquad 1.143<z<1.905 \qquad 2.13c$$

$$\phi(z) = 0 \qquad 1.905<z<2.286 \qquad 2.13d$$

$$\phi(z) = \frac{z-2.286}{.414}\,\phi_s \qquad 2.286<z<2.700 \qquad 2.13e$$

$$\phi(z) = \frac{3.089-z}{.389}\,\phi_s \qquad 2.700<z<3.089 \qquad 2.13f$$

$$\phi(z) = 0 \qquad 3.089<z<4.100 \qquad 2.13g$$

Equations 2.12a and 2.12b can be solved by inspection. For a particle which crosses the aperture plane at the origin of the cup coordinate system, the result is

$$x = v_x t \qquad 2.14a$$

$$y = v_y t \qquad 2.14b$$

The components of the shift vector are simply the values of x and y evaluated for t equal to the transit time of the particle from the aperture to the collector plane. This can be evaluated with the aid of Equation 2.12c, which can be rewritten as

$$\int_0^t dt = \int_0^h \frac{dz}{(v_z^2 - \frac{2z^*e\phi(z)}{Am_p})^{1/2}} \qquad 2.15$$

Inserting the expressions for $\phi(z)$ from Equations 2.13a-2.13g and performing the integrations we find

$$t=t_a+t_b+t_c+t_d+t_e+t_f+t_g \qquad 2.16$$

$$t_a=\left(\frac{2}{v_z}\right)(.762)\frac{\left[1-\left(1-\frac{v_k^2}{v_z^2}\right)^{1/2}\right]}{(v_z^2/v_k^2)} \qquad 2.17a$$

$$t_b=\left(\frac{.381}{v_z}\right)\left(\frac{1}{\left(1-\frac{v_k^2}{v_z^2}\right)}\right) \qquad 2.17b$$

$$t_c=t_a \qquad 2.17c$$

$$t_d=\frac{.381}{v_z} \qquad 2.17d$$

$$t_e=\left(\frac{2}{v_z}\right)(.414)\frac{\left[\left(1+\frac{v_s^2}{v_z^2}\right)^{1/2}-1\right]}{(v_z^2/v_s^2)} \qquad 2.17e$$

$$t_f=\left(\frac{2}{v_z}\right)(.389)\frac{\left[\left(1+\frac{v_s^2}{v_z^2}\right)^{1/2}-1\right]}{(v_z^2/v_s^2)} \qquad 2.17f$$

$$t_g=\frac{1.011}{v_z} \qquad 2.17g$$

Using Equations 2.14a, 2.14b, 2.16, and 2.17a-2.17g the shift vector can be written as

$$S_x=S\left(\frac{v_x}{v_z}\right)h \qquad 2.18a$$

$$S_y=S\left(\frac{v_y}{v_z}\right)h \qquad 2.18b$$

with S, the shift function, defined by

$$S=.743\left(\frac{\left[1-\left(1-\frac{v_k^2}{v_z^2}\right)^{1/2}\right]}{(v_k^2/v_z^2)}\right)+.093\left(\frac{1}{1-(v_k^2/v_z^2)}\right)^{1/2}+.392\left(\frac{\left[\left(1+\frac{v_s^2}{v_z^2}\right)^{1/2}-1\right]}{(v_s^2/v_z^2)}\right)+.340 \qquad 2.19$$

We shall now very briefly consider the sensitive area as a function of the shift vector, which we will denote by $A(\vec{S})$. Because of the shapes of the aperture and the collector, this functional dependence is complicated. As there are 16 separate regions where the dependence is different (see Figure 2.11), an analytic representation is cumbersome. $A(S_x,S_y)$ is given in tabular form in Table 1. A plot of the sensitive area as a function of S_y, with S_x as a parameter, is shown in Figure 2.15.

2.4 Structure and Operation of the Side Sensor

The geometry of the D-cup is quite different from that of the main sensor cups. Figure 2.12 shows its cross section. Its aperture and collector are circular, and it has a metal annulus called the guard ring which is located 1.4 cm above the collector. The outer edge of the guard ring is connected to the side of the cup, while its inner diameter is smaller than the diameter of the aperture. The radii of the aperture, guard ring, and collector are 5.64 cm, 5.13 cm, and 6.35 cm, respectively. The distance from the collector to the guard ring is 1.413 cm, and from the collector to the aperture is 6.000 cm. It has eight grids, two of which are suppressor grids and only one of which is the modulator grid for the positive ion mode. The potential as a function of position for a typical channel is shown in Figure 2.10b.

In addition to measuring positive ions, the D-cup is also used to measure electrons. A different modulator grid is used for the electron mode. The potential as a function of position for a typical channel in the electron mode is shown in Figure 2.10c. The voltage thresholds for the two electron modes are included in appendix A.

2.4a The Grid Transparency

We will first consider the transparency function for the D-cup. The only complication not found in the main sensor cups is caused by the fact that the wires meshes in the different grids are not parallel to each other, but are rotated relative to each other by a specific angle. Also, the Voyager I and Voyager II instruments are different from each other. The mesh orientations for both spacecraft are given in Table 2.2.

We define cup coordinates for the D-cup a fashion analagous to that used for main sensor cups; the z_{cup}-axis is parallel to the cup normal and points into the cup, $\hat{x}_{cup}=\hat{z}_{sc} \times \hat{z}_{cup}$, and $\hat{y}_{cup}=\hat{z}_{cup} \times \hat{x}_{cup}$. The origin of the coordinate system is defined to be the center of the aperture. The transparency of any grid is still given by Equation 2.6 provided v_x and v_y are interpreted as the components of velocity along the directions of the grid wires. The grid orientation as given in Table 2.2 can then be used to rotate from cup coordinates to "grid" coordinates. The resulting expression for the

transparency of the D-cup is

$$T=\prod_{i=1}^{6}\left[1-c\left(1+\frac{v_t^2}{v_z^2}\cos^2(\xi-\alpha_i)\right)^{1/2}\right]\left[1-c\left(1+\frac{v_t^2}{v_z^2}\sin^2(\xi-\alpha_i)\right)^{1/2}\right]\times$$

$$\left[1-c\left(1+\frac{v_t^2\cos^2(\xi-\alpha_m)}{v_z^2\left(1-\frac{v_m^2}{v_z^2}\right)}\right)^{1/2}\right]\left[1-c\left(1+\frac{v_t^2\sin^2(\xi-\alpha_m)}{v_z^2\left(1-\frac{v_m^2}{v_z^2}\right)}\right)^{1/2}\right]\times \qquad 2.20$$

$$\left[1-c\left(1-\frac{v_t^2\cos^2(\xi-\alpha_s)}{v_z^2\left(1-\frac{v_s^2}{v_z^2}\right)}\right)^{1/2}\right]\left[1-c\left(1-\frac{v_t^2\sin^2(\xi-\alpha_s)}{v_z^2\left(1-\frac{v_s^2}{v_z^2}\right)}\right)^{1/2}\right]$$

where the α's are the angles from Table 2.2 which describe the grid orientation, and ξ and v_t are defined by

$$v_t=(v_x^2+v_y^2)^{1/2} \qquad 2.21a$$

$$\xi=\arctan(v_y/v_x) \qquad 2.21b$$

At normal incidence, $T=T_0=(1-c)^{16}=0.68$ and $A_0=56.2\ cm^2$.

2.4b The Sensitive Area

We now proceed to the sensitive area calculation. Because of the guard ring, the sensitive area is the mutual overlap of three circles of different sizes, the centers of which lie on the same line. There are now two independent shift vectors, one for the collector-guard ring shift and one for the collector-aperture shift. Because of the circular symmetry, the sensitive area does not depend upon the direction of the shift vector, only its magnitude. We therefore assume, without loss of generality, that the velocity vector of the incident beam lies in the x-z plane. By assumption, the y-components of the shift vectors are zero. We will denote by S_{ac} and S_{gc} the

magnitude of the (x-directed) shifts between the aperture and collector and between the guard and collector, respectively. It is also convenient to define S_{ag} as the relative shift between the aperture and the guard ring, $S_{ag}=S_{ac}-S_{gc}$.

We will now derive an expression for the overlap area of two circles with radii R_s and R_L ($R_L>R_s$) whose centers are separated by a distance S, as shown in Figures 2.13a, 2.13b and 2.13c. Let the coordinates of the centers of the circles be (0,0) and (s,0). The equations of the two circles are

$$x^2+y^2=R_L^2 \qquad 2.22a$$

$$(x-s)^2+y^2=R_s^2 \qquad 2.22b$$

An important parameter, which we shall call X, is the x-coordinate of the points where the two circles intersect (see Figure 2.13b). X can be determined as a function of s, R_L, and R_s by subtracting Equation 2.22b from 2.22a and solving for x. The result is

$$X=\frac{R_l^2-R_s^2+s^2}{2s} \qquad 2.23$$

Note that X as defined by Equation 2.23 is real and well defined even when the circles do not intersect. In this case $X>R_L$ and the corresponding value of y which simultaneously satisfies Equations 2.22a and 2.22b is imaginary. We shall find it convienient to define X by Equation 2.23 even when the geometrical interpretation of it no longer holds.

Now consider the following three cases, as shown in Figures 2.13a, 2.13b, and 2.13c.

Case I $\quad s\leq R_L-R_s$

In this case the overlap area is obviously just the area of the smaller circle.

$$A=\pi R_s^2 \qquad 2.24a$$

Case II $R_1-R_s<s<R_L+R_s$

The overlap area is given by the following sum of two integrals.

$$A=\int_{s-R_s}^{X}[(x-s)^2-R^2]^{1/2}dx+\int_{X}^{R_L}[x^2-R^2]^{1/2}dx \qquad 2.25$$

This integral is elementary, yielding

$$A=R^2[\tfrac{\pi}{2}+\arcsin Q_1+Q_1(1-Q_1)^{1/2}]+R^2[\tfrac{\pi}{2}-\arcsin Q_2-Q_2(1-Q_2)^{1/2}] \qquad 2.24b$$

$$Q_1=\frac{R_L^2-R_s^2-s^2}{2sR_s} \qquad 2.26a$$

$$Q_2=\frac{R_L^2-R_s^2+s^2}{2sR_L} \qquad 2.26b$$

Case III $s\geq R_L+R_s$

In this case the overlap area is zero.

$$A=0 \qquad 2.24c$$

We shall denote by X_{ac} and X_{gc} the x-coordinates of the points of intersection of the image of the aperture in the plane of the collector and the collector and of the image of the guard in the plane of the collector and the collector, respectively (see Figure 2.14). These can be evaluated with Equation 2.23 by substituting the radius of the collector for R_L, the radius of the aperture(guard ring) for R_s, and $S_{ac}(S_{gc})$ for s.

To determine the overlap area of the three circles, one must consider the following two cases;

Case A: $X_{gc}>X_{ac}$

This is the most frequently encoutered case, and it covers several apparently different situations. These are all shown in Figures 2.14a-2.14c. For all of these cases the sensitive area is given by

$$A=A_{ag}+A_{gc}-A_g \qquad 2.27a$$

where A_{ag} and A_{gc} are the overlap areas of the aperture and the guard ring and

of the guard ring and the collector, respectively, as given by Equations 2.24a-2.24c, and A_g is the area of the guard ring.

Case B: $X_{gc} \leq X_{ac}$

For this case, shown in Figure 2.14d, the sensitive area is the overlap area of the aperture and the collector.

$$A = A_{ac} \qquad 2.27b$$

This completes the derivation of the cup response function.

2.5 The "Cold Plasma" Approximation

The problem of data reduction now formally reduces to inverting a set of integral equations like Equations 2.2 to solve for the distribution function. Unfortunately, this task is very difficult, and a unique solution may not exist. The approach which we have adopted involves paramaterizing the distribution function and then searching parameter space for the "best fit" to the data.

From statistical mechanics we know that the distribution function which describes a gas in thermodynamic equilibrium is the Maxwell-Boltzmann distribution

$$f(\vec{v}) = \frac{N_o}{\pi^{3/2} w^3} \exp\{-(\vec{v}-\vec{V})^2/w^2\} \qquad 2.28$$

where N_o is the particle number density, $\vec{V}$ is the bulk flow velocity, and w is the thermal speed. Although neither the solar wind nor the Jovian magnetospheric plasma is in local thermodynamic equilibrium, there is some empirical justification for using this form for the distribution function. It can be shown that distributions with more than one peak are unstable, and in

the vicinity of the peak one expects the distribution function to be bell shaped. We shall therefore assume that the distribution functions can be approximated by expressions like Equation 2.28.

We now must evaluate the integrals in Equation 2.2b. This cannot be done analytically without further approximations. For the case of a "cold" plasma, i.e. when $|\vec{V}|/w>>1$, we can approximate the dependence of $f(\vec{v})$ on the components of velocity transverse to the cup normal by a product of two delta functions

$$f(\vec{v})\cong \frac{N_o}{w\sqrt{\pi}}\,\delta(v_x-V_x)\;\delta(v_y-V_y)\;\exp\{-(v_z-V_z)^2/w^2\} \qquad 2.29$$

This permits the integrations over v_x and v_y to be performed trivially. The result is

$$I_k^*= \frac{N_0}{w\sqrt{\pi}} \int_{v_k}^{\infty} \exp(-(v_z-V_z)^2/w^2)\; R(V_x,V_y,v_z)\; d_{vz} \qquad 2.30$$

For the D-cup, Equation 2.2b can be evaluated numerically using Equations 2.20, 2.21 and 2.23-2.27. For the main sensor Table 2.1 must be used in addition to Equation 2.9. The use of the lookup table can be eliminated by fitting the area overlap with an easily evaluated function. This approach will be particularly important for the "hot plasma" approximation described hereinafter.

The family of curves representing the sensitive area is shown in Figure 2.15, which shows A plotted as a function of S_y/h, with S_x/h as a parameter.

These functions will be fit by the "trapezoidal approximation"

$$A=A_x(S_x/h)A_y(S_x/h,S_y/h)=\hat{A}_x(S_x/h)\xi(S_x/h)A_y(S_x/h,Sy//h) \qquad 2.31$$

$$A_x=\frac{(S_x/h)+X_r'}{X_r'-X_r}\quad \xi(S_x/h) \qquad -X_r'<S_x/h<X_r \qquad 2.32a$$

$$A_x=1 \qquad -X_r<S_x/h<X_r \qquad 2.32b$$

$$A_x=\frac{(S_x/h)-X_r'}{X_r'-X_r}\quad \xi(-S_x/h) \qquad X_r<S_x/h<X_r' \qquad 2.32c$$

$$A_x=0 \qquad \text{Otherwise} \qquad 2.33d$$

$$A_y=\frac{(S_y/h)+Y_d}{Y_d'-Y_d} \qquad Y_d'<S_y/h<Y_d \qquad 2.33e$$

$$A_y=1 \qquad -Y_d<S_y/h<Y_d \qquad 2.33f$$

$$A_y=\frac{(S_y/h)-Y_u(S_x)}{Y_u'(S_x)-Y_u(S_x)} \qquad Y_u(S_x)<S_y/h<Y_u'(S_x) \qquad 2.33g$$

$$A_y=0 \qquad \text{Otherwise} \qquad 2.33h$$

with

$$X_r=1.10 \qquad 2.34a$$

$$X_r'=4.94 \qquad 2.34b$$

$$Y_d=-2.02 \qquad 2.34c$$

$$Y_d'=-3.62 \qquad 2.34d$$

$$Y_u=\frac{.762\cos\{1.018(S_x/h)+.247\}}{1+0.25(S_x/h)} \qquad 2.34e$$

$$Y_u'=2.50-0.125[(S_x/h)-1]^2 \qquad 2.34f$$

$$\xi(S_x/h)=1.257-0.063(S_x/h)-.126\sqrt{\{(S_x/h)^2-5.1(S_x/h)+6.612\}} \qquad 2.34g$$

All of the quantities defined by Equations 2.34a-2.34f are dimensionless. Y_u and Y_u' are plotted in Figure 2.16. Fiqure 2.17 shows the trapezoidal approximation for A plotted versus S_y/h with S_x/h as a parameter, while Figure 2.18 shows A plotted versus S_x/h for S_y equal to 0. Figure 2.19 shows a 3D plot of $A(\vec{S})$. The values of X_r, X_r', Y_d, Y_d', Y_u, and Y_u' were chosen so as to

match the volume of the solid of Fig. 2.19 as closely as possible with the volume of the solid representing the true area overlap. Figure 2.20 shows a 3D plot of $R(S_x/h,S_y/h)$ for which the "trapezoidal" approximation was used to eveluate the sensitive area and Eq. 2.9 was used to compute the transparency. Appendices B and C contains listings of Fortran programs which compute the integrals in Equation 2.2b for the main sensor cups using the "trapezoidal" approximation and for the D-cup, respectively.

The "cold plasma" approximation was used to test our theoretical response function by analyzing data taken during a cruise maneuver, as described in the next chapter.

2.6 The "Hot Plasma" Approximation for the Main Sensor

When the thermal speed of the plasma is comparable to the magnitude of the bulk streaming velocity Equation 2.30 is no longer valid. This is the case during Voyager I's pass near the Io flux tube. To perform the integral of Equation 2.2b in this case we have fit the previously derived expression for the transparency, Equation 2.9, by an expression with a functional form which permits the integrals over v_x and v_y to be performed analytically. The expression we have used is a sum of two Gaussians

$$T=T_0 \sum_{i=1}^{2} \sum_{j=1}^{2} c_i c_j \exp\left(-a_i\left(\frac{v_x^2}{v_z^2}\right)-a_j\left(\frac{v_y^2}{v_z^2}\right)\right) \qquad 2.35$$

where c_i, c_j, a_i, and a_j are functions of v_z^2/v_k^2 and of v_z^2/v_s^2, and T_0 is the transparency at normal incidence. The values of the c's and a's were determined from Equation 2.9 by the following procedure: We reduced the number of independent parameters to 2 by requiring that $c_1+c_2=1.0$ and that the

integral over v_x and v_y of Eq. 2.2b give the correct answer for an infinitely hot plasma, and then did a nonlinear least-squares fit to determine the best values for the a's and c's.

Using a Maxwell-Boltzmann distribution (Equation 2.28) for $f(\vec{v})$, the "trapezoidal approximation" (Equations 2.31-2.34) for A, and Equation 2.35 for T, Equation 2.2b becomes

$$I_k^* = \frac{T_0 z^* e N_0}{\pi^{3/2} w^3} \int_{v_k}^{\infty} dv_z v_z \exp\left(-\frac{(v_z - V_z)^2}{w^2}\right) \times$$
$$\int_{-\infty}^{\infty}\int_{-\infty}^{\infty} A \sum_{i,j} c_i c_j \exp\left\{-a_i \frac{v_x^2}{v_z^2} - a_j \frac{v_y^2}{v_z^2} - \frac{(v_x - V_x)^2}{w^2} - \frac{(v_y - V_y)^2}{w^2}\right\} dv_x dv_y \qquad 2.36$$

It will be convient to perform the following change of variables

$$X = Sv_x/v_z = S_x/h \qquad 2.37a$$

$$Y = Sv_y/v_z = S_y/h \qquad 2.37b$$

After some algebra Equation 2.36 becomes

$$I_k^* = \frac{N_0 e z^* T_0 R_0}{\pi^{3/2} w^3} \int_{v_k}^{\infty} dv_z \frac{v_z^3}{S^2} \exp\left(-\frac{(v_z - V_z)^2}{w^2}\right) \int_{-\infty}^{\infty}\int_{-\infty}^{\infty} dX dY \, A(X,Y) \sum_{i,j} C_{ij} G_{ix} G_{jy} \qquad 2.38$$

$$C_{ij} = c_i c_j \exp\left\{-\left[\mu_x^2 \left(\frac{a_i w^2}{v_z^2 + a_i w^2}\right) + \mu_y^2 \left(\frac{a_j w^2}{v_z^2 + a_j w^2}\right)\right]\right\} \qquad 2.39a$$

$$G_{ix} = \exp\{-\alpha_i (X - \sigma_x)^2\} \qquad 2.39b$$

$$G_{jy} = \exp\{-\alpha_j (Y - \sigma_y)^2\} \qquad 2.39c$$

$$\alpha_i = \frac{a_i w^2 + v_z^2}{S^2 w^2} \qquad 2.39d$$

$$\sigma_x = \frac{S v_z \mu_x w}{v_z^2 + a_i w^2} \qquad 2.39e$$

$$\sigma_x = \frac{S v_z \mu_y w}{v_z^2 + a_j w^2} \qquad 2.39f$$

$$\vec{\mu} = \vec{V}/w \qquad 2.39g$$

with A(X,Y) defined by Equations 2.31-2.34

We are now ready to carry out the necessary integrations. We will perform the integral over Y first. Regrouping terms in Equation 2.36 we find

$$I_k^*=\frac{N_0 z^* e T_0 A_0}{\pi^{3/2} w^3}\sum_{i,j}\{\int_{v_k}^{\infty} dv_z\left[\frac{v_z^3}{S^2}D_{ij}\int_{-\infty}^{\infty}dX\left(A_x(X)G_{ix}(X)\int_{-\infty}^{\infty}dY\ A_y(X,Y)G_{jy}(Y)\right)\right]\} \qquad 2.40a$$

$$D_{ij}=c_i c_j \exp\{-[(\frac{v_z}{w}-\mu_z)^2+\mu_x^2(\frac{a_i w^2}{v_z^2+a_i w^2})+\mu_y^2(\frac{a_j w^2}{v_z^2+a_j w^2})]\} \qquad 2.40b$$

The Y-integration can be expressed in terms of elementary functions and the Gaussian error function. The result is

$$H_J(X)=\int_{-\infty}^{\infty}dY\ A_Y(X,Y)G_{jY}=\frac{\sqrt{\pi}}{2\sqrt{\alpha_j}}\{\frac{\Phi(Z_u')-\Phi(Z_u)}{Z_u'-Z_u}-\frac{\Phi(Z_d')-\Phi(Z_D)}{Z_d'-Z_d}\} \qquad 2.41a$$

$$\Phi(Z)=Z\ \mathrm{erf}(Z)+(1/\sqrt{\pi})\exp(-Z^2) \qquad 2.41b$$

$$Z_d=\sqrt{\alpha_j}\ (Y_d(X)-\sigma_j) \qquad 2.41c$$

$$Z_d'=\sqrt{\alpha_j}\ (Y_d'(X)-\sigma_j) \qquad 2.41d$$

$$Z_u=\sqrt{\alpha_j}\ (Y_u(X)-\sigma_j) \qquad 2.41e$$

$$Z_u'=\sqrt{\alpha_j}\ (Y_u'(X)-\sigma_j) \qquad 2.41f$$

Equation 2.36 now becomes

$$I_k^*=\frac{N_0 z^* e T_0 A_0}{\pi^{3/2} w^3}\sum_{i=1}^{2}\sum_{j=1}^{2}\{\int_{-\infty}^{\infty}dv_z\left[\frac{v_z^2}{S^2}D_{ij}\int_{-\infty}^{\infty}dX\ A_X(X)G_{iX}(X)H_j(X)\right]\} \qquad 2.42$$

Since the integral over X is now very complicated, it cannot be done without further approximations. If $H_j(X)$ is a slowly varying function of its

argument, we can use the saddle point method to write the integral over X as

$$\int_{-\infty}^{\infty} dX\ A_X(X)G_{iX}(X)H_j(X) \cong H_j(\bar{X}_i)\xi(\bar{X}_i) \int_{-\infty}^{\infty} dX\ A_X(X)G_{iX}(X) \tag{2.43a}$$

$$\bar{X}_i = \frac{\int_{-\infty}^{\infty} |X| A_X(X)G_{iX}(X)dX}{\int_{-\infty}^{\infty} A_X(X)G_{iX}(X)dX} \tag{2.43b}$$

Again, all the integrals can be expressed in terms of elementary functions and the Gaussian error function. The results are

$$F_i = \int_{-\infty}^{\infty} A_X(X)G_{iX}(X)dX = \frac{\sqrt{\pi}}{2\sqrt{\alpha_i}}\left\{\frac{\Phi(Z'_{ri})+\Phi(Z'_{li})-\Phi(Z_{ri})-\Phi(Z_{li})}{Z'_r-Z_r}\right\} \tag{2.44a}$$

$$Z_{ri} = \sqrt{\alpha_i}(X_r-\sigma_i) \tag{2.44b}$$

$$Z'_{ri} = \sqrt{\alpha_i}(X'_r-\sigma_i) \tag{2.44c}$$

$$Z_{li} = \sqrt{\alpha_i}(X_l-\sigma_i) \tag{2.44d}$$

$$Z'_{li} = \sqrt{\alpha_i}(X'_l-\sigma_i) \tag{2.44e}$$

$$X_l = -X_r = -1.10 \tag{2.44f}$$

$$X'_l = -X'_r = -4.94 \tag{2.44g}$$

$$\int_{-\infty}^{\infty} |X| A_x(X)G_{ix}(X)dX = \frac{1}{2\alpha_i}\left\{\frac{\Psi(Z_l)+\Psi(Z'_r)-\Psi(Z'_l)-\Psi(Z_r)+\frac{2}{\sqrt{\pi}}(Z'_r-Z_r)\Phi(\sigma\sqrt{\alpha_i})}{Z'_r-Z_r}\right\} \tag{2.44h}$$

$$\Psi(Z) = (\sigma_i\sqrt{\alpha_i}\ Z-(1/2))\sqrt{\pi}\ \mathrm{erf}(Z)+\sigma_i\sqrt{\alpha_i}\ \exp(-Z^2) \tag{2.44i}$$

We now sumarize the results of this section by rewriting Eq. 2.2 in terms of the functions defined by Eqs. 2.19 and 2.39-2.44 as

$$I_k^* = \frac{z^* e T_0 A_0 N_0}{4\sqrt{\pi}w^3} \sum_{i=1}^{2}\sum_{j=1}^{2}\left\{\int dv_z \frac{v_z^3 D_{ij}}{S^2\sqrt{(\alpha_i\alpha_j)}} H_j(X_i)F_i\right\} \tag{2.45}$$

The integral over v_z in Eq. 2.45 must be performed numerically. To devise an efficient scheme for calculating I_k for many adjacent channels, we

shall rewrite Eqs. 2.2a and 2.2b as

$$I_k = \int_{v_k}^{v_{k+1}} dv_z \; Q(v_z,v_k) + \int_{v_{k+1}}^{\infty} dv_z \; (Q(v_z,v_k)-Q(v_z,v_{k+1}) \qquad 2.46$$

where Q denotes the integrand of Eq. 2.45. The contribution from the second integral on the right side of Eq. 2.46 is called the feedthrough current. The dependence of Q upon v_k is implicit in its dependence on the a's and c's. Since the a's and c's are slowly varying functions of v_k for $v_z \ll v_k$, we can expand the second integrand in Eq. 2.46 in a Taylor series in the a's and c's.

$$\begin{aligned} Q(v_z,v_k)-Q(v_z,v_{k+1}) = {} & Q(v_z,c_1,c_2,a_1,a_2)+(\partial Q/\partial c_1)(c_1(v_z,v_k)-c_1(v_z,v_{k+1})+ \\ & (\partial Q/\partial c_2)(c_2(v_z,v_k)-c_2(v_z,v_{k+1})+(\partial Q/\partial a_1)(a_1(v_z,v_k)-a_1(v_z,v_{k+1})+ \\ & (\partial Q/\partial a_2)(a_2(v_z,v_k)-a_2(v_z,v_{k+1}) \end{aligned} \qquad 2.47$$

This enables us to use compute one value of $Q(v_z)$ and use it in the numerical integration of several channels, greatly reducing the amount of computer time required to simulate an M-mode. Appendix D contains the listing of a Fortran program which utilizes this technique to simulate an M-mode spectrum. We expect that this program can simulate the response of the main sensor cups to a convected Maxwellian of any temperature or flow direction to within about 7%.

2.7 The "Hot Plasma" Approximation for the D-Cup

Except for a small effect due to the alignment of the grids, the D-cup response is azimuthally symmetric about its z-axis. Therefore, the response can only depend upon $v_x^2+v_y^2$ and cannot depend upon v_x and v_y individually. We have fit the the full response function by a function of the form

$$R(\vec{v},v_k,v_s)=\sum_{i=1}^{3} c_i \exp\{-a_i\frac{v_x^2+v_y^2}{v_z^2}\} \qquad 2.48$$

where once again the a_i's and c_i's are functions of v_z^2/Φ_k and Φ_s. Using a Maxwellian for the distribution function and Equation 2.48 for R in Equation 2.2b we obtain

$$I_k^*=\sum_{i=1}^{3} c_i \frac{A_0T_0N_0z^*e}{\pi^{3/2}w^3}\int_{-\infty}^{\infty} dv_z v_z \exp\{-\frac{(v_z-V_z)^2}{w^2}\}\ X$$
$$\int_{-\infty}^{\infty}\exp\{-\frac{(v_x-V_x)^2}{w^2}-\frac{a_iv_x^2}{v_z^2}\}dv_x\int_{-\infty}^{\infty}\exp\{-\frac{(v_y-V_y)^2}{w^2}-\frac{a_iv_y^2}{v_z^2}\}dv_y \qquad 2.49$$

The integration over the transverse components of the velocity are easily done, yielding

$$I_k^*=\sum_{i=1}^{3} c_i \frac{A_0T_0N_0z^*e}{\sqrt{\pi}\,w}\int_{v_k}^{\infty} \frac{v_z dv_z}{(1+a_iw^2/v_z^2)}\exp\{-(\frac{v_z-V_z}{w})^2-\frac{a_i(v_x^2+v_y^2)}{a_iw^2+v_z^2}\} \qquad 2.50$$

As in the case of the main sensor cups, the integration over v_z must be done numerically.

This completes the discussion of the response function of the Voyager PLS experiment.

Chapter 3

Experimental Test of the Response Function

3.1 The Cruise Maneuver

Before the formulas derived in the preceding chapter can be used with confidence to analyze data, they should be tested. Attempts to measure the response of the cups as a function of angle were made prior to launch. This was done by placing the instrument in an evacuated chamber in the path of a beam of charged particles. Data were then taken with the instrument in different orintations.

Unfortunately, it was not possible to test the cup response function to the desired accuracy. Tests were performed with both a proton beam and an electron beam. Since the quantity which is measured is an integral over velocity space of the product of the response function and the distribution function (Eqs. 2.2a,b), it is desirable to have a beam with a small thermal velocity dispersion. The proton beam had too great a velocity dispersion for the desired measurement. The electron beam, although sufficiently narrow, caused the emission of a large number of secondary electrons which contaminated the data. In particular, the response at large angles of incidence was different from what was expected.

The quiet solar wind, on the other hand, has ideal properties for use as a test beam. At 1 AU, the magnitude of its bulk streaming velocity is typically eight times its thermal speed, and this ratio increases with distance from the sun. In order to test the response function, however, the direction of the test beam must be varied. Since the direction of the solar wind is steady to within a few degrees, this requirement can only be met by rotating the spacecraft.

On 14 September 1978, Voyager I, then 4.1 AU from the sun, executed a series of rotations called a cruise maneuver. Data from this particular

maneuver were selected for analysis because during it the solar wind was quiet and the Mach number of the flow was high (~20). The maneuver consisted of ten rotations about the spacecraft z-axis(rolls), ten rotations about the spacecraft y-axis(yaws), and ten more rolls. Each rotation took about 33 minutes. Since the symmetry axis of the main sensor is aligned with the spacecraft z-axis, only the yaws are useful for the purpose of determining the cup response because the angle of the solar wind to the cup normals does not change appreciably during the rolls.

During the cruise maneuver the PLS experiment was taking one M-mode measurement every 96 seconds. Due to telemetry rate constraints, the data from all 128 channels of each spectrum was not sent back to Earth. On alternate spectra, the data from channels 1-72 and 57-128 were transmitted. During the maneuver the solar wind speed was about 380 km/sec, so the peaks in the spectra were never in a channel higher than about 68. Thus, only the spectra containing channels 1-72 could be used for analysis when the beam was oblique to one or more of the cups.

Due to a coincidence, the period between PLS M-mode spectra and the rotation period of the spacecraft during the maneuver were almost commensurate, resulting in the spacecraft having almost the same orientation at the times of corresponding spectra taken in different rotations. Since an odd number (21) of M-mode spectra were taken during each rotation, an upper-half spectrum was taken with the spacecraft in the same orientation as a lower-half spectrum from the previous rotation. We therefore did not lose any angular coverage due to the fact that only 72 of the 128 channels were available from each spectum.

The angular coverage of the cruise maneuver is shown in Figure 3.0, which is a polar plot of a unit vector which points radially away from the

sun. This vector, the nominal solar wind direction, is plotted in cup coordinates at the times of the start of the M-modes for each of the four cups. The polar angle θ and the azimuth angle ϕ of a vector $\vec{V}$ are defined by Equations 3.1a and 3.1b

$$\theta=\cos^{-1}(V_z/\sqrt{(V_x^2+V_y^2+V_z^2)}) \qquad 3.1a$$

$$\phi=\tan^{-1}(V_y/V_x) \qquad 3.1b$$

where V_x, V_y, and V_z are the cartesian components of $\vec{V}$. The numbered points in Fig. 3.1 correspond to the spectra which were analyzed as described hereinafter.

3.2 Analysis of Data Taken During the Cruise Maneuver

To test the response function we adopted the following strategy. We analyzed data from all of the orientations for which there were signals in at least three of the four cups. We then did a simultaneous fit to these data using the "cold" plasma approximation described in Section 2.5. The derived macroscopic plasma parameters were then compared with each other. We also fit an additional spectrum taken when the plasma flow direction was almost aligned with the main sensor symmetry axis. In this case we expect the "unity" response approximation to be valid. Since we have confidence in the parameters we derive at these times we can estimate how much the solar wind is changing between the times of the other measurements and see if the parameters derived from the other measurements stay reasonably steady. If they are, this fact and the goodness of the fits indicates how well we understand the response function. In addition, comparison of the parameters derived from the fits of the solar wind using the "unity" response approximation, where appropriate, with parameters derived from

fits to these same spectra using the "cold beam" approximation indicate the systematic error, if any, which the former approximation introduces.

Nine spectra taken during the cruise maneuver were analyzed. The numerical integrations in Equation 2.30 were done using Simpson's rule. For a term with velocity threshold v_k, we chose a step size of $\Delta v_k/10$. Since the integrand is formally undefined at $v_z=v_k$, the proper limiting value of zero was used.

The spectra consist of a background and one or two peaks. The main peak, due to protons, was fitted. In each cup, about twelve channels around the peak were included. The fits have five parameters; the three components of bulk velocity in spacecraft coordinates, the density, and the thermal speed. The velocity was then rotated into cup coordinates and the currents were computed.

The criterion used to define the "best" fit was the minimization of χ^2, defined by

$$\chi^2=\sum_i (D_i-A_i)^2/(.04D_i)^2 \qquad 3.2$$

where each of the D_i's is the measured current divided by the channel voltage width and the A_i's are the simulated reduced distribution functions. The solution to the extremum problem was found using a gradient search algorithm similar to that described in Bevington (1969). The derivatives with respect to the velocity components and thermal speed were computed numerically, while the derivative with respect to the density was computed analytically.

The results of the analysis of the cruise maneuver are shown in Table 3.1 and Figures 3.2-3.10. Figure 3.2 corresponds to point 1 in Fig. 3.1, Fig. 3.3 to point 2, etc. Figures 3.2-3.10 are plots of reduced

distribution function versus velocity for the nine spectra used. The data are represented by the "staircase" while the fit is represented by the smooth curve. Table 3.1 lists the time, the wind velocity in RTN coordinates, the density, and the thermal speed derived from the fits for each of the spectra. (RTN coordinates are a sun centered orthogonal system. $\hat{r}$ points radially away from the sun; $\hat{t}$ lies in a plane parallel to the ecliptic and points in a positive sense when viewed from the North, and $\hat{n}$ completes a right-handed system.)

The variation in these parameters is about what one expects to find in a quiet solar wind, and the fits are quite good. The fits correctly reproduce the relative heights, positions, and shapes of the spectra in the oblique cups.

The question of choosing the proper criterion for determining the "best fit" deserves more discussion. If one chooses to minimize the square of the difference between the data and the fitting function, there remains the problem of choosing the proper statistical weights. This choice must be made by analyzing the sources of error in the measurement. In our case, there are two main sources of error; electrical noise and digitization error. Since the logarithm of the currents is digitized, this error is a fixed percentage of the signal. This accounts for the weight factor of $1/0.04D_i^2$ in Eq. 3.2. The electrical noise is a more difficult problem. We expect thermal fluctuations in the amplifiers to be seen as fluctuations in the current. The rms power in these current fluctuations should be about the same in all of the channels. Since the reduced distribution function is the current divided by the channel width and the channel width increases with increasing channel number, this component of the noise should be most pronounced in the low channels.

An example of spectra which we expect to be entirely noise are the D-cup spectrum in Fig. 3.4 and the lower channels in the main sensor cups in the same figure. The predominately smooth trace is due to the signal being less than the minimum that can be digitized with our coding scheme; the fluctuations are noise. The predominant smoothness of the curve, especially the lower channels in the B-cup, indicate that the true thermal noise is below the threshold of the detector. We conclude that the noise which we see has another origin. Other sources of noise, such as cosmic rays or interference with other instruments on the spacecraft, are more difficult to estimate. I have accounted for them in my selection of which channels to include in the fits. Unless specifically mentioned, all of the graphs of the results of fits to spectra include all of the data in a particular spectrum and the simulations for all of the channels used in determining the best fit, and no others.

The question of estimating the uncertainty in the macroscopic plasma parameters derived from the previously described fitting procedure deserves discussion. The formal uncertainty in the fit parameters is contained in the so-called error matrix. The properties of this matrix are described in Bevington (1969). The uncertainties which I quote throughout the remainder of this chapter are defined by

$$\sigma_i^2=\epsilon_{ii}\ \chi^2/n_f \qquad 3.3$$

where σ_i is the formal uncertainty in the determination of the i-th parameter, ϵ_{ij} is the error matrix, and n_f is the number of degrees of freedom (number of data points/number of parameters). In the case of linear parameters and Gaussian statistics, σ is simply the standard deviation one would expect to find in the value of the i-th parameter if the same experiment were done many times.

If the uncertainty in the individual data points can be accurately estimated, σ_i^2 is simply equal to ϵ_{ii}. Unfortunately, the values of χ^2 we obtained in the fits of the cruise maneuver were sufficiently large to convince us that we had underestimated the uncertainty in the measurement. The factors which multiply ϵ_{ii} in Eq. 3.3 are an attempt to compensate for this underestimate.

In addition to random errors estimated by σ, there is always the possibility of some systematic error. There are many possible causes for systematic errors. They can be related to the detector, such as uncertainty in the values of the threshold voltages, or they can be related to the plasma itself, such as the presence of suprathermal tails to the distribution functions or thermal anisotropy. In general, systematic errors are more difficult to estimate than random errors.

3.3 Discussion and Conclusions

An examination of Table 3.1 shows that the formal errors in the density and thermal speed are about 3%. In addition, the magnitude of the bulk flow velocity is determined with a precision of less than one percent, and the direction is determined to within 10 arcseconds. We expect that the systematic errors in the determination of these quantities is considerably larger.

The quality of the fits, even at large angles of incidence, gives us great confidence in the accuracy of the response function. For example, compare Figures 3.1, 3.1a, 3.1b, and 3.5. (The following numbering scheme is used; the spectrum in Figure 3.n was taken when the orientation of the spacecraft was such that the nominal solar wind direction corresponded to

the points marked with the number n in Figure 3.0.) In the spectrum of Fig. 3.1, the angles of the solar wind velocity to the A-, B-, and C-cup normals were 35°, 70°, and 55°, respectively. Note that, although the flow is highly oblique, the fit successfully fits the relative heights, locations, and shapes of the peaks.

In Figure 3.1a, the results of simulating the low energy channels in the B-cup, which were not used in the fit, are shown. The simulation shows that the currents in these channels are not all noise, but include a real signal.

Figure 3.1b shows a simulation of what a hypothetical cup with unity response would see in the conditions of Fig. 3.1. Notice that only the location of the peaks remains the same, as all of the peaks are the same height and shape if all of the incident particles reach the collector.

For the case of the B-cup, the effect of the response function is to reduce the height of the peak by a factor of about 5, to broaden it, and to make it skewed. All of these effects can be easily understood qualitatively. The reduction of the height of the peak is caused by the effects of both the sensitive area and the grid transparency. The broadening and skewness of the peak are both caused by the "feedthrough" effect; the contribution to the signal by modulation of particles with $v_z > v_{k+1}$. This effect tends to widen the left side of the peak; there are very few particles which satisfy the above condition on the right side of the peak!

The actual reduction in the size of the signal is much more than the factor of five mentioned in the preceding paragraph. Consider the spectrum shown in Fig. 3.5, taken when the solar wind was flowing down the main sensor symmetry axis. Although the heights of the peaks is about the same

as those in the simulation of Fig. 3.1b, one must remember that the quantity which is actually measured is the current, not the reduced distribution function. Since the current is equal to the reduced distribution function times the channel voltage width, and the channel widths increase with increasing channel number, the ratio of the current in the peak channel in the B-cup of Fig. 3.5 to the same quantity for the spectrum of Fig. 3.1 is about 25. Our response is thus good even when only a few percent of the particles in the beam reach the colector. The accuracy of our expression for the response function over such a wide range of angles and signal strengths is important since in the Io flux tube flyby the flow is highly oblique to the cups.

The sensitivity of the array of four detectors to the direction of the flow is dramatically shown in Figs. 3.8 and 3.8a. The fit for Fig. 3.8a was done assuming that the flow velocity in spacecraft coordinates was the same for all four cups. This neglects effects due to the fact that the spacecraft was spinning while the measurements were being taken. We did another fit to the same data in which we compensated for the change in the spacecraft orientation between the times of the measurements of the channel with the largest current in each cup. The result is shown in Fig. 3.8. This is clearly a much better fit to the data. The angle that the spacecraft rotated through between the time of the measurement of channel 24 (A-cup peak) and channel 46 (C, D-cup peaks) was only about 0.9°.

Since the two spectra shown in Figs. 3.5 and 3.6 were taken when the solar wind velocity was almost parallel to the main sensor symmetry axis, we also fit these with the assumption of unity response. A comparison of the results of these fits with the results of the fits of the corresponding spectra using the full response function is included in Table 3.1. The

quality of the fit, as measured by χ^2, was significantly better for the fits which used the full response function. The x- and y- components of the velocity in spacecraft coordinates agreed to within statisical error, while the z-components of the full response fit exceeded the z-components of unity response fits by about 1%. In addition, the unity response results overestimated the thermal speeds by 7% and underestimated the density by 5%. All of these discrepencies are easily understood. The density difference is caused by the fact that when the flow velocity makes an angle of about 20° to the cup normal, the grid transparency is already slightly less than it is for normal incidence. The other two effects are both caused by the "feedthrough" contribution. The effect of feedthrough is to widen the peak on the low energy side, resulting in a lower estimate of the normal component of the velocity and a higher estimate of the thermal speed.

We must conclude, however, that the unity response approximation is quite good at small angles of incidence, as expected. Uncertainty in the gain of the amplifiers probably introduces a larger error into the density determination than the effect due to the response. Since the response by its nature widens and introduces a certain amount of skewness into the peaks, its effect on the determination of the thermal anisotropy and the heat flux should be considered.

In summary, we have shown that the analytic formulas describing the response function derived in Chapter 2 accurately describe the response of the cups for angles up to 70° for the main sensor cups and 55° for the D-cup. The expressions also correctly predict the complete absence of a signal for angles of incidence $>80^\circ$ for the main sensor cups and $>65^\circ$ for the D-cup.

Chapter 4

The Theory of the Interaction

Between Io and the Jovian Magnetosphere

4.1 Introduction

In Chapter 5 we will present analysis of Voyager I data taken in the vicinity of the satellite Io, shortly after the spacecraft's closest approach to Jupiter. In the present chapter, a description of the plasma environment at Io and a theory of the Io-magnetosphere interaction will be presented. The model plasma parameters which we use in this discussion are the result of a combination of a large number of ground based and in situ measurements. In particular, on its inbound pass the symmetry axis of Voyager I's PLS experiment was pointed in the direction of the corotating flow when the spacecraft flew past Io's orbit, enabling it to make measurements which could be analyzed using the unity response approximation.

Io itself is a large satellite, only slightly smaller than the Moon. Its physical properties are summarized in Table 4.1. Orbiting Jupiter at a distance of 424 thousand kilometers (5.9 R_J), Io is deep within the magnetosphere, which extends to 50-100 R_J. Since the Jovian magnetic field is very strong at Io's orbit (~.02 gauss) and Jupiter's ionosphere is highly conducting, we expect the plasma to rigidly corotate with the planet. Voyager I observed this on its inbound pass (Bagenal and Sullivan (1981)). Because Io's orbital period of 42.8 hours is longer than Jupiter's rotation period of 10 hours, the bulk velocity of the plasma in Io's vicinity is greater than Io's orbital velocity by ~58 km/sec.

One of the great discoveries made by Voyager I was the volcanoes on Io. Io is the most volcanically active body known, and its volcanoes are believed to be the ultimate source of not only the neutral cloud around Io

(which has been observed from Earth) and the plasma torus which surrounds Jupiter at the radius of Io's orbit, but also most of the plasma in the entire Jovian magnetosphere. Voyager I inbound observed two distinct regions in the torus; the inner or cold torus and the outer, hot torus. In the cold torus, where individual peaks in the spectra were resolved, several different ion species, primarily different ionization states of oxygen and sulfur, were observed. The chemical complexity was also present in the hot torus, although the merging of the peaks in the spectra made the analysis more difficult and the results somewhat ambiguous.

To estimate the magnitude of the relevent time and distance scales in the vicinity of Io, we have used the model plasma torus of Johnson and Strobel, consisting of the following species: O^+, O^{++}, S^+, S^{++}, S^{+++}, and electrons. The values of many characteristic plasma parameters for this model torus is given in Table 4.2. A magnetic field strength of .019 Gauss, the value measured by the Voyager I magnetometer experiment (Acuna et al (1981)), was used to estimate the gyroradii and Larmor frequencies. Examination of Table 4.2 indicates that the characteristic time for the plasma to flow past Io (30 sec) is long compared with the Ion gyroperiod (0.5 sec), and short compared with all of the collision times. In addition, the Debye length (65 cm) is very small compared with the radius of Io (1820 km). We therefore expect that the ideal MHD approximation, described hereinafter, is valid and that collisional effects are negligible.

4.2 The Equations Which Describe the Plasma at Io

In section 4.3, we shall present a review and critique of a theory of the Io-magnetosphere interaction which is based on the ideal MHD equations. In the present section we review the derivation of the those equations for the purpose of examining the approximations required for their validity and justifying their use for the purpose of describing the interaction between Io and the Jovian magnetospheric plasma.

We take as our starting point the set of fluid equations which are obtained by taking moments of the kinetic (Boltzmann) equation and summing over the different ionic species. The Boltzmann equation is valid whenever the statistical correlation between the phase space position of two particles can be neglected. This approximation is quite good for the conditions which exist in the Jovian ionosphere, as it is for almost all space plasmas.

The fundamental equations are those of conservation of mass, momentum, and energy, and the Maxwell equations, supplemented by the equation of state, equations for the anisotropic structure of the pressure tensosr, the generalized Ohm's law, and an equation for the heat flux.

The equation of mass conservation is

$$\frac{\partial \rho}{\partial t} = - \frac{\partial}{\partial x_i}(\rho V_i) \qquad 4.1$$

where ρ is the mass density and V_i is the i-th component of the bulk velocity of the plasma as a whole. For the remainder of this chapter, we shall use the Einstein summation convention, i.e. all repeated indices are summed over.

The equation of momentum conservation is

$$\frac{\partial}{\partial t}\left(\rho V_i + \frac{S_i}{c^2}\right) = -\frac{\partial}{\partial x_k}\left(P_{ik} + \rho V_i V_k - T_{ki}\right) + g_i \qquad 4.2$$

where P_{ik} is the pressure tensor, g_i is the local gravitational field, and T_{ik} and S_i are the Maxwell stress tensor and the Poynting vector, respectively, defined by

$$T_{ik} = \frac{1}{4\pi}\left(B_i B_k + E_i E_k - \frac{1}{2}\,\delta_{ik}(E^2 + B^2)\right) \qquad 4.2a$$

$$S_i = \frac{c}{4\pi}\left(\vec{E} \times \vec{B}\right)_i \qquad 4.2b$$

If the equations are written in a non-inertial frame of reference, $\vec{g}$ should include the D'Alembertain forces. If the frame of reference is rotating, the the coriolus force should be included by adding a term $-2\vec{\Omega}\times\vec{V}$ to Eq. 4.2, where $\vec{\Omega}$ is the angular velocity of the reference frame.

The equation of energy conservation is

$$\frac{\partial}{\partial t}\left(\rho V^2 + \epsilon_T + \epsilon_{EM}\right) = -\frac{\partial}{\partial x_k}\left(V_k(\rho V^2 + \epsilon_T) + P_{kj}V_j + S_k + q_k\right) + \rho g_k V_k \qquad 4.3$$

where ϵ_T is the thermal energy per unit volume, q_k is the heat flux vector, and ϵ_{EM} is the electromagnetic energy density, defined by

$$\epsilon_{EM} = \frac{1}{8\pi}(E^2 + B^2) \qquad 4.3a$$

Maxwell's equations are Gauss's law

$$\nabla \cdot \vec{E} = 4\pi\eta \qquad 4.4$$

where η is the electric charge density; the Faraday induction law

$$\nabla \times \vec{E} + \frac{1}{c}\frac{\partial \vec{B}}{\partial t} = 0 \qquad 4.5$$

Ampere's law

$$\nabla \times \vec{B} - \frac{1}{c}\frac{\partial \vec{E}}{\partial t} = \frac{4\pi}{c}\vec{J} \qquad 4.6$$

and the divergence-free condition on $\vec{B}$.

$$\nabla \cdot \vec{B} = 0 \qquad 4.7$$

The equation of state relates ϵ_T to p and ρ, $\epsilon_T = \epsilon_T(p,\rho)$, where p, the scalar pressure, is one-third of the trace of P_{ik}. For a gas of non-relativistic particles with no internal degrees of freedom or long-range interactions the equation of state is

$$\epsilon_T = \frac{3}{2} p \qquad 4.8$$

For any plasma which can be accurately described by the Boltzmann equation, the contribution of long-range forces to the internal energy is small and can be neglected. Therefore, a plasma consisting only of electrons and protons, particles which have no internal degrees of freedom, is accurately described by Eq. 4.8. For a plasma of partially ionized heavy ions, the condition of no internal degrees of freedom is violated if the thermal kinetic energy of the ions or electrons is comparable to the excitation energies. In the hot plasma torus, we do not expect Eq. 4.8 to apply, since the thermal kinetic energy of the plasma is comparable to the excitation energy of the ions.

For a plasma in which the negative ions are electrons, the generalized

Ohm's law is formally given by (see Rossi and Olbert (1970), pp 347-350)

$$\frac{\partial J_i}{\partial t} = -\frac{\partial}{\partial x_k}(J_k V_i + J_i V_k - \eta V_i V_k) + \eta g_i + \\ + \frac{e}{m_e}\frac{\partial P_{e,ik}}{\partial x_k} + \frac{e^2 n_e}{m_e}(\vec{E} + \frac{\vec{V}}{c} \times \vec{B})_i - \frac{e}{m_e}\{(\vec{J} - \eta\vec{V}) \times \frac{\vec{B}}{c}\}_i + (\frac{\delta\vec{J}}{\delta t})_{coll} \qquad 4.9$$

where n_e is the number density of electrons, m_e is the electron mass, and $P_{e,ik}$ is the partial pressure tensor for the electron component of the plasma, and $(\delta J/\delta t)_{coll}$ is the time rate of change of current density due to collisions.

Unfortunately, this set of equations is not closed; there are more unknowns than equations. This situation is usually remedied by making some additional assumption regarding q_i and P_{ik} and neglecting some of the terms in the generalized Ohm's law. One commonly made set of assumptions is that $q_i=0$, P_{ik} is isotropic ($P_{ik}=p\delta_{ik}$), and $\vec{E}=-\vec{V}\times\vec{B}/c$.

In the vicinity of Io, we expect P_{ik} to be gyrotropic; that is, P_{ik} will have cylindrical symmetry about the local direction of $\vec{B}$. This condition must be satisfied whenever the ion gyroradius is small compared to the length scale of gradients of any of the macroscopic plasma parameters. In this case, the pressure tensor can be written as

$$P_{ik} = p_\perp \delta_{ik} + (p_{||} - p_\perp)\frac{B_i B_k}{B^2} \qquad 4.10$$

where $p_{||}$ and $p_\perp$ are called the parallel pressure and the perpendicular pressure, respectively. The equations can then be closed by introducing an equation for the heat flux, appropriate approximations in the generalized Ohm's law and supplementary equations, if neccessary, and an equation relating the parallel and perpendicular pressures. The effect of the

pressure anisotropy in the resulting equations can be expressed in terms proportional to $p_{\parallel}-p_{\perp}$. Since these terms are usually small corrections, they do not qualitatively effect the solutions. We shall therefore neglect them and assume a scalar pressure.

The equations as they now stand are very difficult to solve, and they describe an incredible richness of phenomena which are not of primary importance in understanding the interaction between Io and the Jovian magnetospheric plasma. In particular, we shall be concerned only with changes on time scales long compared to the proton gyroperiod. The characteristic time for the flow of the plasma past Io is of the order of R_{Io}/V, or about 30 sec, while the ion gyroperiods are of the order of 0.5 sec. This enables us to make many further approximations which will greatly simplify the equations.

We start making our approximations with the generalized Ohm's law. For the conditions which we expect to encounter in the flux tube, dimensional analysis (Rossi and Olbert) shows that all of the terms are neglgible compared to the term proportional to $\vec{V}\times\vec{B}$. We therefore can write

$$\vec{E} = -\frac{\vec{V}}{c} \times \vec{B} \qquad 4.11$$

Using Eq. 4.11 and the conservation of mass equation (Eq. 4.1), we can rewrite Faraday's law as

$$(\frac{\partial}{\partial t} + \vec{V} \cdot \nabla)\frac{\vec{B}}{\rho} = (\frac{\vec{B}}{\rho} \cdot \nabla)\vec{V} \qquad 4.12$$

This is called the MHD "frozen-in" law, because it is equivalent to the statement that the magnetic flux linked by any closed curve which moves

along with the plasma does not change with time; hence the field is "frozen-in" to the plasma.

Maxwell's displacement current can be omitted from Ampere's law, yielding

$$\nabla \times \vec{B} = \frac{4\pi}{c} \vec{J} \qquad 4.13$$

Turning now to the equation of momentum conservation, we can safely neglect $\vec{S}$ and the terms in the Maxwell stress tensor which contain $\vec{E}$. While the gravititional term is important in the overall dynamics of the Jovian magnetosphere, it can safely be neglected for a treatment of the interaction with Io. Incorporating these approximations, assuming a scalar pressure, and using the equation of conservation of mass (Eq. 4.1) and some vector identities, we rewrite Eq. 4.2 as

$$(\frac{\partial}{\partial t} + \vec{V} \cdot \nabla)\vec{V} = - \frac{1}{\rho} \nabla p + \frac{1}{4\pi\rho}\{(\vec{B} \cdot \nabla)\vec{B} - \frac{1}{2} \nabla B^2\} \qquad 4.14$$

Using Eq. 4.11 and assuming an ideal gas equation of state and a scalar pressure, the energy equation takes the particularly simple form

$$(\frac{\partial}{\partial t} + \vec{V} \cdot \nabla)(\ln(\frac{p}{\rho^{5/3}})) = - \frac{2}{3p} \nabla \cdot \vec{q} \qquad 4.15$$

Noting that $\ln(p/\rho^{5/3})$ is proportional to the specific entropy of an ideal gas, we interpret this equation saying that if we move along with the gas, the time rate of change of the specific entropy is determined by the divergence of the heat flux. For the case of a gas with a different equation of state, the functional form of the entropy density will be different from $\ln(p/\rho^{5/3})$, but it will still be expressible as a function

of p and ρ. If we further assume that $\nabla\cdot\vec{q}=0$, the energy equation becomes

$$(\frac{\partial}{\partial t} + \vec{V} \cdot \nabla)f(p,\rho) = 0 \qquad 4.16$$

where the functional form of $f(p,\rho)$ depends upon the equation of state of the gas.

Since only the gradient of the pressure enters into the momentum equation, and not the pressure itself, Eq. 4.16 can be used to eliminate p in favor of ρ in Eq. 4.14. The result is

$$(\frac{\partial}{\partial t} + \vec{V} \cdot \nabla)\vec{V} = -c_s^2 \nabla(\ln \rho) + \frac{1}{4\pi\rho}\{(\vec{B} \cdot \nabla)\vec{B} - \frac{1}{2} \nabla B^2\} \qquad 4.17$$

where c_s, the local 'sound' speed, is defined by

$$c_s^2 = (\frac{\partial p}{\partial \rho})_f \qquad 4.17a$$

Equations 4.1, 4.7, 4.12, 4.17 and 4.17a are now a closed set of equations which, with the proper boundary conditions, uniquely determine ρ, $\vec{V}$, and $\vec{B}$. $\vec{E}$ can then be determined Eq. 4.11, n from Gauss's law (Eq. 4.4), and $\vec{J}$ from Ampere's law (eq. 4.13). These equations, with the ideal gas equation of state, are sometimes called the ideal MHD equations. While much simpler than the kinetic equations or the set of moment equations, they are still nonlinear and, therefore, difficult to solve. In fact, they are considerably more complicated than the equations which describe a perfect nonconducting fluid. In the next section we shall apply these equations to the problem of the flow around Io.

4.3 The Io-Magnetosphere Interaction

Since the discovery that the decametric radio bursts from Jupiter are correlated with the phase of Io, the interaction of Io with the surrounding plasma has been a subject of much theoretical interest. Unlike the Earth's Moon, whose only interaction with the solar wind is to cast a geometrical shadow, Io interacts very strongly with the plasma in which it is embedded. It is believed that this interaction is caused by the high electrical conductivity of Io or its ionosphere.

According to the MHD "frozen-in" law, an observer who is moving along with a plasma sees no electric field. Assuming a uniform background flow, an observer moving along with Io would see an electric field given by $\vec{E}=-(\vec{V}\times\vec{B})/c$, where $\vec{V}$ is the velocity of the background flow with respect to Io. But since Io is a good electrical conductor, the electric field in its rest frame must vanish. If we model Io as perfectly conducting sphere, we conclude that there must be a layer charge on its surface to shield out the external electric field. But since the magnetic flux tube linking Io is "frozen" to the satellite, there is effectively a cylindrical obstacle that the plasma must flow around which extends all the way to Jupiter.

In an early discussion of this phenomenon, Goldreich (1969) hypothesized that the Io flux tube would carry field aligned currents (see Figure 4.1). These currents would flow toward Io on one side of the flux tube, cross the magnetic field by flowing through Io or its ionosphere, and flow away from Io on the other side of the flux tube. This current loop would then be closed in Jupiter's ionosphere. The magnitude of the

currents in this model is determined by the electrical conductivity of Io and that of the Jovian ionosphere.

This early model has been superseded by a theory first proposed to explain the anomolously large amount of drag on the Echo weather satellites by Drell (1965) and later extended and applied to Io by Neubauer (1980). We will now discuss this theory in detail and, in the next chapter, use it to interpret in situ measurements taken by Voyager I.

Drell (1965) realized that the effect of a conductor moving through a magnetized plasma is to generate hydromagnetic waves. If the velocity of the conductor is greater than the fast mode phase velocity in the direction of the motion, a bow shock will form. If the velocity of the conductor is slower than the fast mode phase velocity, the result will be a standing system of Alfven waves (see Figure 4.2), consisting of two wings, one along each of the two Alfven characteristics (described hereinafter) which pass through the conductor. In this case one would also expect to find a disturbance associated with the MHD slow mode. The generation of these waves is analogous to the emission of Cerenkov radiation by a particle in a medium which is moving faster than the speed of light in that medium.

The current associated with the Alfven wings is determined primarily by the wave impedence of the plasma as long as the height-integrated conductivity of the conductor is much smaller than the speed of light squared divided by the Alfven speed. Thus, for Io, the magnitude of the current, which can be calculated using the linearized MHD equations, is independent of the conductivity of the Jovian ionosphere.

It is generally believed that Goldreich's model would be valid if the Alfven speed were sufficiently large that the Alfven wave, after reflection

from the Jovian ionosphere, were to again encounter Io. Since estimates show that the round trip travel time of the Alfven wave from Io to Jupiter and back to the latitude of Io's orbit is sufficiently long for Io to move a distance greater than its its own diameter, the Goldreich model does not apply Neubauer (1980).

Neubauer (1980) noted that there is an exact analytical solution to the MHD equations which describes a finite amplitude standing Alfven wave. Our presentation follows Neubauer.

It has long been known that there exists an exact solution of the ideal MHD equations which corresponds to a finite amplitude Alfven wave. To find this solution, we consider the special case where the density does not change with time and the density and the magnitude of the magnetic field have the same value everywhere in space; that is

$$\frac{\partial \rho}{\partial t} = 0 \qquad 4.18$$

$$\frac{\partial \rho}{\partial x_i} = 0 \qquad 4.19$$

$$\frac{\partial B^2}{\partial x_i} = 0 \qquad 4.20$$

This solution is also valid without the previous assumptions about the relation between the density and the pressure (see Eq. 4.17) if we independently require the pressure to have the same value everywhere in

space ($\nabla p = 0$). Eqs. 4.12 and 4.17 can now be written as

$$\frac{\partial \vec{V}_A^*}{\partial t} + (\vec{V} \cdot \nabla)\vec{V}_A^* = (\vec{V}_A^* \cdot \nabla)\vec{V} \qquad 4.21$$

$$(\frac{\partial}{\partial t} + \vec{V} \cdot \nabla)\vec{V} = (\vec{V}_A^* \cdot \nabla)\vec{V}_A^* \qquad 4.22$$

where $\vec{V}_A^*$ is the Alfven velocity, defined by

$$\vec{V}_A^* = \frac{\vec{B}}{\sqrt{(4\pi\rho)}} \qquad 4.23$$

By adding or subtracting Eqs. 4.18 and 4.19, they can be written elegantly in the canonical form

$$(\frac{\partial}{\partial t} + (\vec{V}_A^* + \vec{V}) \cdot \nabla)(\vec{V}_A^* - \vec{V}) = 0 \qquad 4.24$$

$$(\frac{\partial}{\partial t} + (\vec{V}_A^* - \vec{V}) \cdot \nabla)(\vec{V}_A^* + \vec{V}) = 0 \qquad 4.25$$

In Eqs. 4.24 and 4.25 we see that $d\vec{x}/dt=\vec{V}_A^+=\vec{V}+\vec{V}_A^*$ is the equation which defines a characteristic along which the Reimann invariant $\vec{V}_A^-=\vec{V}-\vec{V}_A^*$ stays constant, while $d\vec{x}/dt=\vec{V}_A^-$ defines a charactersitic along which the Riemann invariant $\vec{V}_A^+$ stays constant. (A characteristic is a line along which small amplitude wave packets propagate.) If $\vec{V}_A^+$ is not only constant along the characteristic defined by Eq. 4.24, but also has the same value on all such characteristics, then Eq. 4.24 and 4.25 imply

$$(\frac{\partial}{\partial t} + \vec{V}_A^+ \cdot \nabla)\vec{B} = 0 \qquad 4.26$$

$$(\frac{\partial}{\partial t} + \vec{V}_A^+ \cdot \nabla)\vec{V} = 0 \qquad 4.27$$

This is the finite amplitude Alfven wave. If we further require a

stationary solution, we find

$$(\vec{V}_A^+ \cdot \nabla)\vec{B} = 0 \qquad 4.28$$

$$(\vec{V}_A^+ \cdot \nabla)\vec{V} = 0 \qquad 4.29$$

$$\vec{V}_A^+ = \frac{\vec{B}}{\sqrt{(4\pi\rho)}} + \vec{V} = \text{const} \qquad 4.30$$

$\vec{V}$ and $\vec{B}$, and hence $\vec{E}$, are all constant along lines in the direction of $\vec{V}_A^+$. If we think of $\vec{B}$ ($\vec{V}$) as consisting of the sum of a background field and a (possibly finite) perturbation field, $\delta\vec{B}$ ($\delta\vec{V}$), according to Eq. 4.30 we have

$$\delta\vec{V} = -\frac{\delta\vec{B}}{\sqrt{(4\pi\rho)}} \qquad 4.31$$

The realization that Eq. 4.28-4.31 can be used to describe the interaction between Io and the magnetosphere is due to Neubauer (1980).

We shall now examine this solution in detail. It is important to note that since the characteristics are directional, that is, information can propagate along them in only one direction, this solution can only describe one of the Alfven wings. We can try to construct a solution describing both wings by dividing space into two semi-infinite half spaces, with Io lying in the surface which divides them. In one of the half spaces, we will use the above solution, while in the other, its analog, with $\vec{V}_A^-$ taken to have the same value throughout the entire region. Unfortunately, the solutions which we require for our physical model of the Alfven wing, described herinafter, cannot be patched together at a boundary surface in such a way as to keep both the tangential component of $\vec{E}$ and the normal component of $\vec{B}$ continuous, except in the special case where $\vec{V}_o$ and $\vec{B}_o$ are

perpendicular to each other. This implies that the nature of the interaction directly upstream of Io is not described by this solution. Furthermore, the assumption that $\vec{V}_A^{++}$ has the same value everywhere in a large region of space cannot be true when the "background" magnetic field is the dipole field of a planet. We therefore conclude that this solution can accurately describe the fields only in a region near the Alfven wing, close enough to Io so that the gradients in the background magnetic field can be neglected, yet sufficiently far from the satellite that the effect of the other wing is small. We will discuss other limitations of this model after we have developed it more fully.

We now continue our developement of this special solution. The following important result relating the component of the current density along $\vec{V}_A^{++}$ to the charge density can be obtained by using Eq. 4.24, the MHD "frozen-in" law, and Gauss's law:

$$\eta = (\vec{V}_A^{++} \cdot \vec{J})/c^2 \qquad 4.32$$

Since charge density and current density transform like a four-vector under Lorentz transformation, this implies that in a frame of reference moving with velocity $\vec{V}_A^{++}$ with respect to the frame in which the pattern is stationary the charge density vanishes.

It is convenient to write down the solution in a coordinate system in which one of the axes points along $\vec{V}_A^{++}$. We shall call this direction $\hat{z}$. We will further assume that $\vec{V}$ lies in the x-z plane. Once $\vec{E}(x,y)$ is known for all values of x and y, all of the other quantities are determined. B_x and B_y are computed by taking the cross product of $\vec{V}_A^{*}$ with Eq. 4.11, and B_z can

be computed from Eq. 4.23. The results are

$$B_x = -\frac{cE_y}{|V_A^+|} \qquad 4.33a$$

$$B_y = \frac{cE_x}{|V_A^+|} \qquad 4.33b$$

$$B_z = \sqrt{(B_o^2 - B_x^2 - B_y^2)} \qquad 4.33c$$

$\vec{V}$ is then found from Eq. 4.31.

$$V = V_o - \frac{(\vec{B} - \vec{B}_o)}{\sqrt{(4\pi\rho)}} \qquad 4.34$$

J_x and J_y are computed using Ampere's law.

$$J_x = \frac{c}{4\pi}\frac{\partial B_z}{\partial y} \qquad 4.35a$$

$$J_y = -\frac{c}{4\pi}\frac{\partial B_z}{\partial x} \qquad 4.35b$$

We will now model Io as a perfectly conducting sphere moving through a plasma which, in the absence of the sphere would be at rest and contain a uniform and constant background magnetic field. We will use a frame of reference which is at rest with respect to Io, and take the center of Io as the origin. We define the z-axis to point along $\vec{V}_A^+$, and we seek a solution which is valid for z>0. An example of an appropriate set of boundary conditions is the specification of $\vec{E}(x,y)$ everywhere in the z=0 plane. Unfortunately, our physical model only gives us information about $\vec{E}$ far from the sphere and in the Alfven wing.

Far from the sphere and the Alfven wing, we require that the velocity and the magnetic field be given by

$$\vec{V} = V_o(\cos(\zeta)\ \hat{x}_1 + \sin(\zeta)\ \hat{x}_3) = V_{o\perp}\ \hat{x}_1 + V_{o\parallel}\ \hat{x}_3 \qquad 4.36$$

$$\vec{B} = B_o\ \hat{x}_3 \qquad 4.37$$

where ζ is the angle beween the background flow and the $\hat{x}_1$-axis, $V_{o\parallel}$ and $V_{o\perp}$ are the components of $\vec{V}$ parallel and perpendicular to $\vec{B}$, and $\hat{x}_1$- and $\hat{x}_3$- are related to $\hat{z}$ by the definition of $\vec{V}_A^+$:

$$V_A^+\ \hat{z} = V_o\ \ \hat{x}_1 + \left(\frac{B_o}{\sqrt{(4\pi\rho)}} + V_o\ \right)\ \hat{x}_3 \qquad 4.38$$

The electric field far from the sphere is found from Eq. 4.11 to be

$$\vec{E} = \hat{x}_2\ E_o = \hat{y}\ E_o \qquad 4.39$$

with E_o defined by

$$E_o = \frac{V_{o\perp} B_o}{c} \qquad 4.40$$

Since the sphere is assumed to be a perfect conductor, the electric field in its rest frame must vanish. But, since all quantities are constant along z, we conclude that the electric field must vanish in a semi-infinite cylinder of radius R_{Io}, and that a polarization charge must be present on the surface of the cylinder on which the lines of the electric field in the moving plasma can terminate.

In order to enable us to determine the fields in the vicinity of the cylinder, we must make several further assumptions. First, we assume that the electric charge density vanishes everywhere except at infinity and on the surface of the cylindrical Alfven wing. This, along with our previous assumption that there is no time variation, implies that the electric field

is the gradient of a potential which satisfies Laplace's equation. The boundary conditions are that the potential vanish at the surface of the Alfven wing, and that the electric field far from the wing is that given by Eq. 4.39. The electric field which satisfies Laplace's equation and these boundary conditions is

$$E_x = \frac{2xy}{(x^2 + y^2)^2} R_c^2 E_o \qquad 4.41a$$

$$E_y = (1 - \frac{R_c^2}{(x^2 + y^2)^2} (x^2 - y^2)) E_o \qquad 4.41b$$

The velocity and the magnetic field, from Eq. 4.33 and 4.34, are

$$B_x = -B_o \sin \theta_A (1 - \frac{R_c^2}{(x^2 + y^2)^2} (x^2 - y^2)) \qquad 4.42a$$

$$B_y = B_o \sin \theta_A (\frac{2xy}{(x^2 + y^2)^2} R_c^2) \qquad 4.42b$$

$$B_z = \sqrt{(B_o^2 - B_x^2 - B_y^2)} \qquad 4.42c$$

$$V_x = V_{ox} - (\frac{B_o \sin \theta_A}{\sqrt{(4\pi\rho)}})(\frac{R_c^2 (x^2 - y^2)}{(x^2 + y^2)^2}) \qquad 4.43a$$

$$V_y = - (\frac{B_o \sin \theta_A}{\sqrt{(4\pi\rho)}})(\frac{2xy}{(x^2 + y^2)^2}) \qquad 4.43b$$

$$V_z = V_{oz} - \frac{B_z}{\sqrt{(4\pi\rho)}} \qquad 4.43c$$

where we have introduced the Alfven angle θ_A, defined as the angle between the the Alfven characteristic $\vec{V}_A^{++}$ and the background magnetic field $\vec{B}$. This velocity field is very similar to the potential flow of an incompressible

fluid around an infinite cylinder. The streamlines for this flow are shown in Fig. 4.3.

The surface charge density σ and the surface current density $\vec{K}$, from Gauss's law and Eq. 4.32, are

$$\sigma_s = (2V_{o\perp}B_o \sin \phi)/c \qquad 4.44$$

$$K_z = \frac{cV_{o\perp}B_o \sin \phi}{(V_o^2 + V_A^{+2} + 2V_oV_A^+ \sin \zeta)} \qquad 4.45$$

where ϕ is the polar angle in the x-y plane. Eq. 4.41-4.45 constitute the complete solution for the fields in the vicinity of Io and its Alfven wing.

Far enough from the wing for $\delta\vec{B}$ and $\delta\vec{V}$ to be considered small perturbations, Eqs. 4.42c and 4.43c can be rewritten as

$$B_z = B_o(1 + \sin(\theta_A) \tan(\theta_A))\, R_c^2 \frac{(x^2 - y^2)}{(x^2 + y^2)^2}) \qquad 4.42c'$$

$$V_z = V_{oz} - (\frac{B_o R_c^2 \sin(\theta_A)}{\sqrt{(4\pi\rho)}}) \tan(\theta_a)\, (\frac{x^2 - y^2}{(x^2 + y^2)^2}) \qquad 4.43c'$$

We can also treat the case where the conductivity of Io is large, but finite. In this case, we simply assume that the electric field inside the wing is uniform and y-directed. The electric field outside the wing is still the linear superposition of a uniform field and the field of a line dipole, but the dipole moment is reduced. The fields are still given by Eqs. 4.41-4.43 if R_c is interpreted as the "effective radius" of the Alfven wing. For the case where the currents across $\vec{B}$ flow through Io's ionosphere, rather than through the satellite itself, the same equations are still valid, only now the "effective radius" is greater than R_{Io}.

We shall now examine the validlty of the approximations used in deriving Eq. 4.41-4.45 in more detail. If we relax the restrictive assumptions of Eqs. 4.18-4.20, we find that Eqs. 4.24 and 4.25 become

$$(\frac{\partial}{\partial t} + \vec{V}_A^+ \cdot \nabla)\vec{V}_A^- = -c_s^2 \nabla(\ln \rho) - \frac{\nabla B^2}{8\pi\rho} + \vec{V}_A^*(\frac{\partial}{\partial t} + \vec{V}_A^- \cdot \nabla)(\ln \rho) + \vec{g} \qquad 4.46$$

$$(\frac{\partial}{\partial t} + \vec{V}_A^- \cdot \nabla)\vec{V}_A^+ = -c_s^2 \nabla(\ln \rho) - \frac{\nabla B^2}{8\pi\rho} + \vec{V}_A^*(\frac{\partial}{\partial t} + \vec{V}_A^+ \cdot \nabla)(\ln \rho) + \vec{g} \qquad 4.47$$

The errors committed by making those restrictive assumptions can be estimated by dimensional analysis. We will estimate the order of magnitude of each of the terms which we neglected and compare it to the terms which we have included in the subsequent derivation. In the following equations, the left side is the term whose magnitude we wish to estimate, while the right side is its expected size, in terms of characteristic length, time, and velocity scales of the problem.

To estimate the error in the position and properties of the Alfven wing itself, we consider first Eq. 4.47. For the first term we have

$$\frac{\partial V_A^-}{\partial t} \propto \frac{V_A^*}{T} \approx \frac{V_A^* V}{\pi R_J} \approx \frac{V_A^* V}{3R_J} \qquad 4.48$$

The time in the denominator of the right side of Eq. 4.48 is of the order of one half of the rotation period of Jupiter. We expect changes on this time scale because of the fact that the dipole axis of Jupiter is tilted with respect to the rotation axis. We obtain the term on the far right of Eq. 4.48 by noticing that the corotation velocity is simply the circumference of Io's orbit divided by Jupiter's rotation period. In this

estimate we have neglected the angular velocity of Io compared to the angular velocity of Jupiter.

The second term on the left side of Eq. 4.46 is of order

$$(\vec{V}^{+} \cdot \nabla)V_A^{-} \propto \frac{V_A^{*2}}{L} \qquad 4.49$$

The length L in the denominator can be taken to be the distance of the point in question from Io.

In the same spirit, for the first term on the right side of Eq. 4.46 we have

$$c_s^2 \nabla(\ln \rho) \propto \frac{5c_s^2}{R_J} \qquad 4.50$$

The characteristic length for change in ln ρ is very different in different directions. We know from Voyager measurements and theoretical arguments (Bagenal and Sullivan (1981)) that the characteristic length for changes along $\vec{B}$ near Io is about 1 R_J. In the direction of corotating flow, the characteristic length is on the order of the radius of Io's orbit, about 6 R_J. Radially in towards Jupiter, the gradients are very steep, with a characteristic length of the order of 0.2 R_J. In our estimate of the size of this term we have used the shortest of these three distances.

Assuming the magnetic field of Jupiter to be a dipole field, the size of the second term on the right side of Eq. 4.46 is

$$\frac{|\nabla B^2|}{8\pi\rho} = \frac{-6B^2}{8\pi\rho\,(6R_J)} \propto \frac{V_A^{*2}}{2R_J} \qquad 4.51$$

Using the same arguments, the next two terms are seen to be

$$V_A^* \frac{\partial}{\partial t}(\ln \rho) \propto \frac{V_A^* V}{3R_J} \qquad 4.52$$

$$V_A^* (\vec{V}_A^- \cdot \nabla)(\ln \rho) \propto \frac{V_A^{*2}}{R_J} \qquad 4.53$$

Finally, the gravitational acceleration is primarily due to the centrifugal force, which is of the order of

$$g \propto \frac{V^2}{R_J} \qquad 4.54$$

The solution derived herinbefore will be valid only when the term $(\vec{V}_A^+ \cdot \nabla)V_A^-$ is large compared with all of the others. Comparison of Eqs. 4.48–4.54 shows that this is true as long as $L \ll 1\ R_J$; that is, much closer than 1 R_J to Io.

We cannot use Eq. 4.47 to study the region of validity of our soluion perpendicular to $\vec{V}_A^+$ because the term which determines our solution contains spatial derivatives only along $\vec{V}_A^+$. We therefore must use Eq. 4.46. Each term in that equation will be of the same order as the corresponding term in Eq. 4.46, with two exceptions. Since we are now concerned with errors made when we integrate along a path perpendicular to $\vec{V}_A^+$, the second term on the left side of Eq. 4.46 is of the order of

$$(\vec{V}_A^- \cdot \nabla)V_A^+ \propto \frac{VV_A^*}{L} \qquad 4.55$$

Similarly, the term proportional to $(\vec{V}_A^+ \cdot \nabla)\ln \rho$ vanishes. We conclude that our solution is valid for $L \ll (2V/V_A^*)\ R_J \approx 0.3\ R_J$, or within a few Io

radii of the Alfven wing. These results define what we meant by "near the Alfven wing" and "close enough to Io" in the discussion which followed Eq. 4.31.

Chapter 5

Analysis of Plasma Data

Taken in the Vicintiy of Io

By Voyager I

5.1 The Io Flyby

On 5 March 1979, Voyager I flew through the Jovian system. Its orbit is shown in Figures 5.1, 5.2 and 5.3. Figure 5.1 shows the projection of the spacecraft trajectory into the Jovian equatorial plane, in addition to the orientation of the main sensor symmetry axis and the D-cup normal. As can be seen from these figures, the D-cup was looking into the co-rotating plasma throughout the inbound pass. As the spacecraft approached perijove, the corotating flow swung around towards the main sensors, almost coming down the symmetry axis at closest approach. As the spacecraft receded from Jupiter, the flow direction shifted away from the all of the cups. The closest approach to Io occured on the outbound pass at SCET 1510.

Figures 5.2 and 5.3 are closeups of the Io flyby. Both are in Io-centered coordinates; Fig. 5.2 is also a projection of the orbit into Jupiter's equitatorial plane, while 5.3 plots the distance from the origin of that projection against the height above the plane.

The Io flyby occured on the spacecraft's outbound pass, when Voyager I flew about 20 thousand kilometers due south of the satellite. Though the orbit was planned to fly directly through the flux tube, analysis of the magnetic field data (Acuna et al (1981)) showed that the spacecraft missed the Alfven wing, passing several thousand kilometers upstream of it. Subsequent examination of the plasma data (Belcher (1981)) revealed a signature which was interpreted as being due to the velocity perturbation assocated with the flow around the wing. The approximate position of the Alfven wing in the plane of the spacecraft orbit is shown in Fig. 5.2.

During the Io flyby, the flow direction of a strictly corotating plasma would have been almost perpendicular to the main sensor symmetry axis. Table 5.1 lists the angle between the flow direction of a strictly corotating plasma, corrected for spacecraft aberation, and the normals to each of the PLS cups for each of the useful spectra taken during the flyby. One lower half M-mode spectrum was taken every 192 seconds during the flyby, and there are no useful data in the upper half spectra. The L-modes taken during this time cannot be analyzed because the signal in the A-cup is saturated; that is, the digitized currents were equal to the maximum value for several channels, indicating that the true currents were higher.

5.2 Analysis of the Data

We have analyzed eight spectra taken in the vicinity of Io. Using the same nonlinear least squares fitting technique described in Chapter 3, we have attempted to determine the macroscopic parameters of the plasma at the times of each of these spectra. The velocity determinations were then compared with the predictions of the theory outlined in the previous chapter. We shall first describe the determination of the plasma parameters.

Figures 5.4-5.11 show the reduced distribution function plotted as a function of equivalent proton velocity in each cup for each of the eight spectra. The spectra were taken at SCET (spacecraft event time) 1424, 1451, 1454, 1457, 1500, 1504, 1507, and 1510, rerspectively. As in the spectrum plots of Figs 3.3-3.11, the staircases are the data and the smooth

curves are the "best" fits. All of the spectra are smooth and almost featureless, with a single, broad peak. Furthermore, in each spectrum the peak in the A-cup is in a higher channel than the peaks in the B- and C-cups. The D-cup spectra contain mostly noise, and were not included in the fits.

To determine macroscopic plasma parameters from these spectra is a difficult proposition. Since the flow is so very oblique to all of the cups, the results depend critically upon the cup response function at large angles. In addition, the plasma contains many different kinds of ions, which are probably not in thermal equilibrium. In order to get any results at all, we have had to make some assumptions about the chemical composition and the distribution functions of the various ionic species. These assumptions are:

1. The plasma consists of 4 species, with A/Z^* of 8, 16, 32, and 64.

2. The species all have the same bulk velocity.

3. The distribution function which describes each of the species is a convected Maxwellian.

4. The species all have the same thermal speed.

As discussed in the previous chapter, measurements made by Voyager I inbound (Bagenal and Sullivan (1981)) lead us to expect the plasma to consist of various ionization states of Oxygen and Sulfur. The values of A/Z^* for O^{++}, O^{+}, S^{+++}, S^{++}, S^{+}, and SO_2^{+} are 8, 16, 10 2/3, 16, 32, and 64, respectively. We have not included S^{+++} in our fit in the interest of reducing the number of parameters, and because, since the spectra are so featureless, we do not expect to be able to differentiate between the contribution due to a species with A/Z^* of 10 2/3 and its neighbors with

A/Z^* of 8 and 16. The justification for the inclusion of the species with A/Z^* of 64 is that we expect that the distribution functions will have suprathermal tails, and we hope to be able to account for this in a rough manner by including a very heavy species. In fact, it is impossible to fit the higher channels without it. In some of the fits, the inclusion of the heavy species resulted in driving one of the other densities negative; in these cases we fit the spectra without the heavy species, omitting some of the higher channels. In all of these cases, the derived bulk velocity was almost uneffected by this change.

The assumption of a common bulk velocity is the least likely to be violated of the four which we have made. The component of the bulk velocity perpendicular to the magnetic field is determined by the ideal MHD generalized Ohm's law (Eq. 4.11). Solving this equation for $\vec{V}$, we find

$$\vec{V} = c \frac{\vec{E} \times \vec{B}}{B^2} \qquad 5.1$$

This is the same as the equation for the $\vec{E} \times \vec{B}$ drift velocity of a single particle moving in crossed electric and magnetic fields (see Rossi and Olbert, chapter 2). This is no coincidence; the bulk velocity can be thought of as the average velocity of a large number of particles gyrating around the magnetic field with the same $\vec{E} \times \vec{B}$ drift velocity. Since the latter velocity is independent of the mass or charge of the particle, all species must have the same value of $\vec{V}_\perp$. Although the different species may stream along $\vec{B}$ at different speeds when the magnetic field lines are open, in closed line topology we expect $\vec{V}_\parallel$ will be zero. This is in fact what we found from our analysis of these spectra.

The assumption that the distribution functions are Maxwellian has already been discussed in Chapter 1. Since the self-Maxwellization time for the various species are comparable to or greater than the residence time in the torus (see Table 4.1), we must consider the Maxwellian form as no more than a convient way to parameterize the distribution function. As long as the true distribution functions do not have multiple peaks, which is indicated against by the smoothness of the spectra, a Maxwellian must be a reasonably good approximation to the true distribution function around the maximum. Therefore, our justification for this assumption is that it is a reasonable representation of the true distribution function which enables us to perform the two of the velocity space integrals of Eq. 2.2b analytically.

Unfortunately, the fact that the bulk velocity is so oblique to the cup normals implies that most of the signal comes from particles not near the peak of the distribution function. The simulations indicate that the largest contribution comes from particles about one thermal speed away from the peak. We must conclude that our approximation of Maxwellian distributions is a possible source of error. As mentioned above, the inclusion of a species with a mass to charge ratio of 64 is an attempt to compensate for the presence of suprathermal tails.

The assumption of a common thermal speed for all of the species, like the assumption of the Maxwellian shape for the distribution functions, was motivated partly by physical arguments and partly for computational convience. Since the time scales for equipartition of energy between the various ion species are comparable to or longer than the residence time in the torus (see table 4.1), there is no reason to expect that the different

ion species share a common temperature. We did try to fit the spectra with the assumption of a common temperature for the various species; that we were unable to do so convinced us that the different species do not have the same temperature. Furthermore, there are many physical processes, such as various wave-particle interactions or "pick-up", the process by which the newly-made ions are accelerated up to corotational speed, which tend to produce equal thermal speeds.

Since we really have no way of knowing a priori what the relationship between the thermal speeds of the various species is, it would be nice to be able to vary them independently. Unfortunately, the lack of detail in the spectra makes this impossible. Furthermore, the extra computer time involved in computing the derivatives with respect to each individual thermal speed for the gradient search makes this approach impractical. We must make some assumption which relates the various thermal speeds; the assumption that they are all the same, in addition to being physically plausible, has the advantage that it enables us to greatly reduce the computer time required to fit each spectrum by taking advantage of an approximate symmetry of the response function.

The quantity which we use in our fits is the "reduced distribution function", defined as the current in a given channel divided by the voltage width of that channel. This quantity can be expressed as

$$\frac{I_k}{\Delta\phi_k} \approx \frac{Z^{*2}}{A} \frac{n}{w\sqrt{\pi}} \exp\{-(V_z - v_z)^2/w^2\}\ R(\frac{v_z}{w}, \Delta\phi_k, \phi_s)\ |_{v_z=\bar{v}_k} \qquad 5.2$$

where $R(v_z/w, \Delta\phi_k, \phi_s)$ contains the effect of the response function. It is important to note that to the extent that the dependence of the response

function on the channel width and the suppressor voltage can be ignored, the expression on the right side of Eq. 5.2 depends only on V_z/w and v_z/w, never on v_k. This fact enables us to calculate the value of the "reduced distribution function" in channel k for a species with mass A and charge state Z^* from the value of the "reduced distribution function" in channel k' for a species of mass A' and charge state $Z^{*}{}'$ from the formula

$$\frac{I_{k'}(\bar{v}_{k'})}{\Delta\phi_{k'}} = \left(\frac{Z^{*}{}'}{Z^*}\right)^2 \left(\frac{A}{A'}\right) \left(\frac{I_k(\bar{v}_k)}{\Delta\phi_k}\right) \qquad 5.3$$

if the average proton speeds characterizing channels k and k' are related by

$$\bar{v}_{k'} = \sqrt{\left(\frac{A'}{A}\,\frac{Z^*}{Z^{*}{}'}\right)}\ \bar{v}_k \qquad 5.4$$

This approximation was used in calculating the "best fits" to the spectra shown in Figs. 5.4-5.11. The procedure we followed to simulate a spectrum is as follows: for a given bulk velocity and thermal speed we first computed the reduced distribution function in all 128 channels for a species with A=64 and Z^*=1. We then used Eqs. 5.3 and 5.4 to compute the contribution due to the other species. Since, for a given channel k with average proton speed v_k the value of $v_{k'}$ required by Eq. 5.4 is probably not equal to the average proton speed of any other channel, but rather lies between two channels, we used linear interpolation between the adjacent channels to compute $I_{k'}(v_{k'})/\Delta\phi_{k'}$ for use in Eq. 5.3. For several test cases, the approximate values of the "reduced distribution function" calculated in this way were compared with the values obtained from

calculations done without taking advantage of the scaling law just described. The error introduced never exceeded 6%, and frequently was less than 1%.

The parameters derived from the fits of the spectra of Figs. 5.4-5.11 are given in Table 5.2. In all of these spectra, the geometry is such that the flow is almost perpendicular to the symmetry axis of the main sensor. The A-cup look direction is closest to the flow. We expect the determination of the velocity to be more reliable than the determination of the densities, although the errors in these quantities are correlated. The information about the flow direction is primarily contained in the relative heights of the signals in the three cups; the further the flow direction moves away from the axis of symmetry, the larger the difference between the A-cup signal and the B and C cup signals becomes. The information about the densities is primarily contained in the absolute height of the peaks. If the true flow is closer to the main sensor symmetry axis than the fit indicates, the density will be overestimated, since a larger density is required to produce the same signal in a given cup when the flow is more oblique. Conversely, if the true flow direction is further away from the main sensor symmetry axis than the fit indicates, the density will be underestimated.

There were several spectra taken after the spectrum of 1510 (Fig. 5.11) which we were unable to fit because the difference between the signal in the A-cup and the signals in the B- and C- cups were too large. At about this same time, the magnetometer team noticed a field disturbance which did not fit the model described in Chapter 4 (Acuna et al (1981)). Our difficulty in fitting these spectra might be caused by a change in the

plasma distribution function which is related to this magnetic field disturbance.

5.3 The Flow Around the Alfven Wing

The velocities derived from the fits to the spectra of SCET 1451 through 1510 were compared with the theory which has been derived in Chapter 4. To do this, we did a five parameter nonlinear least squares fit, described hereinafter.

Equations 4.43a, 4.43b, and 4.43c' describe the velocity at every point in space as a function of the background flow velocity $\vec{V}_o$, the magnitude of the magnetic line dipole moment μ ($B_o R_c \sin\theta_A$) of the Alfven wing, and the Alfven Mach angle θ_A. The only difficulty is that the orientation of the coordinate system of Eqs. 4.43 also depends upon three of these five parameters. This is because the z-axis of the coordinates of Eqs. 4.43 points along the Alfven characteristic $\vec{V}_A^+$.

To overcome this difficulty, we devised the following fitting procedure. First we define one set of coordinates, called magnetic coordinates, as follows. The center of Io is taken to be the origin of the coordinate system. The unit vector $-\hat{z}_{mag}$ points in the direction of the extrapolated background magnetic field at the location of the spacecraft at SCET 1500, as quoted in Acuna et al (1981). The unit vector $\hat{x}_{mag}$ lies in the plane containing $\hat{z}_{mag}$ and the direction of strictly corotating flow, making an acute angle with the flow direction, and $\hat{y}_{mag}$ is defined so as to

form a right-handed coordinate system. (The unit vector $\hat{z}_{mag}$ was defined to be antiparallel to the background magnetic field direction because $\vec{B}$ points predominently south near the Jovian equatorial plane. In this way, $\hat{z}_{mag}$ makes an acute angle with Jupiter's angular velocity vector. Compared with a cylindrical coordinate system whose polar axis is Jupiter's spin axis, $\hat{z}_{mag}$ points in the same general direction as $\hat{z}_{cyl}$, $\hat{x}_{mag}$ points in the same general general direction as $\hat{\phi}_{cyl}$, and $\hat{y}_{mag}$ points radially <u>in</u> toward Jupiter.)

To compare the theory with experiment, still another set of coordinates is required. We call this set Alfven coordinates. The origin of these coordinates is also the center of Io. The vector $-\hat{z}_{Alfven}$ points along $\vec{V}_A^+$ (note: this is antiparallel to $\hat{z}$ as defined for Equations 4.32-4.45). The unit vector $\hat{x}_{Alfven}$ lies in the plane determined by $\vec{V}_A^+$ and $\vec{V}_o$, so as to be perpendicular to $\hat{z}_{Alfven}$ and make an acute angle with $\vec{V}_o$. The unit vector $\hat{y}_{Alfven}$ is defined so as to complete a right-handed system. The rotation matrix for the transformation from magnetic coordinates to Alfven coordinates is completely determined by the specification of $\vec{V}_o$ and θ_A. It is given explicitly by

$$\vec{A}_{Alfven} = \tilde{R} \cdot \vec{A}_{mag} \qquad 5.5$$

where

$$\tilde{R} = \begin{pmatrix} \cos\theta_A \cos\alpha & \cos\theta_A \sin\alpha & -\sin\theta_A \\ \sin\alpha & \cos\alpha & 0 \\ \sin\theta_A \sin\alpha & \sin\theta_A \sin\alpha & \cos\theta_A \end{pmatrix} \qquad 5.5a$$

and

$$\sin \alpha = \frac{\vec{V}_o \cdot \hat{y}_{mag}}{\{(\vec{V}_o \cdot \hat{y}_{mag})^2 + (\vec{V}_o \cdot \hat{x}_{mag})^2\}^{1/2}} \qquad 5.5b$$

We are now prepared to outline the fitting procedure. First, the spacecraft position at the time of each of the seven spectra is computed in magnetic coordinates. Then, a first guess for the five paramters is made and used to compute the spacecraft positions in Alfven coordinates. The theoretical velocity at each of the seven spacecraft positions is then computed using Eqs. 4.43 and compared with the measured velocity obtained from the fits to the spectra. The "best fit" values of the five parameters are then found using a gradient search algorithm. These "best fit" parameters are given in Table 5.3, while the measured components of the flow velocity at each of the points are compared with the theoretical values in Figure 5.12.

Since it is important to compare our results with the magnetic field measurements, we shall now sumarize the results of the analysis of the magnetic field data (Acuna et al (1981)). Acuna fit the magnetic field to Neubauer's theory in the following manner. First, they assumed that the background flow was strictly corotational, i.e. they set α equal to zero. Then they assumed a value of θ_A. This defined their coordinate system.

In order to compare their measurements with the theory it was neccessary to separate the perturbation magnetic field from the (non-uniform) background field. The resulting values of $\delta\vec{B}$ were then compared with values predicted by Eqs. 4.42.

At this point they introduced three more free parameters into their model. According to Eqs. 4.42, once the orientation of the Alfven coordinate system has been determined, the only free parameter remaining is the dipole strength. In order to obtain a better fit, the location of the dipole and its direction were varied so as to minimize an appropriately defined χ^2. This process was then repeated with different assumed values for θ_A. The "best" value of θ_A was chosen by the requirements that the dipole location be close to the origin and that the angle between the dipole direction and the $\hat{x}$-direction be small. Their procedure was essentially a five parameter nonlinear least squares fit employing a grid search over the values of θ_A and a gradient search through the space spanned by the other four parameters.

Their analysis resulted in the following estimates for the values of the parameters which are of interest to us: Alfven Mach number 0.15, Alfven speed 400 km/sec, and "effective radius" of Alfven wing 1.1 R_{Io}.

In addition to the analysis using the plasma data alone, we also tested Eq. 4.31. We assumed that the plasma velocity and the magnetic field perturbation are related by

$$\vec{V} = \vec{V}_o + \frac{V_A}{B_o} \delta\vec{B} \qquad 5.6$$

We then performed a linear regression to determine the "best" values for $\vec{V}_o$ and V_A. The results are tabulated in Table 5.3. The value of the Alfven speed is large, about 600 km/sec, while the background velocity has a large component radially in toward Jupiter. Figure 5.14 is a plot, similar to Fig. 5.13, of the projections of $\delta\vec{B}$ and $\delta\vec{V}$ (as determined from the linear

regression) into the plane perpendicular $\hat{z}_{mag}$. As can be seen from this figure, there is a strong anticorrelation between $\delta\vec{B}$ and $\delta\vec{V}$, as expected.

5.4 Discussion and Conclusions

We shall now examine the derived plasma parameters for the eight spectra which we fit (Table 5.3). Figure 5.13 shows, superimposed on the spacecraft trajectory, the projection of the bulk velocity vector into a plane perpendicular to the background magnetic field for each of the seven spectra taken in the vicinity of Io. As the spacecraft passed the flux tube, the radial component of the velocity varied smoothly, decreasing from -4 km/sec at 1451 to -23 km/sec at 1457, then increasing again to 10 km/sec at 1507 before finally decreasing again to 0 in 1510. This is the trend one would expect for the flow around the Alfven wing; as Voyager approached the wing from the direction of Jupiter, it first saw the plasma flowing toward the planet as it passed through streamlines which passed around the side of the flux tube toward Jupiter. As Voyager continued its outbound journey, it passed through streamlines which passed the flux tube on the side away from the planet, hence the outward flow. As Voyager left the flux tube behind, it entered a region where the flow was undisturbed. We conclude that the flow observed by Voyager qualitatively agrees with what we would expect to see if our model is correct.

Unfortunately, the maximum inward flow is much greater than the maximum outward flow, and there seems to be a systematic inflow of plasma towards Jupiter. In addition, there is a correlation between the derived densities and the amount of inflow. The larger the speed of the inflow, the larger the densities. Since we really do not expect there to be such large density

fluctuations, and there is no theoretical reason for this correlation, we shall attempt to explain this effect in terms of a systematic error in our fitting procedure.

As mentioned hereinbefore, an error in the determination of the velocity which changes the angle between the velocity vector and the main sensor symmetry axis will be associated with a corresponding error in the density determination. This can be caused by a violation of any of the assumptions described in the preceding section. If this is the case, we expect that the density changes are artifacts of the fitting procedure, and that the change in the radial component of the velocity is less than the result of the fit. We expect that the overall trend is real, however. Since a negative radial component of plasma velocity corresponds to the flow moving further away from the main sensor symmetry axis, and the more oblique the flow is the less accurate we expect our approximation to be, we expect that this effect can cause an overestimate of the average radial inflow and a corresponding overestimate of the density. Such a systematic error would also have the effect of reducing the large value of V_A which was determined from the linear regression with the magnetic field data so as to bring this estimate of V_A into agreement with the value determined by Acuna et al.

The thermal speeds derived from the fits are all between 30 and 36 km/sec. This is consistent with there being no change in the thermal speed of the plasma throughout the flyby.

The north-south component of all of the velocity vectors is consistent with zero. This is what we expect, considering that the $\hat{B}$ field points almost directly due south, and we do not expect to see any flow along $\hat{B}$.

The azimuthal component of the bulk velocity decreases as Voyager approached the Alfven wing, and then increased again as the spacecraft left the wing. Again, this is just the trend one would expect to see in the flow as it passes around the wing.

We will now procede to examine the paramaters describing the Alfven wing which we determined from the non-linear least squares fit to the theory that was expounded in Chapter 4. We first consider α, which measures the angle between the background flow and rigid corotation. The derived value of 18^{o} is much larger than the expected value of 0. The systematic error described in the preceding paragraph would account for this discrepancy.

The value of our determination of $\vec{V}_o \cdot \hat{z}_{mag}$, the component of the bulk flow along the direction of the background magnetic field, is 0. This is exactly what we expect for a system with closed magnetic field lines. Because the B- and C- cup look directions are symmetric with respect to $\vec{B}$, our measurements are very sensitive to small deviations of this component of velocity. We are therefore very confident that this result is not affected by any systematic error of any kind.

Our derived value of the magnitude of the component of the background flow perpendicular to $\vec{B}$ is 63 km/sec. This is slightly greater than the expected value of 57 km/sec. We consider these values to be consistent to within experimental uncertainties.

Our value of the Alfven velocity is 250 km/sec. It should be emphasized that the only magnetic field data used in this determination was the direction of the background field. The values of the Alfven velocity from the mass density measurements and the measured field strength range from 160-250 km/sec. While the same systematic error would tend to increase the latter of

to be made. These are: only species with A/Z^* of 8, 16, 32, and 64 are present, all of the species have the same streaming velocity, the distribution function of each of the ionic species can be approximated by a convected Maxwellian, and all of the species have the same thermal speed. The velocity determination from seven of these spectra were then used to determine the parameters of a model of the Io-magnetosphere interaction based on the work of Neubauer (1980). Although the quantitative agreement with the theory was not outstanding, the results confirm the overall picture of the plasma flow pattern being analogous to incompressible flow around a cylinder.

The discrepencies between the theory and the observations are probably caused by the violation of one or more of the aforementioned assumptions. We have argued that a systematic error whose primary effect is to cause us to overestimate the angle between the direction of the flow and the main sensor symmetry axis could account for all of the discrepencies. In particular, the assumptions that all of the ion species have the same thermal speed and that the distribution functions can be approximated by convected Maxwellians are certainly violated to some extent and this might be the cause of the systematic error.

An additional complication which we have not discussed before is that the spacecraft potential with respect to the ambient plasma is probably not zero. In a quasi-steady state situation, the net electric current flowing into the spacecraft must be vanish. There are three main contributions to this current; positive ions, electrons, and photoelectrons caused by the sun. In the solar wind, the spacecraft tends to be positively charged, since if the spacecraft were neutral the current due to the photoelectrons would dominate that due to the plasma electrons, the contribution due to the positive ions

being negligible due to their much lower velocities. In the high densities of the Io plasma torus, the situation is reversed; the plasma electron current would overwhelm the photoelectron current, resulting in the spacecraft becoming negatively charged. Analysis of the electron data taken by Voyager I near Io indicate that this is in fact the case (Ed Sittler, private communication).

Unfortunately, the effect of the spacecraft potential is difficult to compensate for. Its effect is largest in the lower channels; in channels for which $\phi_k >> \phi_s c$ the effect is entirely negligible. This effect should be taken into account in future work.

All of these difficulties notwithstanding, we expect that the methods of analyzing the plasma data which we have developed in this thesis can be profitably applied to other spectra, not only those taken at Jupiter, but those from the Saturnian system as well.

References

Acuna, M.H., and F.M. Ness; Standing Alfven Wave Current System at Io: Voyager I Observations. JGR 86:8513-8522 30 September 1981

Bagenal,F. and J.D. Sullivan; Direct Plasma Measurements in the Io Torus and Inner Magnetosphere of Jupiter. JGR 86:8477-8466 30 September 1981

Belcher,J.W., C.K. Goertz, J.D. Sullivan, and M.H. Acuna; Plasma Observations of the Alfven Wave Generated by Io. JGR 86:8508-8512 1981

Bevington,P.R.; Data Reduction and Error Analysis for the Physical Sciences. Mcgraw-Hill 1969

Bridge,H.S., J.W. Belcher, R.J. Butler, A.J. Lazarus, A.M. Mauretic, J.D. Sullivan, G.L. Siscoe, and V.M. Vasyliunas; The Plasma Experiment on the 1977 Voyager Mission. Sp. Sci. Rev. 21:259-287 1977

Drell,S.D.,H.M. Foley, and M.A. Ruderman; Drag and Propulsion in the Ionosphere: An Alfven Propulsion Engine in Space. JGR 70:3131 1965

Goldreich,P., and Lynden-Bell; Io, a Jovian Unipolar Inductor. ApJ 156;59-78 1969

Hill,T.W., and A.J. Dessler; Magnetospheric Models. Chapter 10 in Physics of the Jovian Magnetosphere. A.J. Dessler, editor Cambridge University Press 1983

Johnson,R.E. and D.F. Strobel; Charge Exchange in the Io Torus and Exosphere. JGR 87(A10):10385-10393 1 December 1982

McNutt,R.L., J.W. Belcher, and H.S. Bridge; Positive Ion Observations in the Middle Magnetosphere off Jupiter. JGR 86:8319-43 1981

Neubauer,F.M.; Nonlinear Standing Alfven Wave Current System at Io: Theory. JGR 85:1171-1178 1980

Rossi,B. and S. Olbert; Introduction to the Physics of Space. McGraw-Hill 1970

Tables

Table 2.1

Main Sensor Sensitive Area (Normalized)

S_y \ S_x	0.0	2.0	4.0	6.0	8.0	10.0	12.0	14.0	16.0	18.0	20.0
-16.3	.019	.019	.019	.019	.019	.019	.013	.0	.0	.0	.0
-14.3	.15	.15	.15	.15	.15	.13	.085	.034	.006	.0	.0
-12.3	.40	.40	.40	.40	.363	.305	.225	.127	.062	.019	.0008
-10.3	.70	.70	.70	.67	.60	.50	.383	.248	.144	.063	.0065
-8.3	1.00	1.00	1.00	.93	.82	.69	.53	.370	.227	.108	.0123
-6.3	1.00	1.00	1.00	.93	.82	.69	.53	.370	.227	.108	.0123
-4.3	1.00	1.00	1.00	.93	.82	.69	.53	.370	.227	.108	.0123
-2.3	1.00	1.00	1.00	.93	.82	.67	.51	.367	.227	.108	.0123
-0.3	1.00	1.00	1.00	.91	.75	.60	.45	.328	.212	.108	.0123
1.7	1.00	1.00	.90	.77	.62	.49	.363	.257	.161	.075	.0079
3.7	.88	.80	.71	.59	.46	.347	.243	.156	.084	.030	.0022
5.7	.58	.55	.49	.39	.285	.213	.109	.049	.013	.0	.0
7.7	.28	.275	.252	.205	.138	.069	.023	.002	.0	.0	.0
9.7	.076	.076	.076	.068	.037	.0072	.0	.0	.0	.0	.0
11.7	.0	.0	.0	.0	.0	.0	.0	.0	.0	.0	.0

Table 2.2

Relative Angles of the Grids in the D-cup

Grid	α_1	α_2	α_3	α_4	α_5	α_6	α_M	α_S
Spacecraft								
Voyager I	0°	62°	50°	55°	40°	4°	68°	0°
Voyager II	0°	62°	80°	55°	24°	0°	68°	10°

Table 3.1

Plasma Parameters From Cruise Maneuver on 14 September 1978

Time	Number	V_x	V_y	V_z	V_R	V_T	V_N	N_o	w
2345	1	305.	-8.	225.	378.±1.0	18.2±1.2	-23.8±1.4	.284±.008	19.8±.5
2313	2	221.	-8.	297.	370.±0.4	11.8±0.8	-19.1±0.9	.300±.007	16.5±.3
2315	3	118.	-5.	353.	372.±0.3	9.1±0.8	-12.9±1.0	.294±.009	17.2±.2
2316	4	11.4	-6.4	370.	370.±0.2	10.0±0.8	-16.2±0.8	.293±.009	16.4±.2
2316	4a	10.9	-6.5	368.	368.±0.3	9.5±1.1	-16.0±1.1	.276±.011	17.7±.3
2243	5	17.8	-6.6	370.	371.±0.2	7.0±0.9	-14.1±0.9	.237±.008	17.0±.3
2243	5a	17.5	-7.0	369.	369.±0.3	6.5±1.1	-14.3±1.2	.258±.010	18.3±.3
2211	6	-81.5	-7.8	363.	372.±0.4	8.1±1.0	-15.3±1.0	.304±.012	15.9±.3
2212	7	-184.	-4.7	323.	371.±0.7	10.8±0.9	-13.8±1.0	.291±.009	16.4±.3
2248	8	-276.	-2.1	248.	371.±1.0	13.8±0.6	-13.9±1.0	.258±.006	14.3±.4
2216	9	-341.	-1.6	161.	377.±1.3	9.0±0.7	- 9.8±1.3	.278±.007	18.1±.6

Table 4.1

The Physical Properties of Io

Mass	8.9×10^{22} kg	(4.5×10^{-8} M_E)
Radius	1820 km	
Volume	2.53×10^{10} km^3	
Distance from Jupiter	4.24×10^5 km	(5.9 R_J)
Orbital Speed	17.3 km/sec	
Orbital Period	1.54×10^5 sec	(42hrs, 48mins, 38sec)
Rate of Mass Injection into Torus *	6×10^{29} AMU/sec	

* From Hill et al (1983)

Table 4.2

Parameters of Model Plasma

Electron number density	1900 cm^{-3}
Electron temperature	5 eV
S^{+} density	165 cm^{-3}
S^{++} number density	450 cm^{-3}
S^{+++} number density	65 cm^{-3}
O^{+} number density	600 cm^{-3}
O^{++} number density	20 cm^{-3}
Ion thermal speed	30 km/sec (80 eV)
Mass density	3.2×10^{4} AMU/cm^{3} (5.3×10^{-20} g/cm^{3})
Magnetic field strength	2.1×10^{-2} gauss
Alfven velocity	260 km/sec
Bulk speed of corotating plasma	74.1 km/sec (inertial frame)
	56.8 km/sec (Io rest frame)
Alfven Mach number	0.22
Electron plasma frequency	2.4×10^{6} sec^{-1}
Electron gyrofrequency	3.6×10^{5} sec^{-1}
Ion gyrofrequency	12.6 sec^{-1} (O^{+})
Electron gyroradius	4.24 m
Skin depth	20 km

Table 4.2 continued

Debye length	65 cm
Interparticle distance	8×10^{-2} cm
Number of electrons in Debye sphere	2.3×10^{9}
Ion gyroradius	3 km (O^{+} with w=30 km/sec)
Centrifugal acceleration	33 cm/sec (Io rest frame)
Magnetic energy density	1.6×10^{-5} ergs/cm^3
Thermal energy density	6.3×10^{-7} ergs/cm^3
β	5.2×10^{-2}
Self-Maxwellization times	65 sec (electrons)
	24 days (O^{+})
	47 days (O^{++})
	340 days (S^{+})
	8 days (S^{++})
	12 days (S^{+++})
Thermal relaxation times	50 hrs (ion-electron)
	1-50 days (ion-ion)
Plasma residence time in torus *	30 days
Period of Io	43 hours
Rotation period of Jupiter	10 hours
Plasma time of flight past Io	30 sec

* Estimated from mass injection rate of Table 4.1, assuming that the torus has a radius of 1 R_J.

Table 5.1

Angles Between Cup Normals

and the Flow Direction of a Strictly Corotating Plasma

During Io Flyby on 5 March 1979

SCET	θ_A	θ_B	θ_C	θ_D
1422	57°	86°	89°	163°
1451	64°	93°	96°	169°
1454	64°	93°	96°	169°
1457	65°	94°	97°	169°
1500	66°	95°	98°	170°
1504	67°	95°	98°	171°
1507	67°	96°	99°	171°
1510	68°	96°	99°	171°

Table 5.2

Plasma Parameters Derived From Spectra Taken Near Io

Difference from Corotation

SCET	ΔV_r	ΔV_ϕ	ΔV_z	nO++	n_{O^+}	n_{S^+}	ρ	w	V_A
1422	- 4.9	4.5	- 2.9	593	226	801	3.9	31	210
1451	- 4.2	1.2	- 0.7	702	104	875	4.1	35	200
1454	-13.7	- 2.9	- 1.4	1044	289	1356	6.5	36	160
1457	-22.7	- 6.2	- 0.5	1088	602	1233	6.7	36	160
1500	-16.4	- 7.7	- 0.7	886	338	706	4.2	36	200
1504	4.1	- 5.4	- 3.3	538	228	500	2.8	33	250
1507	9.7	10.0	- 7.1	457	253	500	2.7	33	250
1510	- 5.0	9.5	- 5.6	621	338	682	3.7	32	210

All speeds are in km/sec

n in cm^{-3}

ρ in 10^4 AMU/cm^3

Velocity differences in Jupiter equatorial cylindrical polar coordinates

Table 5.3

Results of Linear Regression to Test Equation 4.31

$\vec{V}_o \cdot \hat{x}_{mag}$	$\vec{V} \cdot \hat{y}_{mag}$	$\vec{V} \cdot \hat{z}_{mag}$	V_A
60 km/sec	13 km/sec	-2 km/sec	600 km/sec

Figure Captions

Figure 2.1 The PLS Experiment. The figure consists of a sketch of instrument, showing the positions of the four cups.

Figure 2.2 The Voyager Spacecraft. The figure consists of a drawing of the spacecraft, showing the location of all of the scientific instruments and the orientation of the axes of the spacecraft coordinate system.

Figure 2.3 The PLS Experiment Aperture Positions. The figure shows the position of the four cups as viewed from along the main sensor symmetry axis, and the directions of the coordinate axes of the cup coordinate system.

Figure 2.4 Main Sensor Cross-section. The figure shows a cross-section of one of the cups in the main cluster, including the positions of the grids and the collector.

Figure 2.5 Main sensor Aperture and Collector Areas. The figure shows the shape and size of the aperture and the collector of a main sensor cup.

Figure 2.6 Modulator Voltage and Collector Current Versus Time. The figure shows the voltage waveform which is impressed on the modulator grid and the resulting collector current waveform for a hypothetical positive ion measurement.

Figure 2.7 Geometry for Grid Transparency Calculation. The figure shows a beam of particles incident on a grid of parallel, cylindrical wires. α is the angle between the beam direction and the normal to the plane of the grid, L is the distance between the centers of two adjacent wires, and d is the wire diameter. The wires run in the $\hat{y}$-direction, and the $\hat{z}$-direction is normal to the grid plane, with $+\hat{z}$ making an acute angle with the direction of the incident beam.

Figure 2.8 Definition of the Shift Vector. The figure shows the outline of the collector of one of the main sensor cups, with the image of the aperture in the collector superposed on it. An incident monoenergetic beam of particles will have the shape of the aperture as it travels through the cup. The shift vector $\vec{S}$ is the vector which lies in the collector plane and points from the point directly underneath the center of the long side of the aperture to the corresponding point on the image of the aperture in the incident beam.

Figure 2.9 Particle Trajectory in a Main Sensor Cup. The figure shows the projection into the x-z plane (cup coordinates) of the path of a particle through one of the main sensor cups. The locations of the nine grids are shown, along with identifying numbers which correspond to the grid numbers in Figure 2.4. The x-component of the shift vector is shown as the difference between the x-coordinate of the particle as it crosses the plane of the aperture grid and the x-coordinate of the particle when it reaches the collector.

Figure 2.10 Potential Versus Distance From Aperture. The figure shows the electrostatic potential inside the cup plotted against z (cup coordinates) in the approximation that the potential depends only on z. Three cases are shown; a) the main sensor, b) the side sensor in positive ion mode, and c) the side sensor in the electron mode.

Figure 2.11 The Sensitive Area of a Main Sensor Cup. The figure shows the 16 distinct regions in which there is a different functional dependence of the sensitive area on the shift vector.

Figure 2.12 Side Sensor Cross-Section. The figure consists of a cross-section of the D-cup, showing the locations of the eight grids and the collector. Compare with Figure 2.4.

Figure 2.13 Common Area of Two Circles. The figure shows the common area of two circles of different radius as a function of the distance between their centers. It also defines the parameter X. If the line connecting the centers of the two circles is taken to be the x axis, with the center of the larger circle at x=0, then X is the x coordinate of the points of intersection of the two circles.

Figure 2.14 Sensitive Area of the D-cup. The D-cup sensitive area is the common area of three circles of different radii all of whose centers lie on the same line. The figure shows four different cases for which different combinations of arcs from the three circles determine the boundary of the common area. The formula for the common area for the cases shown in a,b, and c is given by Equation 2.27a, while the formula for the case shown in d is given by Equation 2.27b. The relative positions of the points X_{AC} and X_{GC} determine which formula is to be used.

Figure 2.15 Main Sensor Sensitive Area Versus S_y/h. The figure shows a family of curves which represent the main sensor sensitive area as a function of the ratio of the y-component of the shift vector divided by the height of the cup, with the x-component of the shift vector as a parameter.

Figure 2.16 Y_u and Y'_u Versus S_x/h. The figure shows a graph of two of the functions required for the trapezoidal approximation to the sensitive area of the main sensor cups.

Figure 2.17 Main Sensor Sensitive Area Versus S_y/h (Trapezoidal Approximation). The figure shows a family of curves which represent the main sensor sensitive area as a function of the ratio of the y-component of the shift vector divided by the height of the cup, with the x-component of the shift vector as a parameter, in the trapezoidal approximation. Compare with Figure 2.15.

Figure 2.18 Main Sensor Sensitive Area Versus $|S_x|/h$ (Trapezoidal Approximation). The plot is valid for S_y equal to zero.

Figure 2.19 3-D Plot of the Sensitive Area Versus X and Y in the Trapezoidal Approximation.

Figure 2.20 3-D Plot of the Full Response Function. The figure shows the full response function plotted versus X and Y, utilizing the trapezoidal approximation (defined by Equations 2.3, 2.9, and 2.31-2.34).

Figure 3.0 The Cruise Maneuver. The figure consists of four lines, each of which has several dots on it. Each line represents a polar plot of the cup coordinates of a hypothetical purely radial solar wind during the cruise maneuver. The dots correspond to the times of the M-mode spectra. Each dot which corresponds to the time of a spectrum which was analyzed is numbered. The spectrum taken when the spacecraft was in the orientation corresponding to point 1 is plotted in Figure 3.1; that corresponding to point 2 is Figure 3.2; etc. The orientation of the spacecraft was the same for the spectra shown in Figures 3.4 and 3.5.

Figure 3.1 Reduced Distribution Function Versus Velocity for Cruise Maneuver Spectrum 1. The staircases are the data, while the smooth curve is the fit.

Figure 3.1a Reduced Distribution Function Versus Velocity for Cruise Maneuver Spectrum 1. The staircases are the data, while the smooth curve is the fit. The lower channels in the B-cup were not used in determining the plasma parameters; they are included to illustrate that the currents in these channels is not only noise, but actually includes some signal.

Figure 3.1b Reduced Distribution Function Versus Velocity for Cruise Maneuver Spectrum 1. The staircases are the data, while the smooth curve is a simulation done assuming "unity" response using the plasma parameters determined from the fit which is plotted in Figure 3.1. Note how the locations of the peaks in the simulation are correct, but their heights and shapes are wrong.

Figure 3.2 Reduced Distribution Function Versus Velocity for Cruise Maneuver Spectrum 2. The staircases are the data, while the smooth curve is the fit.

Figure 3.3 Reduced Distribution Function Versus Velocity for Cruise Maneuver Spectrum 3. The staircases are the data, while the smooth curve is the fit.

Figure 3.4 Reduced Distribution Function Versus Velocity for Cruise Maneuver Spectrum 4. The staircases are the data, while the smooth curve is the fit. This fit was done using the full response function. The data are the same as were fit using the "unity response" approximation for Figure 3.4a.

Figure 3.4a Reduced Distribution Function Versus Velocity for Cruise Maneuver Spectrum 4. The staircases are the data, while the smooth curve is the fit. This fit was done using the "unity" response approximation. The data are the same as were fit using the full response function for Figure 3.4.

Figure 3.5 Reduced Distribution Function Versus Velocity for Cruise Maneuver Spectrum 5. The staircases are the data, while the smooth curve is the fit. This fit was done using the full response function. The data are the same as were fit using the "unity response" approximation for Figure 3.5a. The orientation of the spacecraft was the same as for Spectrum 4.

Figure 3.5a Reduced Distribution Function Versus Velocity for Cruise Maneuver Spectrum 1. The staircases are the data, while the smooth curve is the fit. This fit was done using the "unity response" approximation. The data are the same as were fit using the full response function for Figure 3.5. The orienation of the spacecraft was the same as for Spectrum 4.

Figure 3.6 Reduced Distribution Function Versus Velocity for Cruise Maneuver Spectrum 6. The staircases are the data, while the smooth curve is the fit.

Figure 3.7 Reduced Distribution Function Versus Velocity for Cruise Maneuver Spectrum 7. The staircases are the data, while the smooth curve is the fit.

Figure 3.8 Reduced Distribution Function Versus Velocity for Cruise Maneuver Spectrum 8. The staircases are the data, while the smooth curve is the fit. The change in the orienation of the spacecraft between the times of the peaks in the various cups was corrected for.

Figure 3.8a Reduced Distribution Function Versus Velocity for Cruise Maneuver Spectrum 8. The staircases are the data, while the smooth curve is the fit. The change in the orientation of the spacecraft between the time of the peaks in the different cups was not compensated for. Compare Figure 3.8.

Figure 3.9 Reduced Distribution Function Versus Velocity for Cruise Maneuver Spectrum 9. The staircases are the data, while the smooth curve is the fit.

Figure 4.1 The Goldreich Picture of the Interaction between Io and the Jovian Magnetosphere. Field aligned currents flow in the fluxtube which links Io. The current system is closed in the Jovian ionosphere. A similar system for the southern hemisphere is not shown.

Figure 4.2 Io's Alfven Wings. Two views are shown of the Alfven wing and associated current system. Figure 4.2a shows the Alfven wings as seen looking along the flow direction of the corotating plasma. Figure 4.2b shows the Alfven wings as viewed by an observer located along on the line which connects Jupiter and Io. In model shown here, due to Drell, it is not neccessary to close the current system in the Jovian magnetosphere, so the currents are determined by the Alfven wave impedence of the plasma.

Figure 4.3 The Streamlines of Potential Flow Around an Infinite Cylinder.

Figure 5.1 The Voyager I Jupiter Encounter. The figure shows the projection of the spacecraft trajectory into the Jovian Equatorial plane, along with the directions of the main sensor symmetry axis and the D-cup -z axis. Note how the D-cup points into the corotating flow on the inbound pass, while none of the cups points into the flow on the outbound pass.

Figure 5.2 The Voyager I Io Flyby. The figure shows the trajectory in an Io-centered coordinate system, projected into Jupiter's equatorial plane. The y-axis points toward Jupiter, the x-axis points in the direction of the corotating flow, and the z-axis completes a right-handed system. The axes are labeled in units of Io radii. The circle with its center at the origin is Io; the circle with its center displaced from the origin is the probable position of the Io Alfven wing in the plane of the spacecraft orbit.

Figure 5.3 The Voyager I Io Flyby. The coordinate system used to describe the position of the spacecraft this figure is that defined in the caption for Figure 5.2. The figure shows z plotted against $\sqrt{(x^2 + y^2)}$.

Figure 5.4 Reduced Distribution Function Versus Velocity for the spectrum taken at SCET 1422. The staircases are the data; the smooth curves are the fits. The dropouts in the spectra are caused by interference with another instrument on the spacecraft.

Figure 5.5 Reduced Distribution Function Versus Velocity for the spectrum taken at SCET 1451. The staircases are the data; the smooth curves are the fits. The dropouts in the spectra are caused by interference with another instrument on the spacecraft.

Figure 5.6 Reduced Distribution Function Versus Velocity for the spectrum taken at SCET 1454. The staircases are the data; the smooth curves are the fits. The dropouts in the spectra are caused by interference with another instrument on the spacecraft.

Figure 5.7 Reduced Distribution Function Versus Velocity for the spectrum taken at SCET 1457. The staircases are the data; the smooth curves are the fits. The dropouts in the spectra are caused by interference with another instrument on the spacecraft.

Figure 5.8 Reduced Distribution Function Versus Velocity for the spectrum taken at SCET 1500. The staircases are the data; the smooth curves are the fits. The dropouts in the spectra are caused by interference with another instrument on the spacecraft.

Figure 5.9 Reduced Distribution Function Versus Velocity for the spectrum taken at SCET 1504. The staircases are the data; the smooth curves are the fits. The dropouts in the spectra are caused by interference with another instrument on the spacecraft.

Figure 5.10 Reduced Distribution Function Versus Velocity for the spectrum taken at SCET 1507. The staircases are the data; the smooth curves are the fits. The dropouts in the spectra are caused by interference with another instrument on the spacecraft.

Figure 5.11 Reduced Distribution Function Versus Velocity for the spectrum taken at SCET 1510. The staircases are the data; the smooth curves are the fits. The dropouts in the spectra are caused by interference with another instrument on the spacecraft.

Figure 5.12 Flow Velocity Versus Time. The figure shows the flow velocities determined from the fits to the spectra of Figs. 5.5-5.11. The smooth curves are the velocities determined from a "best fit" to the model of Neubauer. The quantities V_1, V_2 and V_3 are the components of $\vec{V}$ along $\hat{x}_{mag}$, $\hat{y}_{mag}$, and $\hat{z}_{mag}$ respectively.

Figure 5.13 Plasma Bulk Velocity at Different Positions in the Vicinity of Io. The figure shows the projection of the bulk velocity of the plasma into a plane perpendicular to the background magnetic field direction. The points at which the vectors representing the velocities intersect the line which represents the spacecraft orbit corresponds to the position of the spacecraft at the time the velocity measurement was made.

Figure 5.14 $\delta\vec{V}$ and $\delta\vec{B}$ near Io. The figure shows the projection of the deviation from uniform flow $\delta\vec{V}$ and the deviation from a dipole field $\delta\vec{B}$ into a plane perpendicular to the background magnetic field. The points of intersection of the vectors $\delta\vec{V}$ and $\delta\vec{B}$ with the spacecraft trajectory are the positions of the spacecraft at the time of the measurements.

Figures

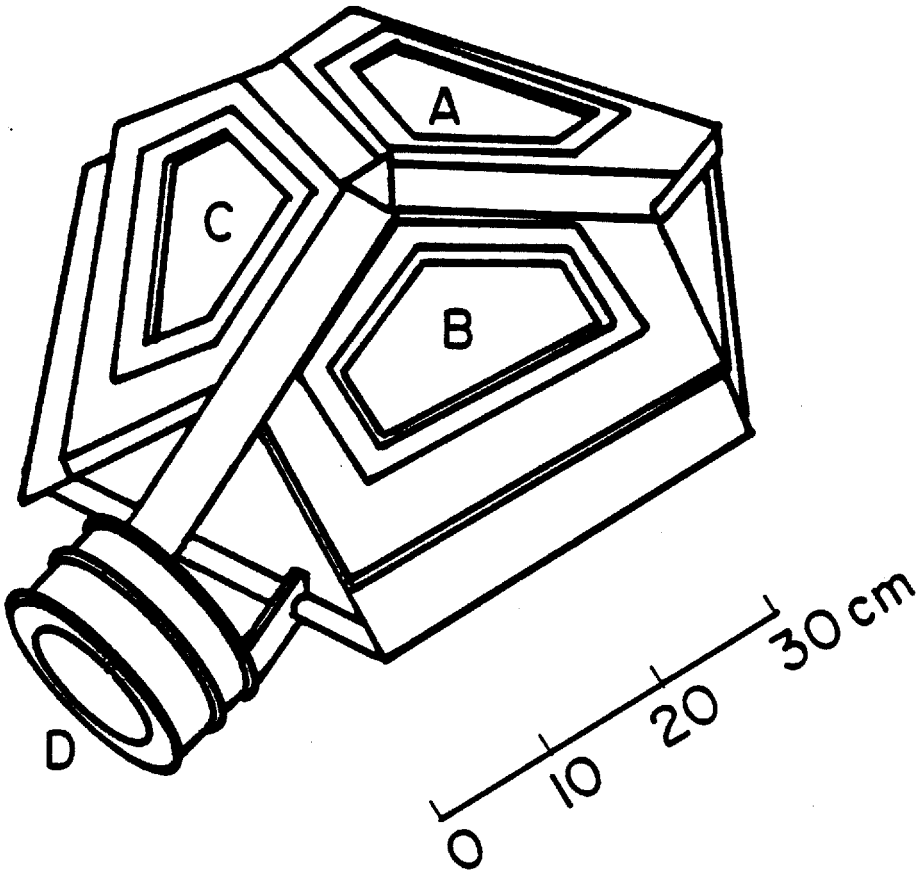

Figure 2.1

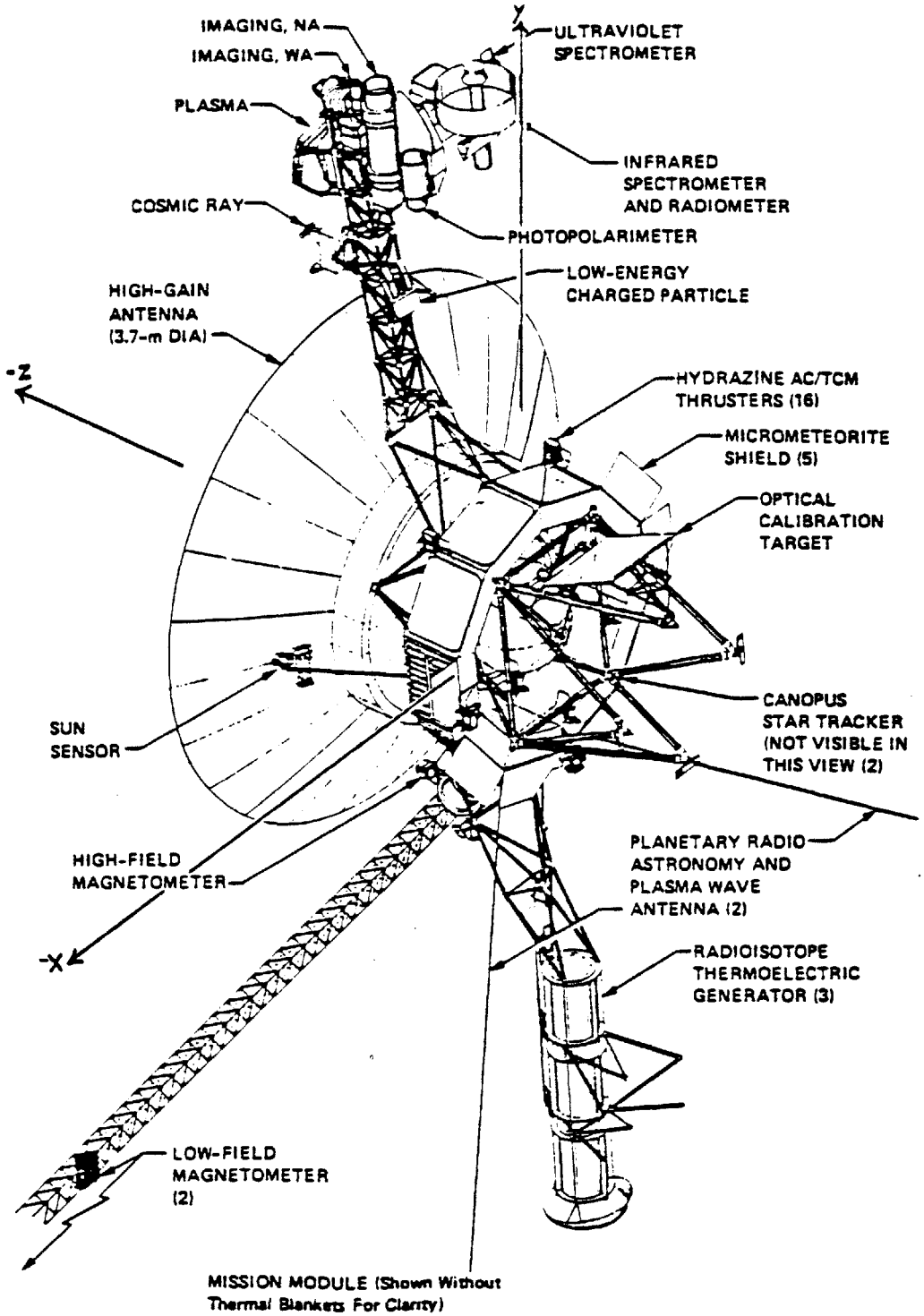
IMAGING, NA
IMAGING, WA
PLASMA
COSMIC RAY
HIGH-GAIN ANTENNA (3.7-m DIA)
-Z
SUN SENSOR
HIGH-FIELD MAGNETOMETER
-X
LOW-FIELD MAGNETOMETER (2)
MISSION MODULE (Shown Without Thermal Blankets For Clarity)
Y
ULTRAVIOLET SPECTROMETER
INFRARED SPECTROMETER AND RADIOMETER
PHOTOPOLARIMETER
LOW-ENERGY CHARGED PARTICLE
HYDRAZINE AC/TCM THRUSTERS (16)
MICROMETEORITE SHIELD (5)
OPTICAL CALIBRATION TARGET
CANOPUS STAR TRACKER (NOT VISIBLE IN THIS VIEW (2)
PLANETARY RADIO ASTRONOMY AND PLASMA WAVE ANTENNA (2)
RADIOISOTOPE THERMOELECTRIC GENERATOR (3)

Figure 2.2

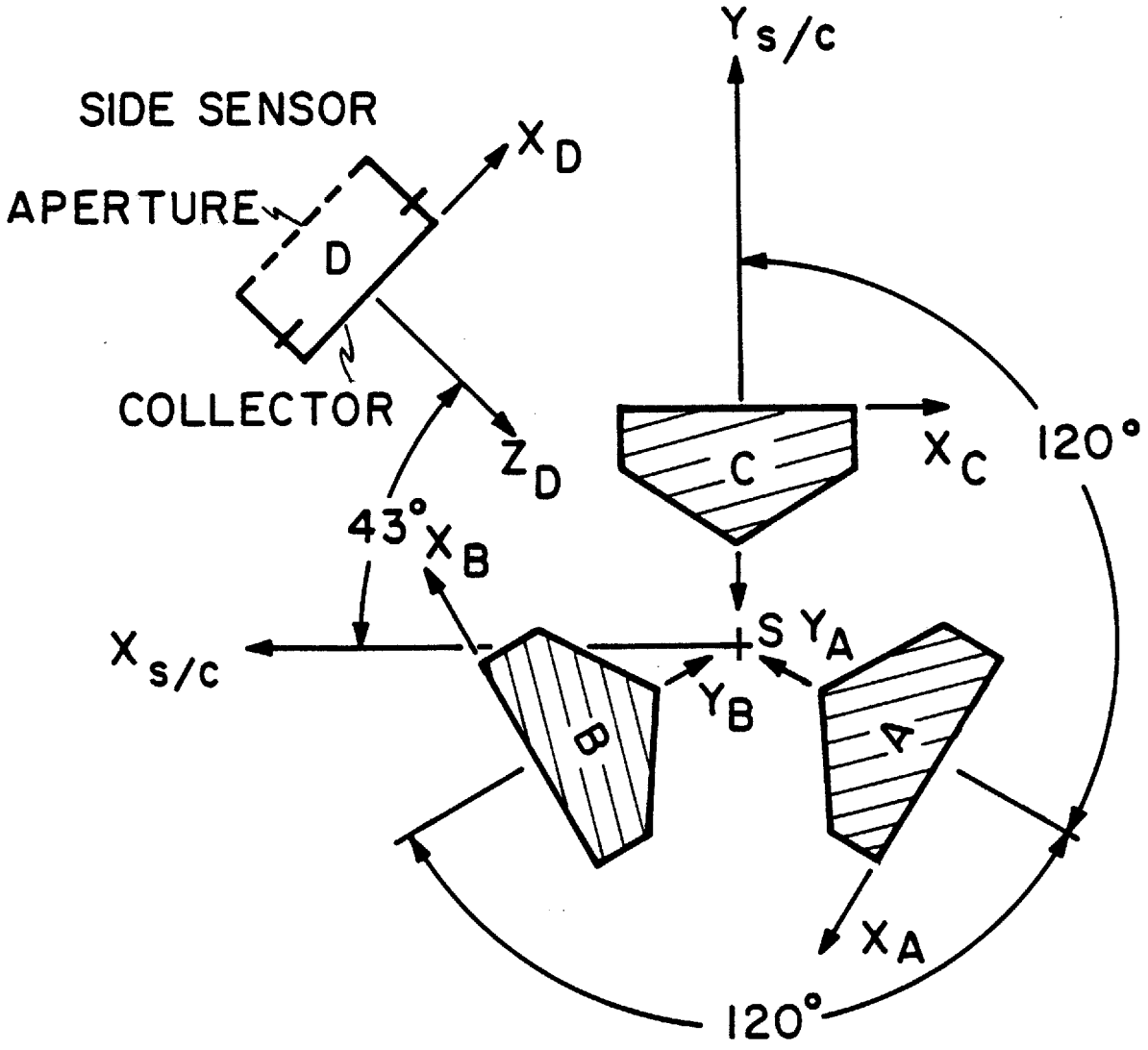
SIDE SENSOR
APERTURE
D
COLLECTOR
X_D
Z_D
$Y_{s/c}$
C
X_C
120°
43°
X_B
$X_{s/c}$
S
Y_A
Y_B
B
A
X_A
120°

Figure 2.3

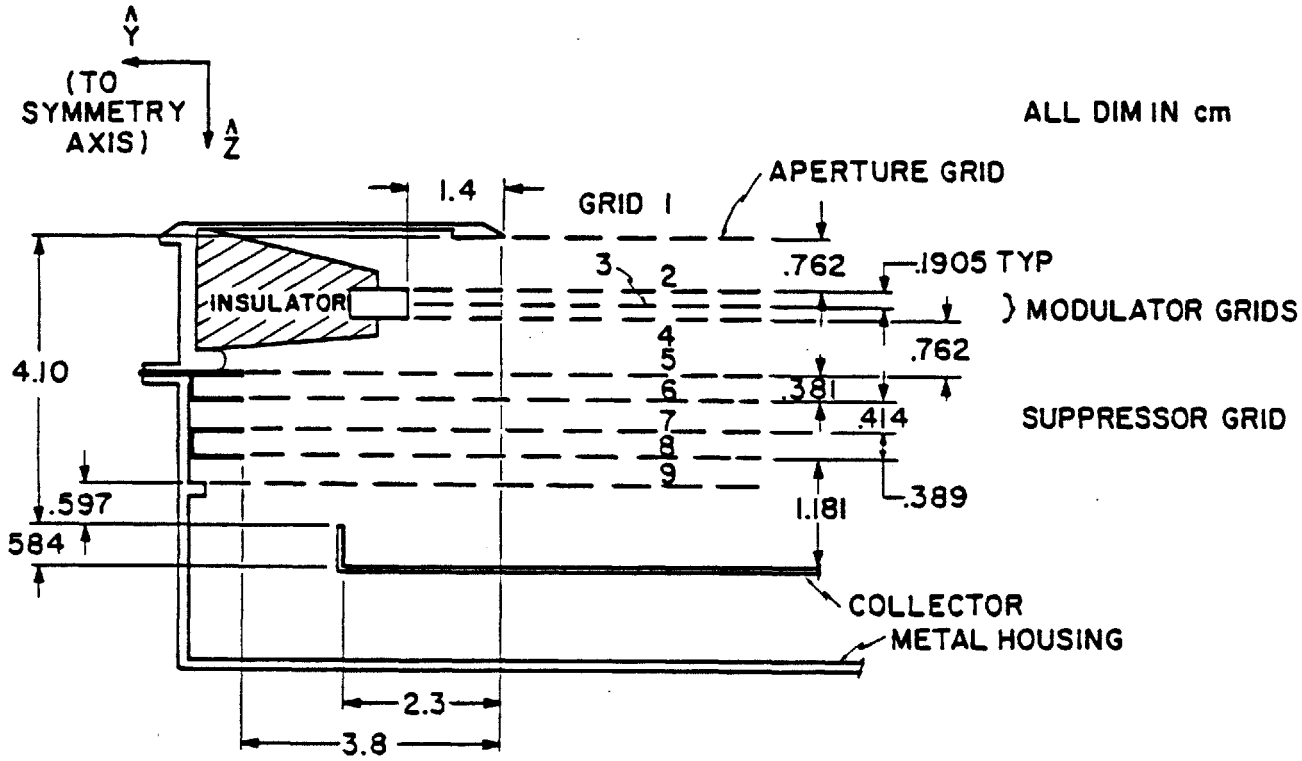

MAIN SENSOR
VERTICAL CUT OF UPPER SEGMENT

Figure 2.4

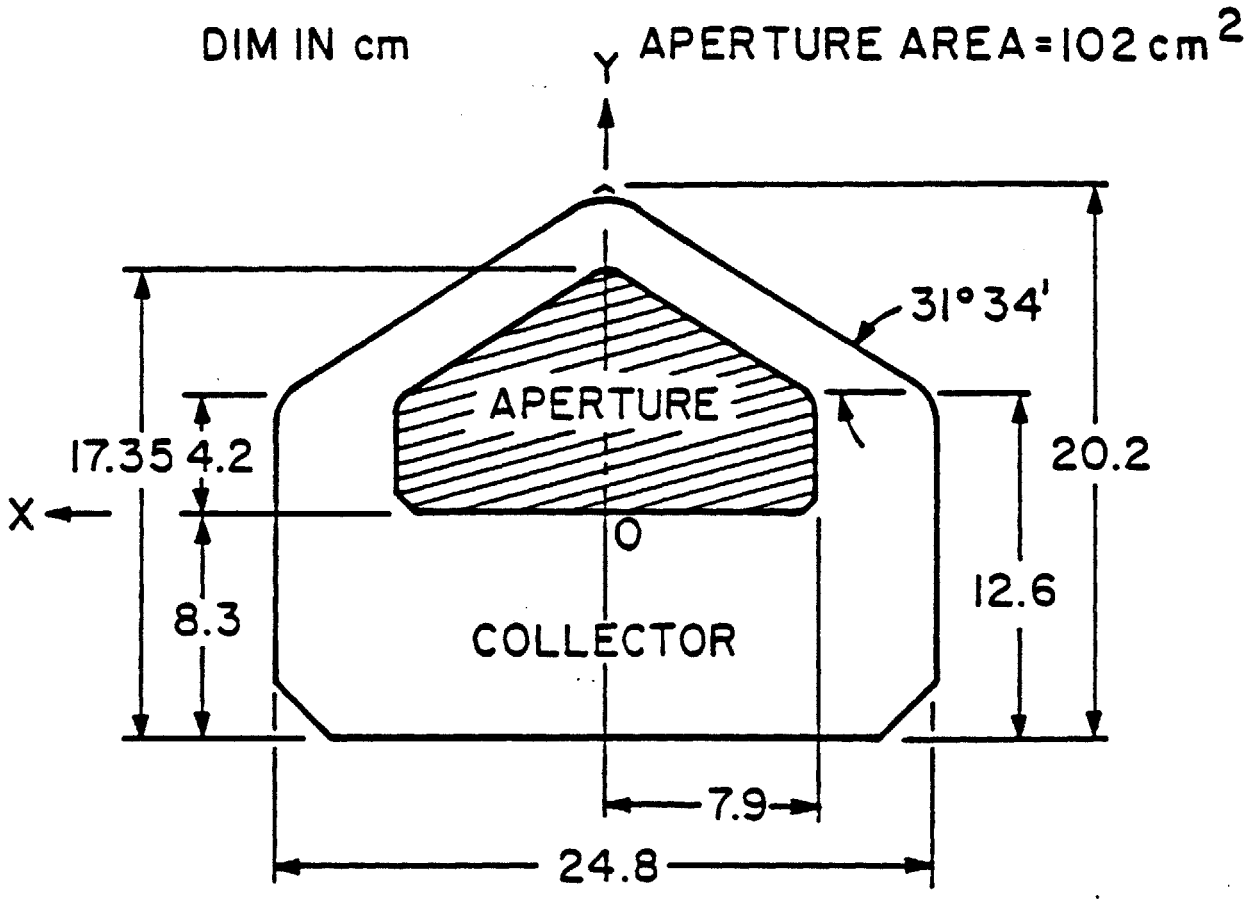

MAIN SENSOR (APERTURE AND COLLECTOR AREAS)

Figure 2.5

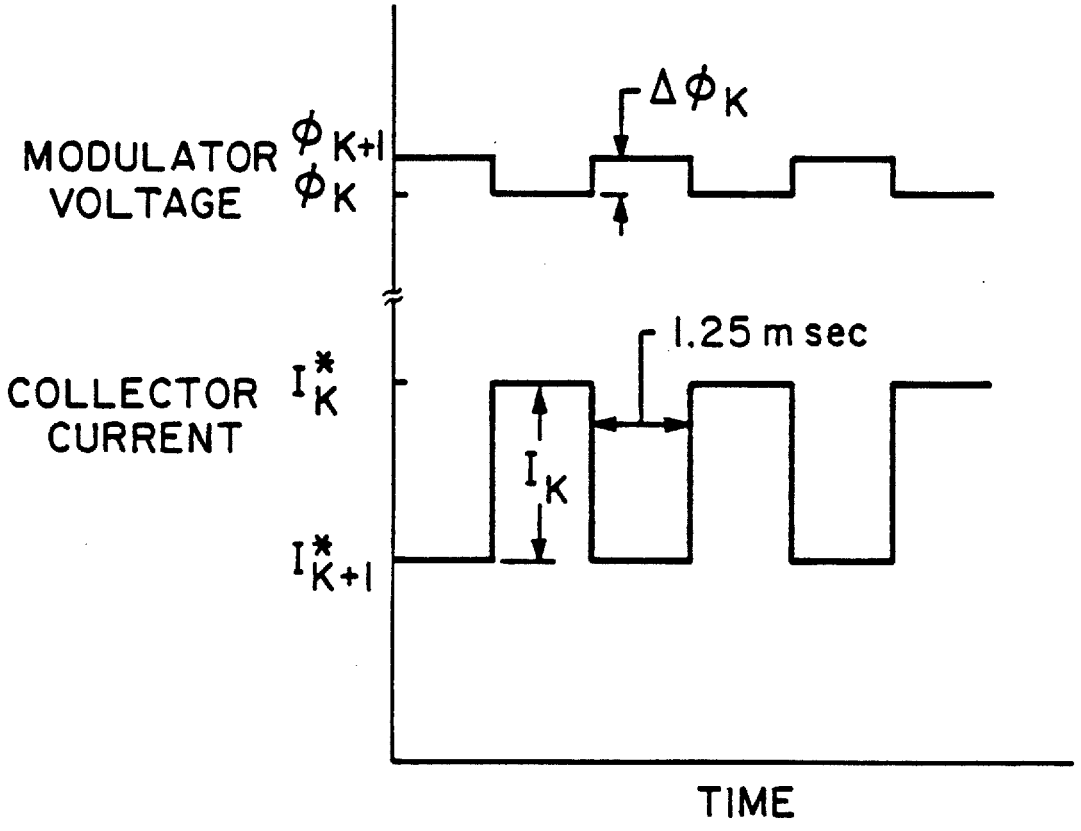

MODULATOR VOLTAGE AND COLLECTOR CURRENT
vs
TIME

Figure 2.6

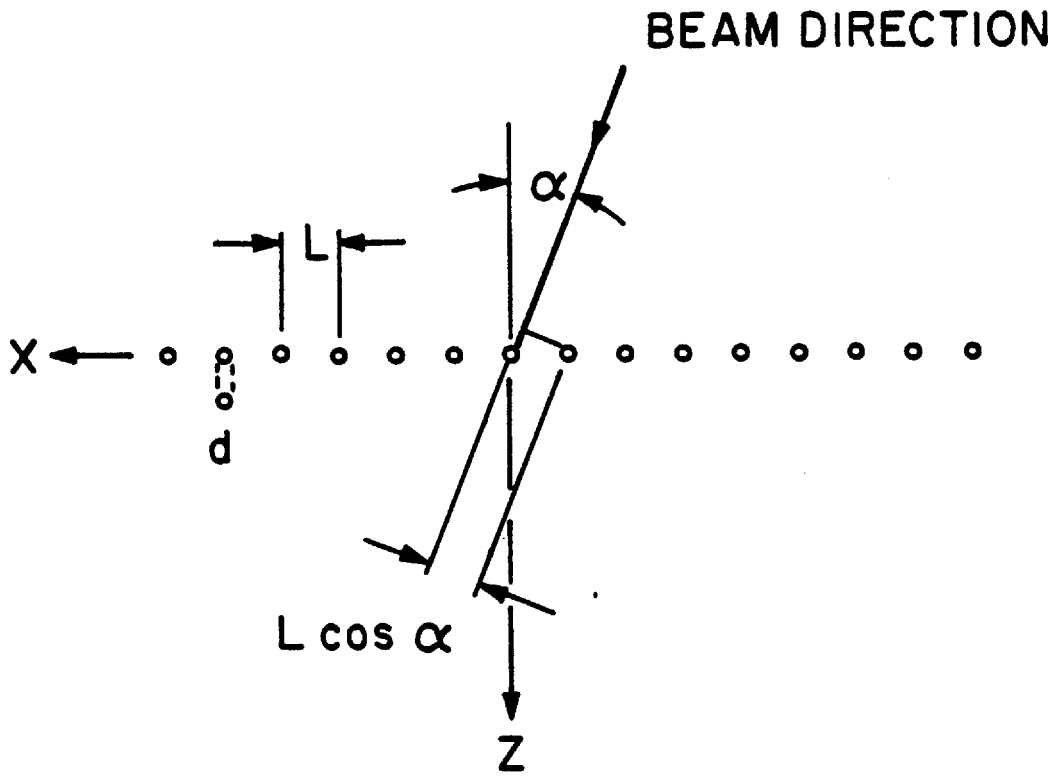

GEOMETRY FOR GRID TRANSPARENCY

Figure 2.7

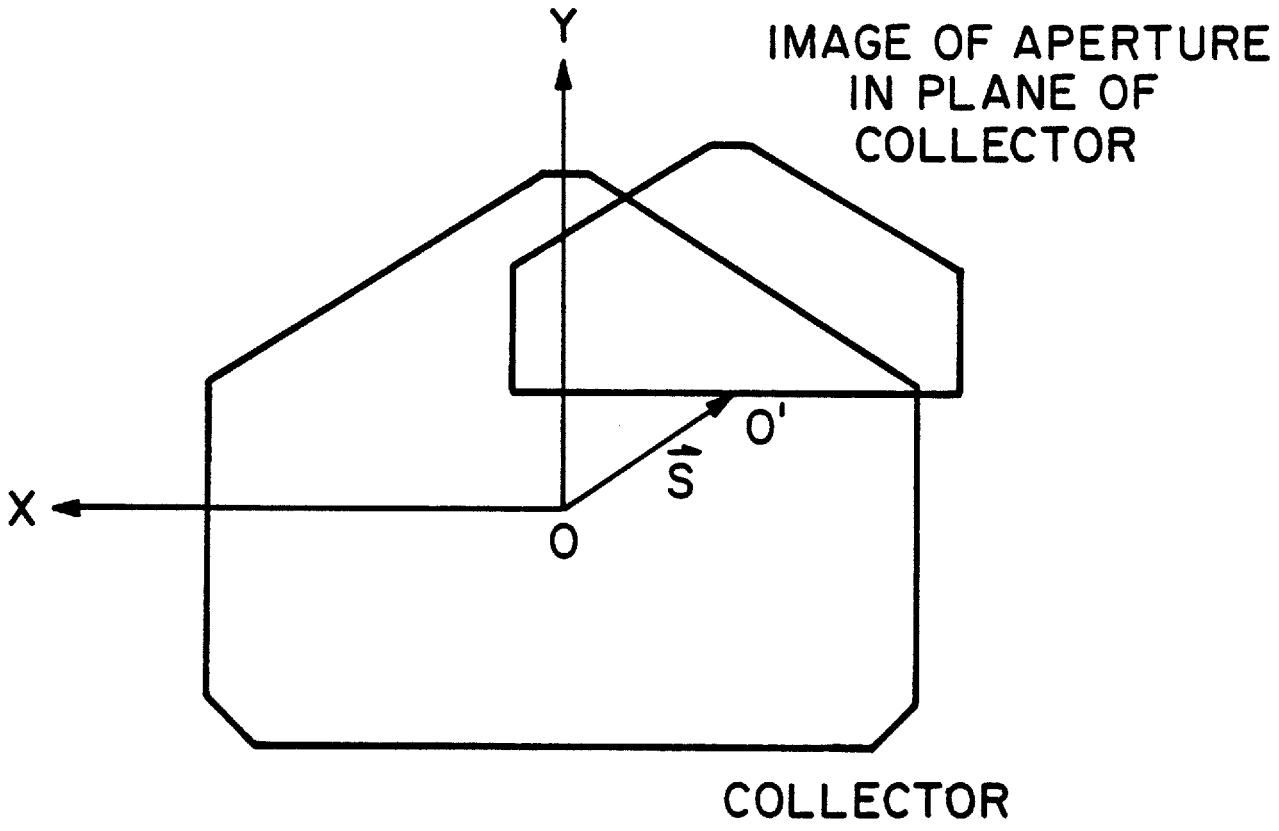

DEFINITION OF SHIFT VECTOR

Figure 2.8

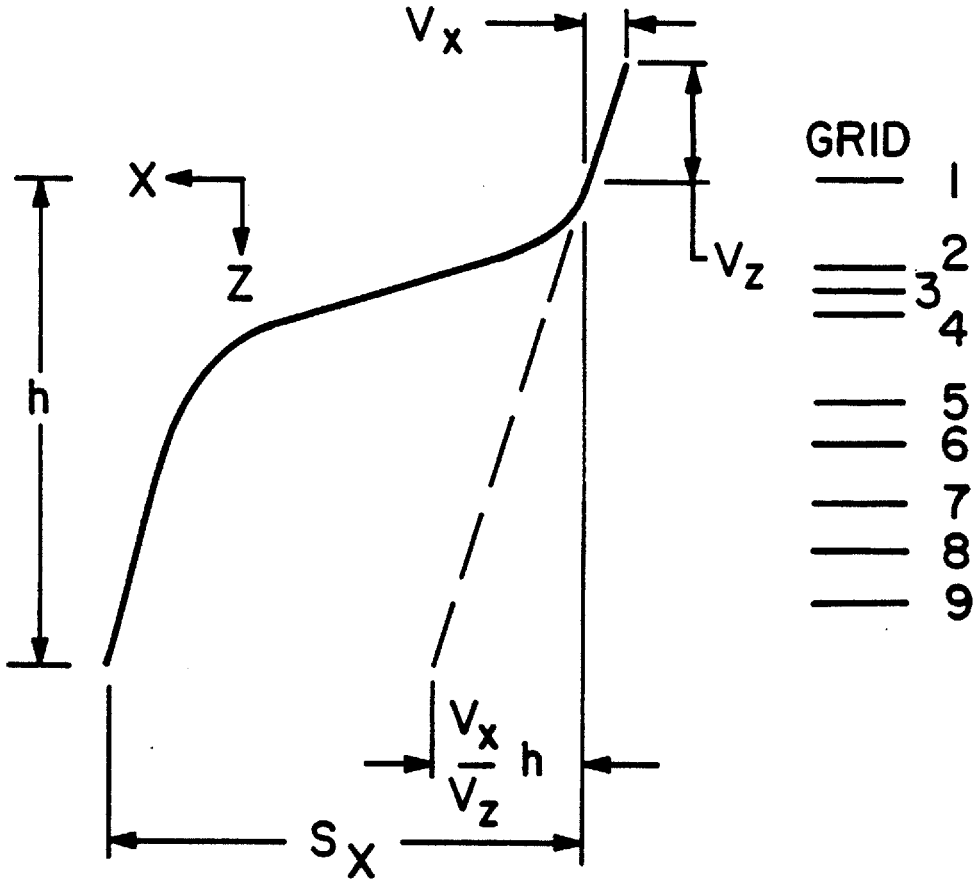

PARTICLE TRAJECTORY
IN A
MAIN SENSOR CUP

Figure 2.9

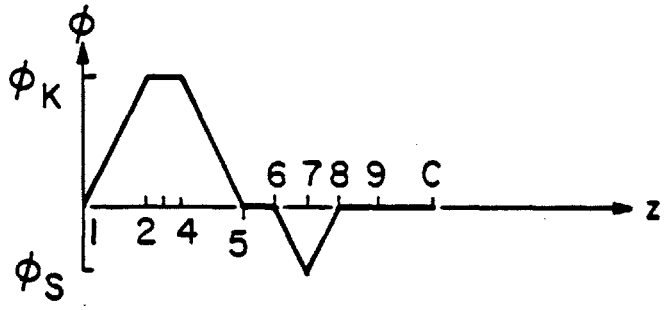

A) MAIN SENSOR

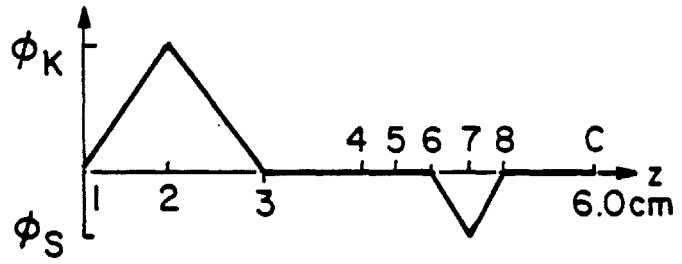

B) SIDE SENSOR-POSITIVE Ion MODE

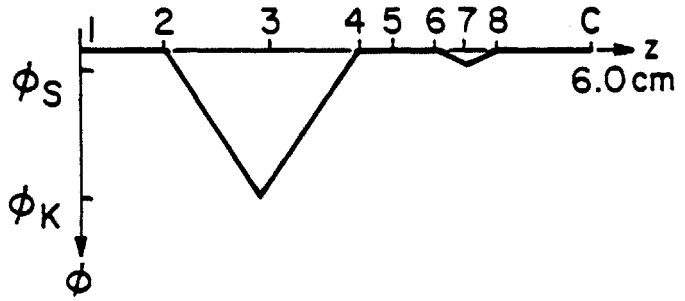

C) SIDE SENSOR-ELECTRON MODE

POTENTIAL vs DISTANCE FROM APERTURE

Figure 2.10

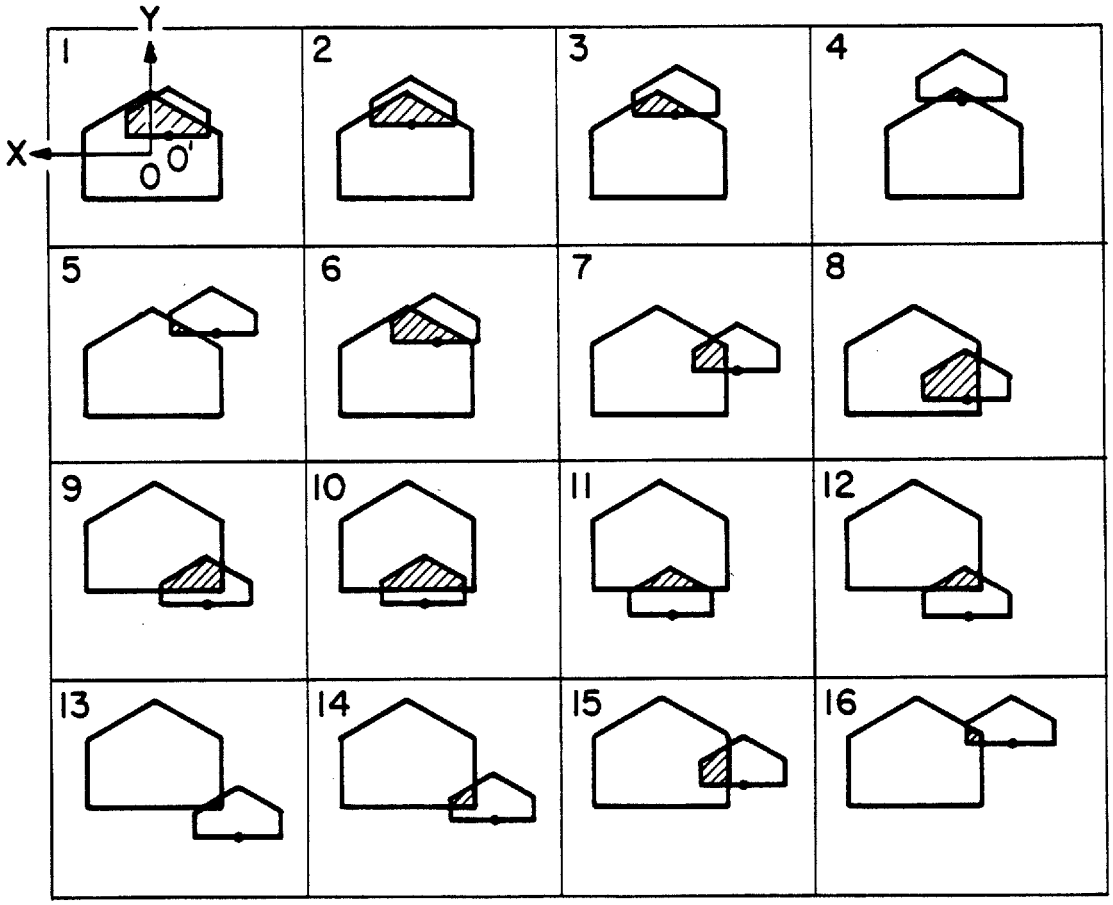

Figure 2.11

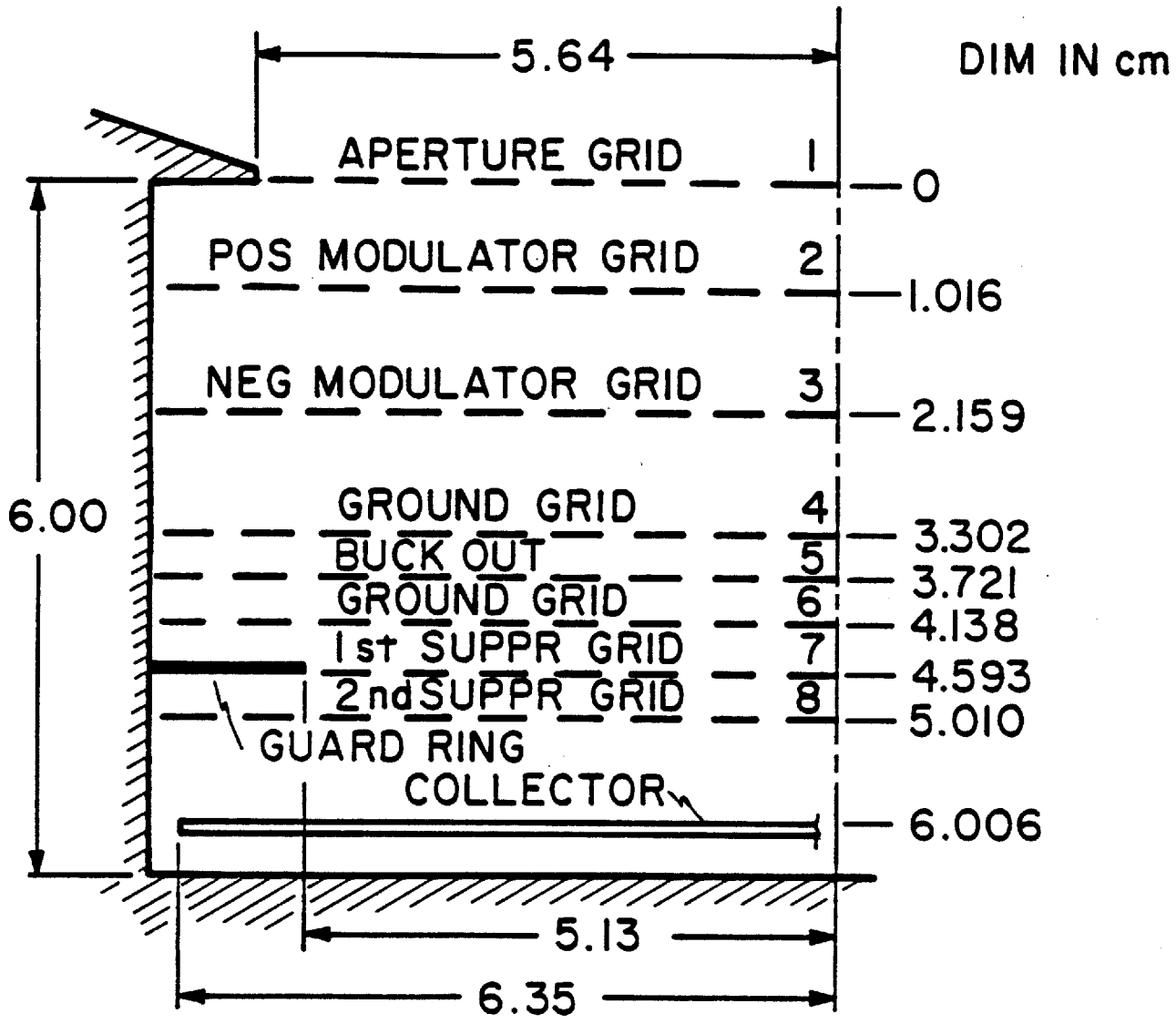

SIDE SENSOR - VERTICAL CUT

Figure 2.12

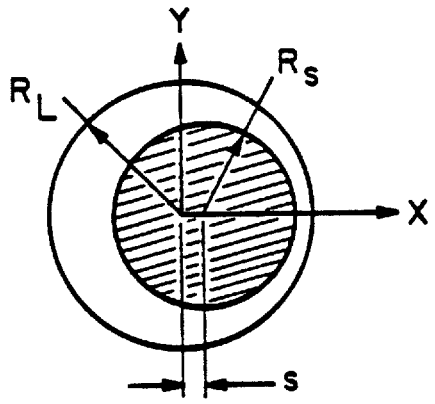

A) $s < R_L - R_S$

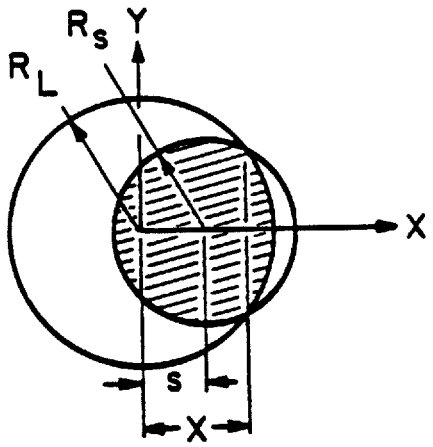

B) $R_L - R_S < s < R_L + R_S$

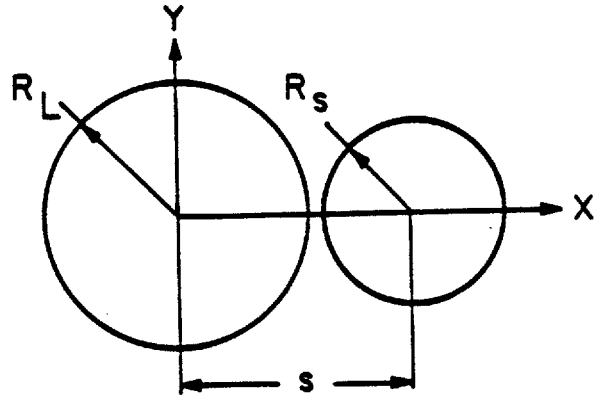

C) $s > R_L + R_S$

COMMON AREA OF TWO CIRCLES

Figure 2.13

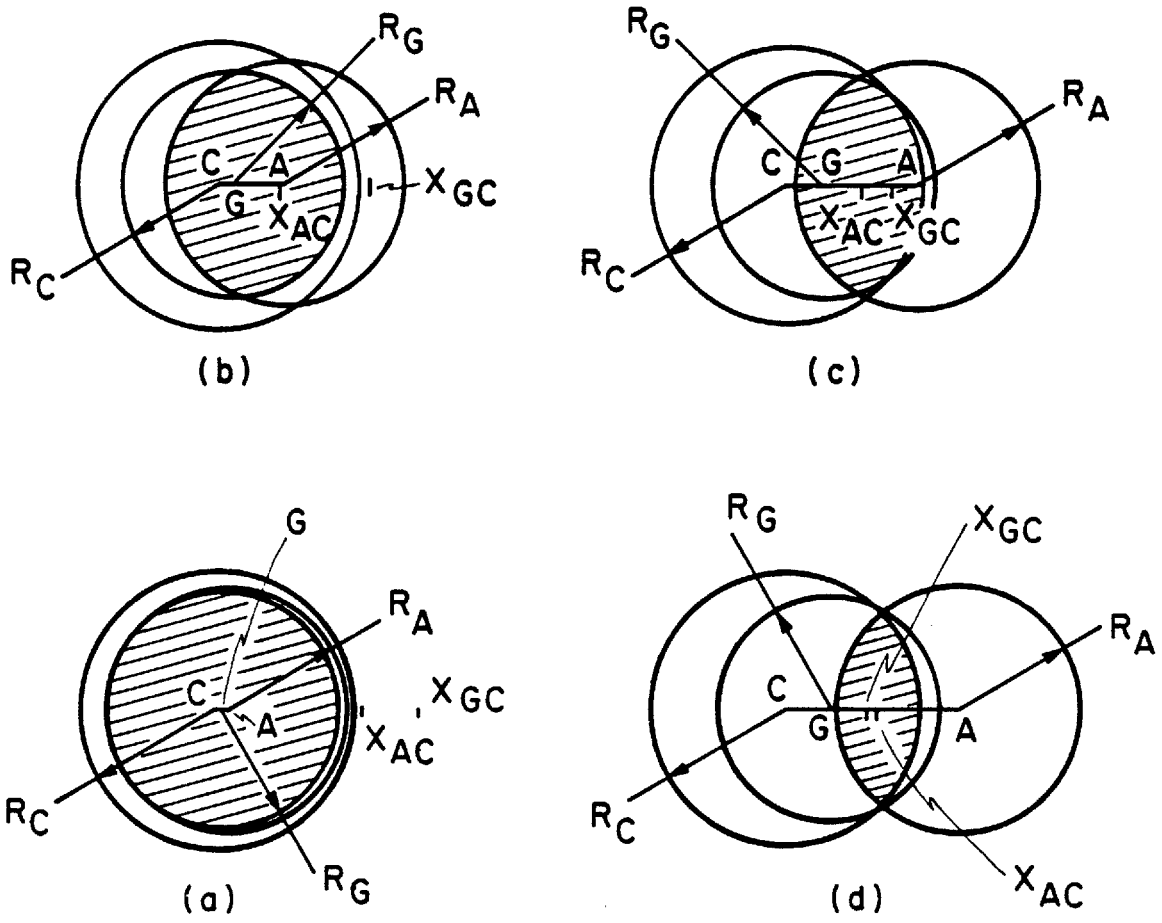
R_G
R_A
C
A
G
X_AC
X_GC
R_C
(b)
R_G
R_A
C
G
A
X_AC
X_GC
R_C
(c)
G
R_A
C
A
X_GC
X_AC
R_C
R_G
(a)
R_G
X_GC
R_A
C
G
A
R_C
X_AC
(d)

Figure 2.14

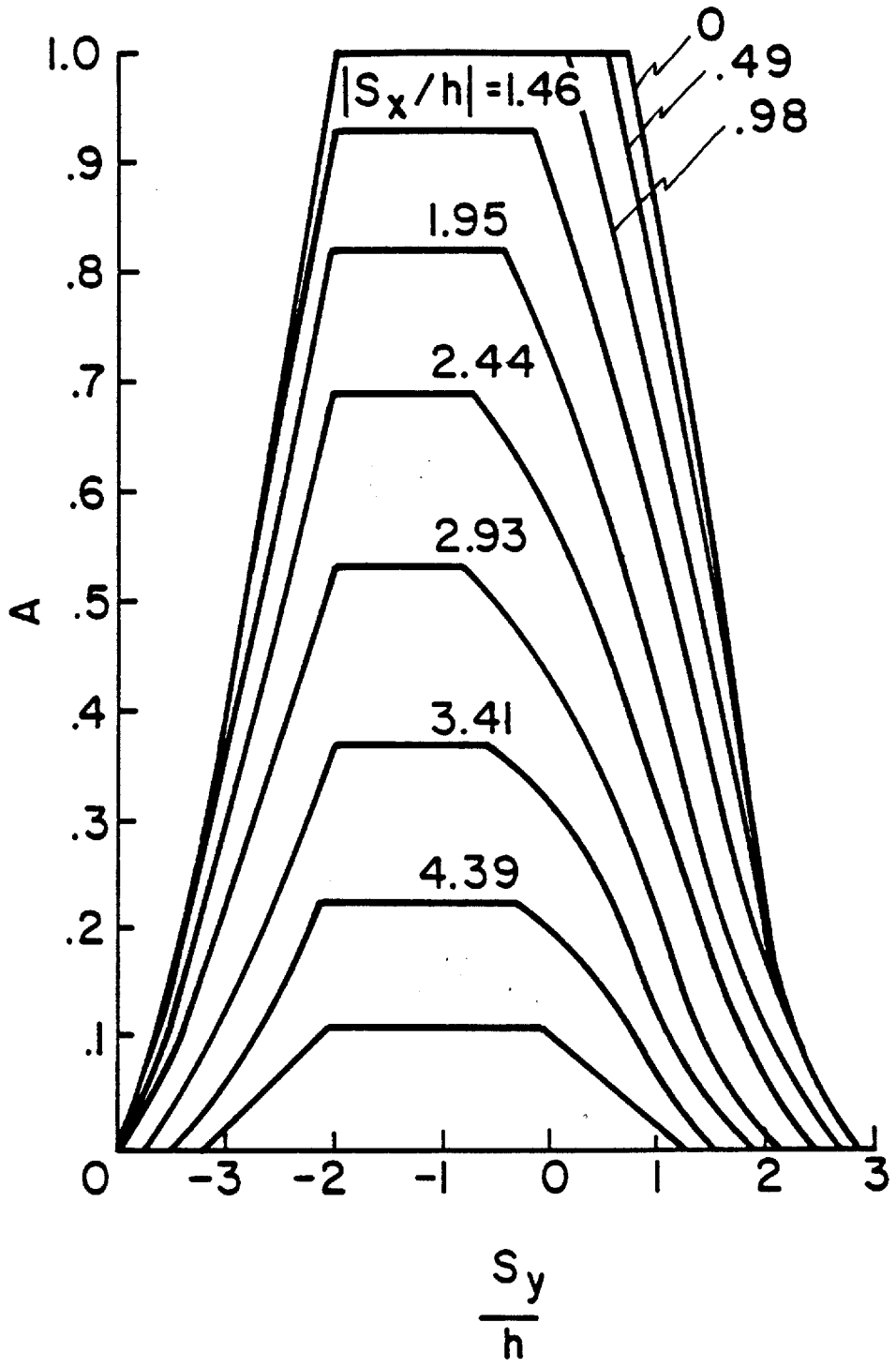

MAIN SENSOR SENSITIVE AREA vs S_y/h

Figure 2.15

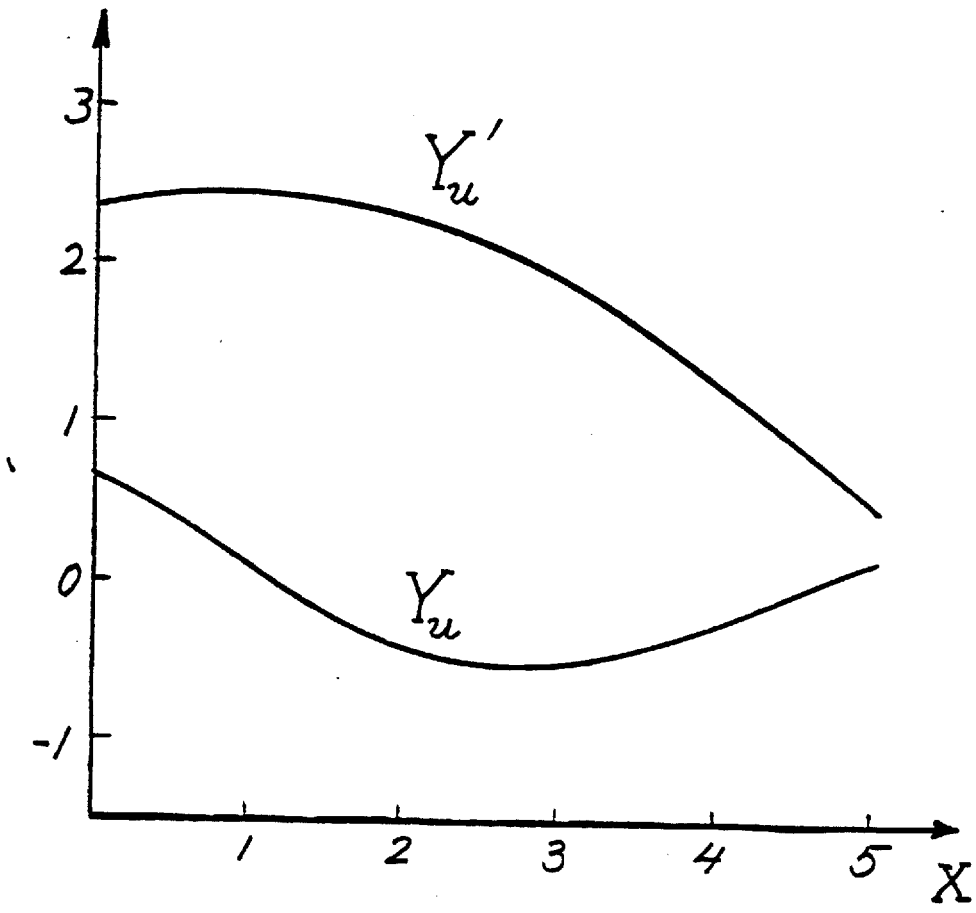

Figure 2.16

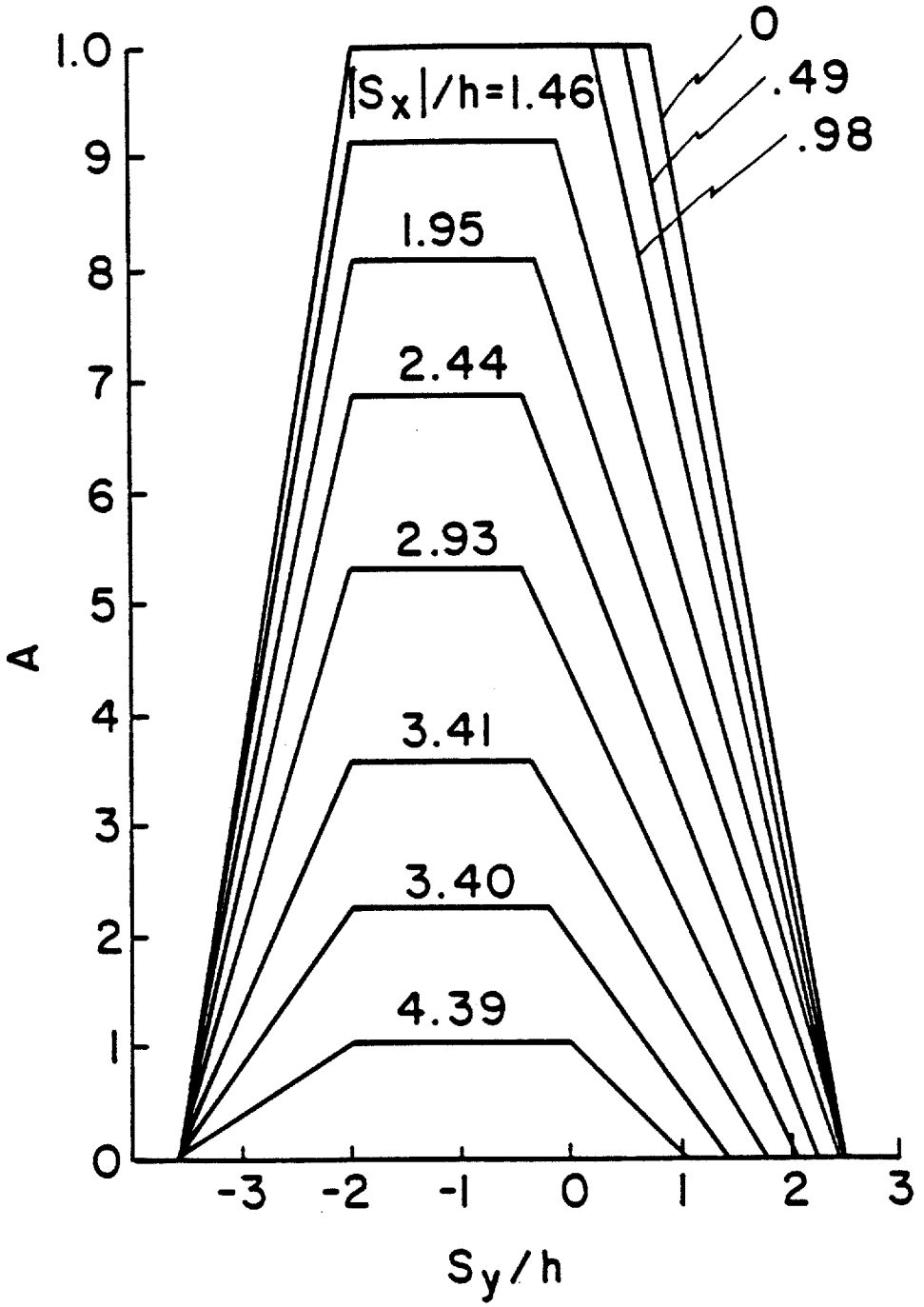

MAIN SENSOR SENSITIVE AREA vs S_y/h

(TRAPEZOIDAL APPROXIMATION)

Figure 2.17

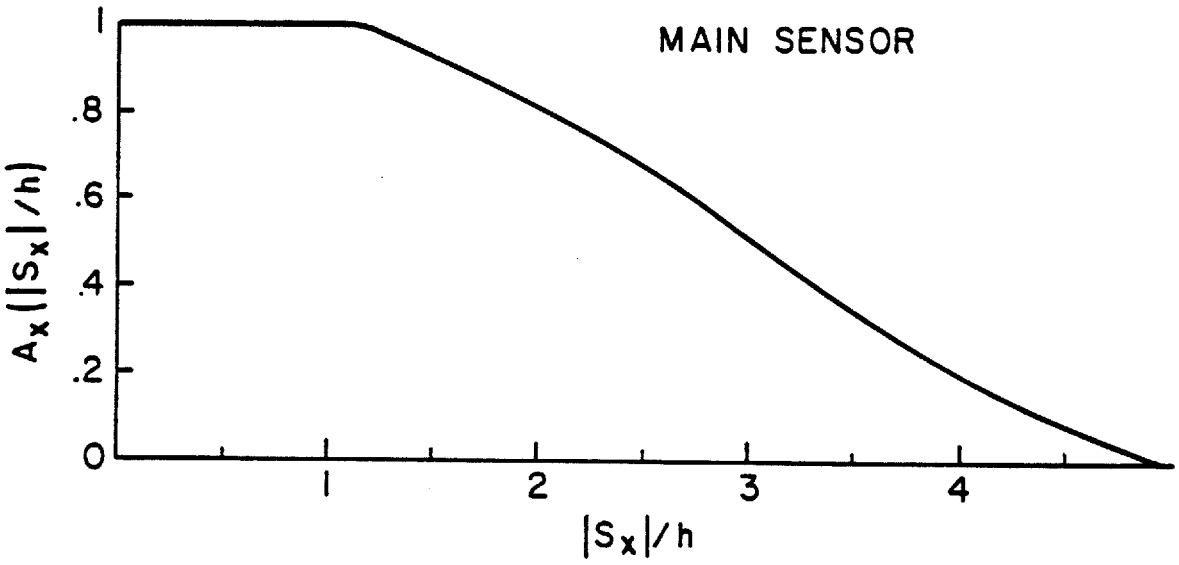

A_x vs $|S_x|/h$
(TRAPEZOIDAL APPROXIMATION)

Figure 2.18

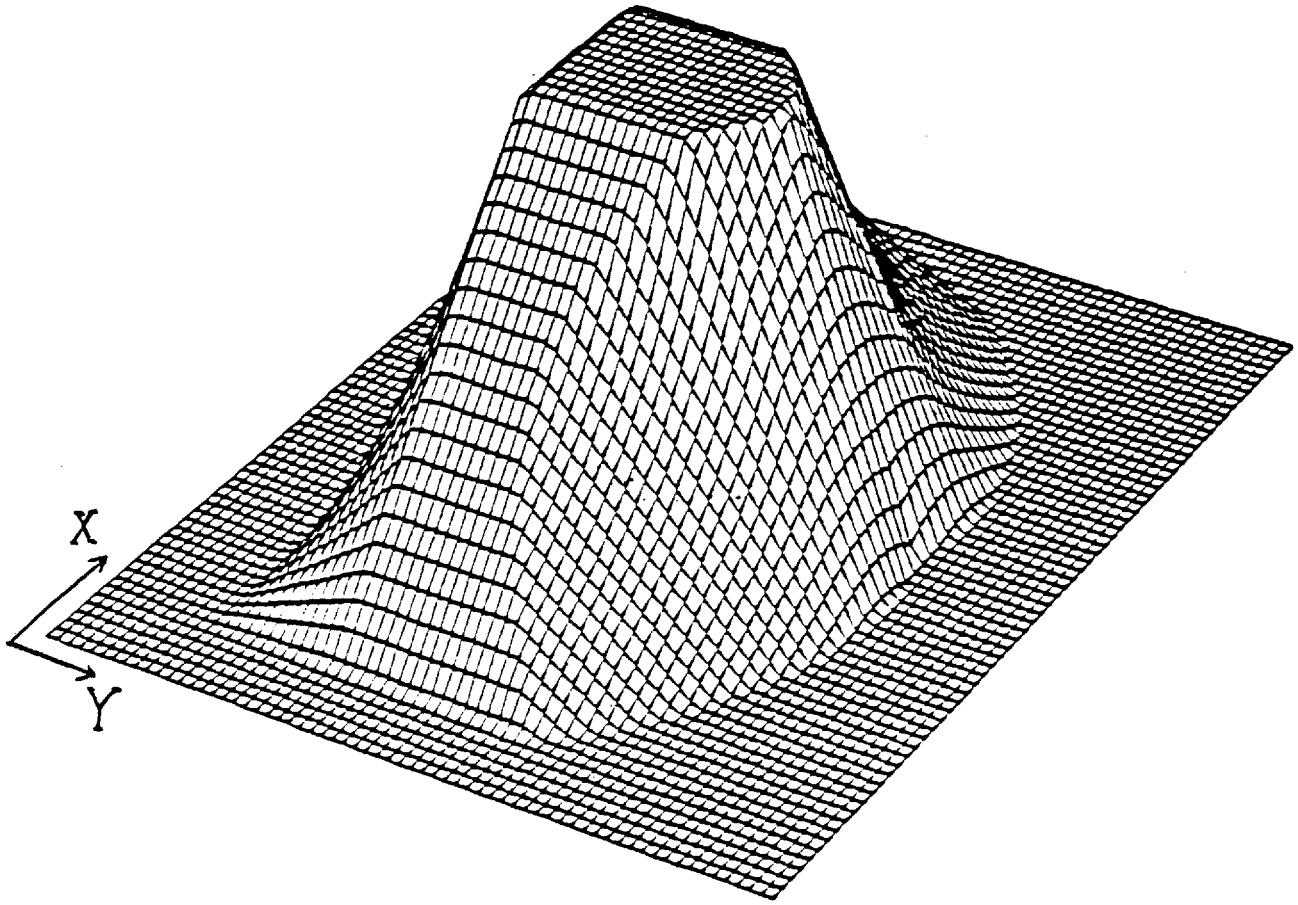

Figure 2.19

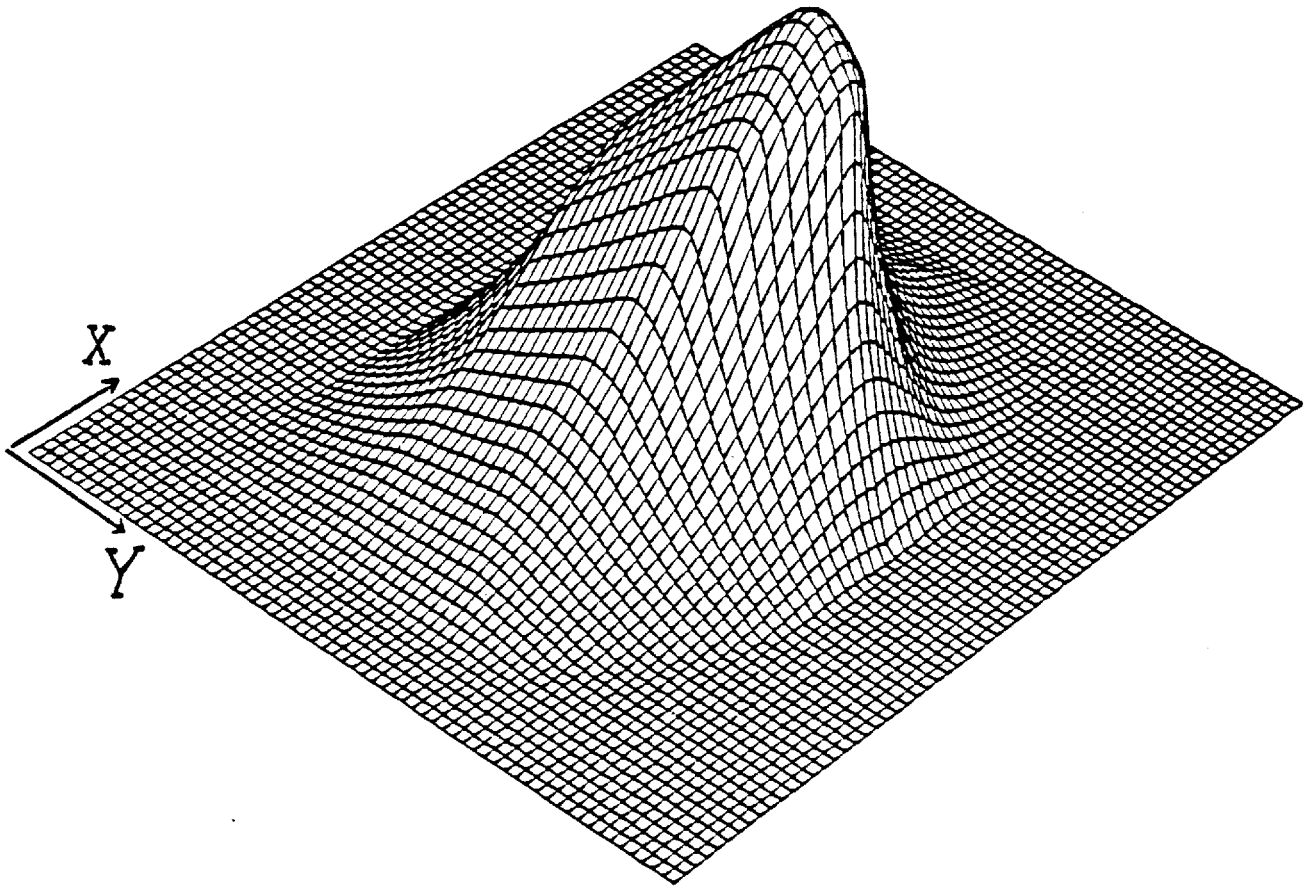

Figure 2.20

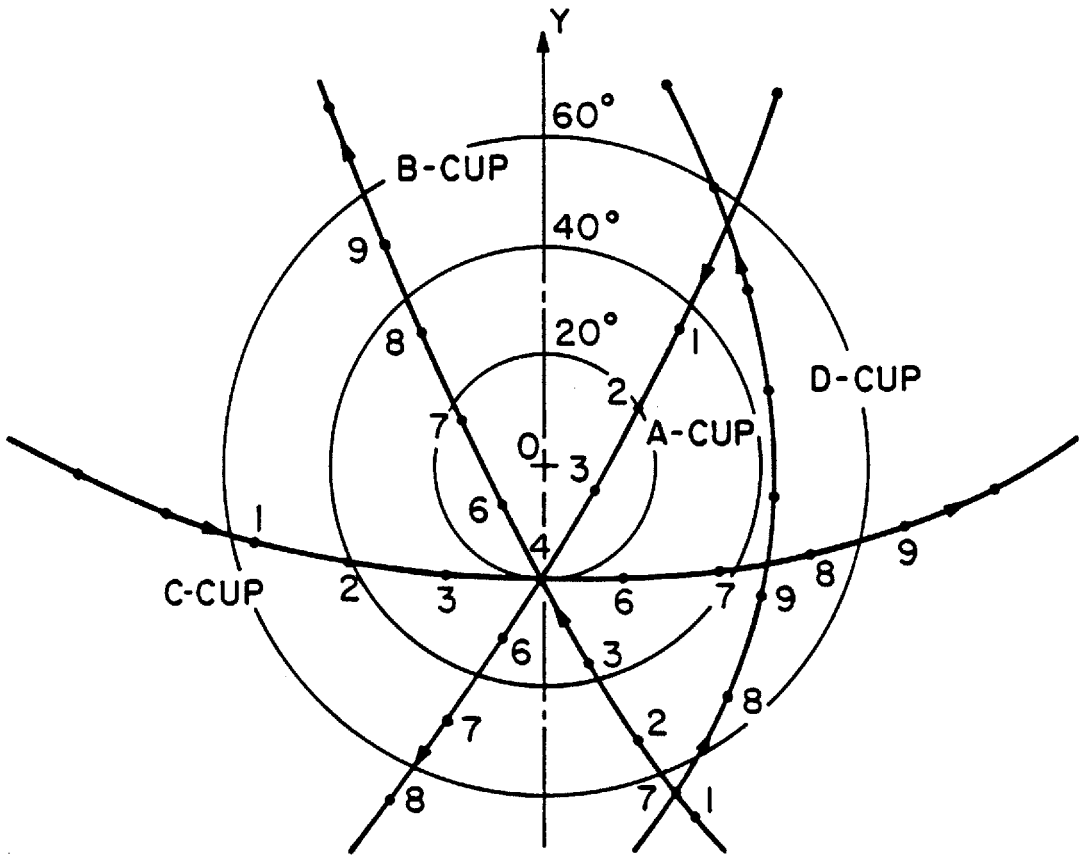

Figure 3.0

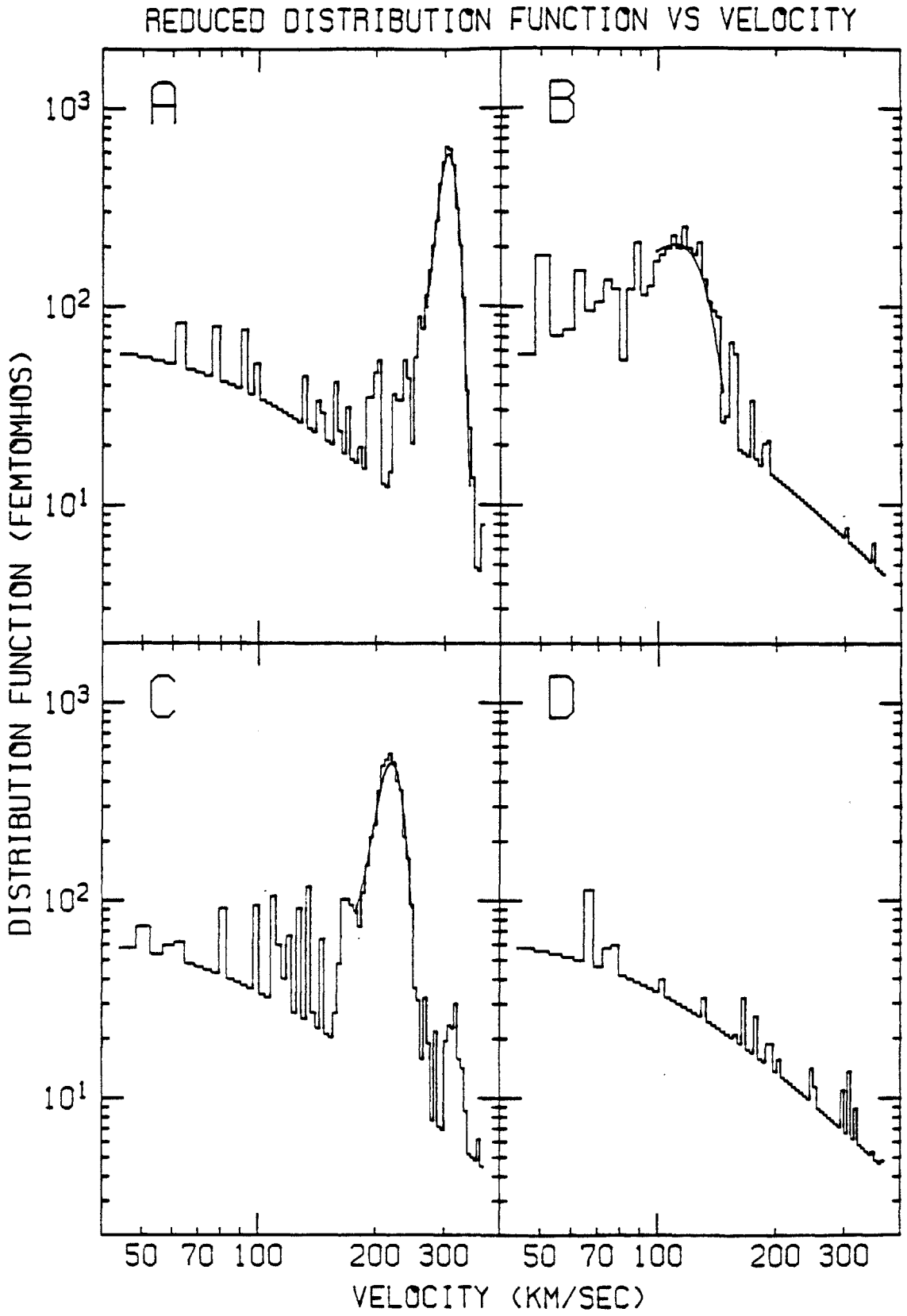
REDUCED DISTRIBUTION FUNCTION VS VELOCITY
A
B
C
D
10^3
10^2
10^1
DISTRIBUTION FUNCTION (FEMTOMHOS)
50 70 100 200 300
50 70 100 200 300
VELOCITY (KM/SEC)

Figure 3.1

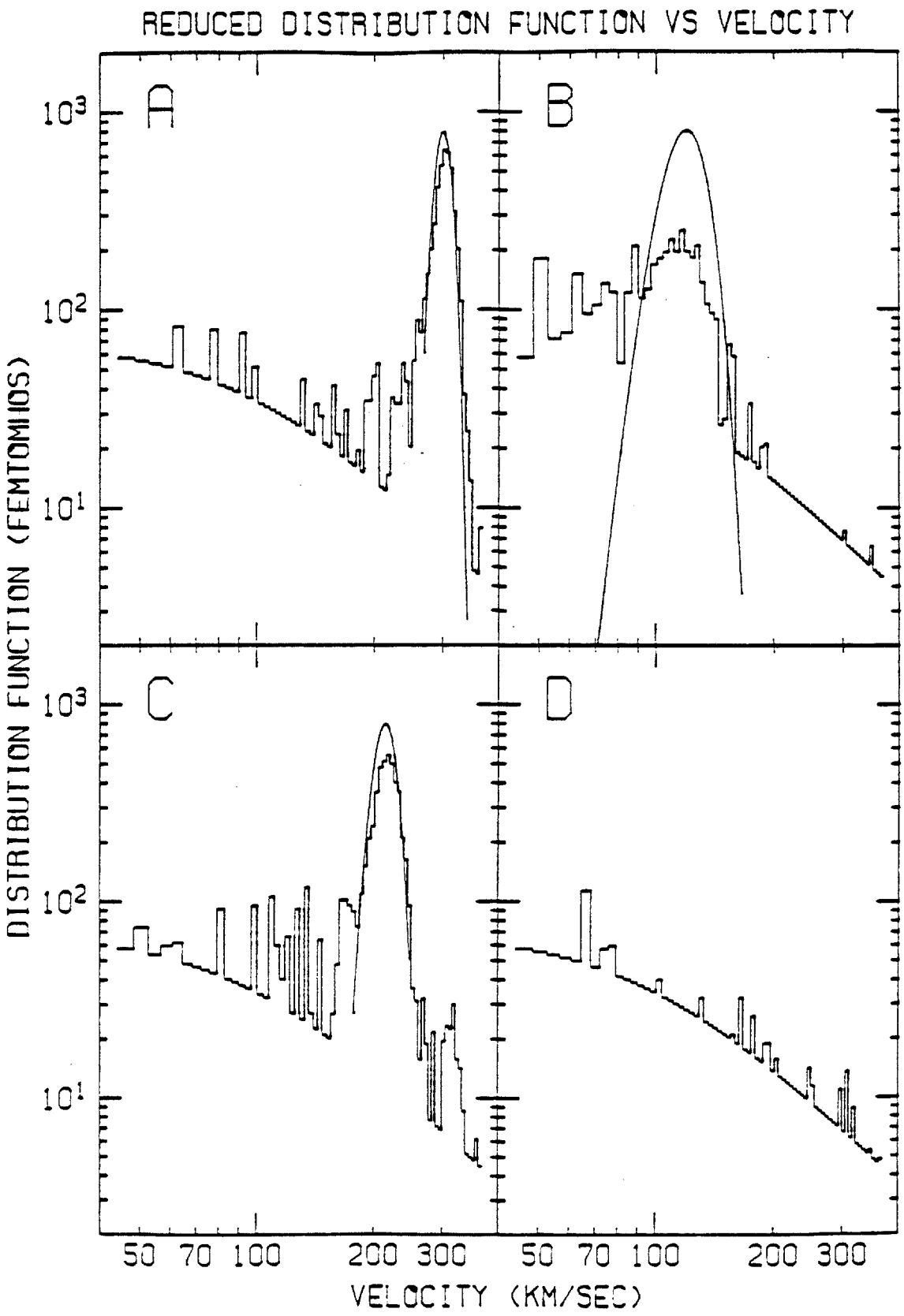
REDUCED DISTRIBUTION FUNCTION VS VELOCITY
A
B
C
D
10^3
10^2
10^1
DISTRIBUTION FUNCTION (FEMTOMHOS)
50 70 100 200 300
50 70 100 200 300
VELOCITY (KM/SEC)

Figure 3.1a

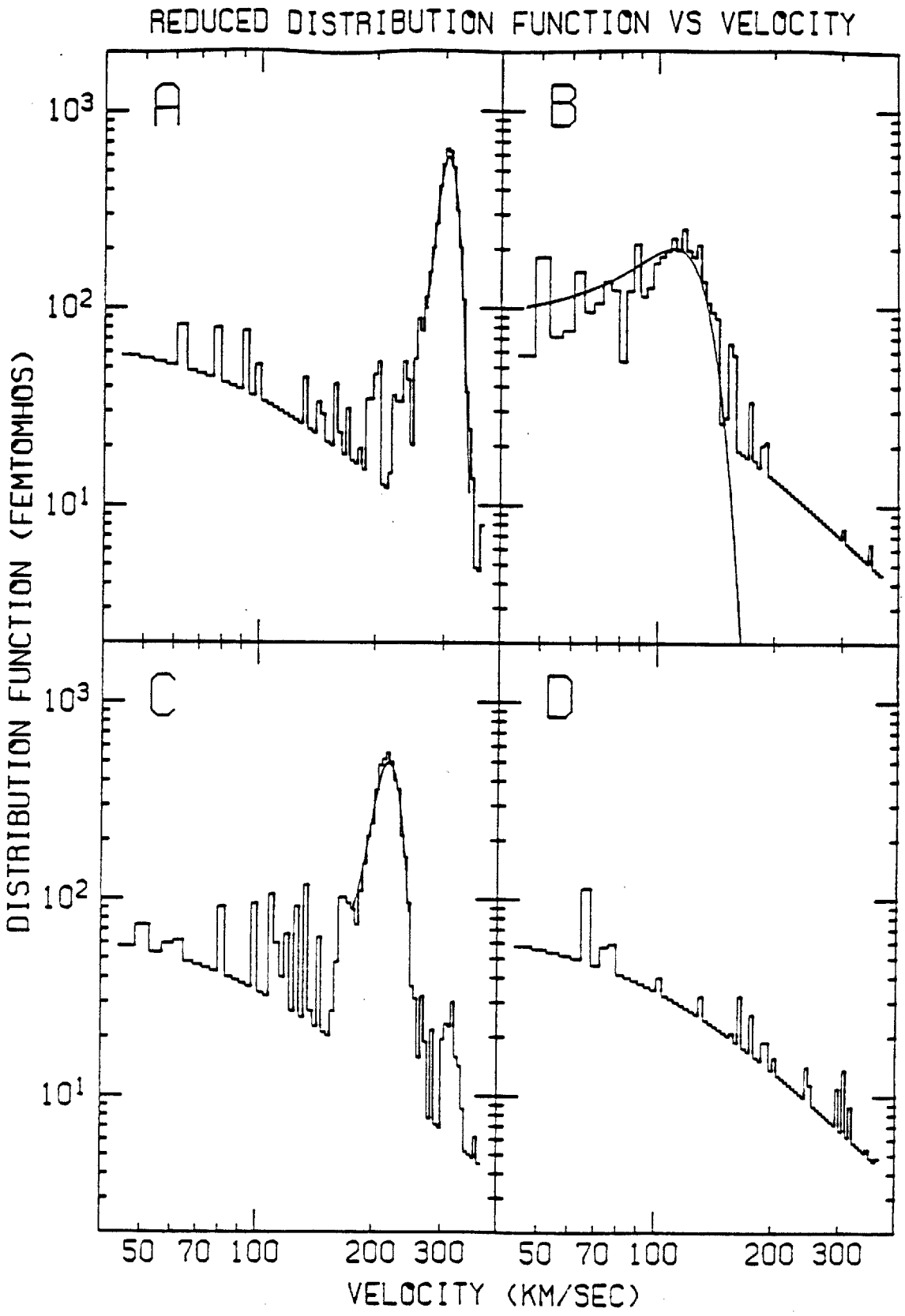
REDUCED DISTRIBUTION FUNCTION VS VELOCITY
A
B
C
D
10^3
10^2
10^1
DISTRIBUTION FUNCTION (FEMTOMHOS)
50 70 100 200 300
50 70 100 200 300
VELOCITY (KM/SEC)

Figure 3.1b

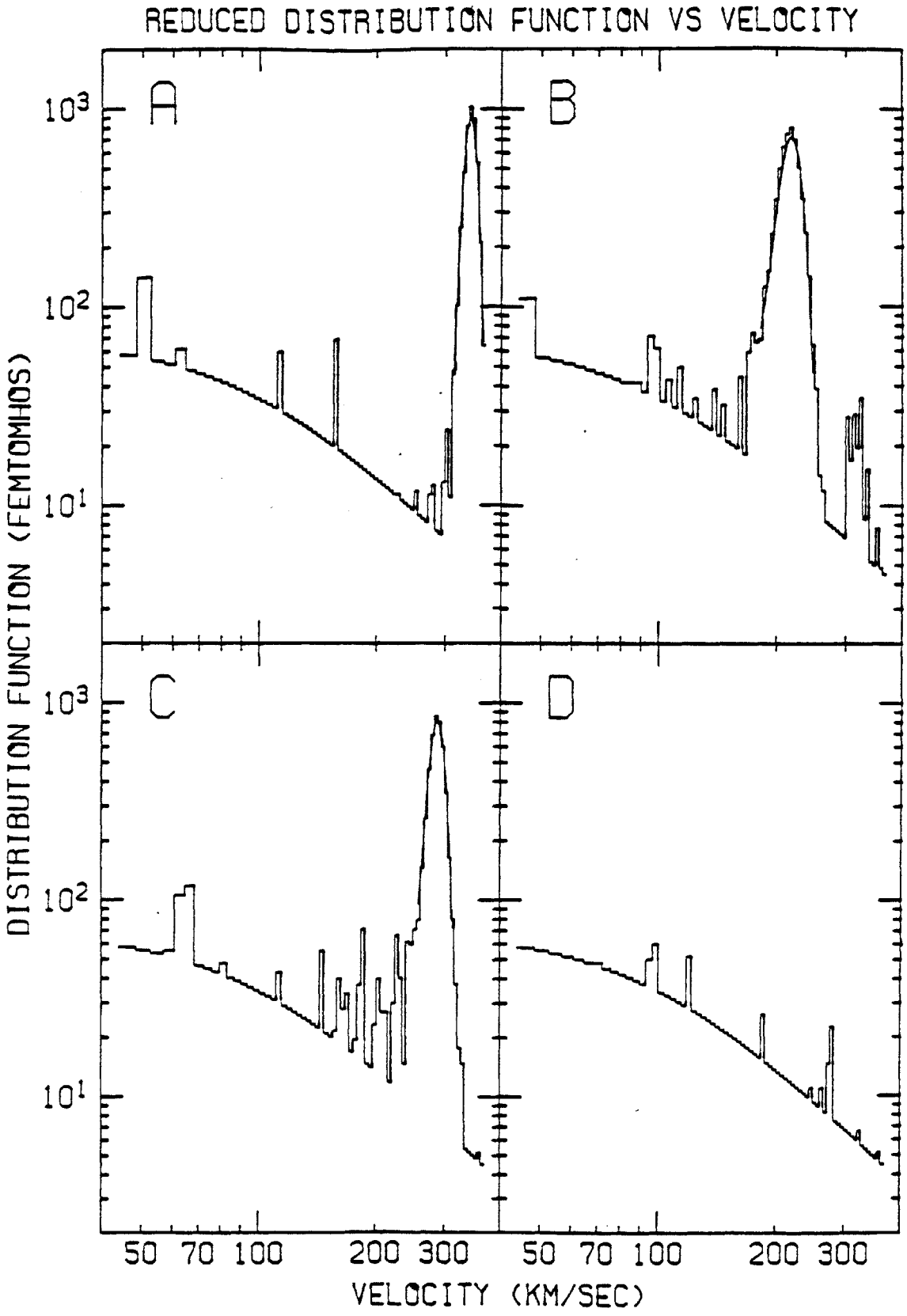
REDUCED DISTRIBUTION FUNCTION VS VELOCITY
A
B
C
D
10^3
10^2
10^1
DISTRIBUTION FUNCTION (FEMTOMHOS)
50 70 100 200 300
50 70 100 200 300
VELOCITY (KM/SEC)

Figure 3.2

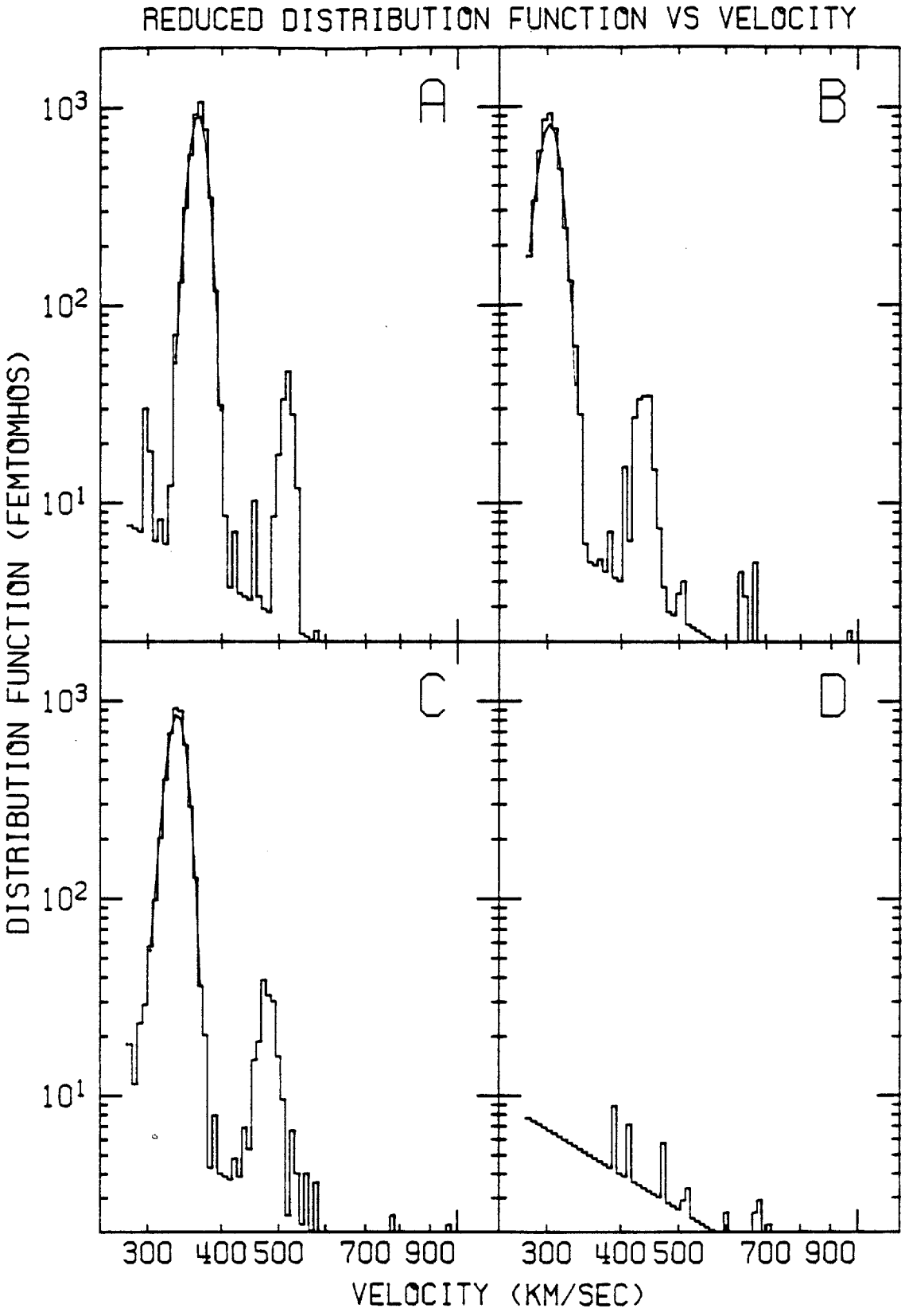
REDUCED DISTRIBUTION FUNCTION VS VELOCITY
A
B
C
D
10^3
10^2
10^1
DISTRIBUTION FUNCTION (FEMTOMHOS)
300 400 500 700 900
300 400 500 700 900
VELOCITY (KM/SEC)

Figure 3.3

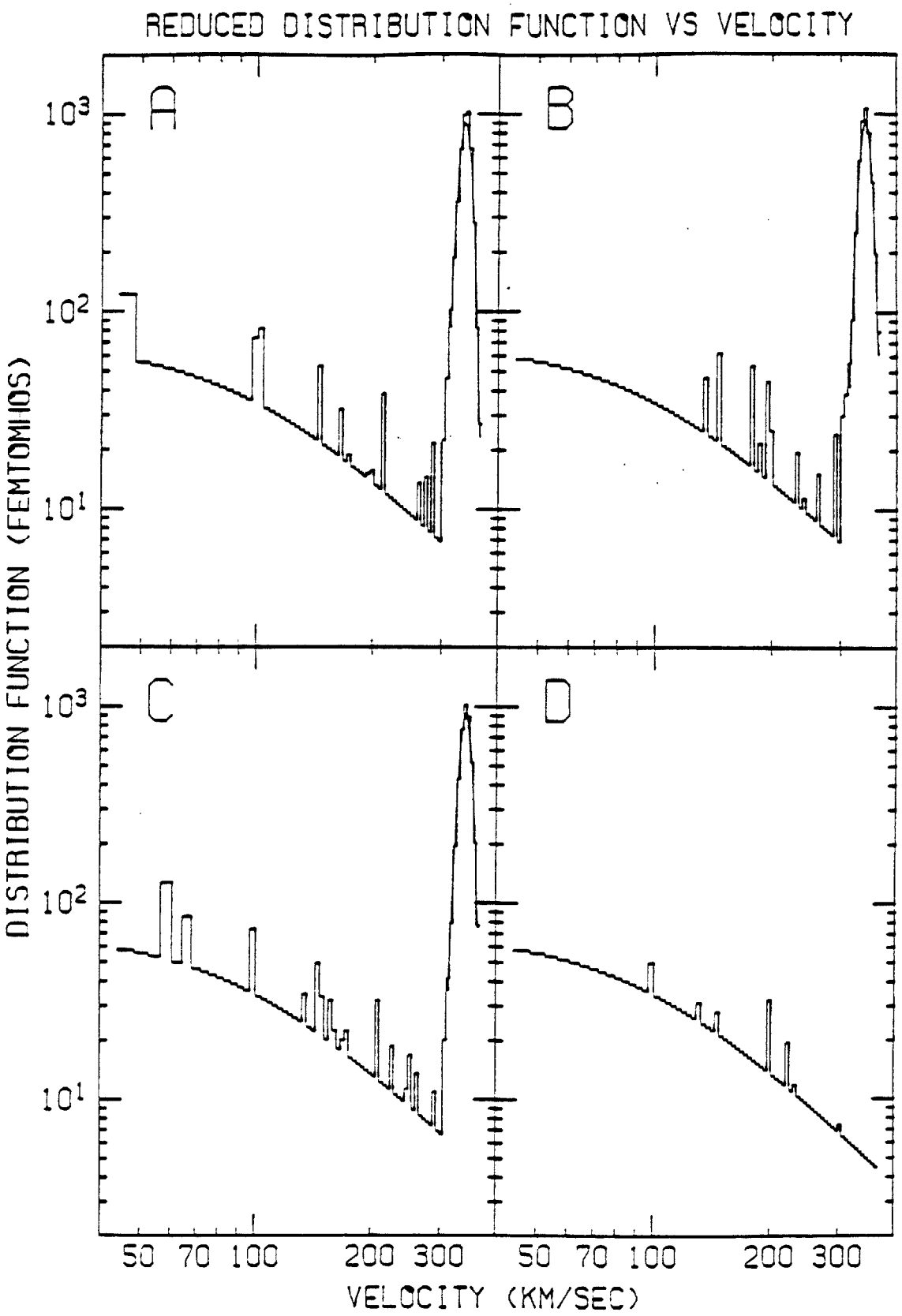
REDUCED DISTRIBUTION FUNCTION VS VELOCITY
A
B
C
D
10^3
10^2
10^1
DISTRIBUTION FUNCTION (FEMTOMIOS)
50 70 100 200 300
50 70 100 200 300
VELOCITY (KM/SEC)

Figure 3.4

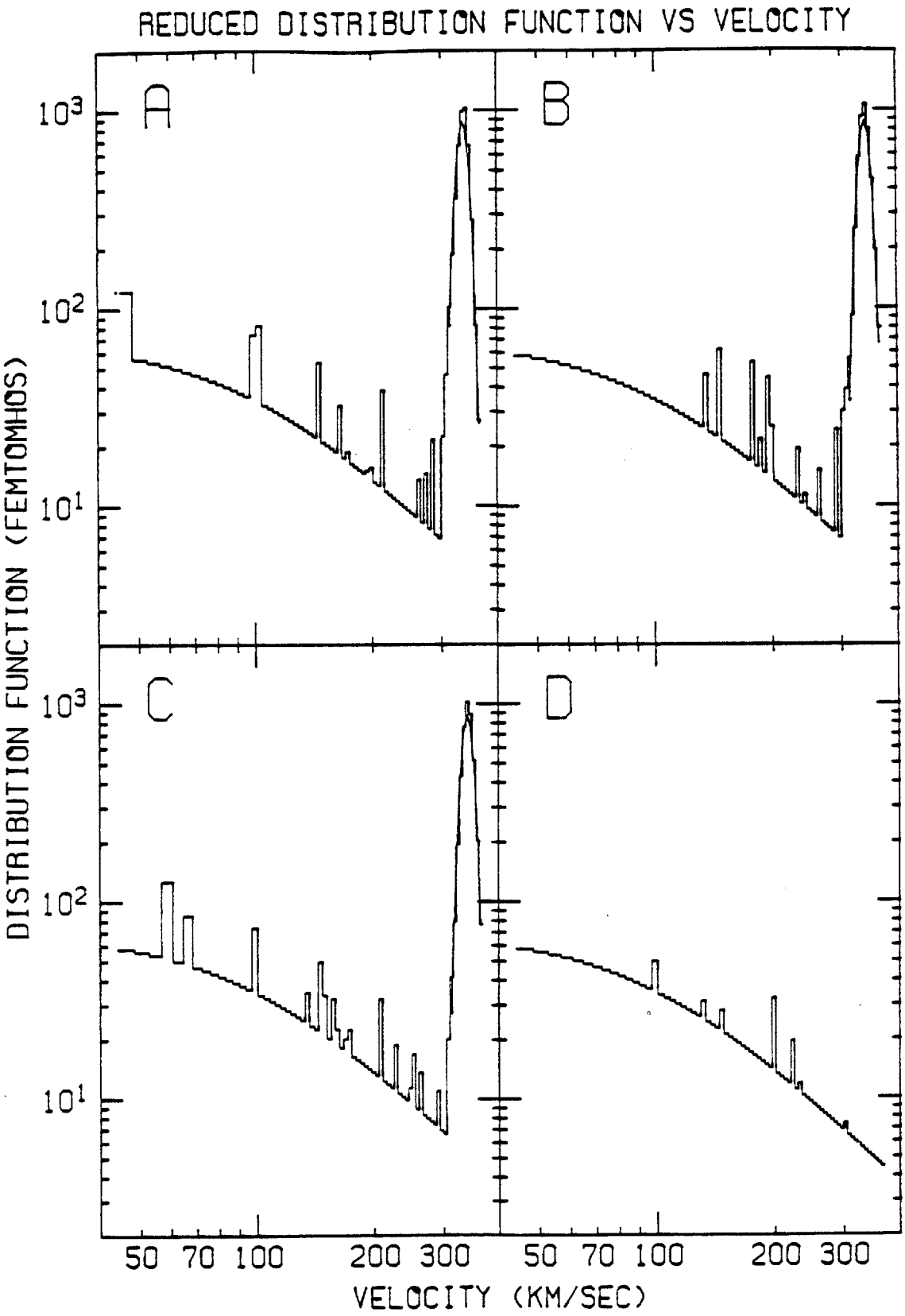
REDUCED DISTRIBUTION FUNCTION VS VELOCITY
A
B
C
D
10^3
10^2
10^1
DISTRIBUTION FUNCTION (FEMTOMHOS)
50 70 100 200 300
50 70 100 200 300
VELOCITY (KM/SEC)

Figure 3.4a

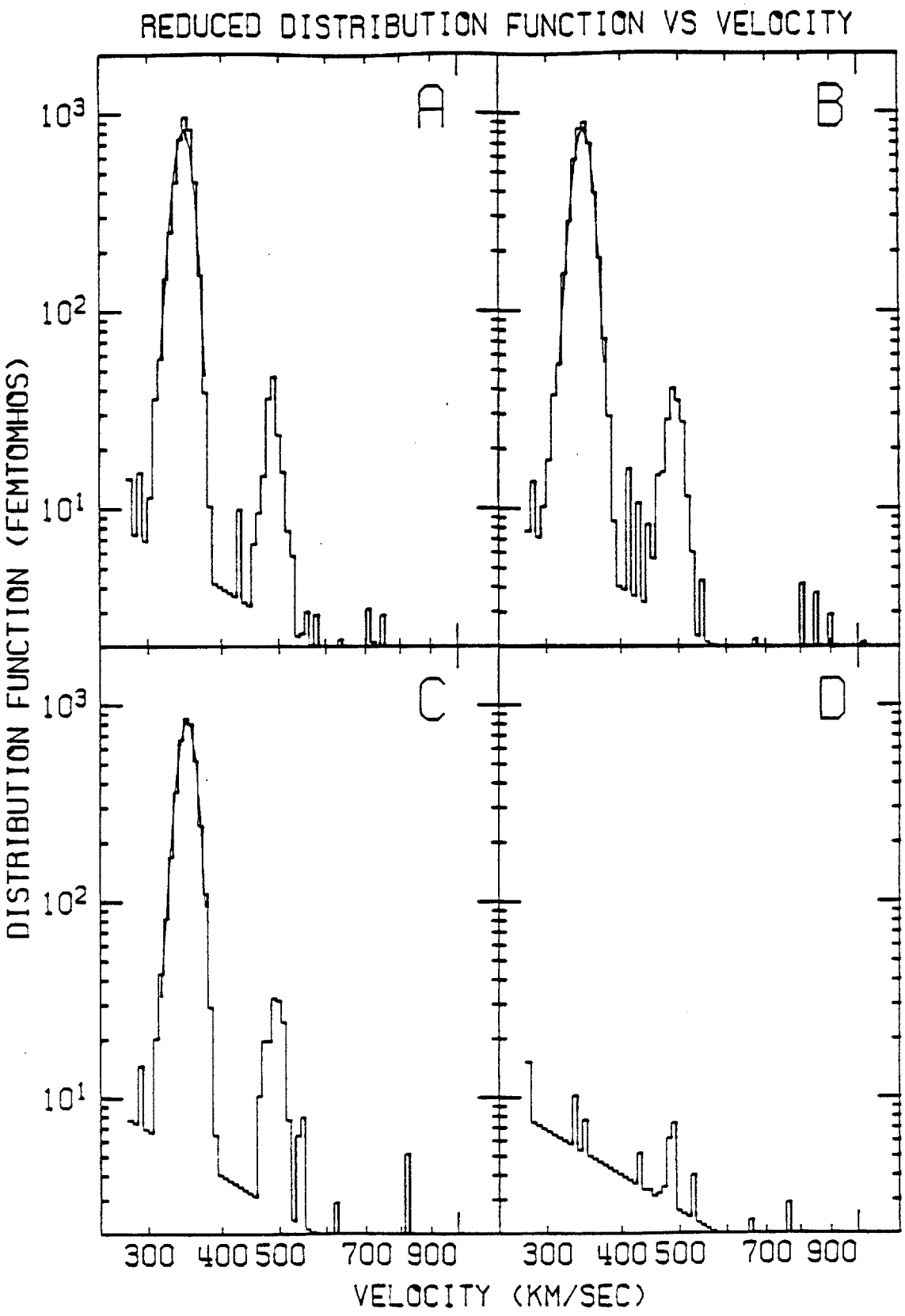
REDUCED DISTRIBUTION FUNCTION VS VELOCITY
A
B
C
D
10^3
10^2
10^1
DISTRIBUTION FUNCTION (FEMTOMHOS)
300 400 500 700 900
300 400 500 700 900
VELOCITY (KM/SEC)

Figure 3.5

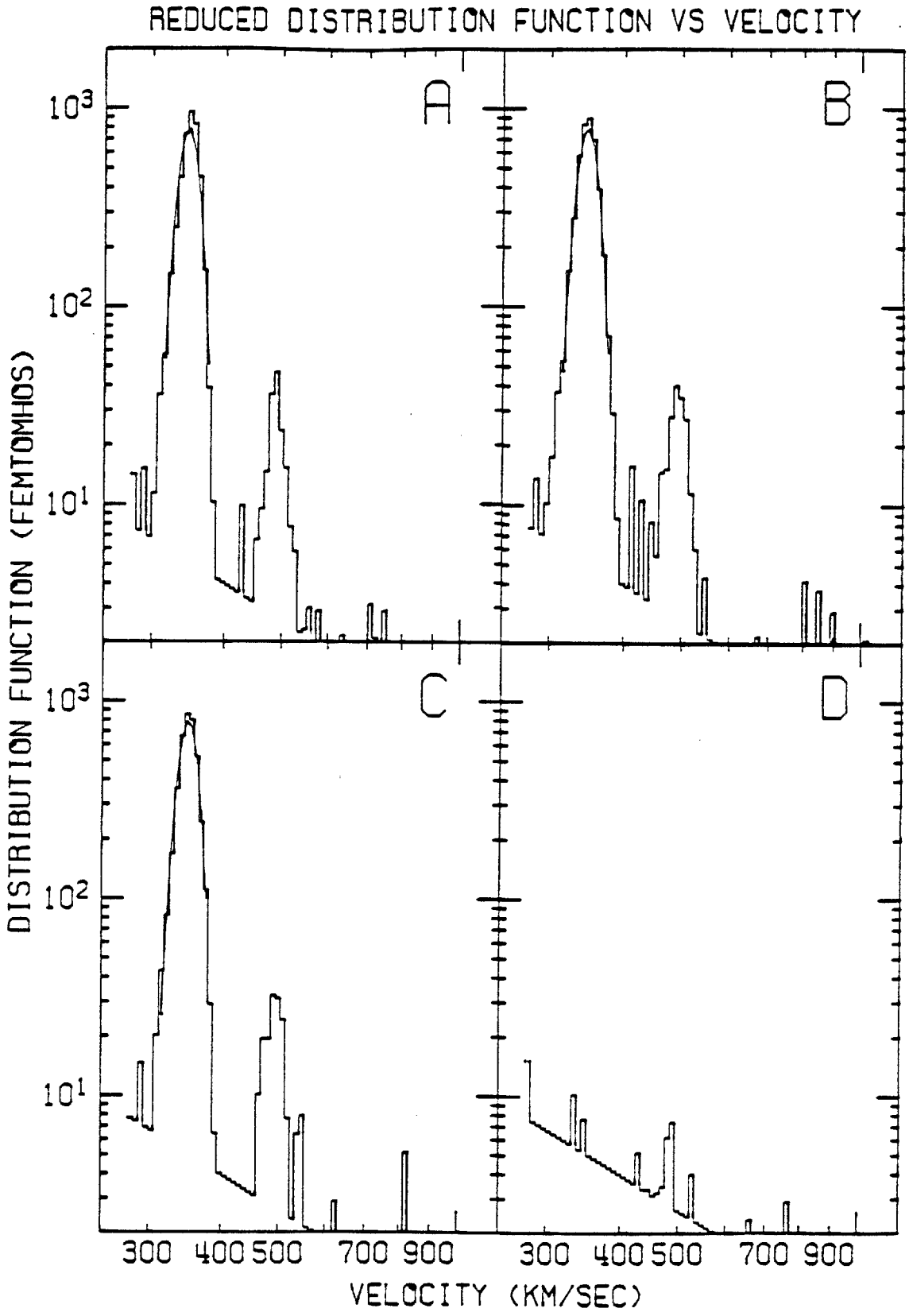
REDUCED DISTRIBUTION FUNCTION VS VELOCITY
A
B
C
D
10^3
10^2
10^1
DISTRIBUTION FUNCTION (FEMTOMHOS)
300 400 500 700 900
300 400 500 700 900
VELOCITY (KM/SEC)

Figure 3.5a

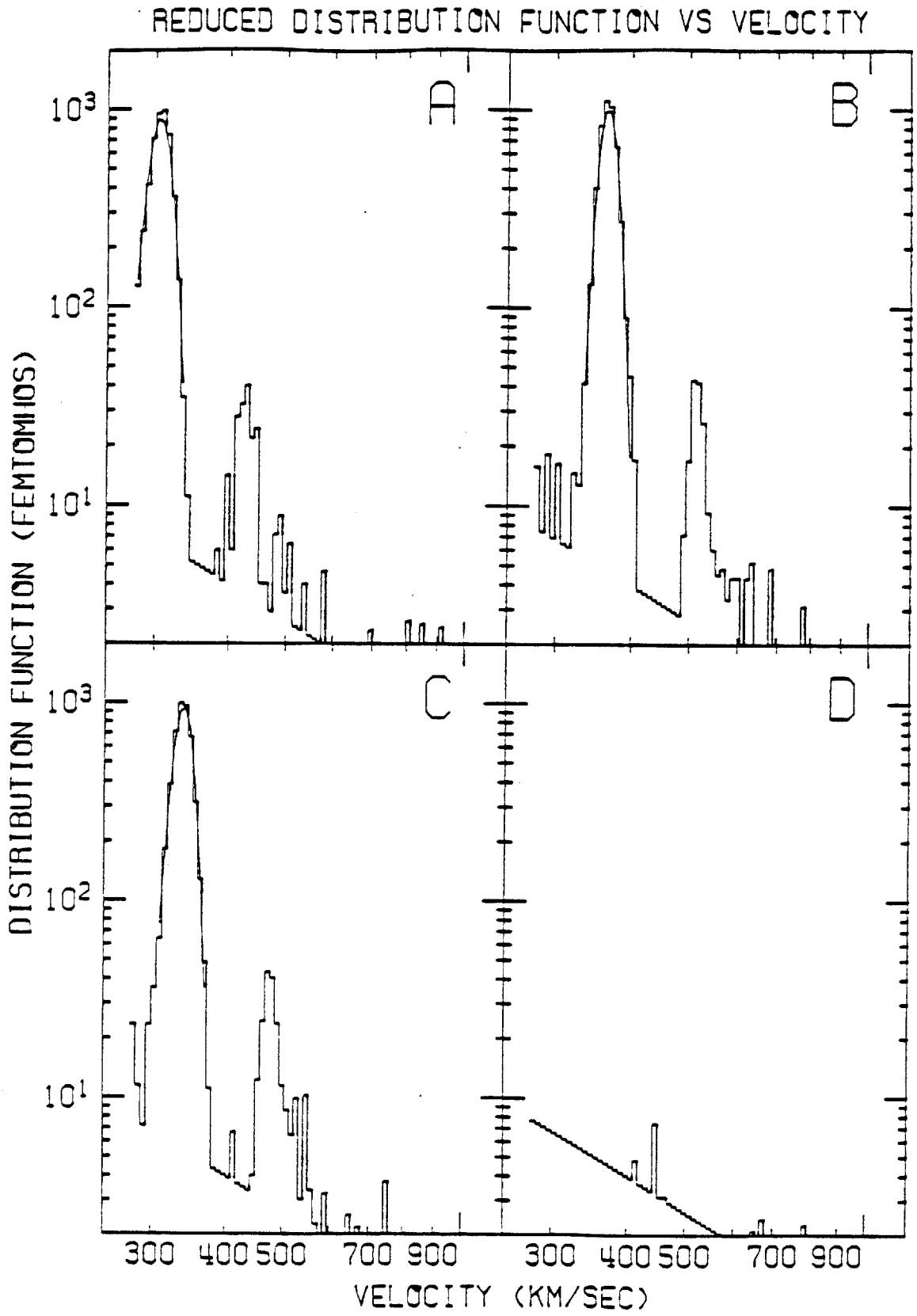
REDUCED DISTRIBUTION FUNCTION VS VELOCITY
A
B
C
D
10^3
10^2
10^1
DISTRIBUTION FUNCTION (FEMTOMHOS)
300 400 500 700 900
300 400 500 700 900
VELOCITY (KM/SEC)

Figure 3.6

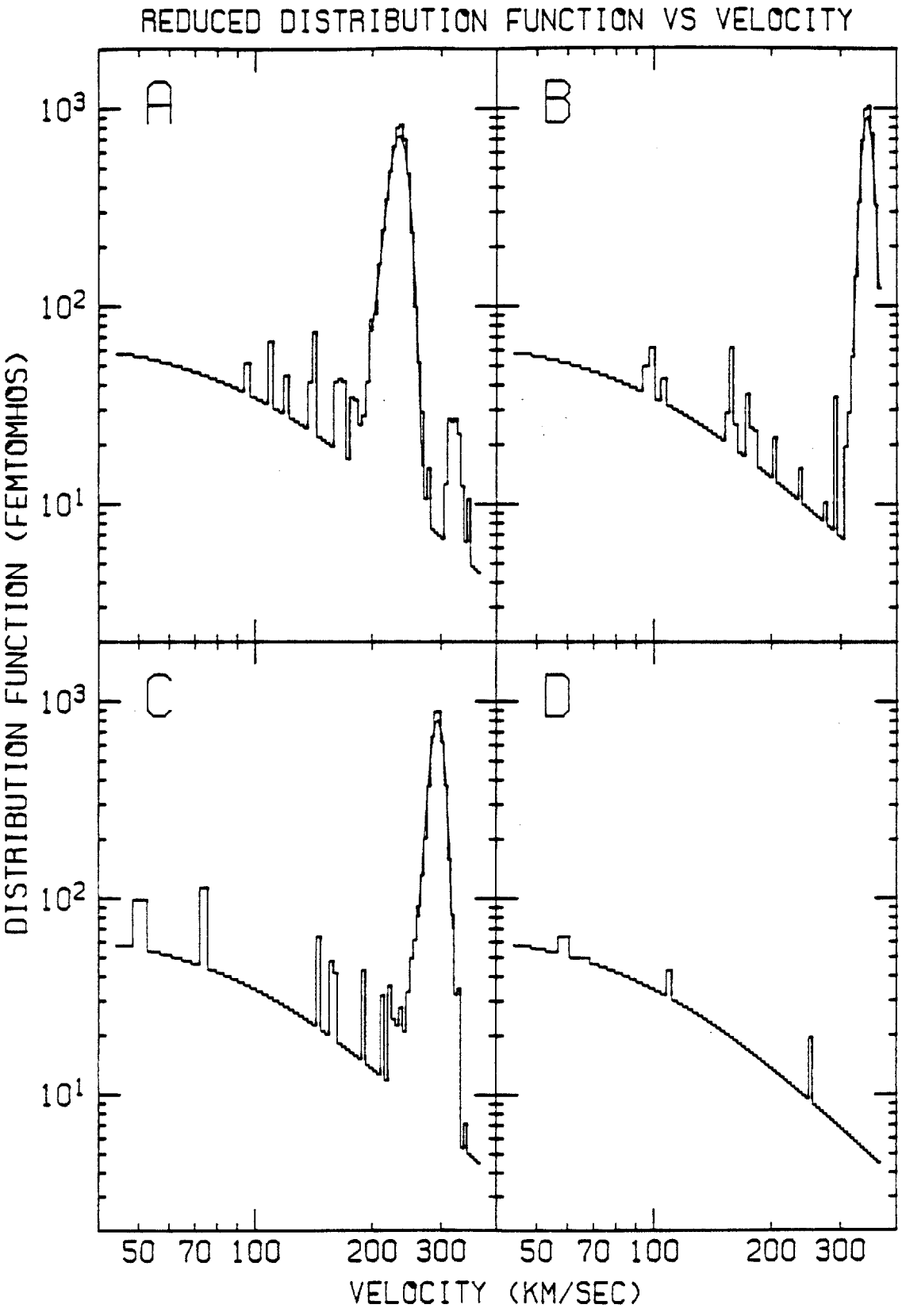
REDUCED DISTRIBUTION FUNCTION VS VELOCITY
A
B
C
D
10^3
10^2
10^1
DISTRIBUTION FUNCTION (FEMTOMHOS)
50 70 100 200 300
50 70 100 200 300
VELOCITY (KM/SEC)

Figure 3.7

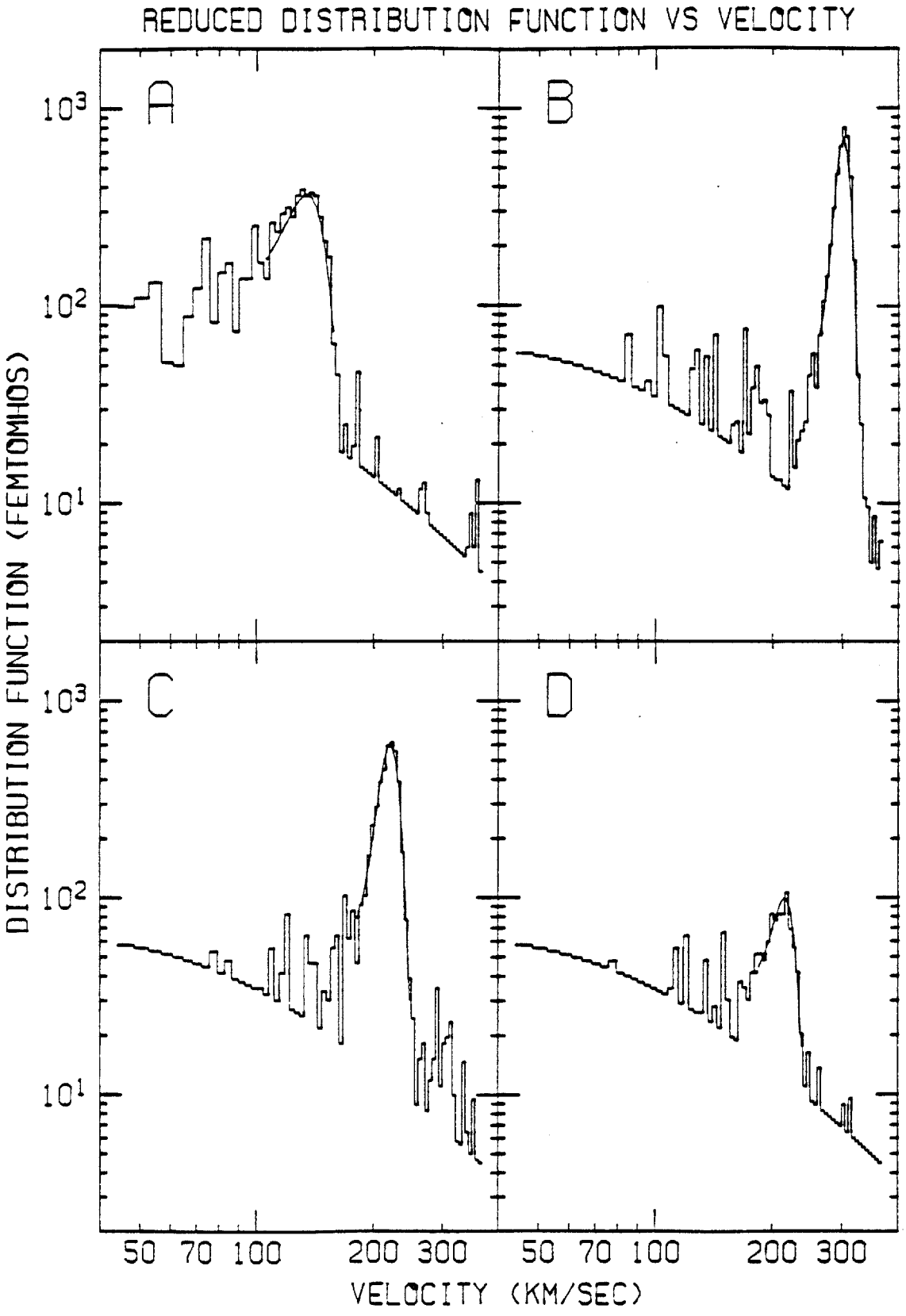
REDUCED DISTRIBUTION FUNCTION VS VELOCITY
A
B
C
D
10^3
10^2
10^1
DISTRIBUTION FUNCTION (FEMTOMHOS)
50 70 100 200 300
50 70 100 200 300
VELOCITY (KM/SEC)

Figure 3.8

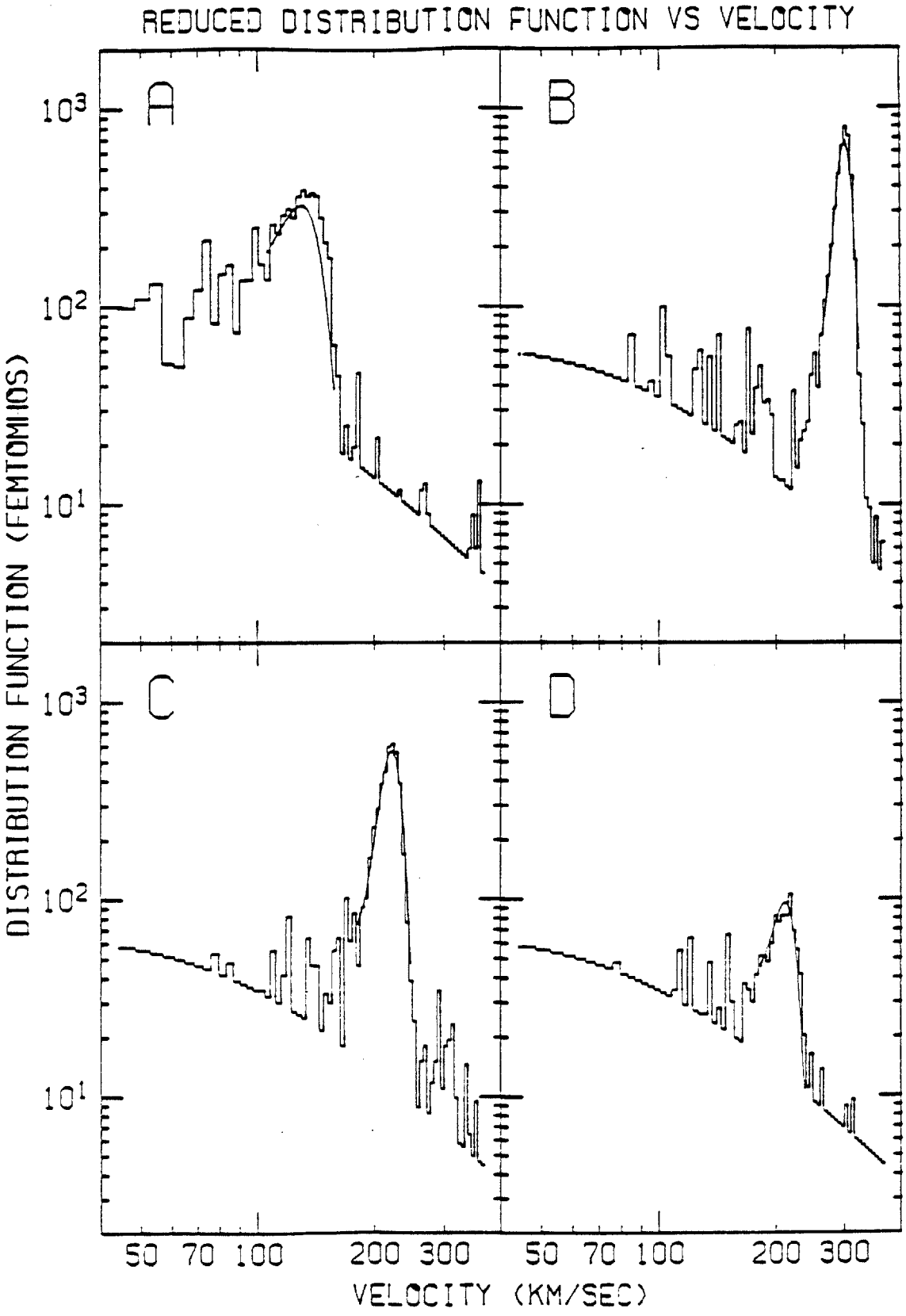
REDUCED DISTRIBUTION FUNCTION VS VELOCITY
A
B
C
D
10^3
10^2
10^1
DISTRIBUTION FUNCTION (FEMTOMHOS)
50 70 100 200 300
50 70 100 200 300
VELOCITY (KM/SEC)

Figure 3.8a

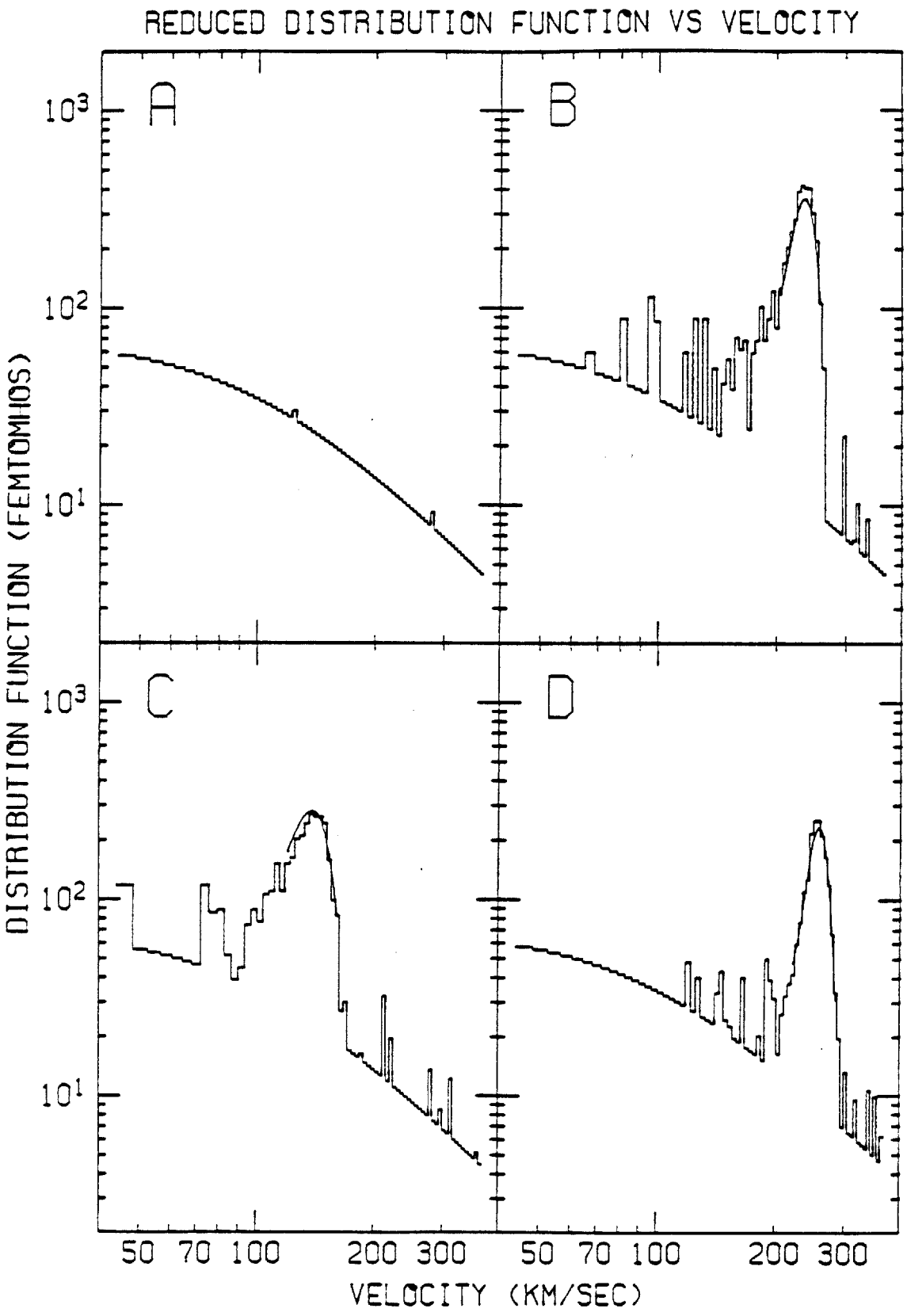
REDUCED DISTRIBUTION FUNCTION VS VELOCITY
A
B
C
D
10^3
10^2
10^1
DISTRIBUTION FUNCTION (FEMTOMHOS)
50 70 100 200 300
50 70 100 200 300
VELOCITY (KM/SEC)

Figure 3.9

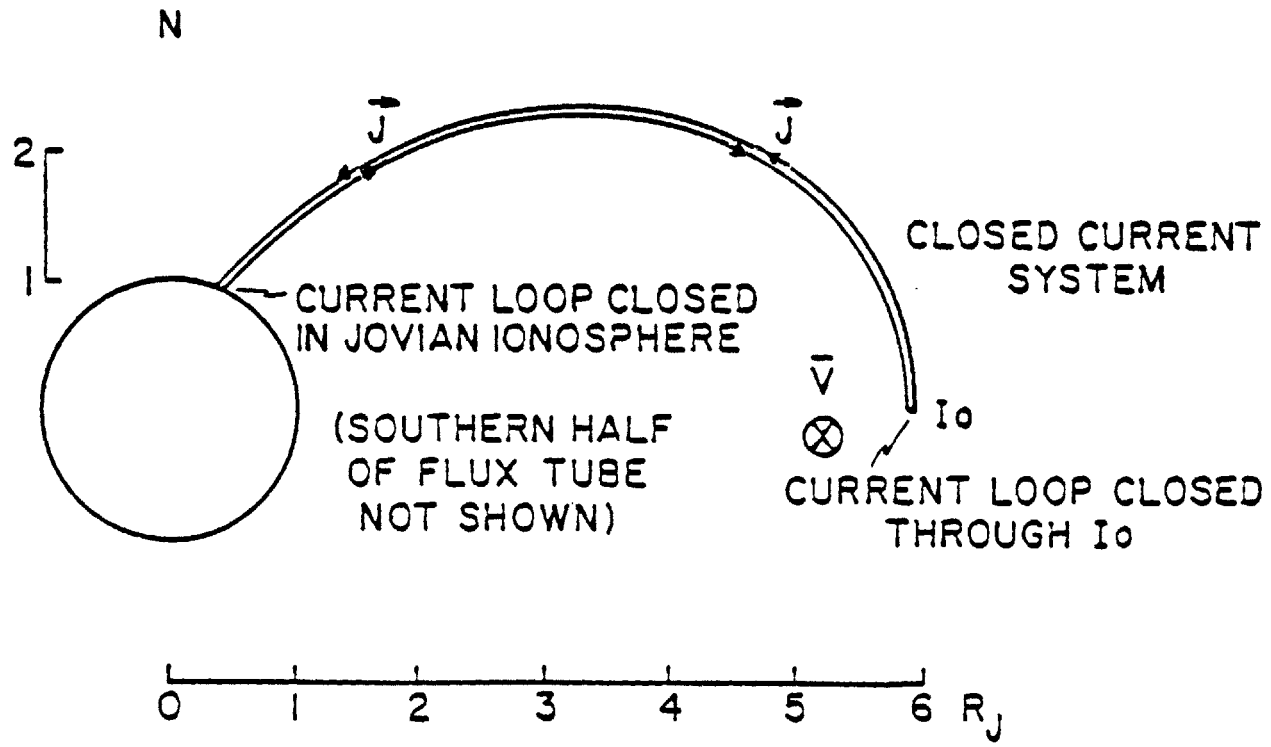

Io FLUX TUBE-NORTHERN HEMISPHERE

Figure 4.1

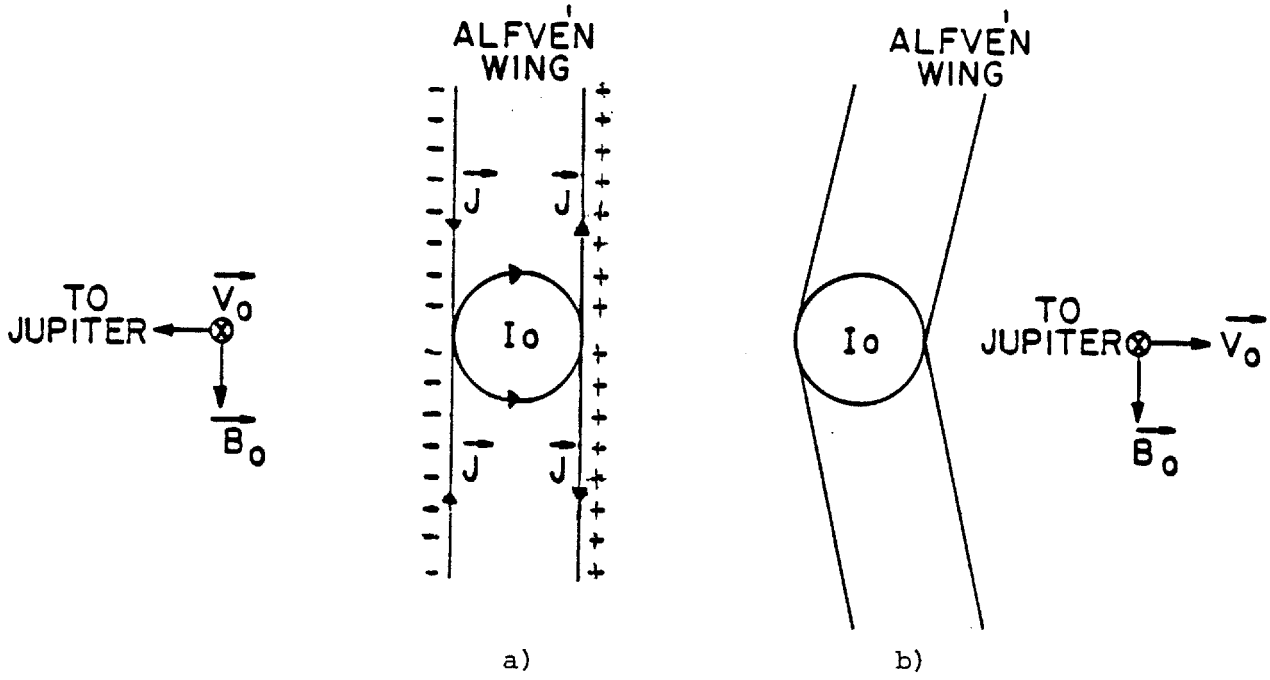
ALFVEN WING
TO JUPITER
$\vec{V}_o$
$\vec{B}_o$
$\vec{J}$
Io
a)
ALFVEN WING
Io
TO JUPITER
$\vec{V}_o$
$\vec{B}_o$
b)

Figure 4.2

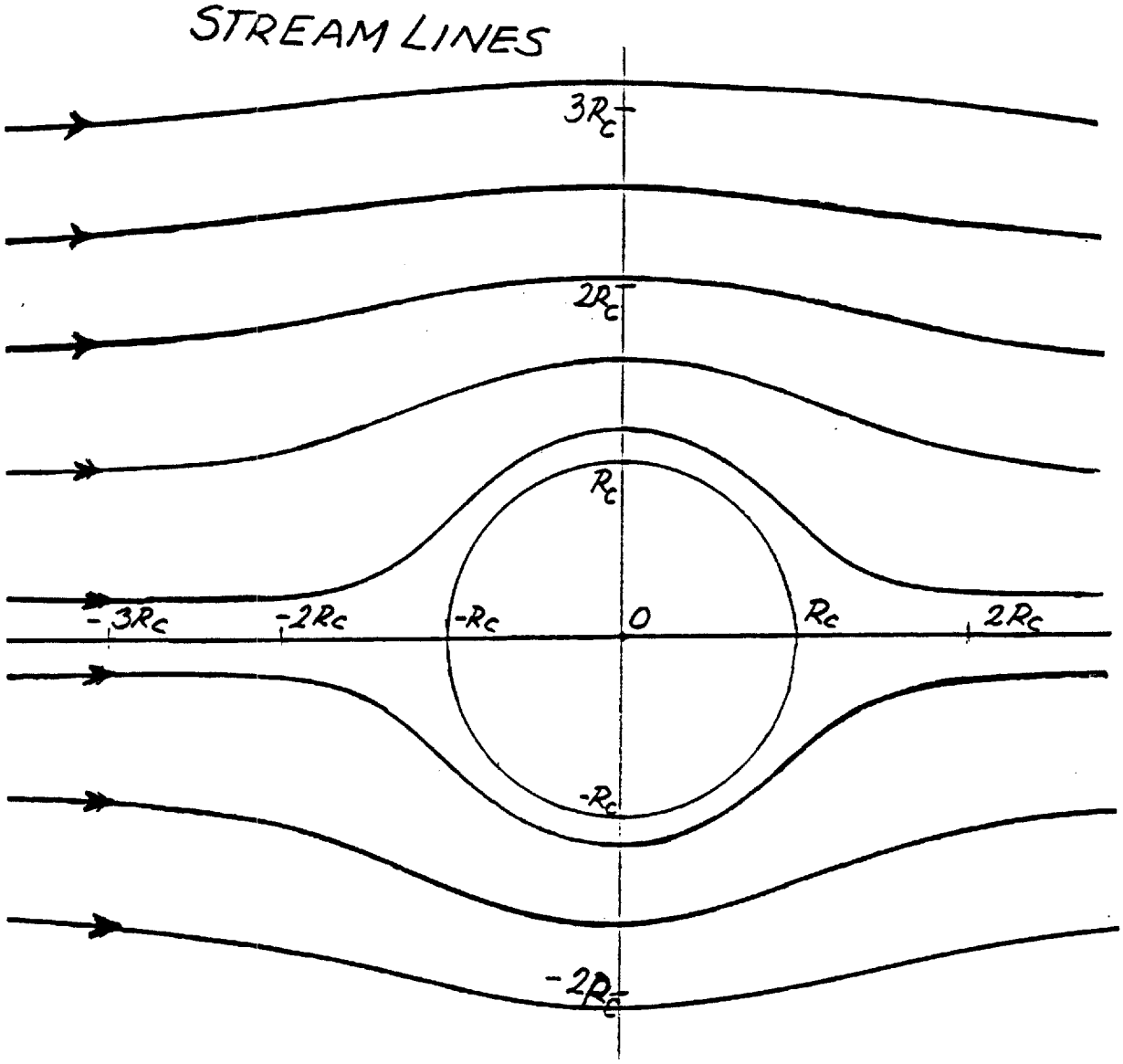

Figure 4.3

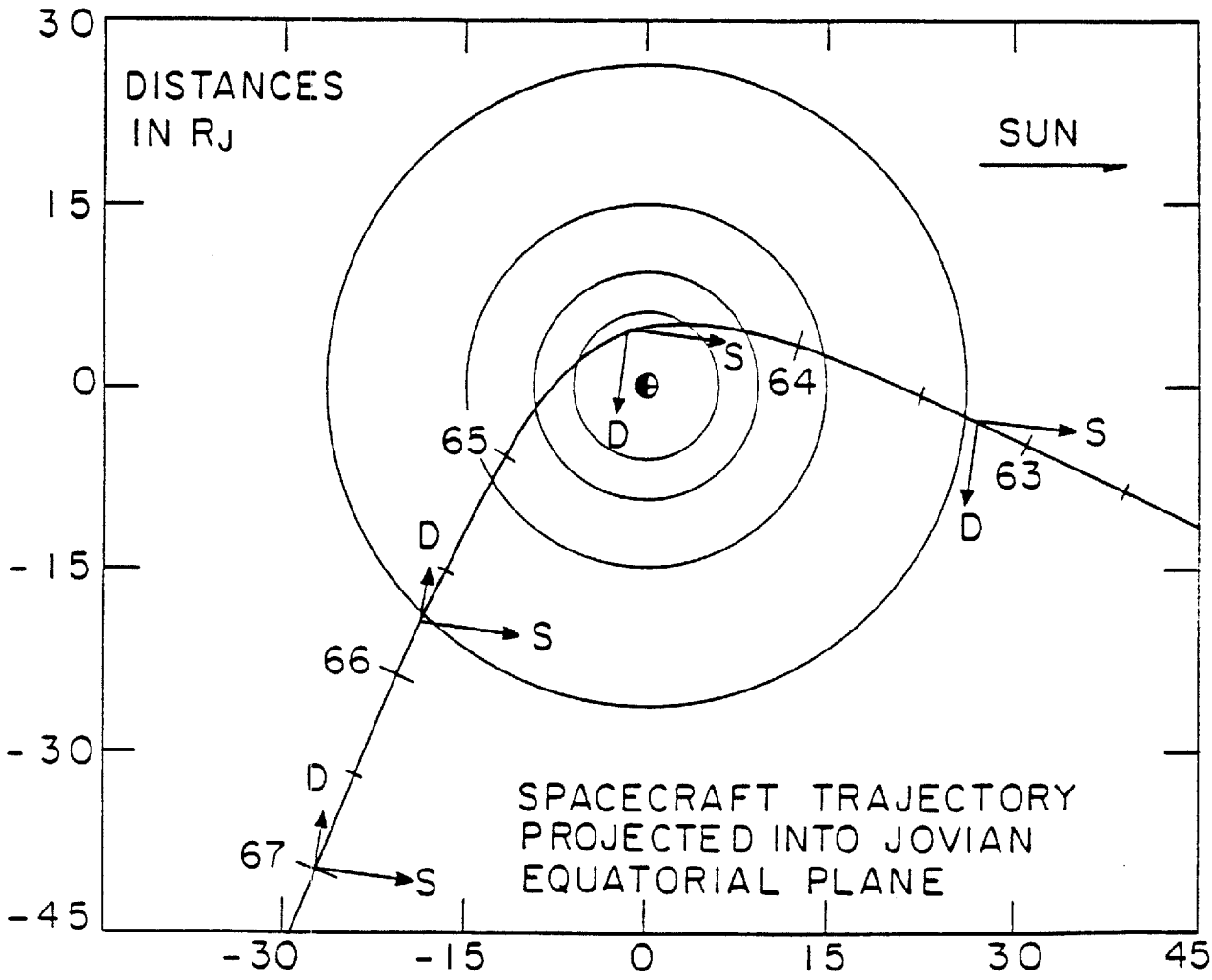
30
15
0
-15
-30
-45
-30
-15
0
15
30
45
DISTANCES
IN R_J
SUN
S
64
D
65
S
63
D
D
S
66
D
67
S
SPACECRAFT TRAJECTORY
PROJECTED INTO JOVIAN
EQUATORIAL PLANE

Figure 5.1

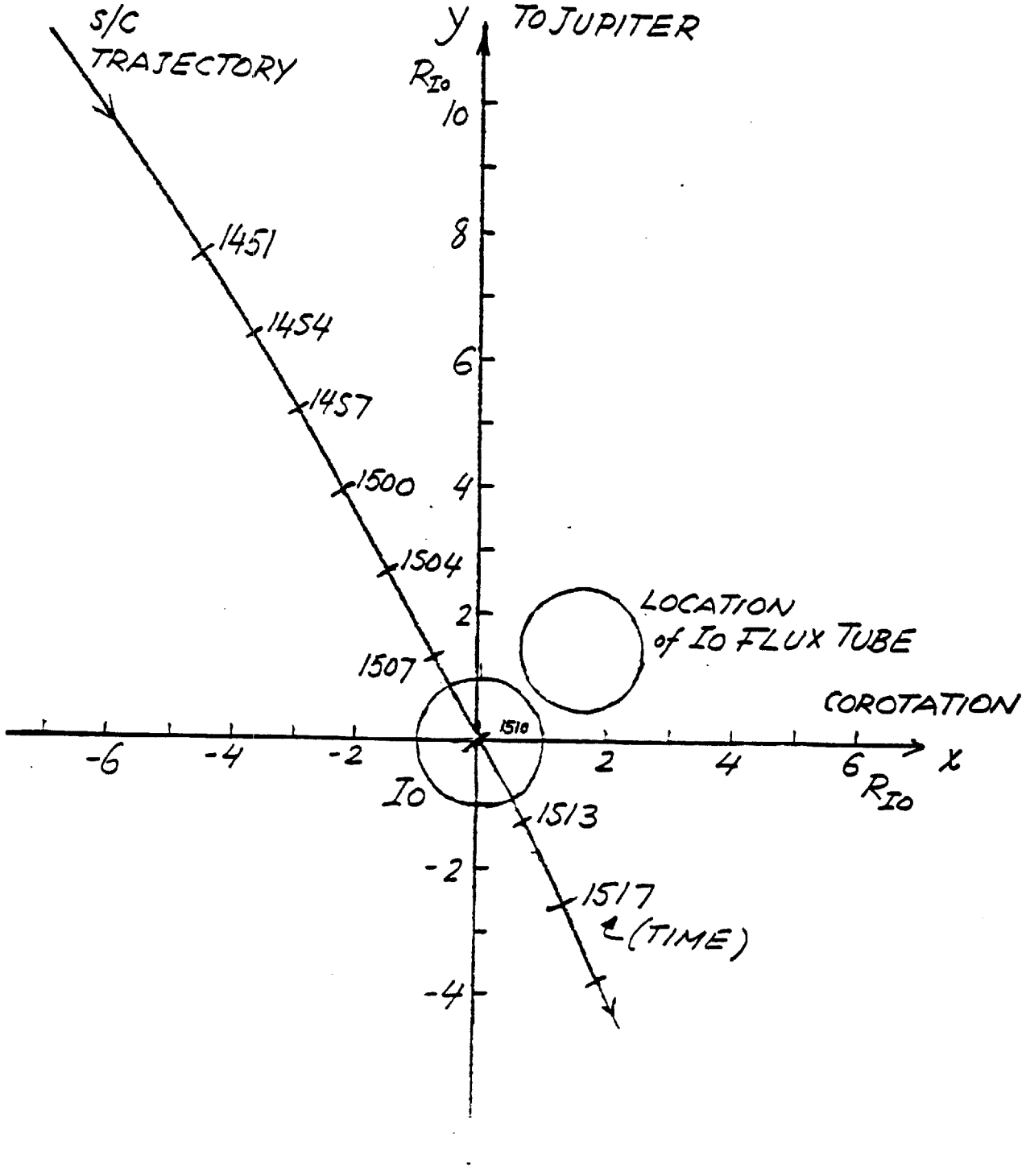
S/C
TRAJECTORY
y
TO JUPITER
R_{Io}
10
8
6
4
2
-2
-4
1451
1454
1457
1500
1504
1507
1510
1513
1517
(TIME)
LOCATION
of Io FLUX TUBE
COROTATION
-6
-4
-2
2
4
6
R_{Io}
x
Io

Figure 5.2

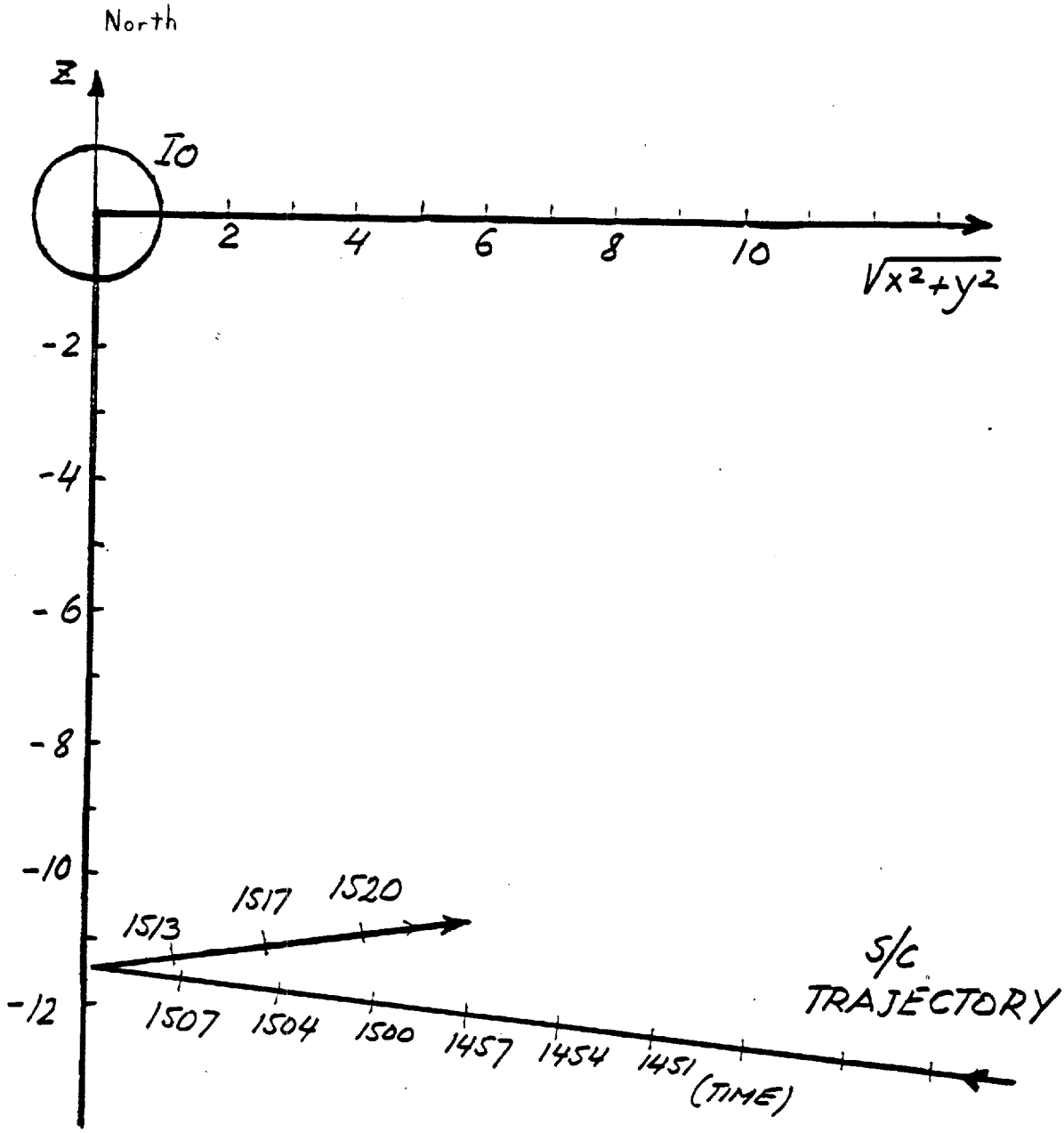
North
Z
Io
2
4
6
8
10
$\sqrt{x^2+y^2}$
-2
-4
-6
-8
-10
-12
1513
1517
1520
1507
1504
1500
1457
1454
1451
(TIME)
S/C
TRAJECTORY

Figure 5.3

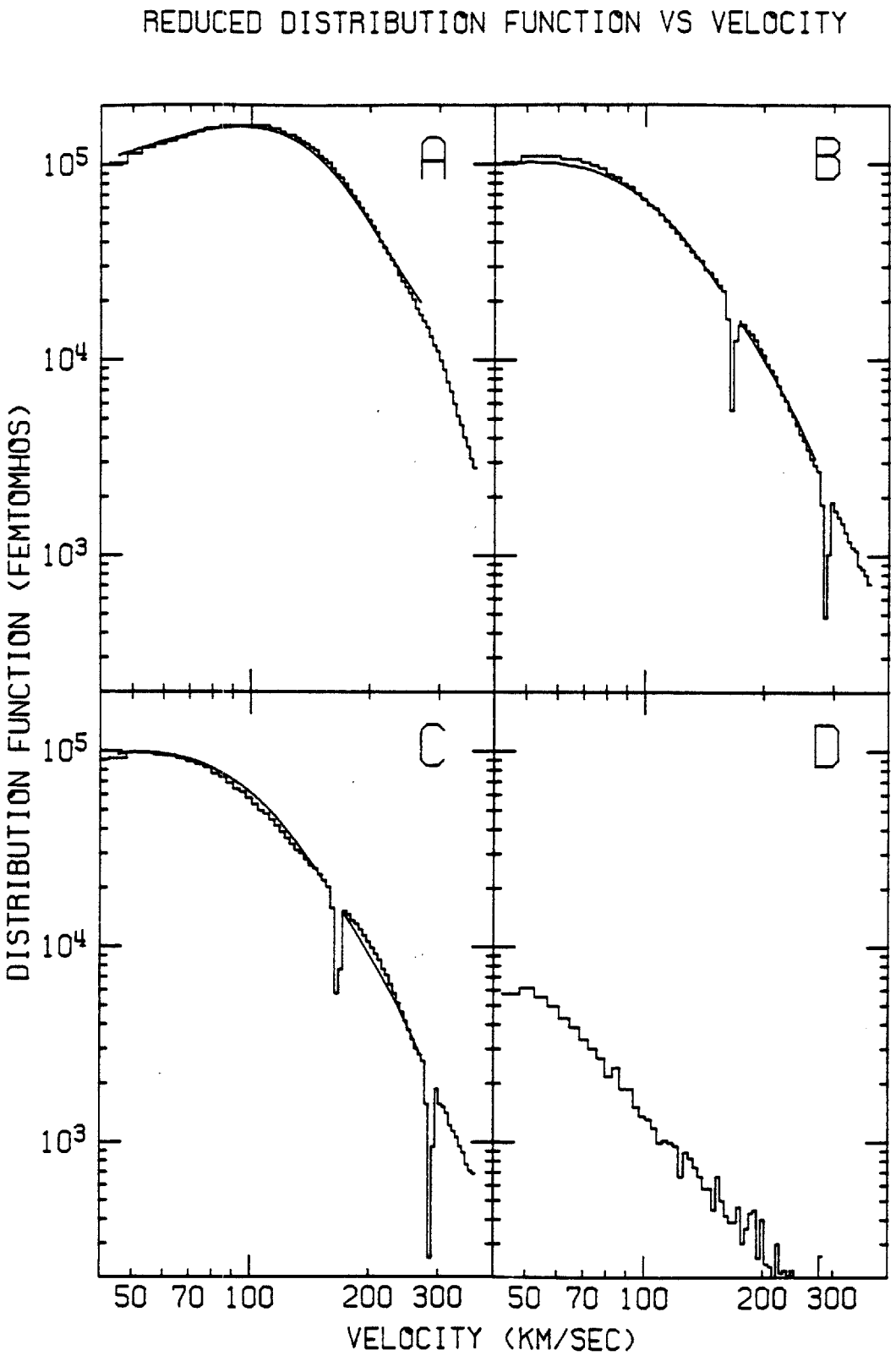
REDUCED DISTRIBUTION FUNCTION VS VELOCITY
A
B
C
D
10^5
10^4
10^3
DISTRIBUTION FUNCTION (FEMTOMHOS)
50 70 100 200 300
50 70 100 200 300
VELOCITY (KM/SEC)

Figure 5.4

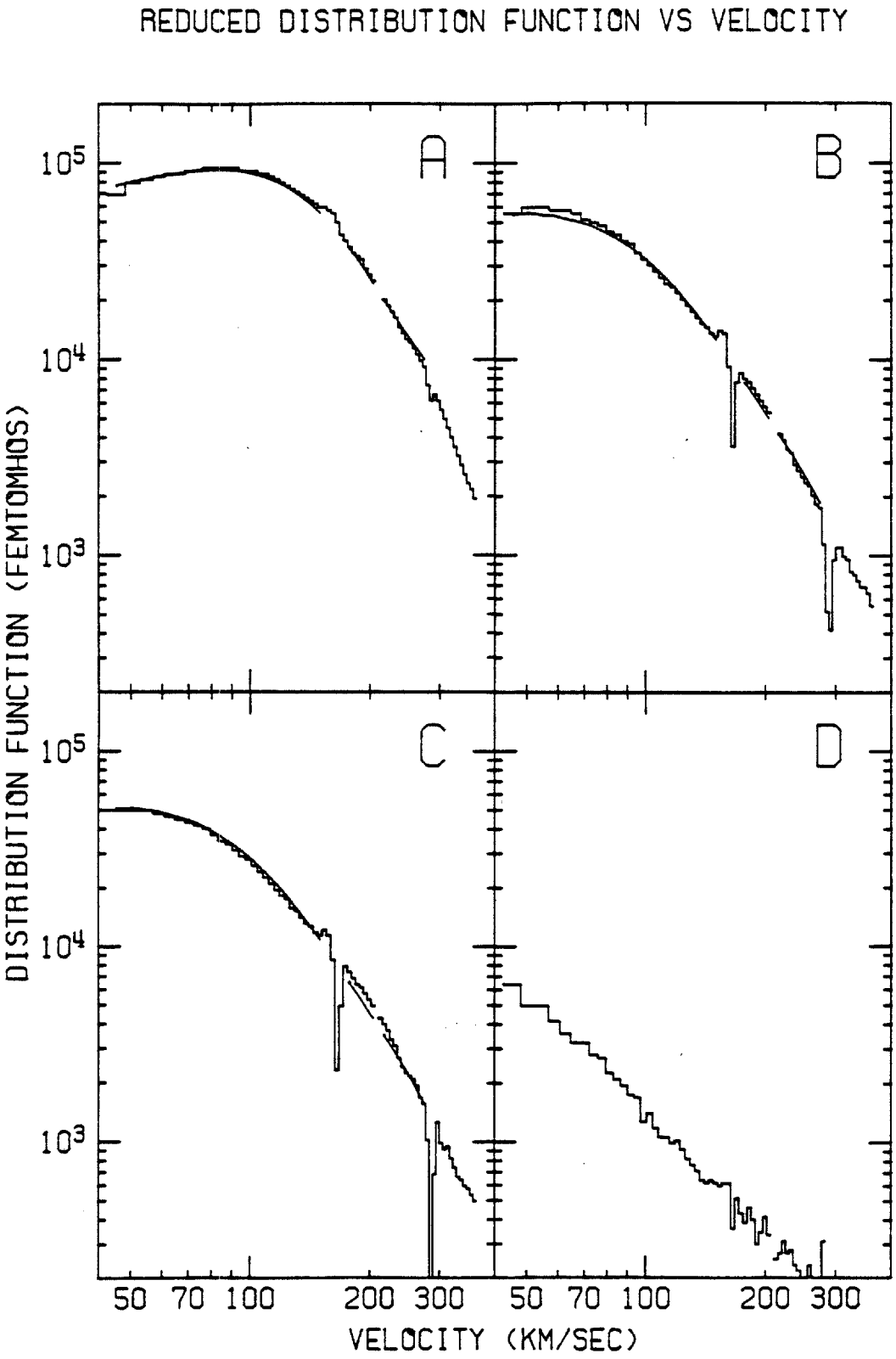
REDUCED DISTRIBUTION FUNCTION VS VELOCITY
A
B
C
D
10^5
10^4
10^3
DISTRIBUTION FUNCTION (FEMTOMHOS)
50 70 100 200 300
VELOCITY (KM/SEC)

Figure 5.5

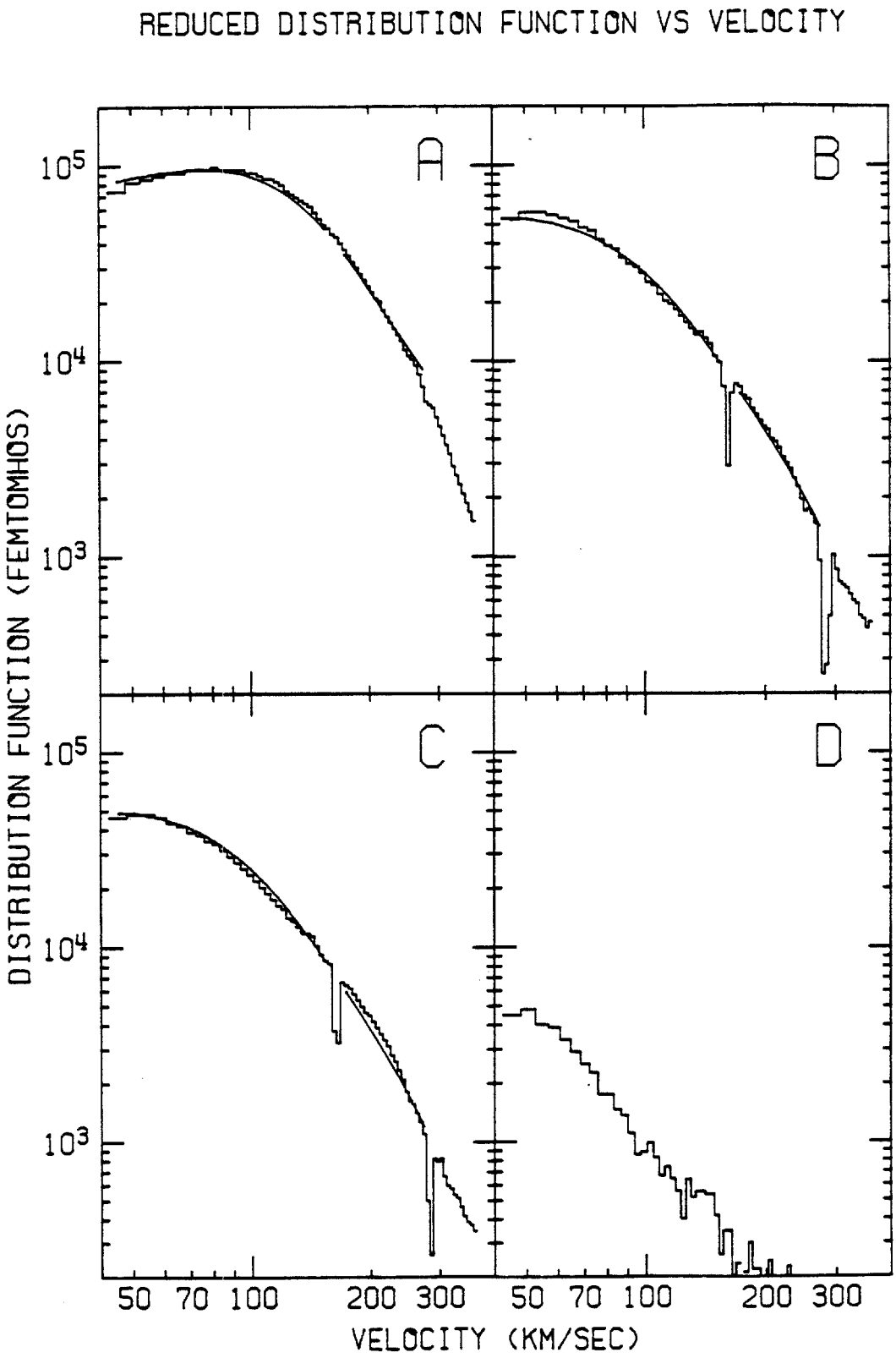
REDUCED DISTRIBUTION FUNCTION VS VELOCITY
A
B
C
D
10^5
10^4
10^3
DISTRIBUTION FUNCTION (FEMTOMHOS)
50 70 100 200 300
VELOCITY (KM/SEC)

Figure 5.6

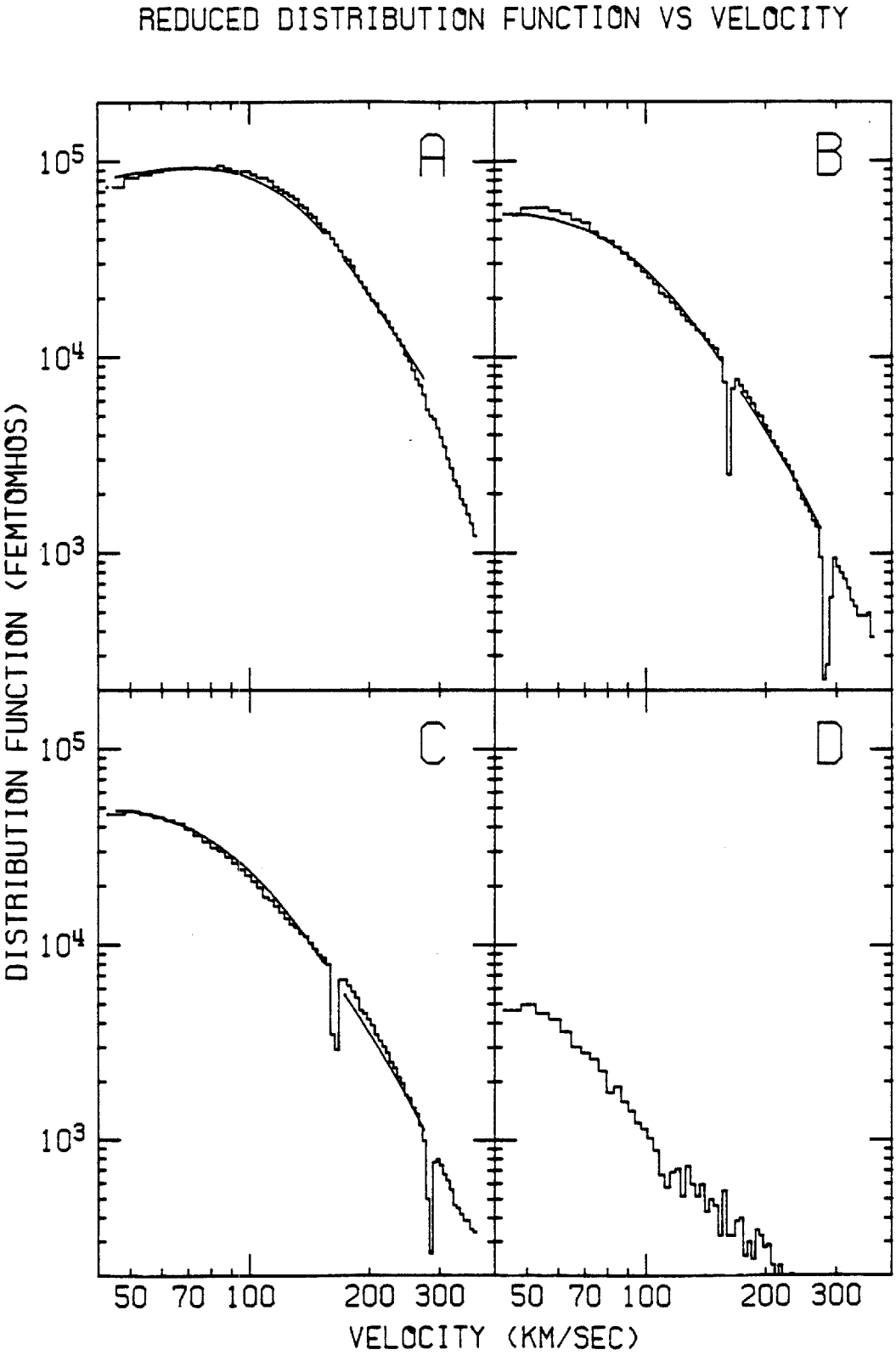
REDUCED DISTRIBUTION FUNCTION VS VELOCITY
A
B
C
D
10^5
10^4
10^3
DISTRIBUTION FUNCTION (FEMTOMHOS)
50 70 100 200 300
VELOCITY (KM/SEC)

Figure 5.7

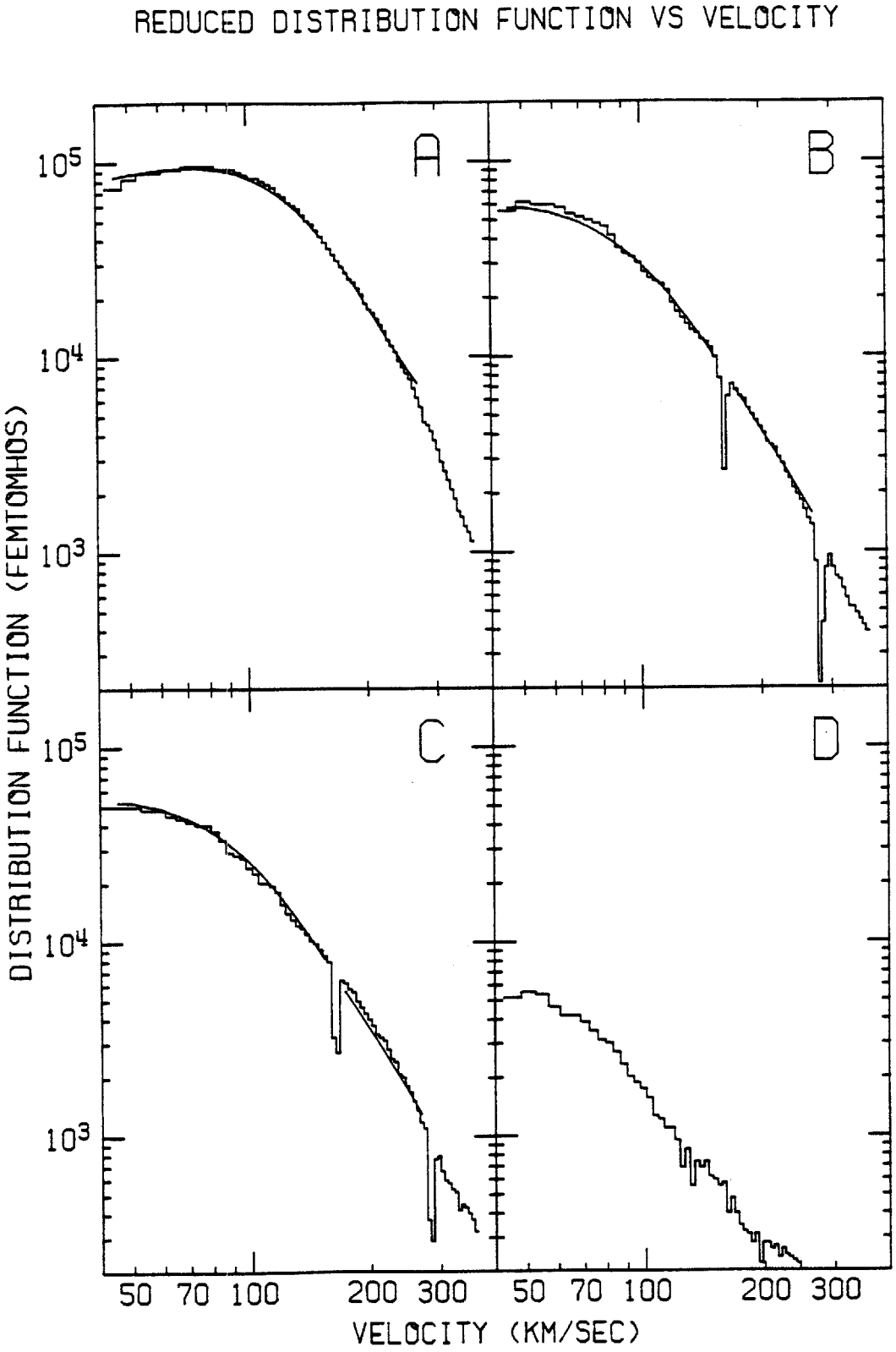
REDUCED DISTRIBUTION FUNCTION VS VELOCITY
A
B
C
D
10^5
10^4
10^3
DISTRIBUTION FUNCTION (FEMTOMHOS)
50 70 100 200 300
VELOCITY (KM/SEC)

Figure 5.8

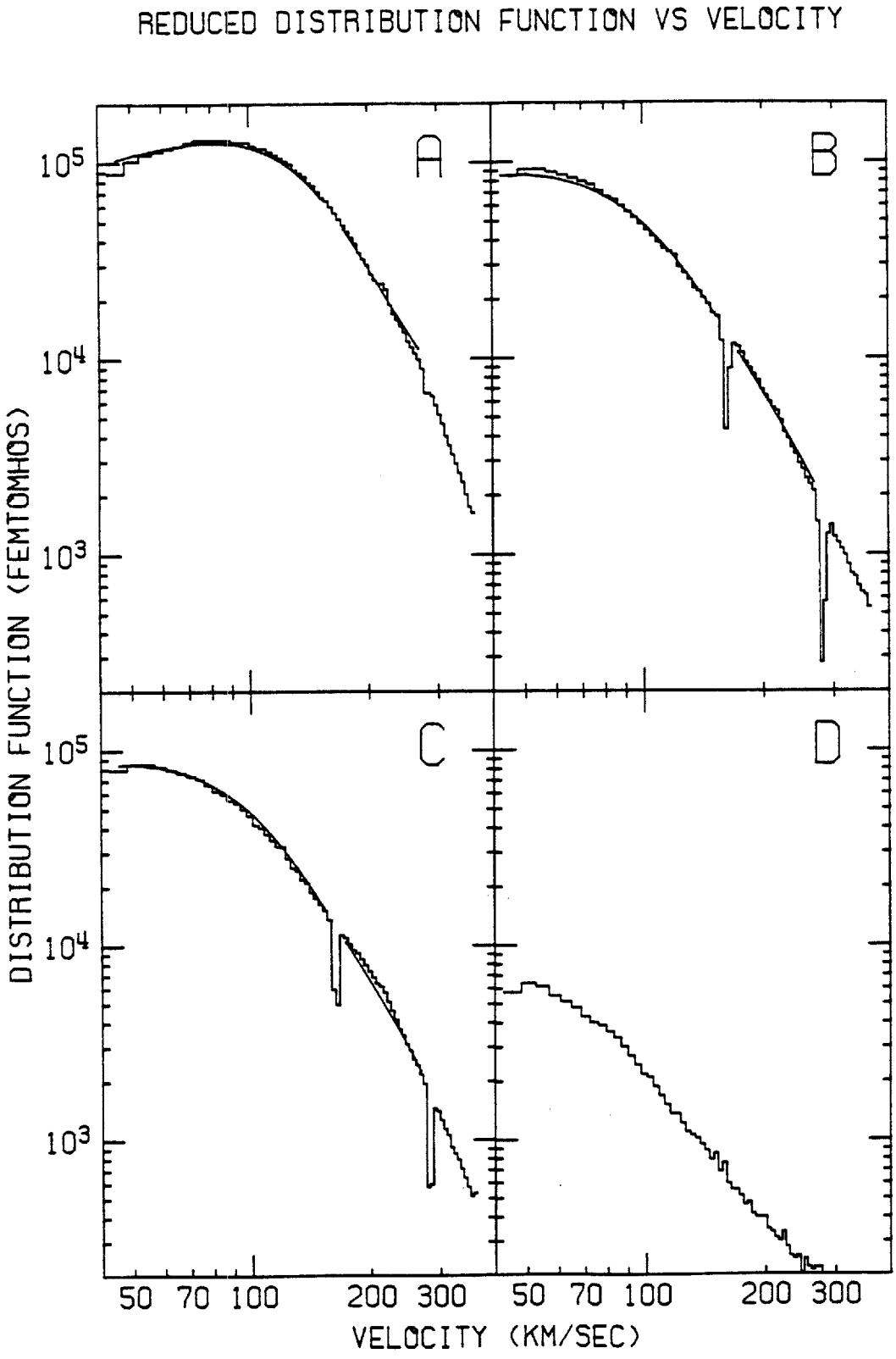
REDUCED DISTRIBUTION FUNCTION VS VELOCITY
A
B
C
D
10^5
10^4
10^3
DISTRIBUTION FUNCTION (FEMTOMHOS)
50 70 100 200 300
VELOCITY (KM/SEC)

Figure 5.9

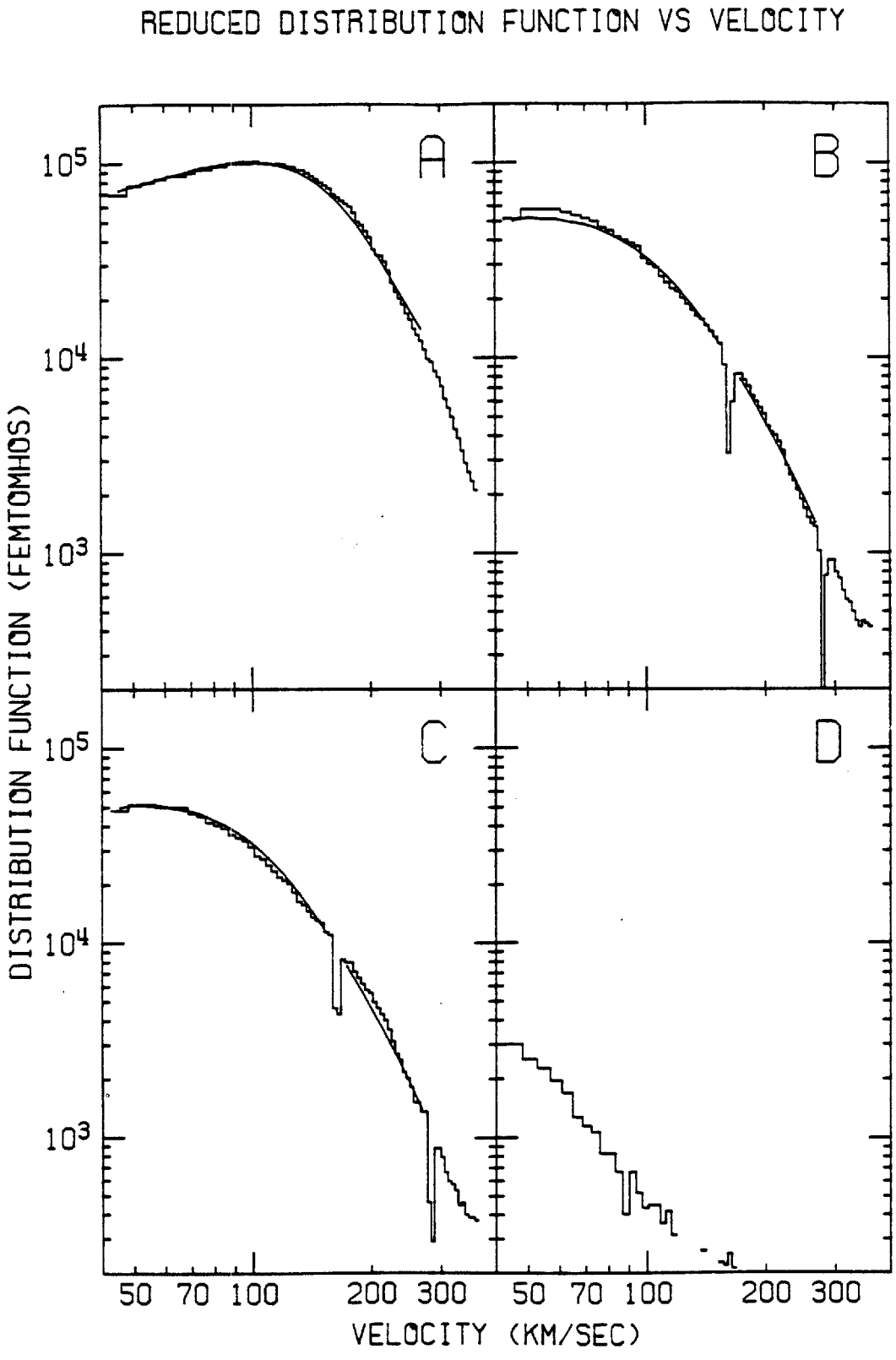
REDUCED DISTRIBUTION FUNCTION VS VELOCITY
A
B
C
D
10^5
10^4
10^3
DISTRIBUTION FUNCTION (FEMTOMHOS)
50 70 100 200 300
VELOCITY (KM/SEC)

Figure 5.10

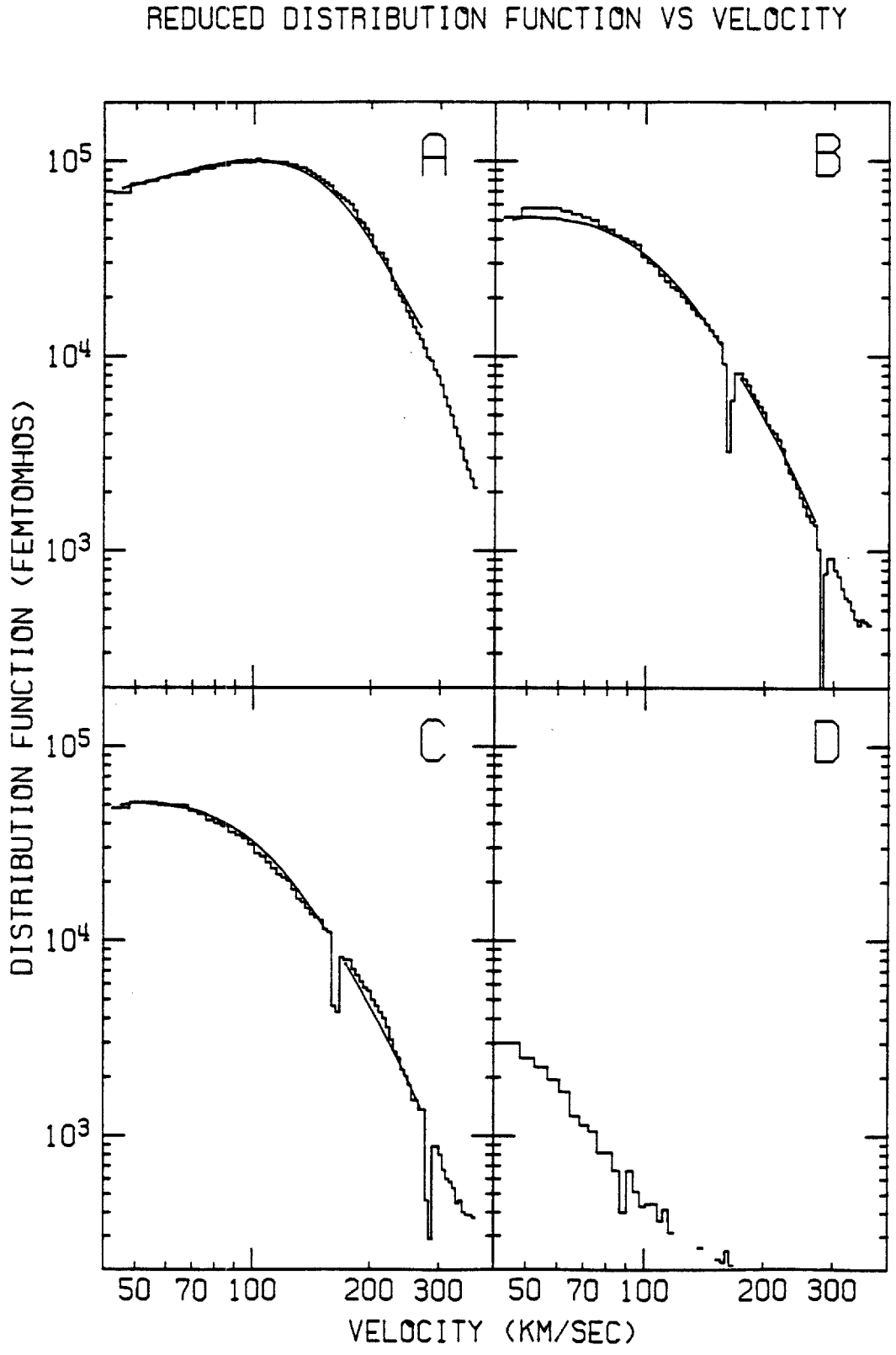
REDUCED DISTRIBUTION FUNCTION VS VELOCITY
A
B
C
D
10^5
10^4
10^3
DISTRIBUTION FUNCTION (FEMTOMHOS)
50 70 100 200 300
VELOCITY (KM/SEC)

Figure 5.11

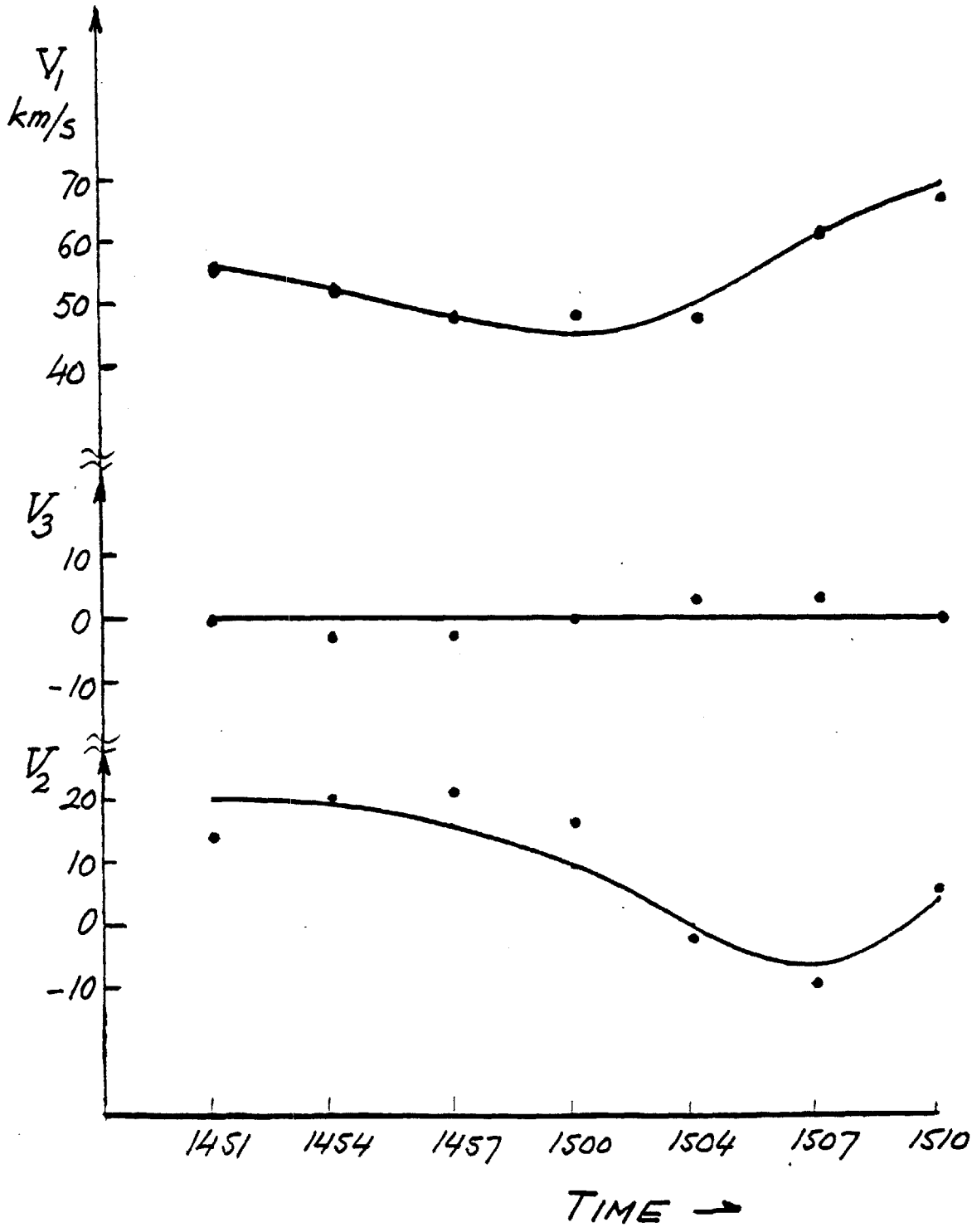
V1
km/s
70
60
50
40
V3
10
0
-10
V2
20
10
0
-10
1451
1454
1457
1500
1504
1507
1510
TIME →

Figure 5.12

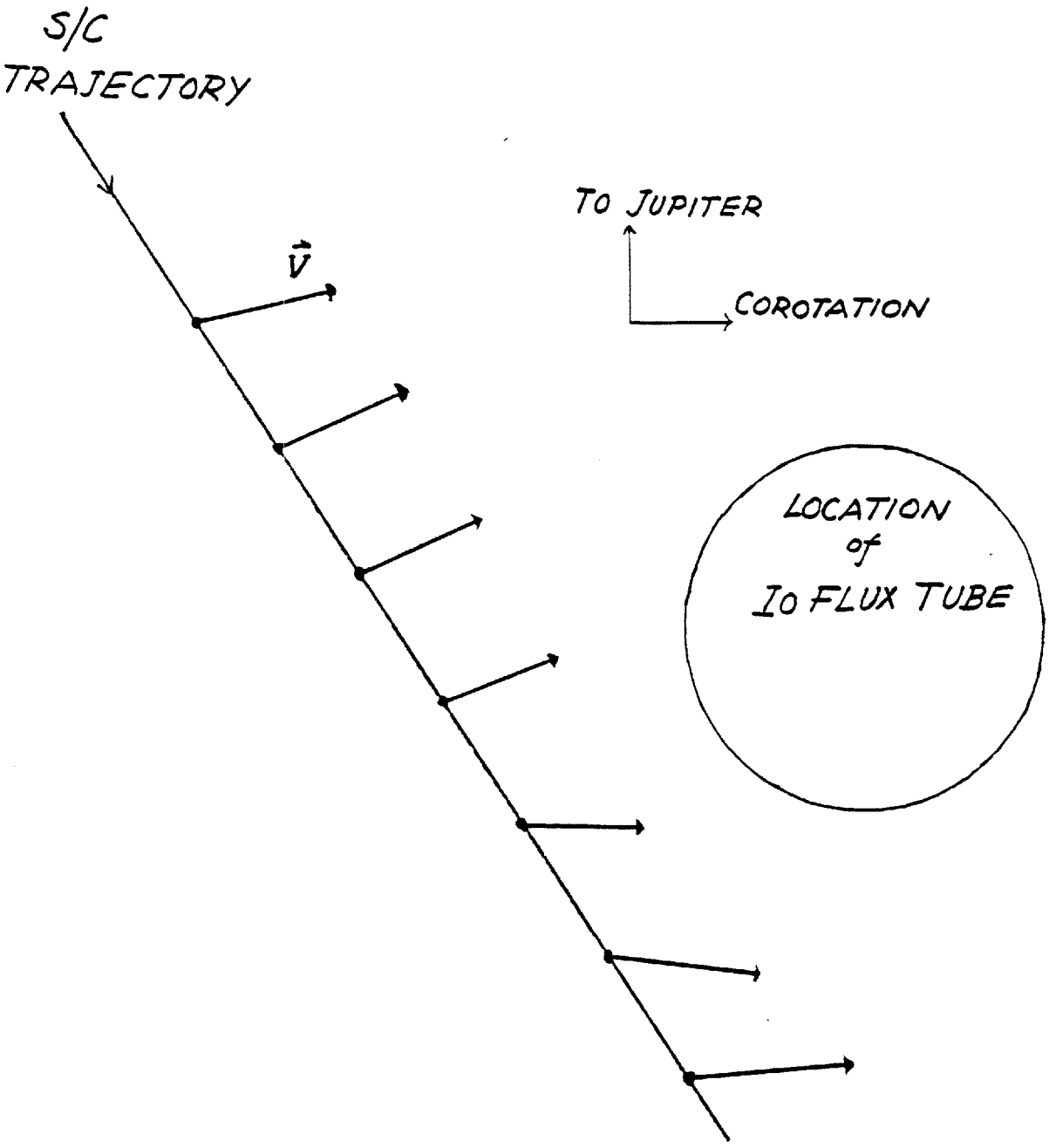
S/C
TRAJECTORY
$\vec{V}$
TO JUPITER
COROTATION
LOCATION
of
Io FLUX TUBE

Figure 5.13

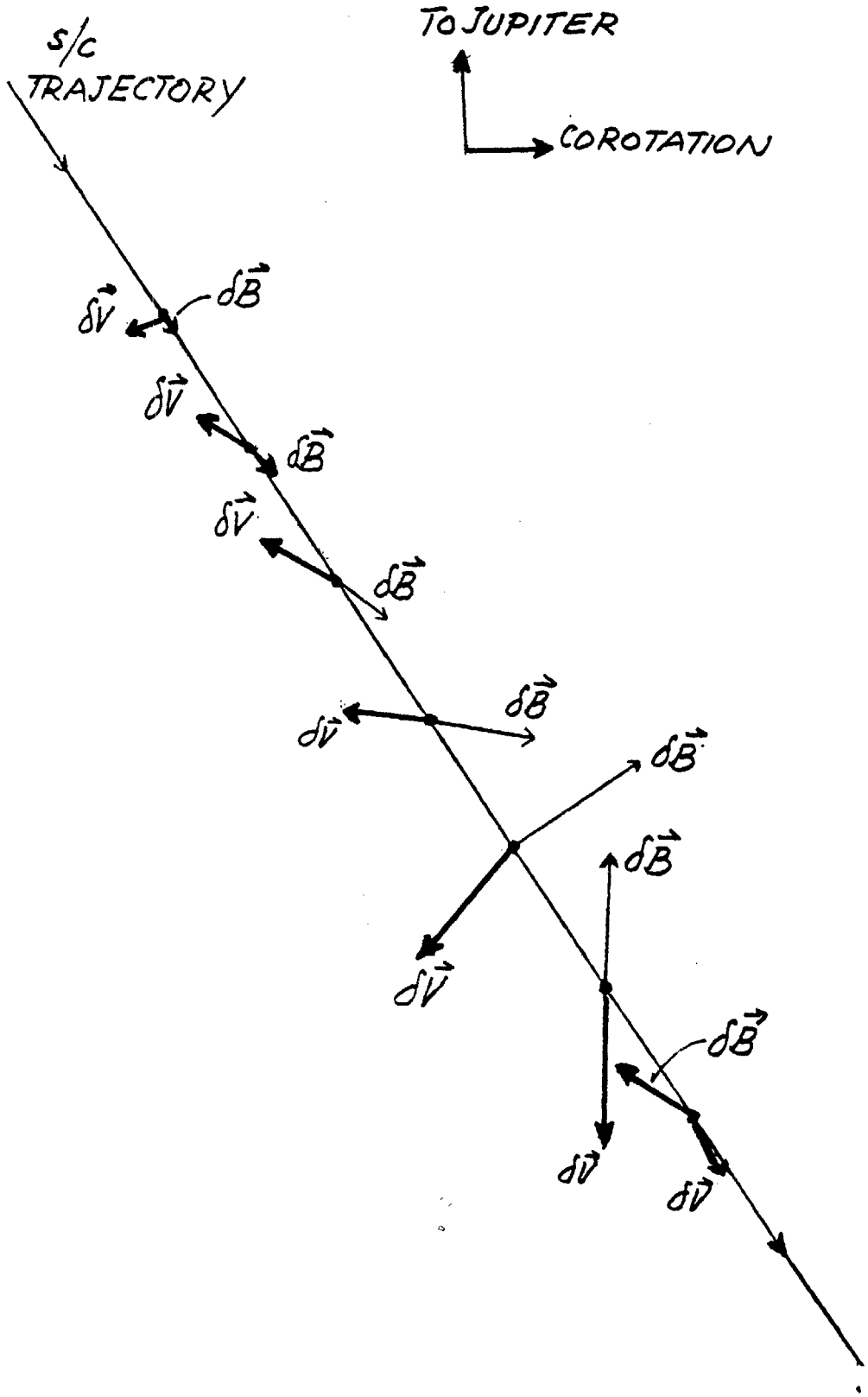

Figure 5.14

Appendix A

Table of nominal constants for MUS.

The delta values are the full width.

M.mode. K = 1.036633

REGULATOR STEP	THRESHOLD VOLTAGE	PEAK VOLTAGE	AVERAGE VOLTAGE	DELTA VOLTAGE
1	10.0000	12.1980	11.0990	2.19795
2	12.1980	14.4764	13.3372	2.27846
3	14.4764	16.8383	15.6574	2.36192
4	16.8383	19.2868	18.0626	2.44846
5	19.2868	21.8249	20.5559	2.53815
6	21.8249	24.4561	23.1405	2.63112
7	24.4561	27.1836	25.8198	2.72751
8	27.1836	30.0110	28.5973	2.82742
9	30.0110	32.9420	31.4765	2.93100
10	32.9420	35.9803	34.4612	3.03836
11	35.9803	39.1300	37.5552	3.14967
12	39.1300	42.3951	40.7625	3.26505
13	42.3951	45.7797	44.0874	3.38466
14	45.7797	49.2884	47.5340	3.50865
15	49.2884	52.9256	51.1070	3.63718
16	52.9256	56.6960	54.8108	3.77042

PROTONS

REGULATOR STEP	AVERAGE SPEED	DELTA SPEED
1	46.0847	4.57437
2	50.5391	4.32440
3	54.7646	4.13652
4	58.8288	3.99184
5	62.7640	3.87860
6	66.5979	3.78922
7	70.3517	3.71844
8	74.0422	3.66253
9	77.6828	3.61877
10	81.2848	3.58509
11	84.8573	3.55996
12	88.4083	3.54213
13	91.9447	3.53067
14	95.4725	3.52478
15	98.9968	3.52381
16	102.522	3.52729

Table of nominal constants for MJS.

The delta values are the full width.

M mode. K = 1.036633

MODULATOR STEP	THRESHOLD VOLTAGE	PEAK VOLTAGE	AVERAGE VOLTAGE	DELTA VOLTAGE
17	56.6960	60.6045	58.6502	3.90854
18	60.6045	64.6562	62.6304	4.05171
19	64.6562	68.8564	66.7563	4.20013
20	68.8564	73.2104	71.0334	4.35400
21	73.2104	77.7239	75.4671	4.51350
22	77.7239	82.4027	80.0633	4.67885
23	82.4027	87.2529	84.8278	4.85023
24	87.2529	92.2809	89.7669	5.02792
25	92.2809	97.4930	94.8869	5.21210
26	97.4930	102.896	100.194	5.40303
27	102.896	108.497	105.696	5.60097
28	108.497	114.303	111.400	5.80614
29	114.303	120.322	117.313	6.01883
30	120.322	126.561	123.442	6.23932
31	126.561	133.029	129.795	6.46788
32	133.029	139.734	136.381	6.70482

PROTONS

MODULATOR STEP	AVERAGE SPEED	DELTA SPEED
17	106.053	3.53475
18	109.594	3.54587
19	113.147	3.56033
20	116.716	3.57790
21	120.304	3.59835
22	123.914	3.62150
23	127.548	3.64718
24	131.209	3.67531
25	134.900	3.70569
26	138.622	3.73830
27	142.378	3.77303
28	146.169	3.80980
29	149.998	3.84853
30	153.867	3.88921
31	157.778	3.93175
32	161.731	3.97613

Table of nominal constants for MJS.

The delta values are the full width.

M mode. K = 1.036633

MODULATOR STEP	THRESHOLD VOLTAGE	PEAK VOLTAGE	AVERAGE VOLTAGE	DELTA VOLTAGE
33	139.734	146.684	143.209	6.95042
34	146.684	153.889	150.287	7.20505
35	153.889	161.358	157.624	7.46898
36	161.358	169.101	165.230	7.74258
37	169.101	177.127	173.114	8.02621
38	177.127	185.447	181.287	8.32024
39	185.447	194.072	189.760	8.62503
40	194.072	203.013	198.543	8.94098
41	203.013	212.282	207.648	9.26830
42	212.282	221.890	217.086	9.60791
43	221.890	231.850	226.870	9.95996
44	231.850	242.174	237.012	10.3247
45	242.174	252.877	247.526	10.7029
46	252.877	263.972	258.425	11.0950
47	263.972	275.474	269.723	11.5015
48	275.474	287.396	281.435	11.9229

PROTONS

MODULATOR STEP	AVERAGE SPEED	DELTA SPEED
33	165.731	4.02234
34	169.777	4.07030
35	173.872	4.12004
36	178.018	4.17149
37	182.216	4.22468
38	186.468	4.27957
39	190.776	4.33617
40	195.141	4.39446
41	199.566	4.45434
42	204.051	4.51605
43	208.599	4.57947
44	213.211	4.64449
45	217.889	4.71125
46	222.634	4.77977
47	227.449	4.84991
48	232.335	4.92197

Table of nominal constants for MJS.

The delta values are the full width.

M mode. K = 1.036633

MODULATOR STEP	THRESHOLD VOLTAGE	PEAK VOLTAGE	AVERAGE VOLTAGE	DELTA VOLTAGE
49	287.396	299.756	293.576	12.3596
50	299.756	312.568	306.162	12.8123
51	312.568	325.850	319.209	13.2817
52	325.850	339.618	332.734	13.7683
53	339.618	353.891	346.755	14.2727
54	353.891	368.687	361.289	14.7954
55	368.687	384.024	376.355	15.3374
56	384.024	399.923	391.973	15.8992
57	399.923	416.405	408.164	16.4817
58	416.405	433.490	424.948	17.0854
59	433.490	451.202	442.346	17.7114
60	451.202	469.562	460.382	18.3601
61	469.562	488.594	479.078	19.0327
62	488.594	508.324	498.459	19.7300
63	508.324	528.777	518.551	20.4526
64	528.777	549.979	539.378	21.2019

PROTONS

MODULATOR STEP	AVERAGE SPEED	DELTA SPEED
49	237.294	4.99552
50	242.327	5.07096
51	247.437	5.14831
52	252.624	5.22735
53	257.892	5.30808
54	263.241	5.39071
55	268.674	5.47504
56	274.193	5.56147
57	279.798	5.64981
58	285.493	5.73984
59	291.279	5.83177
60	297.158	5.92602
61	303.132	6.02197
62	309.203	6.12003
63	315.373	6.21999
64	321.644	6.32227

Table of nominal constants for MJS.

The delta values are the full width.

M mode. K = 1.036633

MODULATOR STEP	THRESHOLD VOLTAGE	PEAK VOLTAGE	AVERAGE VOLTAGE	DELTA VOLTAGE
81	1016.92	1056.00	1036.46	39.0840
82	1056.00	1096.52	1076.26	40.5156
83	1096.52	1138.52	1117.52	41.9998
84	1138.52	1182.06	1160.29	43.5383
85	1182.06	1227.19	1204.62	45.1333
86	1227.19	1273.98	1250.58	46.7866
87	1273.98	1322.48	1298.23	48.5005
88	1322.48	1372.76	1347.62	50.2773
89	1372.76	1424.88	1398.82	52.1191
90	1424.88	1478.90	1451.89	54.0283
91	1478.90	1534.91	1506.91	56.0076
92	1534.91	1592.97	1563.94	58.0591
93	1592.97	1653.16	1623.06	60.1860
94	1653.16	1715.55	1684.35	62.3909
95	1715.55	1780.22	1747.89	64.6763
96	1780.22	1847.27	1813.75	67.0457

PROTONS

MODULATOR STEP	AVERAGE SPEED	DELTA SPEED
81	445.869	8.40751
82	454.349	8.55270
83	462.976	8.70063
84	471.752	8.85173
85	480.681	9.00559
86	489.764	9.16213
87	499.007	9.32216
88	508.410	9.48468
89	517.978	9.65058
90	527.713	9.81964
91	537.619	9.99188
92	547.698	10.1671
93	557.955	10.3459
94	568.391	10.5278
95	579.012	10.7134
96	589.820	10.9025

Table of nominal constants for MJS.

The delta values are the full widths.

M mode. K = 1.036633

MODULATOR STEP	THRESHOLD VOLTAGE	PEAK VOLTAGE	AVERAGE VOLTAGE	DELTA VOLTAGE
65	549.979	571.958	560.968	21.9785
66	571.958	594.741	583.349	22.7837
67	594.741	618.360	606.550	23.6184
68	618.360	642.843	630.601	24.4836
69	642.843	668.224	655.533	25.3804
70	668.224	694.534	681.379	26.3103
71	694.534	721.808	708.171	27.2739
72	721.808	750.081	735.944	28.2732
73	750.081	779.390	764.735	29.3088
74	779.390	809.772	794.581	30.3826
75	809.772	841.268	825.520	31.4956
76	841.268	873.917	857.593	32.6492
77	873.917	907.762	890.840	33.8452
78	907.762	942.848	925.305	35.0852
79	942.848	979.218	961.033	36.3704
80	979.218	1016.92	998.069	37.7026

PROTONS

MODULATOR STEP	AVERAGE SPEED	DELTA SPEED
65	328.018	6.42646
66	334.498	6.53276
67	341.085	6.64139
68	347.782	6.75213
69	354.590	6.86498
70	361.513	6.98037
71	368.552	7.09766
72	375.709	7.21749
73	382.988	7.33985
74	390.390	7.46432
75	397.918	7.59155
76	405.574	7.72088
77	413.361	7.85297
78	421.282	7.98780
79	429.338	8.12496
80	437.533	8.26465

Table of nominal constants for MJS.

The delta values are the full widths.

M mode. K = 1.036633

MODULATOR STEP	THRESHOLD VOLTAGE	PEAK VOLTAGE	AVERAGE VOLTAGE	DELTA VOLTAGE
97	1847.27	1916.77	1882.02	69.5017
98	1916.77	1988.82	1952.79	72.0476
99	1988.82	2063.51	2026.16	74.6870
100	2063.51	2140.93	2102.22	77.4229
101	2140.93	2221.19	2181.06	80.2590
102	2221.19	2304.39	2262.79	83.1992
103	2304.39	2390.63	2347.51	86.2471
104	2390.63	2480.04	2435.34	89.4065
105	2480.04	2572.72	2526.38	92.6816
106	2572.72	2668.80	2620.76	96.0769
107	2668.80	2768.40	2718.60	99.5964
108	2768.40	2871.64	2820.02	103.245
109	2871.64	2978.67	2925.15	107.027
110	2978.67	3089.61	3034.14	110.948
111	3089.61	3204.63	3147.12	115.012
112	3204.63	3323.85	3264.24	119.225

PROTONS

MODULATOR STEP	AVERAGE SPEED	DELTA SPEED
97	600.819	11.0948
98	612.011	11.2910
99	623.402	11.4907
100	634.995	11.6942
101	646.792	11.9013
102	658.799	12.1126
103	671.020	12.3275
104	683.457	12.5467
105	696.115	12.7697
106	708.998	12.9971
107	722.111	13.2285
108	735.457	13.4641
109	749.042	13.7044
110	762.868	13.9489
111	776.941	14.1979
112	791.266	14.4515

Table of nominal constants for MJS.

The delta values are the full widths.

M mode. K = 1.036633

MODULATOR STEP	THRESHOLD VOLTAGE	PEAK VOLTAGE	AVERAGE VOLTAGE	DELTA VOLTAGE
113	3323.85	3447.44	3385.65	123.593
114	3447.44	3575.56	3511.50	128.120
115	3575.56	3708.38	3641.97	132.813
116	3708.38	3846.06	3777.22	137.679
117	3846.06	3988.78	3917.42	142.722
118	3988.78	4136.73	4062.75	147.948
119	4136.73	4290.09	4213.41	153.367
120	4290.09	4449.08	4369.59	158.988
121	4449.08	4613.89	4531.49	164.812
122	4613.89	4784.74	4699.32	170.848
123	4784.74	4961.85	4873.29	177.105
124	4961.85	5145.44	5053.64	183.594
125	5145.44	5335.76	5240.60	190.320
126	5335.76	5533.05	5434.41	197.293
127	5533.05	5737.57	5635.31	204.520
128	5737.57	5949.59	5843.58	212.012

PROTONS

MODULATOR STEP	AVERAGE SPEED	DELTA SPEED
113	805.847	14.7099
114	820.688	14.9730
115	835.795	15.2410
116	851.173	15.5133
117	866.825	15.7917
118	882.759	16.0743
119	898.977	16.3628
120	915.487	16.6565
121	932.293	16.9553
122	949.400	17.2594
123	966.814	17.5695
124	984.542	17.8852
125	1002.59	18.2066
126	1020.96	18.5342
127	1039.66	18.8675
128	1058.70	19.2069

Table of nominal constants for MJS.

The delta values are the full width.

E_1 mode. K = 1.074608

MODULATOR STEP	THRESHOLD VOLTAGE	PEAK VOLTAGE	AVERAGE VOLTAGE	DELTA VOLTAGE
1	10.0000	14.4765	12.2382	4.47647
2	14.4765	19.2869	16.8817	4.81044
3	19.2869	24.4563	21.8716	5.16934
4	24.4563	30.0113	27.2337	5.55501
5	30.0113	35.9807	32.9960	5.96947
6	35.9807	42.3956	39.1881	6.41483
7	42.3956	49.2890	45.8423	6.89343
8	49.2890	56.6967	52.9928	7.40773
9	56.6967	64.6571	60.6769	7.96040
10	64.6571	73.2114	68.9343	8.55431
11	73.2114	82.4040	77.8077	9.19254
12	82.4040	92.2823	87.3431	9.87837
13	92.2823	102.898	97.5900	10.6154
14	102.898	114.305	108.601	11.4074
15	114.305	126.564	120.434	12.2584
16	126.564	139.737	133.150	13.1730

	ELECTRONS	
MODULATOR STEP	AVERAGE SPEED	DELTA SPEED
1	2067.48	381.335
2	2432.31	348.319
3	2770.76	328.585
4	3093.20	316.292
5	3405.69	308.703
6	3712.22	304.342
7	4015.56	302.344
8	4317.81	302.157
9	4620.60	303.422
10	4925.25	305.891
11	5232.89	309.388
12	5544.48	313.787
13	5860.87	318.995
14	6182.84	324.944
15	6511.10	331.582
16	6846.33	338.874

Table of nominal constants for MJS.

The delta values are the full widths.

L Mode.

MODULATOR STEP	THRESHOLD VOLTAGE	PEAK VOLTAGE	AVERAGE VOLTAGE	DELTA VOLTAGE
1	10.0000	30.0113	20.0056	20.0113
2	30.0113	56.6968	43.3541	26.6855
3	56.6968	92.2825	74.4897	35.5857
4	92.2825	139.737	116.010	47.4543
5	139.737	203.018	171.377	63.2814
6	203.018	287.405	245.212	84.3870
7	287.405	399.937	343.671	112.532
8	399.937	550.001	474.969	150.064
9	550.001	750.114	650.058	200.113
10	750.114	1016.97	883.542	266.855
11	1016.97	1372.83	1194.90	355.858
12	1372.83	1847.37	1610.10	474.544
13	1847.37	2480.19	2163.78	632.815
14	2480.19	3324.06	2902.12	843.872
15	3324.06	4449.38	3886.72	1125.32
16	4449.38	5950.02	5199.70	1500.64

PROTON

MODULATOR STEP	AVERAGE SPEED	DELTA SPEED
1	59.9357	32.0763
2	90.0803	28.4129
3	118.668	28.7616
4	148.385	30.6730
5	180.531	33.6197
6	216.070	37.4585
7	255.889	42.1787
8	300.895	47.8334
9	352.069	54.5151
10	410.501	62.3493
11	477.421	71.4897
12	554.227	82.1219
13	642.519	94.4626
14	744.134	108.767
15	861.181	125.329
16	996.092	144.493

Table of nominal constants for MJS.

The delta values are the full widths.

E_2 Mode. K = 1.333522

MODULATOR STEP	THRESHOLD VOLTAGE	PEAK VOLTAGE	AVERAGE VOLTAGE	DELTA VOLTAGE
1	10.0000	30.0113	20.0056	20.0113
2	30.0118	56.6968	43.3541	26.6855
3	56.6968	92.2825	74.4897	35.5857
4	92.2825	139.737	116.010	47.4543
5	139.737	203.018	171.377	63.2814
6	203.018	287.405	245.212	84.3870
7	287.405	399.937	343.671	112.532
8	399.937	550.001	474.969	150.064
9	550.001	750.114	650.058	200.113
10	750.114	1016.97	883.542	266.855
11	1016.97	1372.83	1194.90	355.858
12	1372.83	1847.37	1610.10	474.544
13	1847.37	2480.19	2163.78	632.815
14	2480.19	3324.06	2902.12	843.872
15	3324.06	4449.38	3886.72	1125.32
16	4449.38	5950.02	5199.70	1500.64

MODULATOR STEP	ELECTRONS AVERAGE SPEED	ELECTRONS DELTA SPEED
1	2564.08	1374.53
2	3860.12	1217.55
3	5085.13	1232.49
4	6358.58	1314.40
5	7736.11	1440.67
6	9259.03	1605.17
7	10965.3	1807.44
8	12893.9	2049.76
9	15086.9	2336.08
10	17590.8	2671.79
11	20458.4	3063.48
12	23749.7	3519.09
13	27533.2	4047.91
14	31887.6	4660.86
15	36903.3	5370.59
16	42684.5	6191.81

Appendix B

```
      SUBROUTINE CUPINT(DN,U,W,NSTEP,CUR)                                DD 00010
      IMPLICIT REAL*8(A-H,O-Z)                                           DD 00020
      REAL*8 U(3),VZSUP/134.9/,RO/100./,ECHRGE/1.6E-19/                  DD 00030
      REAL*8 PI/3.14152654/                                              DD 00040
      REAL*8 AMVZ(128)/                                                  DD 00050
     +    46.06,  50.50,  54.73,  58.79,  62.72,  66.56,  70.31,  74.00,DD 00060
     +    77.63,  81.23,  84.80,  88.35,  91.89,  95.41,  98.93, 102.46,DD 00070
     +   105.99, 109.52, 113.07, 116.64, 120.23, 123.83, 127.47, 131.12,DD 00080
     +   134.81, 138.53, 142.28, 146.07, 149.90, 153.77, 157.67, 161.62,DD 00090
     +   165.62, 169.66, 173.76, 177.90, 182.09, 186.34, 190.65, 195.01,DD 00100
     +   199.43, 203.91, 208.46, 213.07, 217.74, 222.48, 227.29, 232.18,DD 00110
     +   237.13, 242.16, 247.27, 252.45, 257.71, 263.06, 268.49, 274.00,DD 00120
     +   279.60, 285.29, 291.08, 296.95, 302.92, 308.99, 315.15, 321.42,DD 00130
     +   327.79, 334.26, 340.84, 347.54, 354.34, 361.26, 368.29, 375.44,DD 00140
     +   382.71, 390.11, 397.63, 405.28, 413.06, 420.98, 429.03, 437.22,DD 00150
     +   445.54, 454.02, 462.64, 471.41, 480.33, 489.41, 498.64, 508.04,DD 00160
     +   517.60, 527.32, 537.22, 547.29, 557.54, 567.97, 578.58, 589.38,DD 00170
     +   600.37, 611.55, 622.93, 634.52, 646.30, 658.30, 670.51, 682.94,DD 00180
     +   695.58, 708.46, 721.56, 734.89, 748.47, 762.28, 776.34, 790.65,DD 00190
     +   805.22, 820.05, 835.14, 850.51, 866.15, 882.07, 898.27, 914.77,DD 00200
     +   931.56, 948.65, 966.05, 983.76,1001.80,1020.10,1038.80,1057.90/DD 00210
      REAL*8 AMDVZ(128)/                                                 DD 00220
     +     4.57,   4.32,   4.13,   3.99,   3.88,   3.79,   3.72,   3.66,DD 00230
     +     3.62,   3.58,   3.56,   3.54,   3.53,   3.52,   3.52,   3.53,DD 00240
     +     3.53,   3.54,   3.56,   3.58,   3.59,   3.62,   3.65,   3.67,DD 00250
     +     3.70,   3.74,   3.77,   3.81,   3.84,   3.89,   3.93,   3.97,DD 00260
     +     4.02,   4.07,   4.11,   4.17,   4.22,   4.28,   4.33,   4.40,DD 00270
     +     4.45,   4.51,   4.58,   4.64,   4.70,   4.78,   4.85,   4.92,DD 00280
     +     4.99,   5.06,   5.15,   5.22,   5.31,   5.38,   5.47,   5.56,DD 00290
     +     5.65,   5.73,   5.83,   5.92,   6.02,   6.11,   6.22,   6.32,DD 00300
     +     6.42,   6.53,   6.63,   6.75,   6.86,   6.97,   7.10,   7.21,DD 00310
     +     7.33,   7.46,   7.59,   7.71,   7.85,   7.98,   8.12,   8.25,DD 00320
     +     8.41,   8.54,   8.70,   8.84,   9.00,   9.15,   9.32,   9.47,DD 00330
     +     9.65,   9.81,   9.98,  10.16,  10.34,  10.52,  10.70,  10.89,DD 00340
     +    11.09,  11.28,  11.48,  11.69,  11.89,  12.10,  12.32,  12.53,DD 00350
     +    12.76,  12.99,  13.22,  13.45,  13.69,  13.94,  14.18,  14.44,DD 00360
     +    14.70,  14.96,  15.23,  15.50,  15.78,  16.06,  16.35,  16.64,DD 00370
     +    16.94,  17.24,  17.56,  17.87,  18.20,  18.50,  18.90,  19.10/DD 00380
      CUR=0.D0                                                           DD 00390
      VZT=AMVZ(NSTEP)-AMDVZ(NSTEP)/2.D0                                  DD 00400
      VZ=VZT                                                             DD 00410
      X1=(VZ-U(3))/W                                                     DD 00420
      IF (X1 .GT. 3.D0) RETURN                                           DD 00430
      DVZ=AMDVZ(NSTEP)/10.D0                                             DD 00440
      N=0                                                                DD 00450
   10 CONTINUE                                                           DD 00460
      N=N+1                                                              DD 00470
      NN=MOD(N,2)                                                        DD 00480
      VZ=VZ+DVZ                                                          DD 00490
      X1=(VZ-U(3))/W                                                     DD 00500
      IF (X1 .LT. -5.D0) GO TO 10                                        DD 00510
      IF(X1 .GT. 3.D0) GO TO 100                                         DD 00520
      P1=(VZT/VZ)**2                                                     DD 00530
      P2=(VZSUP/VZ)**2                                                   DD 00540
      X=DABS(U(1)/VZ)                                                    DD 00550
```

```
      Y=U(2)/VZ                                                          DD 00560
      CALL TRANSP(X,Y,P1,P2,T)                                           DD 00570
      CALL AREAOV(X,Y,P1,P2,R)                                           DD 00580
      IF(NN .EQ. 1)CUR=CUR+R*T*DEXP(-X1**2)*VZ*2.D0                      DD 00590
      IF(NN .EQ. 0)CUR=CUR+R*T*DEXP(-X1**2)*VZ                           DD 00600
      GO TO 10                                                           DD 00610
  100 CONTINUE                                                           DD 00620
      CUR=CUR*RO*ECHRGE*DN/(W*DSQRT(PI))*1.E20*DVZ*2.D0/3.D0             DD 00630
C      CUR=CUR+R*T*DEXP(-X1**2)*VZ                                       DD 00640
C      CUR=CUR*RO*ECHRGE*DN/(W*DSQRT(PI))*1.E20*DVZ                      DD 00650
      RETURN                                                             DD 00660
      END                                                                DD 00670
      SUBROUTINE TRANSP(X,Y,P1,P2,T)                                     DD 00680
      IMPLICIT REAL*8(A-H,O-Z)                                           DD 00690
      C=1/42.D0                                                          DD 00700
      X2=X**2                                                            DD 00710
      Y2=Y**2                                                            DD 00720
      T=((1.D0-C*DSQRT(1.D0+X2))*(1.D0-C*DSQRT(1.D0+Y2)))**5             DD 00730
      T=T*((1.D0-C*DSQRT(1.D0+X2/(1.D0-P1)))*                            DD 00740
     *   (1.D0-C*DSQRT(1.D0+Y2/(1.D0-P1))))**3                           DD 00750
      T=T*(1.D0-C*DSQRT(1.D0+X2/(1.D0+P2)))*                             DD 00760
     *   (1.D0-C*DSQRT(1.D0+Y2/(1.D0+P2)))                               DD 00770
      RETURN                                                             DD 00780
      END                                                                DD 00790
      SUBROUTINE AREAOV(X,Y,P1,P2,R)                                     DD 00800
      IMPLICIT REAL*8 (A-H,O-Z)                                          DD 00810
      REAL*8 A/.338D0/,B/.197D0/,C/.093D0/,D/.372D0/                     DD 00820
      SHIFT=A+B*2*(DSQRT(1.D0+P2)-1.D0)/P2+C/DSQRT(1.D0-P1)+             DD 00830
     +   D*2*(1.D0-DSQRT(1.D0-P1))/P1                                    DD 00840
      X1=SHIFT*X                                                         DD 00850
      Y1=SHIFT*Y                                                         DD 00860
      IF (X1 .GT. 4.94D0) GO TO 100                                      DD 00870
      R=(4.94D0-X1)/3.84D0                                               DD 00880
      IF (X1 .LT. 1.1D0) R=1.D0                                          DD 00890
      IF (Y1 .LT. -2.02D0) GO TO 10                                      DD 00900
      Y3=YU(X1)                                                          DD 00910
      Y4=YUP(X1)                                                         DD 00920
      IF (Y1-Y3) 1,1,2                                                   DD 00930
    1 RETURN                                                             DD 00940
    2 IF (Y1 .GT. Y4) GO TO 100                                          DD 00950
      R=R*(Y4-Y1)/(Y4-Y3)                                                DD 00960
      RETURN                                                             DD 00970
   10 IF (Y1 .LT. -3.63D0) GO TO 100                                     DD 00980
      R=R*(3.63D0+Y1)/1.61D0                                             DD 00990
      RETURN                                                             DD 01000
  100 R=0.D0                                                             DD 01010
      RETURN                                                             DD 01020
      END                                                                DD 01030
      FUNCTION YU(X)                                                     DD 01040
      IMPLICIT REAL*8 (A-H,O-Z)                                          DD 01050
      A=.762D0                                                           DD 01060
      B=1.018D0                                                          DD 01070
      C=.247D0                                                           DD 01080
      D=.25D0                                                            DD 01090
      YU=A*DCOS(B*X+C)/(1.D0+D*X)                                        DD 01100
```

```
RETURN                                                          DD 01110
END                                                             DD 01120
FUNCTION YUP(X)                                                 DD 01130
IMPLICIT REAL*8 (A-H,O-Z)                                       DD 01140
A=2.5D0                                                         DD 01150
B=0.125D0                                                       DD 01160
YUP=A-B*(X-1.D0)**2                                             DD 01170
RETURN                                                          DD 01180
END                                                             DD 01190
```

Appendix C

```
      SUBROUTINE DCPINT(DN,U,W,NSTEP,CUR)                                    DD 00010
      IMPLICIT REAL*8 (A-H,O-Z)                                              DD 00020
      REAL*8 U(3),VZSUP/134.9/,ECHRGE/1.6E-19/,PI/3.141592654/,RC/6.35/,DD 00030
     ,  RG/5.1308/,RA/5.6438/,                                               DD 00040
     ,  RCG2/13.99739136/,RCA2/8.47002156/,RAG2/5.5273698/,RO/82.7/          DD 00050
      REAL*8 AMVZ(128)/                                                      DD 00060
     +    46.06,  50.50,  54.73,  58.79,  62.72,  66.56,  70.31,  74.00,DD 00070
     +    77.63,  81.23,  84.80,  88.35,  91.89,  95.41,  98.93, 102.46,DD 00080
     +   105.99, 109.52, 113.07, 116.64, 120.23, 123.83, 127.47, 131.12,DD 00090
     +   134.81, 138.53, 142.28, 146.07, 149.90, 153.77, 157.67, 161.62,DD 00100
     +   165.62, 169.66, 173.76, 177.90, 182.09, 186.34, 190.65, 195.01,DD 00110
     +   199.43, 203.91, 208.46, 213.07, 217.74, 222.48, 227.29, 232.18,DD 00120
     +   237.13, 242.16, 247.27, 252.45, 257.71, 263.06, 268.49, 274.00,DD 00130
     +   279.60, 285.29, 291.08, 296.95, 302.92, 308.99, 315.15, 321.42,DD 00140
     +   327.79, 334.26, 340.84, 347.54, 354.34, 361.26, 368.29, 375.44,DD 00150
     +   382.71, 390.11, 397.63, 405.28, 413.06, 420.98, 429.03, 437.22,DD 00160
     +   445.54, 454.02, 462.64, 471.41, 480.33, 489.41, 498.64, 508.04,DD 00170
     +   517.60, 527.32, 537.22, 547.29, 557.54, 567.97, 578.58, 589.38,DD 00180
     +   600.37, 611.55, 622.93, 634.52, 646.30, 658.30, 670.51, 682.94,DD 00190
     +   695.58, 708.46, 721.56, 734.89, 748.47, 762.28, 776.34, 790.65,DD 00200
     +   805.22, 820.05, 835.14, 850.51, 866.15, 882.07, 898.27, 914.77,DD 00210
     +   931.56, 948.65, 966.05, 983.76,1001.80,1020.10,1038.80,1057.90/DD 00220
      REAL*8 AMDVZ(128)/                                                     DD 00230
     +     4.57,   4.32,   4.13,   3.99,   3.88,   3.79,   3.72,   3.66,DD 00240
     +     3.62,   3.58,   3.56,   3.54,   3.53,   3.52,   3.52,   3.53,DD 00250
     +     3.53,   3.54,   3.56,   3.58,   3.59,   3.62,   3.65,   3.67,DD 00260
     +     3.70,   3.74,   3.77,   3.81,   3.84,   3.89,   3.93,   3.97,DD 00270
     +     4.02,   4.07,   4.11,   4.17,   4.22,   4.28,   4.33,   4.40,DD 00280
     +     4.45,   4.51,   4.58,   4.64,   4.70,   4.78,   4.85,   4.92,DD 00290
     +     4.99,   5.06,   5.15,   5.22,   5.31,   5.38,   5.47,   5.56,DD 00300
     +     5.65,   5.73,   5.83,   5.92,   6.02,   6.11,   6.22,   6.32,DD 00310
     +     6.42,   6.53,   6.63,   6.75,   6.86,   6.97,   7.10,   7.21,DD 00320
     +     7.33,   7.46,   7.59,   7.71,   7.85,   7.98,   8.12,   8.25,DD 00330
     +     8.41,   8.54,   8.70,   8.84,   9.00,   9.15,   9.32,   9.47,DD 00340
     +     9.65,   9.81,   9.98,  10.16,  10.34,  10.52,  10.70,  10.89,DD 00350
     +    11.09,  11.28,  11.48,  11.69,  11.89,  12.10,  12.32,  12.53,DD 00360
     +    12.76,  12.99,  13.22,  13.45,  13.69,  13.94,  14.18,  14.44,DD 00370
     +    14.70,  14.96,  15.23,  15.50,  15.78,  16.06,  16.35,  16.64,DD 00380
     +    16.94,  17.24,  17.56,  17.87,  18.20,  18.50,  18.90,  19.10/DD 00390
      CUR=0.D0                                                               DD 00400
      IF(U(1) .EQ. 0.D0 .AND. U(2) .EQ. 0.D0) GO TO 1                        DD 00410
      PHI=DATAN2(U(2),U(1))                                                  DD 00420
      GO TO 2                                                                DD 00430
    1 PHI=0.D0                                                               DD 00440
    2 VT2=U(1)**2+U(2)**2                                                    DD 00450
      VZT=AMVZ(NSTEP)-AMDVZ(NSTEP)/2.D0                                      DD 00460
      VZ=VZT                                                                 DD 00470
      X1=(VZ-U(3))/W                                                         DD 00480
      IF (X1 .GT. 3.D0) RETURN                                               DD 00490
      DVZ=AMDVZ(NSTEP)/10.D0                                                 DD 00500
      N=0                                                                    DD 00510
   10 CONTINUE                                                               DD 00520
      N=N+1                                                                  DD 00530
      NN=MOD(N,2)                                                            DD 00540
      VZ=VZ+DVZ                                                              DD 00550
```

```
      X1=(VZ-U(3))/W                                                    DD 00560
      IF (X1 .LT. -5.D0) GO TO 10                                       DD 00570
      IF (X1 .GT. 3.D0)GO TO 500                                        DD 00580
      P1=(VZT/VZ)**2                                                    DD 00590
      P2=(VZSUP/VZ)**2                                                  DD 00600
      PSI=VT2/VZ**2                                                     DD 00610
      CALL TRNSPD(PSI,PHI,P1,P2,T)                                      DD 00620
      CALL SHIFT(PSI,P1,P2,DCA,DCG,DAG)                                 DD 00630
      IF (DCA .EQ. 0.D0) GO TO 150                                      DD 00640
      XCG=(RCG2+DCG**2)/(2.D0*DCG)                                      DD 00650
      XCA=(RCA2+DCA**2)/(2.D0*DCA)                                      DD 00660
      IF (XCA-XCG) 100,200,200                                          DD 00670
  100 CALL CLAROV(RCG2,RC,RG,DCG,A1)                                    DD 00680
      CALL CLAROV(RAG2,RA,RG,DAG,A2)                                    DD 00690
      R=A1+A2-R0                                                        DD 00700
      GO TO 250                                                         DD 00710
  150 R=R0                                                              DD 00720
      GO TO 250                                                         DD 00730
  200 CALL CLAROV(RCA2,RC,RA,DCA,R)                                     DD 00740
  250 CONTINUE                                                          DD 00750
      IF(NN .EQ. 1)CUR=CUR+R*T*DEXP(-X1**2)*VZ*2.D0                     DD 00760
      IF(NN .EQ. 0)CUR=CUR+R*T*DEXP(-X1**2)*VZ                          DD 00770
      GO TO 10                                                          DD 00780
  500 CONTINUE                                                          DD 00790
      CUR=CUR*ECHRGE*DN/(W*DSQRT(PI))*1.0D20*DVZ*2.D0/3.D0              DD 00800
      RETURN                                                            DD 00810
      END                                                               DD 00820
      SUBROUTINE TRNSPD(PSI,PHI,P1,P2,T)                                DD 00830
      IMPLICIT REAL*8 (A-H,O-Z)                                         DD 00840
      REAL*8 C/.02381D0/,A1/0.D0/,A2/1.0821D0/,A3/.8727D0/,             DD 00850
     ,   A4/.9599D0/,A5/.6981D0/,A6/.0698D0/,AM/1.1868D0/,AS/0.D0/      DD 00860
      T=(1.D0-C*DSQRT(1.D0+PSI*DCOS(PHI-A1)**2))*                       DD 00870
     *  (1.D0-C*DSQRT(1.D0+PSI*DSIN(PHI-A1)**2))*                       DD 00880
     *  (1.D0-C*DSQRT(1.D0+PSI*DCOS(PHI-A2)**2))*                       DD 00890
     *  (1.D0-C*DSQRT(1.D0+PSI*DSIN(PHI-A2)**2))*                       DD 00900
     *  (1.D0-C*DSQRT(1.D0+PSI*DCOS(PHI-A3)**2))*                       DD 00910
     *  (1.D0-C*DSQRT(1.D0+PSI*DSIN(PHI-A3)**2))*                       DD 00920
     *  (1.D0-C*DSQRT(1.D0+PSI*DCOS(PHI-A4)**2))*                       DD 00930
     *  (1.D0-C*DSQRT(1.D0+PSI*DSIN(PHI-A4)**2))*                       DD 00940
     *  (1.D0-C*DSQRT(1.D0+PSI*DCOS(PHI-A5)**2))*                       DD 00950
     *  (1.D0-C*DSQRT(1.D0+PSI*DSIN(PHI-A5)**2))*                       DD 00960
     *  (1.D0-C*DSQRT(1.D0+PSI*DCOS(PHI-A6)**2))*                       DD 00970
     *  (1.D0-C*DSQRT(1.D0+PSI*DSIN(PHI-A6)**2))*                       DD 00980
     *  (1.D0-C*DSQRT(1.D0+PSI*DCOS(PHI-AM)**2/(1.D0-P1)))*             DD 00990
     *  (1.D0-C*DSQRT(1.D0+PSI*DSIN(PHI-AM)**2/(1.D0-P1)))*             DD 01000
     *  (1.D0-C*DSQRT(1.D0+PSI*DCOS(PHI-AS)**2/(1.D0+P2)))*             DD 01010
     *  (1.D0-C*DSQRT(1.D0+PSI*DSIN(PHI-AS)**2/(1.D0+P2)))              DD 01020
      RETURN                                                            DD 01030
      END                                                               DD 01040
      SUBROUTINE CLAROV(R2,RL,RS,D,A)                                   DD 01050
      IMPLICIT REAL*8 (A-H,O-Z)                                         DD 01060
      REAL*8 PI/3.141592654D0/                                          DD 01070
      IF (D-RL+RS) 1,1,2                                                DD 01080
    1 A=PI*RS**2                                                        DD 01090
      RETURN                                                            DD 01100
```

```
2 IF(D-RL-RS) 3,4,4                                                    DD 01110
3 QS=(R2-D**2)/(2.D0*D*RS)                                             DD 01120
  QL=(R2+D**2)/(2.D0*D*RL)                                             DD 01130
  A=RS**2*(PI/2.D0+DARSIN(QS)+QS*DSQRT(1.D0-QS**2))+                   DD 01140
 + RL**2*(PI/2.D0-DARSIN(QL)-QL*DSQRT(1.D0-QL**2))                     DD 01150
  RETURN                                                               DD 01160
4 A=0.D0                                                               DD 01170
  RETURN                                                               DD 01180
  END                                                                  DD 01190
  SUBROUTINE SHIFT(PSI,P1,P2,DCA,DCG,DAG)                              DD 01200
  IMPLICIT REAL*8(A-H,O-Z)                                             DD 01210
  S=.495D0+.720D0*(1.D0-DSQRT(1.D0-P1))/P1+                            DD 01220
 +  .290D0*(DSQRT(1.D0+P2)-1.D0)/P2                                    DD 01230
  B=S/(.166D0+.139D0*(DSQRT(1.D0+P2)-1.D0)/P2)                         DD 01240
  DCA=DSQRT(PSI)*6.D0*S                                                DD 01250
  DCG=DCA/B                                                            DD 01260
  DAG=DCA-DCG                                                          DD 01270
  RETURN                                                               DD 01280
  END                                                                  DD 01290
```

Appendix D

```
      SUBROUTINE ABCCUR(DN,W,U1,A,Z,NCHN,DISTF)                          DIS00010
      IMPLICIT REAL*8 (A-H,O-Z)                                          DIS00020
      REAL*8 CM(100),VZSC2,SCPOT/-12.5D0/                                DIS00030
      COMMON/CM/CM,N13                                                   DIS00040
      INTEGER*4 NCHN(2),NSTEP(129)/22,16,10,6,41*4,84*2/,NFIRST          DIS00050
      INTEGER*4 NTAIL(2)                                                 DIS00060
      INTEGER MFIRST(128)/3,6,10,13,17,20,23,26,29,                      DIS00070
     , 32,35,38,39,41,42,44,45,46,48,49,50,52,53,54,55,56,58,59,60,61,   DIS00080
     , 63,64,65,66,67,68,70,71,72,73,74,75,76,77,78,80,81,82,83,84,85,   DIS00090
     , 86,87,88,89,90,92,93,94,95,96,97,98,99,100,101,102,103,104,105,   DIS00100
     , 106,107,108,109,110,111,112,113,115,49*0/                         DIS00110
      REAL*4 AMA1,AMA2,AMC1,AMSFT,ABCS                                   DIS00120
      REAL*4 AAAVZ,AAVZ,AVZ,AAADVZ,AADVZ,ADVZ,DVOLT                      DIS00130
      REAL*8 U(3),ZX(4,2),ZY(4,2,2),U1(3),AA(2),SS(2),CC(2)              DIS00140
      REAL*8 A1(2),XBAR(2),A2(2),B(2,2),D(2,2),AC(2),CRR(129)/129*0.D0/  DIS00150
      REAL*8 X(4)/-4.94D0,-1.10D0,1.10D0,4.94D0/,                        DIS00160
     ,     Y(4,2)/-3.63D0,-2.02D0,2.02D0,3.63D0,                         DIS00170
     ,    -3.63D0,-2.02D0,2.02D0,3.63D0/                                 DIS00180
      REAL*8 R/100./,T/.65/,ECHRGE/1.6D-19/,SQRTPI/1.772453851/          DIS00190
      REAL*8 PI/3.141592654/,PRESET/Z7FFFFFFF/,DISTF(128),CUR1(241,5,2)  DIS00200
      COMMON/TRNPAR/AMA1(100,129),AMA2(100,129),AMC1(100,129),           DIS00210
     ,  AMSFT(100,129)                                                   DIS00220
      COMMON/ABCSET/ABCS(241,4,2)                                        DIS00230
      COMMON/VZ/AAAVZ(22,5),AAVZ(4,40),AVZ(2,84),AAADVZ(22,5),           DIS00240
     ,   AADVZ(4,40),ADVZ(2,84),DVOLT(128),NFIRST(129)                   DIS00250
      DO 1 I=1,128                                                       DIS00260
      IF(I .GE. 80)MFIRST(I)=I+36                                        DIS00270
    1 DISTF(I)=0.D0                                                      DIS00280
C     THE FOLLOWING LINE IS FOR NON-ZERO SPACECRAFT POTENTIAL            DIS00290
      VZSC2=2.D0*Z*ECHRGE*SCPOT/(A*1.67D-27*1.D6*W**2)                   DIS00300
C                                                                        DIS00310
      CONST=R*T*Z*ECHRGE*1.0D20/SQRTPI*DN                                DIS00320
      NCHAN1=NCHN(1)                                                     DIS00330
      NCHAN2=NCHN(2)                                                     DIS00340
      NCHAN3=NCHN(2)+1                                                   DIS00350
      NTAIL(1)=NFIRST(NCHAN1)                                            DIS00360
      NTAIL(2)=MFIRST(NCHAN2)-1                                          DIS00370
      CALL SETCUR(W,U1,A,Z,NTAIL,1,CUR1)                                 DIS00380
      NTAIL(1)=MFIRST(NCHAN1)                                            DIS00390
      NTAIL(2)=99+NFIRST(NCHAN2)-NSTEP(NCHAN2)                           DIS00400
      CALL SETCUR(W,U1,A,Z,NTAIL,2,CUR1)                                 DIS00410
C                                                                        DIS00420
C     NORMALIZE VELOCITY                                                 DIS00430
C                                                                        DIS00440
      DO 3 I=1,3                                                         DIS00450
    3 U(I)=U1(I)/W                                                       DIS00460
C                                                                        DIS00470
C     INTEGRATE ACROSS CURRENT CHANNEL                                   DIS00480
C                                                                        DIS00490
      DO 2700 NCHAN=NCHAN1,NCHAN3                                        DIS00500
      CURENT=0.D0                                                        DIS00510
      NS=NSTEP(NCHAN)                                                    DIS00520
      DO 2600 JJ=1,NS                                                    DIS00530
      G=0.D0                                                             DIS00540
C                                                                        DIS00550
```

```
C     SELECT VALUE OF VZ,DVZ                                                DIS00560
C                                                                           DIS00570
      IF(NCHAN .GE. 6 .AND. NCHAN .LE. 45)GO TO 10                          DIS00580
      IF(NCHAN .GE. 46)GO TO 20                                             DIS00590
      VZ=DBLE(AAAVZ(JJ,NCHAN))*DSQRT(Z/A)/W                                 DIS00600
      DVZ=DBLE(AAADVZ(JJ,NCHAN))*DSQRT(Z/A)                                 DIS00610
      GO TO 100                                                             DIS00620
   10 VZ=DBLE(AAVZ(JJ,NCHAN-5))*DSQRT(Z/A)/W                                DIS00630
      DVZ=DBLE(AADVZ(JJ,NCHAN-5))*DSQRT(Z/A)                                DIS00640
      GO TO 100                                                             DIS00650
   20 VZ=DBLE(AVZ(JJ,NCHAN-45))*DSQRT(Z/A)/W                                DIS00660
      DVZ=DBLE(ADVZ(JJ,NCHAN-45))*DSQRT(Z/A)                                DIS00670
  100 CONTINUE                                                              DIS00680
C     THE FOLLOWING LINE CORRECTS FOR NON-ZERO SPACECRAFT POTENTIAL         DIS00690
      VZ2=VZ**2+VZSC2                                                       DIS00700
      IF(VZ2 .LT. 0.D0)GO TO 2600                                           DIS00710
      X1=(DSQRT(VZ2)-U(3))**2                                               DIS00720
C                                                                           DIS00730
C     X1=(VZ-U(3))**2                                                       DIS00740
      IF (X1 .GT. 16.D0) GO TO 2600                                         DIS00750
C                                                                           DIS00760
C     ASSIGN VALUES OF RESPONSE PARAMETERS                                  DIS00770
C                                                                           DIS00780
      S=DBLE(AMSFT(JJ,NCHAN))                                               DIS00790
      CC(1)=DBLE(AMC1(JJ,NCHAN))                                            DIS00800
      CC(2)=1.0D0-CC(1)                                                     DIS00810
      AC(1)=DBLE(AMA1(JJ,NCHAN))                                            DIS00820
      AC(2)=DBLE(AMA2(JJ,NCHAN))                                            DIS00830
      AA(1)=(AC(1)+VZ**2)/S**2                                              DIS00840
      AA(2)=(AC(2)+VZ**2)/S**2                                              DIS00850
      SS(1)=S*VZ*U(1)/(VZ*VZ+AC(1))                                         DIS00860
      SS(2)=S*VZ*U(1)/(VZ*VZ+AC(2))                                         DIS00870
C                                                                           DIS00880
C     COMPUTE CURRENTS                                                      DIS00890
C                                                                           DIS00900
      DO 2020 L=1,4                                                         DIS00910
      ZX(L,1)=DSQRT(AA(1))*(X(L)-SS(1))                                     DIS00920
 2020 ZX(L,2)=DSQRT(AA(2))*(X(L)-SS(2))                                     DIS00930
      XBAR(1)=(PSI(ZX(2,1),SS(1),AA(1))+PSI(ZX(4,1),SS(1),AA(1))-           DIS00940
     -   PSI(ZX(1,1),SS(1),AA(1))-PSI(ZX(3,1),SS(1),AA(1))+                DIS00950
     +   (ZX(4,1)-ZX(3,1))*FUN(SS(1),AA(1)))/                              DIS00960
     /  (DSQRT(PI*AA(1))*                                                   DIS00970
     *  (PHI(ZX(4,1))+PHI(ZX(1,1))-PHI(ZX(3,1))-PHI(ZX(2,1))))             DIS00980
      XBAR(2)=(PSI(ZX(2,2),SS(2),AA(2))+PSI(ZX(4,2),SS(2),AA(2))-           DIS00990
     -   PSI(ZX(1,2),SS(2),AA(2))-PSI(ZX(3,2),SS(2),AA(2))+                DIS01000
     +   (ZX(4,2)-ZX(3,2))*FUN(SS(2),AA(2)))/                              DIS01010
     /  (DSQRT(PI*AA(2))*                                                   DIS01020
     *  (PHI(ZX(4,2))+PHI(ZX(1,2))-PHI(ZX(3,2))-PHI(ZX(2,2))))             DIS01030
      IF (DABS(XBAR(1))-1.1D0) 2021,2021,2022                               DIS01040
 2021 A2(1)=1.0D0                                                           DIS01050
      GO TO 2023                                                            DIS01060
 2022 A2(1)=1.257D0-0.063D0*DABS(XBAR(1))-                                  DIS01070
     -   0.126D0*DSQRT(XBAR(1)**2-5.10D0*DABS(XBAR(1))+6.612D0)             DIS01080
 2023 CONTINUE                                                              DIS01090
      IF (DABS(XBAR(2))-1.1D0) 2026,2026,2027                               DIS01100
```

```
 2026 A2(2)=1.0D0                                                        DIS01110
      GO TO 2028                                                         DIS01120
 2027 A2(2)=1.257D0-0.063D0*DABS(XBAR(2))-                               DIS01130
     -   0.126D0*DSQRT(XBAR(2)**2-5.10D0*DABS(XBAR(2))+6.612D0)         DIS01140
 2028 CONTINUE                                                           DIS01150
      Y(3,1)=.762D0*DCOS(1.018D0*XBAR(1)+.247D0)/(1.0D0+.25D0*XBAR(1))   DIS01160
      Y(3,2)=.762D0*DCOS(1.018D0*XBAR(2)+.247D0)/(1.0D0+.25D0*XBAR(2))   DIS01170
      Y(4,1)=2.5D0-0.125D0*(XBAR(1)-1.0D0)**2                            DIS01180
      Y(4,2)=2.5D0-0.125D0*(XBAR(2)-1.0D0)**2                            DIS01190
C     WRITE(6,*)XBAR(1),Y(3,1),Y(4,1)                                    DIS01200
      SS(1)=S*VZ*U(2)/(VZ*VZ+AC(1))                                      DIS01210
      SS(2)=S*VZ*U(2)/(VZ*VZ+AC(2))                                      DIS01220
      DO 2030 L=1,4                                                      DIS01230
      ZY(L,1,1)=DSQRT(AA(1))*(Y(L,1)-SS(1))                              DIS01240
      ZY(L,2,1)=DSQRT(AA(1))*(Y(L,2)-SS(1))                              DIS01250
      ZY(L,1,2)=DSQRT(AA(2))*(Y(L,1)-SS(2))                              DIS01260
 2030 ZY(L,2,2)=DSQRT(AA(2))*(Y(L,2)-SS(2))                              DIS01270
      A1(1)=(PHI(ZX(1,1))+PHI(ZX(4,1))-PHI(ZX(3,1))-PHI(ZX(2,1)))/       DIS01280
     /   (ZX(4,1)-ZX(3,1))                                               DIS01290
      A1(2)=(PHI(ZX(1,2))+PHI(ZX(4,2))-PHI(ZX(3,2))-PHI(ZX(2,2)))/       DIS01300
     /   (ZX(4,2)-ZX(3,2))                                               DIS01310
 2049 CONTINUE                                                           DIS01320
      DO 2500 I=1,2                                                      DIS01330
      DO 2450 J=1,2                                                      DIS01340
      B(I,J)=(PHI(ZY(4,I,J))-PHI(ZY(3,I,J)))/(ZY(4,I,J)-ZY(3,I,J))-      DIS01350
     -   (PHI(ZY(1,I,J))-PHI(ZY(2,I,J)))/(ZY(1,I,J)-ZY(2,I,J))          DIS01360
      D(I,J)=-U(1)**2*AC(I)/(VZ**2+AC(I))-U(2)**2*AC(J)/(VZ**2+AC(J))    DIS01370
      IF (D(I,J) .LT. -50.0D0) GO TO 2050                                DIS01380
      D(I,J)=CC(I)*CC(J)*DEXP(D(I,J))/DSQRT(AA(I)*AA(J))                 DIS01390
      GO TO 2051                                                         DIS01400
 2050 D(I,J)=0.                                                          DIS01410
 2051 CONTINUE                                                           DIS01420
      G=(VZ/S)**2*D(I,J)*A1(I)*A2(I)*B(I,J)/4+G                          DIS01430
 2450 CONTINUE                                                           DIS01440
 2500 CONTINUE                                                           DIS01450
      CUR=VZ*DEXP(-X1)*G*DVZ                                             DIS01460
      CURENT=CURENT+CUR                                                  DIS01470
C     WRITE(6,2) JJ,CUR,CURENT,VZ                                        DIS01480
    2 FORMAT(' JJ,CUR,CURENT,VZ=',I4,,3D16.7)                            DIS01490
 2600 CONTINUE                                                           DIS01500
      CRR(NCHAN)=CURENT                                                  DIS01510
 2700 CONTINUE                                                           DIS01520
C      WRITE(6,9000)(CRR(I),I=NCHAN1,NCHAN3)                             DIS01530
 9000 FORMAT(5D16.6)                                                     DIS01540
C                                                                       DIS01550
C    CALCULATE CONTRIBUTION FROM "TAIL"                                 DIS01560
C                                                                       DIS01570
      DO 3000 NCHAN=NCHAN1,NCHAN2                                        DIS01580
      DISTF(NCHAN)=CRR(NCHAN)-CRR(NCHAN+1)                               DIS01590
      IF(NCHAN .NE. N13)GO TO 17                                         DIS01600
      CM(1)=CRR(NCHAN)                                                   DIS01610
      IF(NCHAN .LE. 4)CM(1)=DISTF(NCHAN)                                 DIS01620
   17 NF=NFIRST(NCHAN)                                                   DIS01630
      IF(NCHAN .LE. 4)GO TO 2775                                         DIS01640
      NF1=NFIRST(NCHAN+1)-1                                              DIS01650
```

```
      N=NSTEP(NCHAN)+1                                                  DIS01660
      DO 2725 I=NF,NF1                                                  DIS01670
      IF(CUR1(I,1,1) .EQ. PRESET) GO TO 3000                            DIS01680
      IF(CUR1(I,1,1) .EQ. 0.D0) GO TO 2725                              DIS01690
      DISTF(NCHAN)=DISTF(NCHAN)+CUR1(I,1,1)+                            DIS01700
     +   CUR1(I,2,1)*DBLE(AMSFT(N,NCHAN)-ABCS(I,1,1))+                  DIS01710
     +   CUR1(I,3,1)*DBLE(AMA1(N,NCHAN)-ABCS(I,2,1))+                   DIS01720
     +   CUR1(I,4,1)*DBLE(AMA2(N,NCHAN)-ABCS(I,3,1))+                   DIS01730
     +   CUR1(I,5,1)*DBLE(AMC1(N,NCHAN)-ABCS(I,4,1))                    DIS01740
C     WRITE(6,9001)I,NCHAN,DISTF(NCHAN)                                 DIS01750
 9001 FORMAT(' I,NCHAN,DISTF(NCHAN)='I4,2D16.7)                         DIS01760
      N=N+1                                                             DIS01770
 2725 CONTINUE                                                          DIS01780
      N1=N                                                              DIS01790
      N2=NSTEP(NCHAN+1)+1                                               DIS01800
      IF(NCHAN .EQ. N13)CM(2)=DISTF(NCHAN)                              DIS01810
      GO TO 2750                                                        DIS01820
 2775 CONTINUE                                                          DIS01830
      I=1                                                               DIS01840
      N1=NSTEP(NCHAN)+1                                                 DIS01850
      N2=NSTEP(NCHAN+1)+1                                               DIS01860
 2750 DO 2900 LL=N1,100                                                 DIS01870
      M=1                                                               DIS01880
      IF(I .GE. MFIRST(NCHAN))M=2                                       DIS01890
      IF(CUR1(I,1,M) .EQ. 0.D0)GO TO 2900                               DIS01900
      IF(CUR1(I,1,M) .EQ. PRESET)GO TO 3000                             DIS01910
      DISTF(NCHAN)=DISTF(NCHAN)+                                        DIS01920
     +   CUR1(I,2,M)*DBLE(AMSFT(LL,NCHAN)-AMSFT(N2,NCHAN+1))+           DIS01930
     +   CUR1(I,3,M)*DBLE(AMA1(LL,NCHAN)-AMA1(N2,NCHAN+1))+             DIS01940
     +   CUR1(I,4,M)*DBLE(AMA2(LL,NCHAN)-AMA2(N2,NCHAN+1))+             DIS01950
     +   CUR1(I,5,M)*DBLE(AMC1(LL,NCHAN)-AMC1(N2,NCHAN+1))              DIS01960
      IF(NCHAN .EQ. N13)CM(I-NF1+2)=DISTF(NCHAN)                        DIS01970
      IF(NCHAN .EQ. N13 .AND. NCHAN .LE. 4)CM(I+1)=DISTF(NCHAN)         DIS01980
      I=I+1                                                             DIS01990
      N2=N2+1                                                           DIS02000
 2900 CONTINUE                                                          DIS02010
 3000 CONTINUE                                                          DIS02020
 5000 CONTINUE                                                          DIS02030
      DO 5001 NCHAN=1,128                                               DIS02040
 5001 DISTF(NCHAN)=DISTF(NCHAN)*CONST/DBLE(DVOLT(NCHAN))                DIS02050
      RETURN                                                            DIS02060
      END                                                               DIS02070
      FUNCTION FUN(SIGMA,ALPHA)                                         DIS02080
      IMPLICIT REAL*8 (A-H,O-Z)                                         DIS02090
      REAL*8 SQRTPI/1.772453851/                                        DIS02100
      X=SIGMA*DSQRT(ALPHA)                                              DIS02110
      FUN1=2.0D0*SQRTPI*X*DERF(X)                                       DIS02120
      IF (DABS(X) .GT. 10.0D0) GO TO 1                                  DIS02130
      FUN1=FUN1+2.0D0*DEXP(-X*X)                                        DIS02140
    1 FUN=FUN1                                                          DIS02150
      RETURN                                                            DIS02160
      END                                                               DIS02170
      FUNCTION PHI(Z)                                                   DIS02180
      IMPLICIT REAL*8 (A-H,O-Z)                                         DIS02190
      SQRTPI=1.772453851                                                DIS02200
```

```
      IF (DABS(Z) .GT. 10.D0) GO TO 1                                   DIS02210
      PHI=Z*DERF(Z)+DEXP(-Z*Z)/SQRTPI                                   DIS02220
      RETURN                                                            DIS02230
    1 PHI=Z*DERF(Z)                                                     DIS02240
      RETURN                                                            DIS02250
      END                                                               DIS02260
      FUNCTION PSI(Z,SIGMA,ALPHA)                                       DIS02270
      IMPLICIT REAL*8 (A-H,O-Z)                                         DIS02280
      SQRTPI=1.772453851                                                DIS02290
      PSI=SQRTPI*DERF(Z)*(-.5D0+SIGMA*DSQRT(ALPHA)*Z)                   DIS02300
      IF (DABS(Z) .GT. 10.D0) RETURN                                    DIS02310
      PSI=PSI+SIGMA*DSQRT(ALPHA)*DEXP(-Z*Z)                             DIS02320
      RETURN                                                            DIS02330
      END                                                               DIS02340
```

```
      SUBROUTINE SETCUR(W,U1,A,Z,NTAIL,M,CUR1)                          CUR00010
C                                                                       CUR00020
C     THIS PROGRAM COMPUTES THE CURRENTS IN THE TAIL AND THE DERIVATIVES CUR00030
C           OF THOSE CURRENTS WITH RESPECT TO THE PARAMETERS            CUR00040
C                 WHICH DESCRIBE THE RESPONSE FUNCTION                  CUR00050
C                                                                       CUR00060
      IMPLICIT REAL*8 (A-H,O-Z)                                         CUR00070
      INTEGER NTAIL(2),M                                                CUR00080
      REAL*8 U(3),ZX(4,2),ZY(4,2,2),U1(3),AA(2),SS(2),CC(2)             CUR00090
      REAL*8 SCPOT/-12.5D0/,ECHRGE/1.6D-19/                             CUR00100
      REAL*8 A1(2),XBAR(2),A2(2),B(2,2),D(2,2),AC(2),PRESET/Z7FFFFFFF/  CUR00110
      REAL*8 X(4)/-4.94D0,-1.10D0,1.10D0,4.94D0/,CUR1(241,5,2)          CUR00120
      REAL*8 Y(4,2)/-3.63D0,-2.02D0,2.02D0,3.63D0,                      CUR00130
     ,    -3.63D0,-2.02D0,2.02D0,3.63D0/                               CUR00140
      REAL*8 PI/3.141592654D0/,DCUR(4)/0.D0,.05D0,.001D0,.01D0/         CUR00150
      REAL*4 ABCS,TVZ,TDVZ                                              CUR00160
      COMMON /ABCSET/ABCS(241,4,2)                                      CUR00170
      COMMON /TAIL/TVZ(241),TDVZ(241)                                   CUR00180
C   THE FOLLOWING LINE IS FOR NON-ZERO SPACECRAFT POTENTIAL             CUR00190
      VZSC2=2.D0*Z*ECHRGE*SCPOT/(A*1.67D-27*1.D6*W**2)                  CUR00200
C                                                                       CUR00210
C                                                                       CUR00220
C     NORMALIZE THE VELOCITY                                            CUR00230
C                                                                       CUR00240
      DO 1 I=1,3                                                        CUR00250
    1 U(I)=U1(I)/W                                                      CUR00260
 2000 CONTINUE                                                          CUR00270
      NT1=NTAIL(1)                                                      CUR00280
      NT2=NTAIL(2)                                                      CUR00290
      DO 3700 JJ=NT1,NT2                                                CUR00300
C                                                                       CUR00310
C     CHOOSE VZ AND DVZ                                                 CUR00320
C                                                                       CUR00330
      VZ=DBLE(TVZ(JJ))*DSQRT(Z/A)/W                                     CUR00340
      VZ2=VZ**2+VZSC2                                                   CUR00350
      IF(VZ2 .LT. 0.D0) GO TO 3690                                      CUR00360
      DVZ=DBLE(TDVZ(JJ))*DSQRT(Z/A)                                     CUR00370
C     THE FOLLOWING LINE IS FOR NON-ZERO SPACECRAFT CHARGE              CUR00380
      X1=(DSQRT(VZ2)-U(3))                                              CUR00390
C                                                                       CUR00400
C     X1=(VZ-U(3))                                                      CUR00410
      IF (X1 .LT. -4.D0) GO TO 3690                                     CUR00420
      IF (X1 .GT. 4.D0) GO TO 3800                                      CUR00430
      X1=X1**2                                                          CUR00440
C                                                                       CUR00450
C     THIS LOOP COMPUTES THE DERIVATIVES                                CUR00460
C                                                                       CUR00470
      DO 3600 KK=1,4                                                    CUR00480
      G=0.D0                                                            CUR00490
      S=DBLE(ABCS(JJ,1,M))                                              CUR00500
      CC(1)=DBLE(ABCS(JJ,4,M))                                          CUR00510
      AC(1)=DBLE(ABCS(JJ,2,M))                                          CUR00520
      AC(2)=DBLE(ABCS(JJ,3,M))                                          CUR00530
      IF(KK .EQ. 2)S=S+DCUR(2)                                          CUR00540
      IF(KK .EQ. 3)AC(1)=AC(1)+DCUR(3)                                  CUR00550
```

```
      IF(KK .EQ. 4)AC(2)=AC(2)+DCUR(4)                                  CUR00560
      CC(2)=1.0D0-CC(1)                                                 CUR00570
      AA(1)=(AC(1)+VZ**2)/S**2                                          CUR00580
      AA(2)=(AC(2)+VZ**2)/S**2                                          CUR00590
      SS(1)=S*VZ*U(1)/(VZ*VZ+AC(1))                                     CUR00600
      SS(2)=S*VZ*U(1)/(VZ*VZ+AC(2))                                     CUR00610
      DO 3020 L=1,4                                                     CUR00620
      ZX(L,1)=DSQRT(AA(1))*(X(L)-SS(1))                                 CUR00630
 3020 ZX(L,2)=DSQRT(AA(2))*(X(L)-SS(2))                                 CUR00640
      XBAR(1)=(PSI(ZX(2,1),SS(1),AA(1))+PSI(ZX(4,1),SS(1),AA(1))-       CUR00650
     -   PSI(ZX(1,1),SS(1),AA(1))-PSI(ZX(3,1),SS(1),AA(1))+            CUR00660
     +   (ZX(4,1)-ZX(3,1))*FUN(SS(1),AA(1)))/                          CUR00670
     /  (DSQRT(PI*AA(1))*                                               CUR00680
     *  (PHI(ZX(4,1))+PHI(ZX(1,1))-PHI(ZX(3,1))-PHI(ZX(2,1))))         CUR00690
      XBAR(2)=(PSI(ZX(2,2),SS(2),AA(2))+PSI(ZX(4,2),SS(2),AA(2))-       CUR00700
     -   PSI(ZX(1,2),SS(2),AA(2))-PSI(ZX(3,2),SS(2),AA(2))+            CUR00710
     +   (ZX(4,2)-ZX(3,2))*FUN(SS(2),AA(2)))/                          CUR00720
     /  (DSQRT(PI*AA(2))*                                               CUR00730
     *  (PHI(ZX(4,2))+PHI(ZX(1,2))-PHI(ZX(3,2))-PHI(ZX(2,2))))         CUR00740
      IF (DABS(XBAR(1))-1.1D0) 3021,3021,3022                           CUR00750
 3021 A2(1)=1.0D0                                                       CUR00760
      GO TO 3023                                                        CUR00770
 3022 A2(1)=1.257D0-0.063D0*DABS(XBAR(1))-                              CUR00780
     -   0.126D0*DSQRT(XBAR(1)**2-5.10D0*DABS(XBAR(1))+6.612D0)        CUR00790
 3023 CONTINUE                                                          CUR00800
      IF (DABS(XBAR(2))-1.1D0) 3026,3026,3027                           CUR00810
 3026 A2(2)=1.0D0                                                       CUR00820
      GO TO 3028                                                        CUR00830
 3027 A2(2)=1.257D0-0.063D0*DABS(XBAR(2))-                              CUR00840
     -   0.126D0*DSQRT(XBAR(2)**2-5.10D0*DABS(XBAR(2))+6.612D0)        CUR00850
 3028 CONTINUE                                                          CUR00860
      Y(3,1)=.762D0*DCOS(1.018D0*XBAR(1)+.247D0)/(1.0D0+.25D0*XBAR(1))  CUR00870
      Y(3,2)=.762D0*DCOS(1.018D0*XBAR(2)+.247D0)/(1.0D0+.25D0*XBAR(2))  CUR00880
      Y(4,1)=2.5D0-0.125D0*(XBAR(1)-1.0D0)**2                           CUR00890
      Y(4,2)=2.5D0-0.125D0*(XBAR(2)-1.0D0)**2                           CUR00900
      SS(1)=S*VZ*U(2)/(VZ*VZ+AC(1))                                     CUR00910
      SS(2)=S*VZ*U(2)/(VZ*VZ+AC(2))                                     CUR00920
      DO 3030 L=1,4                                                     CUR00930
      ZY(L,1,1)=DSQRT(AA(1))*(Y(L,1)-SS(1))                             CUR00940
      ZY(L,2,1)=DSQRT(AA(1))*(Y(L,2)-SS(1))                             CUR00950
      ZY(L,1,2)=DSQRT(AA(2))*(Y(L,1)-SS(2))                             CUR00960
 3030 ZY(L,2,2)=DSQRT(AA(2))*(Y(L,2)-SS(2))                             CUR00970
  999 FORMAT(8D10.2)                                                    CUR00980
      A1(1)=(PHI(ZX(1,1))+PHI(ZX(4,1))-PHI(ZX(3,1))-PHI(ZX(2,1)))/      CUR00990
     /   (ZX(4,1)-ZX(3,1))                                             CUR01000
      A1(2)=(PHI(ZX(1,2))+PHI(ZX(4,2))-PHI(ZX(3,2))-PHI(ZX(2,2)))/      CUR01010
     /   (ZX(4,2)-ZX(3,2))                                             CUR01020
      DO 3500 I=1,2                                                     CUR01030
      DO 3450 J=1,2                                                     CUR01040
      B(I,J)=(PHI(ZY(4,I,J))-PHI(ZY(3,I,J)))/(ZY(4,I,J)-ZY(3,I,J))-     CUR01050
     -   (PHI(ZY(1,I,J))-PHI(ZY(2,I,J)))/(ZY(1,I,J)-ZY(2,I,J))         CUR01060
      D(I,J)=-U(1)**2*AC(I)/(VZ**2+AC(I))-U(2)**2*AC(J)/(VZ**2+AC(J))   CUR01070
      IF (D(I,J) .LT. -50.D0) GO TO 3050                                CUR01080
      D(I,J)=CC(I)*CC(J)*DEXP(D(I,J))/DSQRT(AA(I)*AA(J))                CUR01090
      GO TO 3051                                                        CUR01100
```

```
 3050 D(I,J)=0.D0                                                        CUR01110
 3051 CONTINUE                                                           CUR01120
      G1=(VZ/S)**2*D(I,J)*A1(I)*A2(I)*B(I,J)/4                           CUR01130
      G=G+G1                                                             CUR01140
C                                                                        CUR01150
C     COMPUTE DERIVATIVE WITH RESPECT TO C ANALYTICALLY                  CUR01160
C                                                                        CUR01170
      IF (KK .NE. 1) GO TO 3440                                          CUR01180
      IF (I+J .EQ. 2)GD=G1*2.0D0/CC(1)                                   CUR01190
      IF (I+J .EQ. 3)GD=G1*(CC(2)-CC(1))/(CC(2)*CC(1))+GD                CUR01200
      IF (I+J .EQ. 4)GD=GD-G1*2.0D0/CC(2)                                CUR01210
 3440 CONTINUE                                                           CUR01220
 3450 CONTINUE                                                           CUR01230
 3500 CONTINUE                                                           CUR01240
C                                                                        CUR01250
C     COMPUTE DERIVATIVES NUMERICALLY                                    CUR01260
C                                                                        CUR01270
      CUR1(JJ,KK,M)=VZ*DEXP(-X1)*G*DVZ                                   CUR01280
      IF(KK .NE. 1)CUR1(JJ,KK,M)=                                        CUR01290
     =    ((CUR1(JJ,KK,M)-CUR1(JJ,1,M))/DCUR(KK))                       CUR01300
 3550 CONTINUE                                                           CUR01310
      CUR1(JJ,5,M)=VZ*DEXP(-X1)*GD*DVZ                                   CUR01320
 3600 CONTINUE                                                           CUR01330
      GO TO 3700                                                         CUR01340
 3690 CONTINUE                                                           CUR01350
      CUR1(JJ,1,M)=0.D0                                                  CUR01360
 3700 CONTINUE                                                           CUR01370
      RETURN                                                             CUR01380
 3800 CONTINUE                                                           CUR01390
      DO 3850 L=JJ,200                                                   CUR01400
      CUR1(L,1,M)=PRESET                                                 CUR01410
 3850 CONTINUE                                                           CUR01420
      RETURN                                                             CUR01430
      END                                                                CUR01440
```

```
      SUBROUTINE PREP                                                   PRE00010
      INTEGER NSTP(5)/20,14,8,4,2/                                      PRE00020
      REAL*4 VOLT(228),CW(227),RATIO/1.036633/                          PRE00030
      REAL*4 DVZ(2,129),VZT(228)                                        PRE00040
      REAL*4 AAAVZ,AAVZ,AVZ,TVZ,AAADVZ,AADVZ,ADVZ,TDVZ,DVOLT            PRE00050
      COMMON /VZ/AAAVZ(22,5),AAVZ(4,40),AVZ(2,84),AAADVZ(22,5),         PRE00060
     ,   AADVZ(4,40),ADVZ(2,84),DVOLT(128),NFIRST(129)                  PRE00070
      COMMON /TAIL/TVZ(241),TDVZ(241)                                   PRE00080
C                                                                       PRE00090
C     GENERATE TABLE OF THRESHOLD SPEEDS AND CHANNEL WIDTHS             PRE00100
C                                                                       PRE00110
      DO 1 K=1,228                                                      PRE00120
    1 VOLT(K)=RATIO**(K-1)*60.-50.                                      PRE00130
      DO 2 K=1,227                                                      PRE00140
      IF(K .LE. 128)DVOLT(K)=VOLT(K+1)-VOLT(K)                          PRE00150
    2 CW(K)=ALOG(VOLT(K+1)/VOLT(K))*.5                                  PRE00160
      VZT(1)=43.76871                                                   PRE00170
      DO 3 K=1,227                                                      PRE00180
    3 VZT(K+1)=VZT(K)*EXP(CW(K))                                        PRE00190
C                                                                       PRE00200
C     GENERATE TABLE OF SPEEDS FOR INTEGRATION OF FIRST 5 CHANNELS      PRE00210
C                                                                       PRE00220
      DO 4 NCHAN=1,5                                                    PRE00230
      NFIRST(NCHAN)=1                                                   PRE00240
      AAAVZ(2,NCHAN)=1.02*VZT(NCHAN)                                    PRE00250
      AAAVZ(1,NCHAN)=(VZT(NCHAN)+AAAVZ(2,NCHAN))/2.                     PRE00260
      DVZ(1,NCHAN)=AAAVZ(2,NCHAN)-AAAVZ(1,NCHAN)                        PRE00270
      NSTEP=NSTP(NCHAN)                                                 PRE00280
      DVZ(2,NCHAN)=(VZT(6)-AAAVZ(2,NCHAN))/FLOAT(NSTEP)                 PRE00290
      AAADVZ(1,NCHAN)=DVZ(1,NCHAN)*4./3.                                PRE00300
      AAADVZ(2,NCHAN)=(DVZ(1,NCHAN)+DVZ(2,NCHAN))/3.                    PRE00310
      DO 4 N=1,NSTEP                                                    PRE00320
      AAADVZ(N+2,NCHAN)=DVZ(2,NCHAN)*2./3.                              PRE00330
      IF(MOD(N,2) .EQ. 1)AAADVZ(N+2,NCHAN)=DVZ(2,NCHAN)*4./3.           PRE00340
      IF(N .EQ. NSTEP)AAADVZ(N+2,NCHAN)=DVZ(2,NCHAN)/3.                 PRE00350
 4    AAAVZ(N+2,NCHAN)=AAAVZ(N+1,NCHAN)+DVZ(2,NCHAN)                    PRE00360
C                                                                       PRE00370
C     GENERATE TABLE OF INTEGRATION VELOCITIES FOR CHANNELS 6-45        PRE00380
C                                                                       PRE00390
      DO 5 NCHAN=6,45                                                   PRE00400
      DVZ(1,NCHAN)=(VZT(NCHAN+1)-VZT(NCHAN))/4                          PRE00410
      AADVZ(1,NCHAN-5)=DVZ(1,NCHAN)*4./3.                               PRE00420
      AADVZ(2,NCHAN-5)=DVZ(1,NCHAN)*2./3.                               PRE00430
      AADVZ(3,NCHAN-5)=DVZ(1,NCHAN)*4./3.                               PRE00440
      AADVZ(4,NCHAN-5)=DVZ(1,NCHAN)/3.                                  PRE00450
      DO 5 NSTEP=1,4                                                    PRE00460
    5 AAVZ(NSTEP,NCHAN-5)=VZT(NCHAN)+FLOAT(NSTEP)*DVZ(1,NCHAN)          PRE00470
C                                                                       PRE00480
C     GENERATE TABLE OF INTEGRATION VELOCITIES FOR CHANNELS 46-128      PRE00490
C                                                                       PRE00500
      DO 6 NCHAN=46,129                                                 PRE00510
      DVZ(1,NCHAN)=(VZT(NCHAN+1)-VZT(NCHAN))/2.                         PRE00520
      ADVZ(1,NCHAN-45)=DVZ(1,NCHAN)*4./3.                               PRE00530
      ADVZ(2,NCHAN-45)=DVZ(1,NCHAN)/3.                                  PRE00540
      DO 6 NSTEP=1,2                                                    PRE00550
```

```
      SUBROUTINE DATARD                                                 FXR00010
C                                                                       FXR00020
C    THIS SUBROUTINE READS DATA FOR ANALYSIS.  DATA SELECTION           FXR00030
C       INFORMATION IS READ FROM UNIT 8.  THE CONTROL VARIABLES ARE:    FXR00040
C             ITYM     TIME OF SPECTRUM TO BE ANALYZED                  FXR00050
C             CC       NOISE CURRENT                                    FXR00060
C             CN       STATISTICAL UNCERTAINTY DUE TO NOISE             FXR00070
C             NP       1=FIT VELOCITY,4=KEEP VELOCITY FIXED             FXR00080
C             LCHAN    ARRAY INDICATING WHICH CHANNELS ARE TO BE FIT    FXR00090
C       THE DATA ARE READ FROM UNIT 2.  THE FIRST SPECTRUM OF MODE       FXR00100
C       TYPE ITLMOD TAKEN LATER THAN THE TIME SPECIFIED BY ITYM IS       FXR00110
C       CHOSEN FOR ANALYSIS.  THE CHANNELS INDICATED BY T IN LCHAN ARE   FXR00120
C       READ INTO DRAY.  THE STATISTICAL WEIGHT FOR EACH DATA POINT IS   FXR00130
C       THEN COMPUTED AND STORED IN WRAY                                 FXR00140
C                                                                       FXR00150
      INTEGER*4 NCHN(2),NFIRST                                          FXR00160
      INTEGER*4 NINT,NPTS,NPARM,NP,ITLMOD,JTLMOD                        FXR00170
      INTEGER NSY/31536000/,NSD/86400/,NSH/3600/,NSM/60/,JTYM(6),ITYM(6)FXR00180
      REAL*4 CURRNT(512)                                                FXR00190
      REAL*4 SHIFT(100),A1(100),A2(100),C1(100)                         FXR00200
      REAL*4 AMA1,AMA2,AMC1,AMSFT,ABCS                                  FXR00210
      REAL*4 AS,BS,C,CN,CC                                              FXR00220
      REAL*4 AAAVZ,AAVZ,AVZ,TVZ,AAADVZ,AADVZ,ADVZ,TDVZ,DVOLT            FXR00230
      REAL*8 DRAY,WRAY,PARM                                             FXR00240
      LOGICAL*1 LCHAN,LT                                                FXR00250
      COMMON/LCHAN/LCHAN(128,4),CN,CC                                   FXR00260
      COMMON /ABCSET/ABCS(241,4,2)                                      FXR00270
      COMMON /VZ/AAAVZ(22,5),AAVZ(4,40),AVZ(2,84),AAADVZ(22,5),         FXR00280
     ,   AADVZ(4,40),ADVZ(2,84),DVOLT(128),NFIRST(129)                  FXR00290
      COMMON/CFIT/NPTS,NPARM,PARM(10),DRAY(512),WRAY(512),NP            FXR00300
      COMMON/AS/AS(72,4),BS(72,4),C(4),NINT(72,4)                       FXR00310
      COMMON/TRNPAR/AMA1(100,129),AMA2(100,129),AMC1(100,129),          FXR00320
     ,  AMSFT(100,129)                                                  FXR00330
      LOGICAL*1 LARRY                                                   FXR00340
      REAL*8 ARRY(512),ARRY1(512,6)                                     FXR00350
      C(1)=16.                                                          FXR00360
      C(2)=4.                                                           FXR00370
      C(3)=2.                                                           FXR00380
C     C(4)=1.                                                           FXR00390
      C(4)=18.                                                          FXR00400
      READ (8,*) NPTS,NPARM,NP                                          FXR00410
      READ (8,*) (PARM(I),I=1,10)                                       FXR00420
      READ (8,*) ITYM,ITLMOD                                            FXR00430
      T=(ITYM(1)-1979)*NSY+ITYM(2)*NSD+ITYM(3)*NSH+ITYM(4)*NSM+ITYM(5)  FXR00440
      READ (8,*) CN,CC                                                  FXR00450
      READ (8,300) LCHAN                                                FXR00460
  300 FORMAT (64L1)                                                     FXR00470
    1 READ (2,350) JTYM,JTLMOD                                          FXR00480
  350 FORMAT('0',6I5,'  JTLMOD=',I4)                                    FXR00490
      IF(JTLMOD .EQ. 1)NET=64                                           FXR00500
      IF(JTLMOD .EQ. 2)NET=512                                          FXR00510
      T1=(JTYM(1)-1979)*NSY+JTYM(2)*NSD+JTYM(3)*NSH+JTYM(4)*NSM+JTYM(5) FXR00520
      READ(2,400) (CURRNT(I),I=1,NET)                                   FXR00530
  400 FORMAT(1X,4E12.3)                                                 FXR00540
      IF (T1-T) 1,2,2                                                   FXR00550
```

```
      2 IF(JTLMOD-ITLMOD) 1,3,1                                                 FXR00560
      3 CONTINUE                                                                FXR00570
        WRITE(35)(CURRNT(I),I=1,NET)                                            FXR00580
        N=0                                                                     FXR00590
        DO 20 NCP=1,4                                                           FXR00600
        DO 10 NCHAN=1,128                                                       FXR00610
        IF(.NOT. LCHAN(NCHAN,NCP)) GO TO 10                                     FXR00620
        N=N+1                                                                   FXR00630
        IF (ITLMOD .EQ. 1) N1=NCHAN+16*(NCP-1)                                  FXR00640
        IF (ITLMOD .EQ. 2) N1=NCHAN+128*(NCP-1)                                 FXR00650
        DRAY(N)=CURRNT(N1)                                                      FXR00660
        WRAY(N)=DSQRT((4.D-2*DRAY(N))**2+(DBLE(CN)/DBLE(DVOLT(NCHAN)))**2)      FXR00670
     10 CONTINUE                                                                FXR00680
     20 CONTINUE                                                                FXR00690
        READ(1,*)ABCS                                                           FXR00700
        DO 30 I=1,128                                                           FXR00710
        READ(15)(SHIFT(J),J=1,60)                                               FXR00720
        READ(25)(SHIFT(J),J=61,100)                                             FXR00730
        READ(16)(A1(J),J=1,60)                                                  FXR00740
        READ(26)(A1(J),J=61,100)                                                FXR00750
        READ(17)(A2(J),J=1,60)                                                  FXR00760
        READ(27)(A2(J),J=61,100)                                                FXR00770
        READ(18)(C1(J),J=1,60)                                                  FXR00780
        READ(28)(C1(J),J=61,100)                                                FXR00790
        DO 29 J=1,100                                                           FXR00800
        AMSFT(J,I)=SHIFT(J)                                                     FXR00810
        AMA1(J,I)=A1(J)                                                         FXR00820
        AMA2(J,I)=A2(J)                                                         FXR00830
        AMC1(J,I)=C1(J)                                                         FXR00840
     29 CONTINUE                                                                FXR00850
     30 CONTINUE                                                                FXR00860
        READ(30,9100)NINT                                                       FXR00870
        READ(30,9101)AS                                                         FXR00880
        READ(30,9101)BS                                                         FXR00890
   9100 FORMAT(20I4)                                                            FXR00900
   9101 FORMAT(5D16.7)                                                          FXR00910
        LARRY=.TRUE.                                                            FXR00920
        RETURN                                                                  FXR00930
        END                                                                     FXR00940
        SUBROUTINE SIMCOM(PARM,LARRY,ARRY,ARRY1)                                FXR00950
        LOGICAL*1 LCHAN,LARRY                                                   FXR00960
        INTEGER*4 NCHN(2),NPTS,NPARM,NP,NINT                                    FXR00970
C     THE FOLLOWING STATEMENT IS A MODIFICATION                                 FXR00980
C       REAL*4 V0(3)/41.2,28.95,3.5/,DB(3)/-25.8,33.0,37.2/                     FXR00990
C                                                                               FXR01000
        REAL*4 AS,BS,C,CN,CC                                                    FXR01010
        REAL*4 AAAVZ,AAVZ,AVZ,TVZ,AAADVZ,AADVZ,ADVZ,TDVZ,DVOLT                  FXR01020
        REAL*8 DN/1.D0/,A/64.D0/,Z/1.D0/,DIST(128),PARM(10)                     FXR01030
        REAL*8 F(71,4),WSP,VSC(3),VCP(3),ARRY1(512,6),ARRY(512)                 FXR01040
        COMMON/LCHAN/LCHAN(128,4),CN,CC                                         FXR01050
        COMMON/VZ/AAAVZ(22,5),AAVZ(4,40),AVZ(2,84),AAADVZ(22,5),                FXR01060
       ,   AADVZ(4,40),ADVZ(2,84),DVOLT(128),NFIRST(129)                        FXR01070
       ,COMMON/AS/AS(72,4),BS(72,4),C(4),NINT(72,4)                             FXR01080
        WSP=PARM(4)                                                             FXR01090
        VSC(1)=PARM(1)                                                          FXR01100
```

```
      VSC(2)=PARM(2)                                                    FXR01110
      VSC(3)=PARM(3)                                                    FXR01120
C    THE FOLLOWING TWO STATEMENTS ARE A MODIFICATION                    FXR01130
C     DO 9991 MP=1,3                                                    FXR01140
C9991 VSC(MP)=DBLE(VO(MP))+PARM(3)*DBLE(DB(MP))                         FXR01150
C                                                                       FXR01160
      NP=0                                                              FXR01170
      DO 300 NCP=1,3                                                    FXR01180
      CALL VSCCP(VSC,NCP,VCP)                                           FXR01190
      NCHN(1)=1                                                         FXR01200
      NCHN(2)=127                                                       FXR01210
C     WRITE(6,9000)DN,WSP,VCP,A,Z                                       FXR01220
 9000 FORMAT(5D16.7)                                                    FXR01230
      CALL ABCCUR(DN,WSP,VCP,A,Z,NCHN,DIST)                             FXR01240
C     WRITE(6,9000)(DIST(NN),NN=1,71)                                   FXR01250
      DO 100 J=1,4                                                      FXR01260
      DO 100 NCHAN=1,71                                                 FXR01270
      N1=NINT(NCHAN,J)                                                  FXR01280
      N2=N1+1                                                           FXR01290
      F(NCHAN,J)=(DBLE(AS(NCHAN,J))*DIST(N1)+                           FXR01300
     +   DBLE(BS(NCHAN,J))*DIST(N2))*DBLE(C(J))                         FXR01310
  100 CONTINUE                                                          FXR01320
      DO 150 NCHAN=1,71                                                 FXR01330
      IF(.NOT. LCHAN(NCHAN,NCP))GO TO 150                               FXR01340
      NP=NP+1                                                           FXR01350
C     ARRY(NP)=PARM(5)**2*F(NCHAN,1)+PARM(6)**2*F(NCHAN,2)+             FXR01360
C    +  PARM(7)**2*F(NCHAN,3)+PARM(8)**2*F(NCHAN,4)+                    FXR01370
C    +  DBLE(CC)/DVOLT(NCHAN)                                           FXR01380
      ARRY(NP)=PARM(5)*F(NCHAN,1)+PARM(6)*F(NCHAN,2)+                   FXR01390
     +  PARM(7)*F(NCHAN,3)+PARM(8)*F(NCHAN,4)+DBLE(CC)/DVOLT(NCHAN)     FXR01400
      IF(.NOT. LARRY)GO TO 150                                          FXR01410
      DO 130 NSP=1,4                                                    FXR01420
C 130 ARRY1(NP,NSP)=F(NCHAN,NSP)*2.D0*PARM(NSP+4)                       FXR01430
  130 ARRY1(NP,NSP)=F(NCHAN,NSP)                                        FXR01440
  150 CONTINUE                                                          FXR01450
  300 CONTINUE                                                          FXR01460
      RETURN                                                            FXR01470
      END                                                               FXR01480
      SUBROUTINE VSCCP(VSC,NCP,VCP)                                     FXR01490
      REAL*8 TM(9,4),VJE(3),VSC(3),TJESC(9),VCP(3),T(9),V(3)            FXR01500
      DATA TM/0.5,0.8137977,0.2961981,  -0.8660254,0.4698463,0.1710101, FXR01510
     1   0.,-0.3420201,0.9396926,                                       FXR01520
     2        0.5,-0.8137977,-0.2961981,  0.8660254,0.4698463,0.1710101,FXR01530
     *0.,-0.3420201,0.9396926,                                          FXR01540
     3 -1.,0.,0.,  0.,-0.9396926,-0.3420201,  0.,-0.3420201,0.9396926,  FXR01550
     4   -0.6819984,-0.02552388,-0.7309082,                             FXR01560
     * 0.7313537,-0.02380140,-0.6815829,  0.,-0.9993908,0.03489950/     FXR01570
      CALL DVTRNS(VCP,TM(1,NCP),VSC)                                    FXR01580
      RETURN                                                            FXR01590
      END                                                               FXR01600
      SUBROUTINE DVTRNS (VP,T,V)                                        FXR01610
C VP = TV+VO                                                            FXR01620
      REAL*8 VP(1),T(1),V(1)                                            FXR01630
      VP(1) = T(1)*V(1)+T(4)*V(2)+T(7)*V(3)                             FXR01640
      VP(2) = T(2)*V(1)+T(5)*V(2)+T(8)*V(3)                             FXR01650
```

```
      VP(3) = T(3)*V(1)+T(6)*V(2)+T(9)*V(3)                    FXR01660
      RETURN                                                   FXR01670
      END                                                      FXR01680
```